UNIVERSITY OF SOUTHAMPTON

FACULTY OF NATURAL AND ENVIRONMENTAL SCIENCES

Chemistry

SYNTHESIS OF COORDINATION COMPLEXES USING MIXED DONOR CHALCOGENOETHER MACROCYCLES TO INVESTIGATE HARD/SOFT METAL TO LIGAND INTERACTIONS

by

Paolo A. Farina

Thesis for the degree of Doctor of Philosophy

NOVEMBER 2013

UNIVERSITY OF SOUTHAMPTON

ABSTRACT

FACULTY OF NATURAL AND ENVIRONMENTAL SCIENCES

Chemistry

Thesis for the degree of Doctor of Philosophy

SYNTHESIS OF COORDINATION COMPLEXES USING MIXED DONOR CHALCOGENOETHER MACROCYCLES TO INVESTIGATE HARD/SOFT METAL TO LIGAND INTERACTIONS

Paolo Alberto Farina

Improvements to the synthesis of Group 16 mixed donor macrocycles are reported. The mixed donor chalcogenoether macrocycles [15]aneO_3S_2, [18]aneO_2S_4 and [18]aneO_4E_2 (E= S, Se and Te) can coordinate a range of both soft and hard Lewis acids. Complexes investigating hard Lewis acids focussed on Ca(II), Sr(II), Sc(III) and Y(III) halides. The Group 2 metals are coordinated to all the donors in the macrocycle, importantly the metal centres showed an affinity for the softer donor (S, Se) as well as the harder donor (O). This interaction was maintained even after trace ingress of water. The lattice energies of the starting metal precursors were important in accessing the coordination chemistry of Ca(II) and Sr(II), CaI_2 and SrI_2 both gave products of the type [MI_2(macrocycle)]. Similarly ScI_3 was reacted with the macrocyclic ligands to give ionic solids [ScI_2(macrocycle)][I]. The analogous Y(III) and Sc(III) chlorides were also synthesised by using the halide abstractor $FeCl_3$ and [$ScCl_3(THF)_3$] and [$YCl_2(THF)_5$][$YCl_4(THF)_2$] to give complexes of the type [MCl_2(macrocycle)][$FeCl_4$]. The macrocycles bind hexadentate (pentadentate in case of [15]aneO_3S_2) to the Group 3 cations. Softer and borderline Lewis acids $Sn(XF_n)_2$ and $Pb(XF_n)_2$ (X=B, P; n= 4, 6 respectively) form complexes with the Group 16 donor macrocycles. The coordination compounds exhibit a range of unusual coordination modes for the weakly coordinating fluoroanions ($[BF_4]^-$ μ^2, κ^2 and κ^1; $[PF_6]^-$ κ^3 and κ^2). Pb(II) and Sn(II) were shown to encourage the hydrolysis of the $[PF_6]^-$ anion and the decomposition of [18]aneO_4Te_2. Sn(II) also cleaved the other [18]aneO_4E_2 (E= S, Se) macrocycles, the complex [Sn([18]aneO_4S_2)($HO(CH_2)_2OH$)][BF_4]$_2$ is the first structural evidence for metal mediated ring opening of a saturated oxa-thia macrocycle. A series of coordination complexes of Sb(III), a soft Lewis acid, halides were investigated. Structural comparisons between the analogous fluoro-, chloro- and iodo-antimony(III) complexes showed the corresponding halide greatly influenced the Lewis behaviour of Sb(III). X-ray crystallography, ^{1}H (and where appropriate ^{19}F, ^{31}P, ^{45}Sc, ^{77}Se and ^{125}Te) NMR spectroscopy, elemental analysis, conductivity measurements and IR spectroscopy were used to characterise the complexes in this study.

Contents

List of tables

List of figures

DECLARATION OF AUTHORSHIP

I, Paolo Alberto Farina

declare that the thesis entitled

"SYNTHESIS OF COORDINATION COMPLEXES USING MIXED DONOR CHALCOGENOETHER MACROCYCLES TO INVESTIGATE HARD/SOFT METAL TO LIGAND INTERACTIONS"

and the work presented in the thesis are both my own, and have been generated by me as the result of my own original research. I confirm that:

- this work was done wholly or mainly while in candidature for a research degree at this University;
- where any part of this thesis has previously been submitted for a degree or any other qualification at this University or any other institution, this has been clearly stated;
- where I have consulted the published work of others, this is always clearly attributed;
- where I have quoted from the work of others, the source is always given. With the exception of such quotations, this thesis is entirely my own work;
- I have acknowledged all main sources of help;
- where the thesis is based on work done by myself jointly with others, I have made clear exactly what was done by others and what I have contributed myself;
- Parts of this work have been published as:

P. Farina, W. Levason and G. Reid, *Dalton Transactions,* 2013, **42**, 89

P. Farina, T. Latter, W. Levason and G. Reid, *Dalton Transactions,* 2013, **42**, 4714

P. Farina, W. Levason and G. Reid, *Polyhedron*, 2013, **55**, 102-108

M. J.D. Champion, P. Farina, W. Levason and G. Reid, *Dalton Transactions*, 2013, **42**, 13179

C. Beattie, P. Farina, W. Levason, G. Reid, *Dalton Transactions*, 2013, 2013, **42**, 15183

Siged: ……..

Date:……

Acknowledgements

I would firstly like to thank my supervisors Professor William Levason and Professor Gillian Reid, not only for their invaluable guidance and experience throughout the course of my PhD, but also for facilitating me with (overall) an exciting and enjoyable 'blue skies' project.

Special mention should go to Dr. Andreas Danopoulos and Dr. Steven J. Simpson for forging me onto a PhD journey, without which I would not have met some truly wonderful people whom I will subsequently acknowledge:

To my 'wife' Sarah Hobbs and life-long confidant Rowena Thomas, fellow residents of 35 Northcote Rd; not to be forgotten Chrissie Wicking (honorary housemate); thank you so much for just being generally awesome (MI7).

These people have first and foremost made living in Southampton not just bearable but even pleasant and therefore I would also like to thank Pete Wells, Peter Cummings and the extraordinary pair "The Benjamins". And a shout out to the Canoe Polo society too.

To the members of labs 2005 and 2007, I will take away many fond memories of you guys.

With regards to this work, Professor Levason requires a special thank you for taking the time to collect multinuclear NMR spectra for a great majority of the compounds. Dr. Michael Webster and Dr. Wenjian Zhang for their invaluable support and advice regarding X-ray crystallography. I would also like to thank and acknowledge my two faithful project students, Thomas Latter and Christopher Beattie, who contributed to work discussed in this thesis.

Finally my family, especially my mum, for just being there regardless of the situation- the best rock a guy could stand on.

Definitions and Abbreviations

Ar^F	fluorinated aryl
bipy	2,2'-bipyridine
Cp	cyclopentadienyl
Cp*	pentamethylcyclopentadienyl
dmso	dimethyl sulfoxide
EI	electron ionisation
ESI	electrospray ionisation
HSAB	Hard Soft Acid Base
IR	infrared
MS	mass spectrometry
NMR	nuclear magnetic resonance
phen	1,10-phenanthroline
THF	tetrahydrofuran
ΣVdW	sum of the Van der Waals

Macrocycles and Ligands:

[9]aneO_2S	1,4,7-dioxathiacyclononane
[9]aneO_2Te	1,4,7-dioxatelluracyclononane
[9]aneOS_2	1,4,7-oxadithiacyclononane
[9]aneS_3	1,4,7-trithiacyclononane
Me_3-tacn	1,4,7-trimethyl-1,4,7-triazacyclononane
[10]aneS_3	1,4,8-trithiacyclodecane
12-crown-4	1,4,7,10-tetraoxacyclododecane
[14]aneS_4	1,4,8,11-tetrathiacyclotetradecane
dibenzo-14-N_2O_2	dibenzo-1,8-dioxa-4,11-diazacyclotetradecine
15-crown-5	1,4,8,10,13-pentaoxacyclopentadecane
[15]aneO_3S_2	1,4,7-trioxa-10,13-dithiacyclopentadecane
mn-15-O_3S_2	1,4,7-trioxa-10,13-dithiacyclopentadec-11-ene-11,12-dicarbonitrile

[16]aneS_4	1,5,9,13-tetrathiacyclohexadecane
[16]aneSe_4	1,5,9,13-tetraselenacyclohexadecane
[18]aneO_4S_2	1,4,10,13-tetraoxa-7,16-dithiacyclooctadecane
[18]aneO_2S_4	1,10-dioxa-4,7,13,16-tetrathiacyclooctadecane
mn-18-O_4S_2	1,4,7,10-tetraoxa-13,16-dithiacyclooctadec-14-ene-14,15-dicarbonitrile
[18]aneO_4Se_2	1,4,10,13-tetraoxa-7,16-diselenacyclooctadecane
[18]aneO_4Te_2	1,4,10,13-tetraoxa-7,16-ditelluracyclooctadecane
[18]aneS_6	1,4, 7,10,13,16-hexathiacyclooctadecane
18-crown-6	1,4, 7,10,13,16-hexaoxacyclooctadecane
1,5-dibenzothia-18-crown-6	dibenzo-1,4,7,10,13-pentaoxa-16-thiacyclooctadecine
dicyclohexyl-18-crown-6	icosahydrodibenzo-1,4,7,10,13,16-hexaoxacyclooctadecine
benzo-18-crown-6	benzo-1,4,7,10,13,16-hexaoxacyclooctadecine
[28]aneS_8	1,4,8,11,15,18,22,25-octathiacyclooctacosane
^{n}decyl–SNS	S-decyl-N-(decylthio)thiohydroxylamine
^{t}Bu–SNS	S-(tert-butyl)-N-(tert-butylthio)thiohydroxylamine
2,6-^{i}PrC_6H_3-BIAN	1,2-bis((2,6-diisopropylphenyl)azanyl)-acenaphthylene

1. Introduction

1.1 Macrocycles

Macrocycles are an important and varied class of compounds which have a widespread role within chemistry. They include porphyrins in biological systems such as haemoglobin, Schiff-base pyrrole macrobicycles that can stabilise and trap metal ions and small molecules and macrotetrolide antibiotics such as nonactin (Figure 1.1) for selective sequestration of K^+ over the other alkali metal ions [1] [2]. Further to this, macrocycles can incorporate many donor types and architectures for catalyst design and function; they have been used to emulate more complex systems for example vanadium-sulfur macrocycle complexes to mimic vanadium nitrogenase [3].

Their prevalence can be attributed to their limitless potential and synthetic flexibility, based on variable ring sizes, donor types, number of donors present, distances between donors and rigidity of the ring framework; with the case of the trivalent pnictogens there is also the pendant group that can be used for further steric and electronic fine tuning.

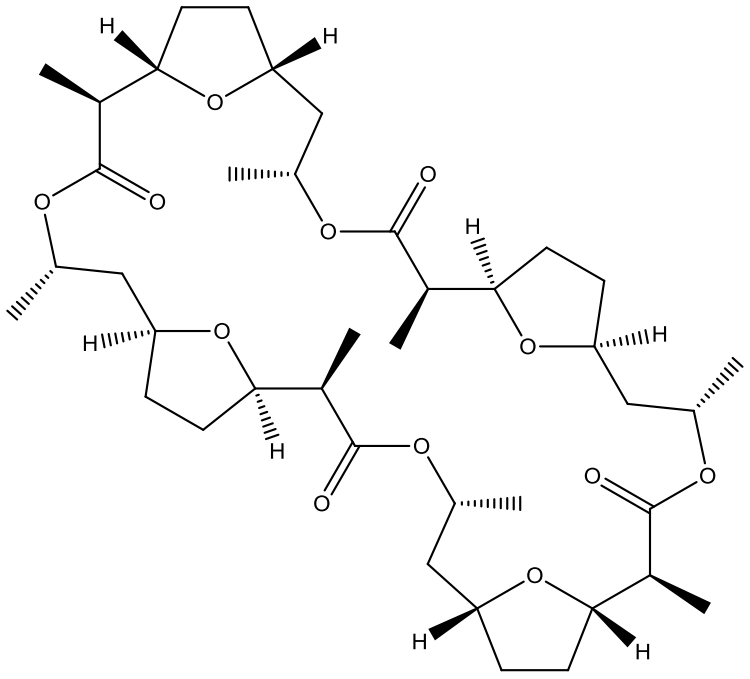

Figure 1.1 The skeleton notation for the antibiotic nonactin [2].

Ever since the observation of the macrocyclic effect by Cabbiness and Margerum in 1969, macrocycles have been an integral ligand class in coordination chemistry [4]. The effect was first identified by studying the increased thermodynamic stability and kinetic inertness of Cu(II) tetra-amine complexes.

The macrocyclic effect incorporates an increase in both the kinetic and thermodynamic stability afforded to the complex. The kinetic influence can be viewed as the relative lability of the coordinated bonds in macrocyclic systems compared to those in open chain chelates (Figure 1.2). To break the metal-ligand bond requires its elongation, which with the macrocycle framework causes a distortion throughout the whole ring and therefore unfavourable conformational strain. In contrast, the open chain ligands can "unfasten" relatively easily beginning with a terminal donor and then the others sequentially [5].

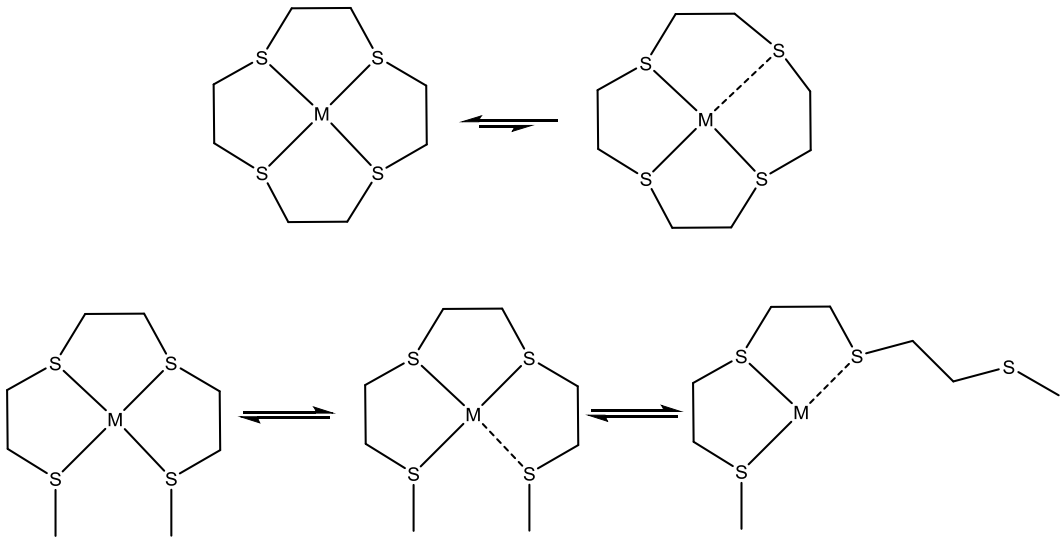

Figure 1.2 Reaction scheme comparing [12]aneS_4 and 2,5,8,11-tetrathiadodecane illustrating the kinetic contribution to the macrocyclic effect.

The thermodynamic influence can be considered as the combination of an enthalpic and entropic effect; the former is still a subject of uncertainty. The entropic effect derives from an increase in the number of configurational degrees of freedom the ligand gains from its dissociation from the metal centre. 'Free' macrocycles on the whole will have less degrees of freedom than their open chain counterparts, therefore

although there is still an entropy gain from the macrocycle's dissociation, it is markedly less than when an open chain chelate dissociates.

Many factors, usually co-dependent, help determine the enthalpic contribution to the thermodynamic influence of the macrocyclic effect [6]. These include compatibility of metal ion size to the macrocyclic cavity, any variance between the bond energies of the participating donors and the Lewis acid, any ligand conformational changes after coordination and crucially the difference in solvation energies for macrocycles relative to open chain chelates.

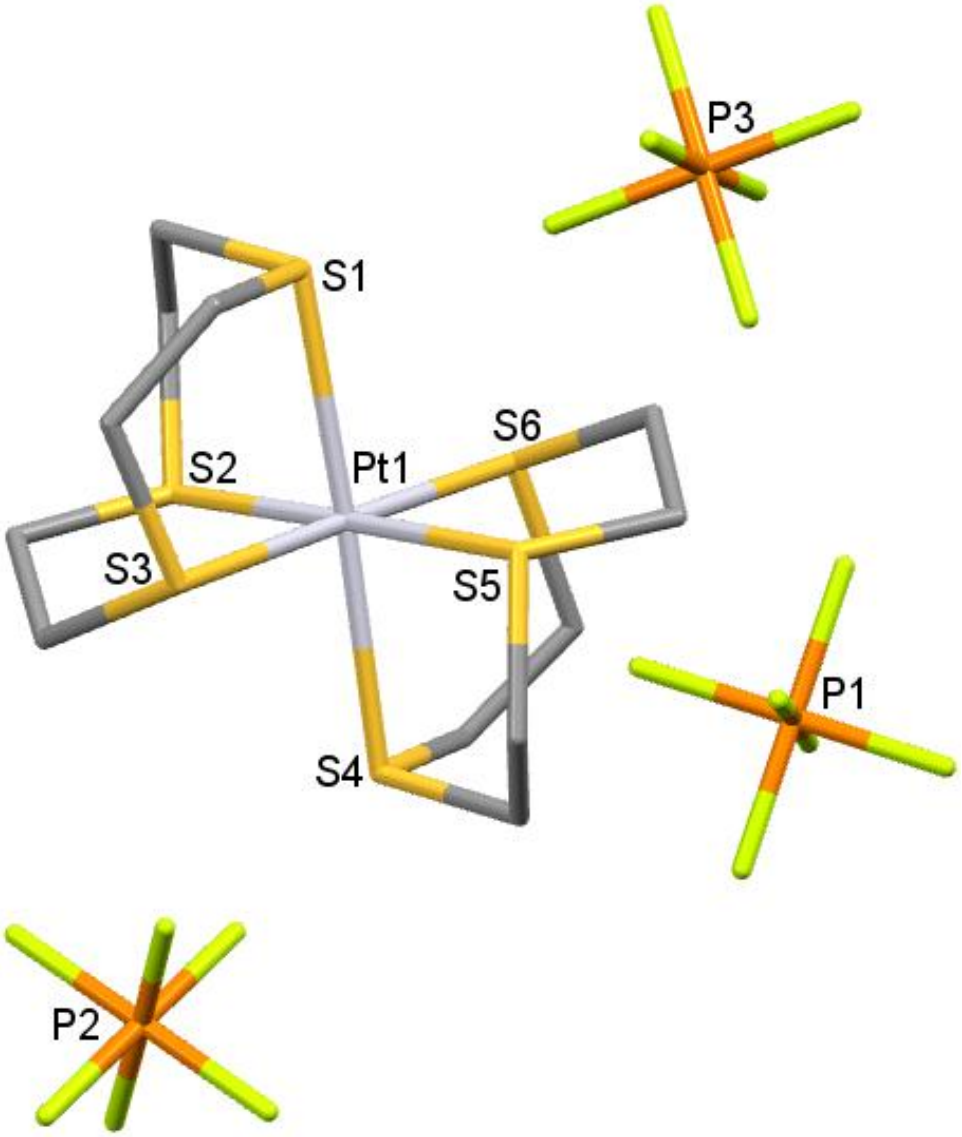

Figure 1.3 Structure of $[Pt([9]aneS_3)_2][PF_6]_3$. H atoms are omitted for clarity [7].

The macrocyclic effect also distinguishes macrocycles from other non-macrocyclic ligands in that the increase in coordination potential helps them to readily solubilise metal salts which are insoluble. This allows for a more straight forward approach to the coordination chemistry of the metal salt. An exemplar case is in the formation of “purple benzene”; potassium permanganate (normally completely insoluble in organic solvents such as benzene) is readily solubilised in benzene by the presence of dissolved 18-crown-6 giving an immediately striking purple colouration to the solvent [8].

Also due to their stabilising properties, macrocycles can be considered as protecting groups for metal ion centres, they have led to the stabilisation of unusual metal oxidation states and coordination geometries. Such as Pt(III) Figure 1.3, Pd(III), Au(II) with thiacrowns [7 9 10].

In tandem with the macrocyclic effect, other factors also help govern the coordination behaviour of macrocycles working either synergistically or antagonistically towards the isolation of the complex.

Preorganisation of the macrocycle is discussed further in Chapter 2. HSAB (Hard Soft Acid Base) theory can help predict the affinity of the macrocyclic donors to the target Lewis acid. It is a widely applicable, qualitative theory that states hard Lewis acids will more likely coordinate to hard Lewis bases with the opposite true for soft Lewis acids [11]. Expanding research in the area of coordination chemistry has uncovered many exceptions [12 13 14].

Traditionally, macrocycles based around S, N, P and As donor atoms have been geared more towards coordination with the transition block elements, whereas their polyether analogues are better suited for complexation to the alkali and alkaline earth metals [15]. Despite this, crown ethers have been found coordinated to most types of metal ion [15 16].

1.2 Heterocrown and Crown ether coordination chemistry

Crown ethers have been widely used in coordination chemistry and to date there are over 2050 structurally authenticated complexes based solely on 18-crown-6 (arguably the most recognisable crown ether) [17]. Although normally coordinated both hexadentate and planar, 18-crown-6 complexes have shown a range of denticities and conformations of the macrocyclic framework [16 18 19 20 21].

As part of this study a few novel crown-ether complexes were synthesised and are discussed briefly as a comparison to the mixed chalcogenoether macrocycle complexes in the relevant Chapters. With regards to the known crown ether complexes they represent a point of comparison by being the 'hardest' chalcogenoether macrocycles for coordination to the target Lewis acids.

Conversely, thiacrowns and selenacrowns represent the 'softest' widely explored Group 16 donor macrocycles and are the other reference point [22 23]. Their complexes are also discussed in the introductions in the relevant chapters.

Heterocrown ethers are the middle ground, incorporating hard macrocyclic O-donors as well as softer S/Se/Te donors. Their chemistry is less explored than that of the homoleptic crowns already mentioned. Here is discussed the advances in mixed chalcogenoether macrocycle coordination chemistry [22]. Examples with Ca(II), Sc(III), Pb(II), and Sb(III) are discussed in the relevant Chapters.

The other Main Group and f-block metal complexes include a small number of examples with the alkali metals, Ba(II), La(III), Lu(III), Nd(III), Ge(II) and Bi(III). By far the majority of examples reside with the middle to late d-block metals, Groups 9-12.

Barium(II) and the alkali metal cations form *endodentate* complexes with [18]aneO_4S_2. Other compounds contain Cu(I) which binds in an *exocyclic* to the S-donors and is the cause of the twisted geometries; they are all lamellar copper(I) isothiocyanate based coordination polymers with

[18]aneO$_4$S$_2$ moieties which ligate the s-block metals, although, not with all the macrocyclic donors (the s-block metals show a preference for the O-donors) [24] [25]. Caesium(I) and barium(II) coordinate to all the donors by virtue of their increased radius [26] [27].

The f-block metals La(III), Lu(III) and Nd(III) have only been coordinated to mixed chalcogenoether donor macrocycles in the last few years and there are few structural examples. [La(ClO$_4$)$_2$([18]aneO$_4$S$_2$)(H$_2$O)][ClO$_4$], [LaI$_2$([18]aneO$_4$S$_2$)(H$_2$O)][I], [LaI$_3$([18]aneO$_4$S$_2$)] and [LaI$_3$([18]aneO$_4$Se$_2$)] all have a very similar structure with the metal bound to all the macrocyclic donors *endocyclic*, three other co-ligands occupy a *meridian* giving a 9-coordinate metal centre [12] [28]. The macrocycle is fairly planar with the E-donor atoms (E= S, Se) puckered *syn*. In contrast, Lu(III) is only 8-coordinate in [LuI$_2$([18]aneO$_4$S$_2$)][I] and [LuI$_2$([18]aneO$_4$Se$_2$)][I] and the two coordinated iodides are mutually *cis* and the macrocycle is much more folded around the metal. The complex [NdI$_3$([18]aneO$_4$Se$_2$)] lacks structural authentication but there is spectroscopic evidence for its existence [28]. These complexes mark some of the first examples of soft chalcogenoether coordination to the hard electropositive f-block metal cations and, in parallel to the work discussed later in this study, highlight a much greater coordination chemistry between hard Lewis metal centres and soft Lewis bases.

The p-block metals Ge(II) and Bi(III) form well defined, discrete complexes with oxa-thia macrocycles. They are [GeCl([15]aneO$_3$S$_2$)][GeCl$_3$], [GeCl([18]aneO$_3$S$_3$)][Y] (Y= GeCl$_3^-$ or CF$_3$SO$_3^-$) and [BiCl$_3$(15-mn-O$_3$S$_2$)] and [BiCl$_3$(18-mn-O$_4$S$_2$)] [29] [30]. The germanium(II) complexes are all cationic *endodentate* systems showing a preference for the harder O-donors. In the 18-membered ring complexes the metal binds to only four of the available six donors (O$_3$S) reflecting the small radius of germanium. The Bi(III) complexes are directly analogous to the Sb(III) counterparts discussed in Chapter 7.

In general the geometries observed for the complexes of Groups 9-10 are dominated by the stereochemical preferences of the metal cation centre giving either octahedral or square planar geometries [22]. Examples of the type of complex include [PdCl$_2$([18]aneO$_4$S$_2$)] (κ^2-S$_2$) [31],

$[Co([20]aneO_2S_4)][ClO_4]_2$ (κ^6) [32], $[Pt([18]aneO_2S_4)][PF_6]_2$ (κ^4-S_4) Figure 1.4 [33], $[Ni([18]aneO_2S_4)][BF_4]_2$ (κ^6) Figure 1.5 [34], $[Pd([15]aneO_3S_2)_2][PF_6]_2$ (*exo*-κ^2-S_2) [35], $[Co([9]aneOS_2)_2][ClO_4]_2$ (κ^3) [36] etc. A strong preference for the S-donors is evident, and in several cases some or all the O-donors remained uncoordinated.

$PdCl_2$ and $PtCl_2$ provide the first structurally authenticated examples of complexes with $[18]aneO_4E_2$ (E= Se, Te), $[PdCl_2([18]aneO_4Se_2)]$ and $[PtCl_2([18]aneO_4E_2)]$ Figure 1.6. They strongly resemble the oxa-thia analogue and only coordinate *via* the soft donors [37]. The only other examples containing heavier chalcogenoethers are two similar square planar complexes of oxa-selena benzo-crowns with Pd(II) Figure 1.7, that interact solely through the neutral selenium donors [38] [39].

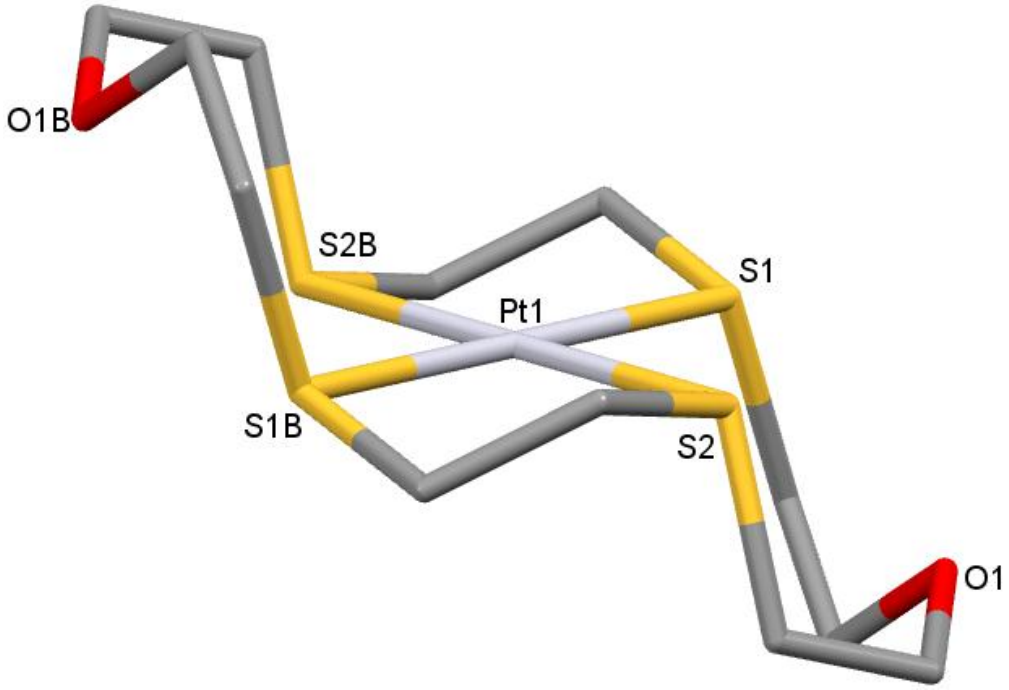

Figure 1.4 Structure of the cation in $[Pt([18]aneO_2S_4)][PF_6]_2$. H atoms are omitted for clarity [33].

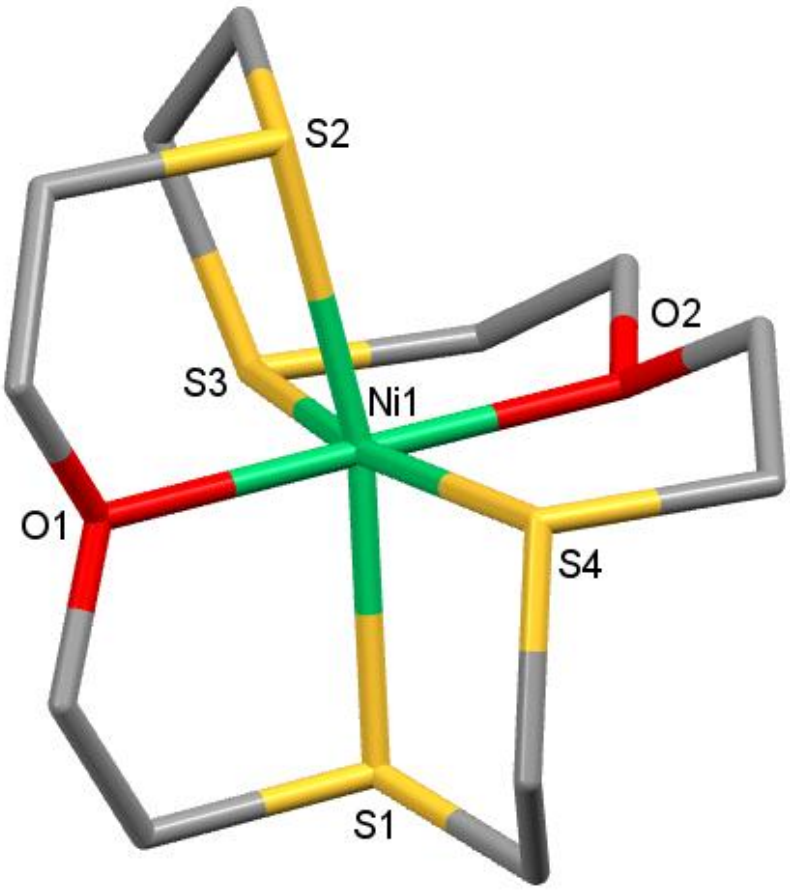

Figure 1.5 Structure of the cation in [Ni([18]aneO$_2$S$_4$)][BF$_4$]$_2$. H atoms are omitted for clarity [34]

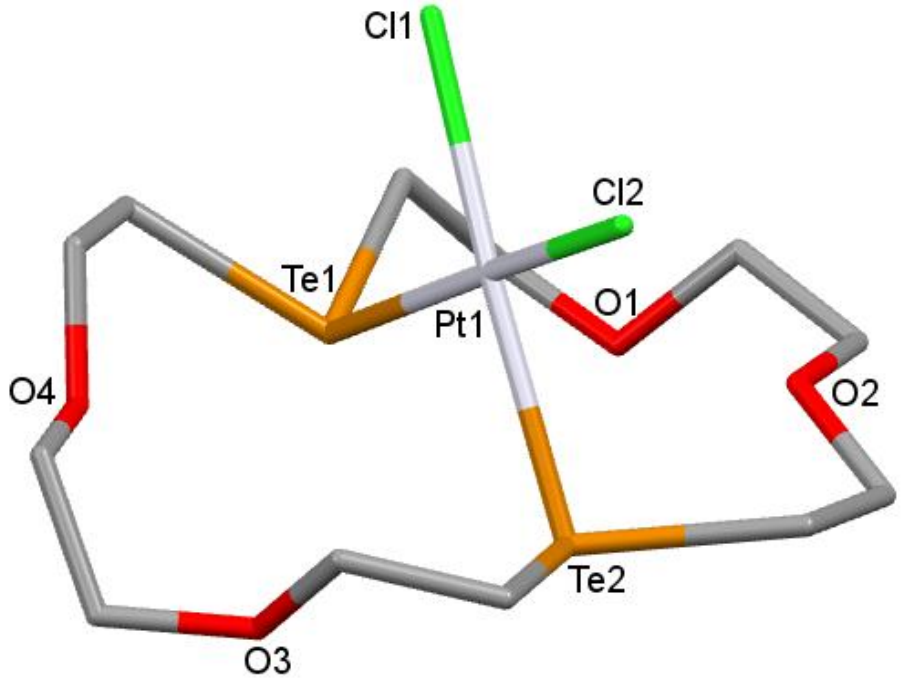

Figure 1.6 Structure of [PtCl$_2$([18]aneO$_4$Te$_2$)]. H atoms are omitted for clarity [37]

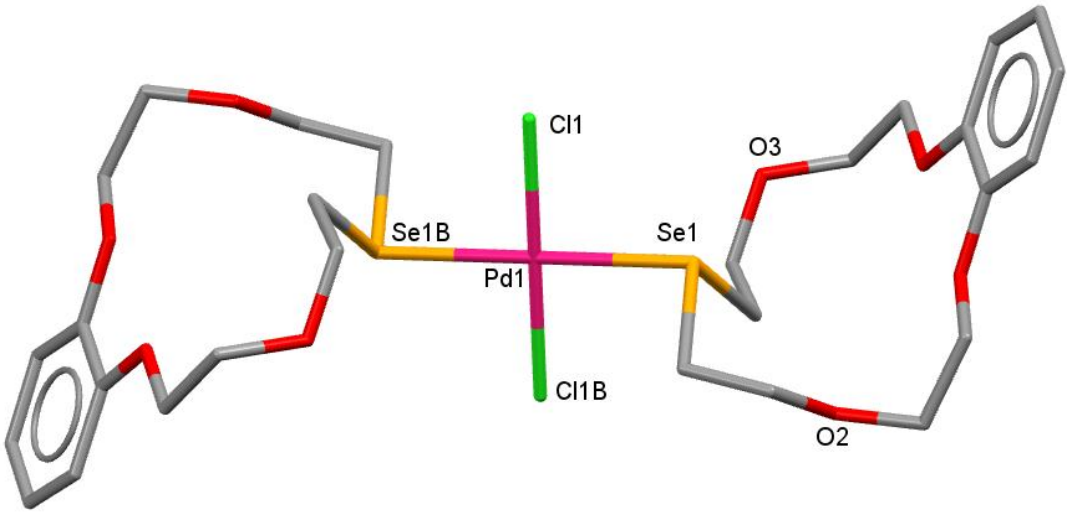

Figure 1.7 Structure of $[PdCl_2(benzo\text{-}[15]aneO_4Se)_2]$. H atoms are omitted for clarity [38].

The complexes of Group 11 have even more unusual geometries, (especially Ag(I)), dependent on a number of factors, including small changes in the ring architecture, counter-anions used and solvent conditions [22]. The Cu(II) complexes $[Cu([18]aneO_2S_4)][ClO_4]_2$ [40] and $[Cu([9]aneOS_2)_2][BF_4]_2$ [34] are octahedral coordinating to all the macrocyclic donors. Cu(I) is relatively softer and its complexes, such as $[Cu([18]aneO_2S_4)][ClO_4]$, tend to be tetrahedral coordinating to only the sulfur donor atoms [40]. Other Cu(I) oxa-thia macrocycle complexes gave mono-, di- and polymeric coordination compounds dependant on the ring size [41] [42] [43]. Silver complexes display an extensive range in coordination numbers and conformations due to there not being an energetic driving force to a particular geometry in a d^{10} species and hence factors such as steric-influences become more pronounced, and from the substantial focus the metal cation has received with oxa-thia macrocycles [22]. Notable examples are the sulfur-bridged chain polymer $\infty[Ag([15]aneO_3S_2)][PF_6]$ (Figure 1.8) [44] which is also a rare example of *endodentate* coordination of $[15]aneO_3S_2$, and the related complexes $[Ag([18]aneO_2S_4)][PF_6]$ and $[Ag([18]aneO_2S_4)][PF_6]_2$ [45]. The former was electrochemically oxidised to the latter (Ag(I) to Ag(II)) giving rise to a highly unusual structure (Figure 1.9) with a 4+2+2 coordination sphere, the Ag(II) sits square planar to the four S-donors, the O-donors are directional to the metal but folded away mutually *cis* and there are long contacts to a κ^2-PF_6 group.

Gold has three reasonably accessible oxidation states and all three form complexes with [9]aneOS$_2$. Au(I) adopts a distorted tetrahedral AuS$_4$ core with the O donors not interacting, Au(II) and Au(III) instead form square planar AuS$_4$ cores with long Au–O contacts [46]. The stability of the complexes are significantly different between the three oxidation states. In [{AuCl}$_2$([18]aneO$_4$S$_2$)] the Au(I) is linear coordinating to only the S donors and forms a discrete dimer [47].

Group 12 has relatively few examples; only one zinc complex is known [Zn([18]aneO$_4$S$_2$)(H$_2$O)$_3$)][ClO$_4$]$_2$. The zinc(II) is octahedral coordinating to three aquo ligands and an O$_2$S donor set from the macrocycle [12]. Complexes with cadmium, [Cd([18]aneO$_2$S$_4$)][ClO$_4$]$_2$ and [Cd([9]aneOS$_2$)$_2$][ClO$_4$]$_2$ are octahedral [48]. [Cd(NO$_3$)([18]aneO$_4$S$_2$)][Cd(NO$_3$)$_4$], [Cd(ClO$_4$)$_2$([18]aneO$_4$S$_2$)] show distorted geometries and higher coordination numbers seven (O$_5$S$_2$) and eight (O$_6$S$_2$) respectively [12]. Hg(II) tends to form complexes with oxa-thia macrocycles *via* the softer donors only, adopting distorted tetrahedral environments [48] . In certain cases where the macrocyclic framework adopts an appropriate conformation the ether donors also interact [49].

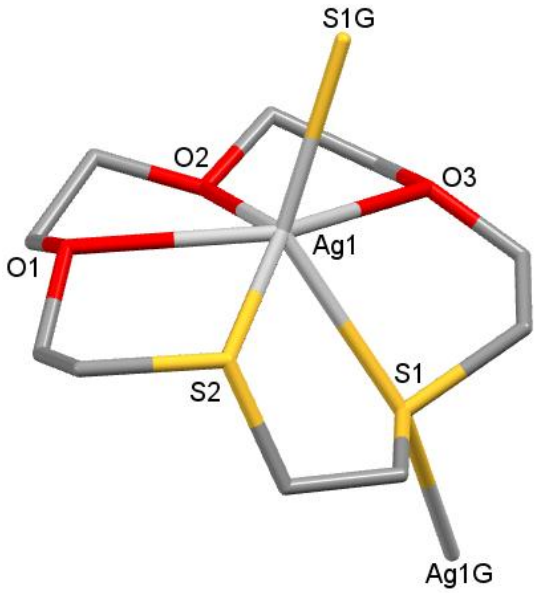

Figure 1.8 Structure of the cation in ∞[Ag([15]aneO$_3$S$_2$)][PF$_6$]. H atoms are omitted for clarity. S1G and Ag1G refer to the sequential donor/acceptor atoms in the chain polymer. [44].

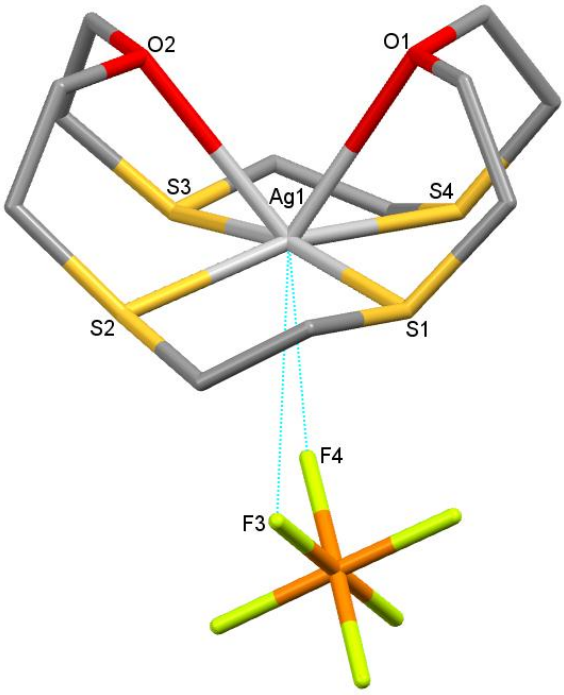

Figure 1.9 Structure showing the coordination environment around the metal centre in [Ag([18]aneO$_2$S$_4$)][PF$_6$]$_2$. H atoms are omitted for clarity [45].

The preferential coordination to the sulfur donors observed by the low valent metals of Groups 9-12 is expected and readily predictable by HSAB theory [11]. It would follow that coordination complexes of the earlier transition metals (Groups 4-6) would see a shift in the donor preferences

towards the harder O-donors as the metals become more electropositive and highly charged.

Spectroscopic data (UV-visible and ^{1}H NMR spectroscopy) on the orange-yellow complex [$TiCl_4$([15]aneO_3S_2)] showed the macrocycle bound κ^2 *via* the thioether donors rather than the ether oxygens [14]. Ti(IV) is a hard oxophilic centre that should have a distinctive preference for harder Lewis bases such as OR_2.

The unexpected nature of [$TiCl_4$([15]aneO_3S_2)] can be explained by the extensive comparative studies done on VCl_3 and $CrCl_3$ with crown ethers (12-crown-4, 15-crown-5 and 18-crown-6), thiacrown ([12]aneS_4) and the oxa-thia crowns ([9]aneOS_2, [15]aneO_3S_2 and [18]aneO_3S_3) [13 50 51 52 53]. The range of octahedral complexes obtained had interesting differences, the crown ether complexes were easily hydrolysed, dissociating an O-donor to form a metal-aquo bond whereas, surprisingly, the thiacrowns were more stable towards moisture. In the mixed donor macrocyclic systems, again the preference was for the sulfur donor over the ether oxygens even on these hard, oxophilic centres. Structural authentication of some of the complexes allowed examination of the $-OCH_2CH_2O-$ and $-SCH_2CH_2S-$ linked chelate rings. The shorter M-O distances resulted in considerable ring strain in the octahedral complexes, the longer M-S instead helped to alleviate this strain by having less acute chelate angles [13]. The behaviour of the Group 5, 6 and, presumably, 4, 1st row metals highlight that a lot of factors contribute to the observed coordination chemistry, not just HSAB theory. These recent examples hint at a much broader chemistry available for hard Lewis acids with soft Lewis bases than previously thought.

1.3 Characterisation Techniques

The compounds to be discussed in the majority of cases are novel and importantly represent the first examples of their kind. The general application of the following methods has been fundamental to the authentication and in-depth analysis of these complexes.

1.3.1 Single Crystal X-ray crystallography

The most powerful technique for unambiguously authenticating the macrocyclic complexes formed as part of this study is single crystal X-ray crystallography. Macrocyclic chemistry has developed largely during the era of efficient computerised crystallographic analysis and is a routine technique for the determination of macrocyclic structures [54].

Determining the structure of macrocyclic coordination compounds has been the best way to confirm the 'incompatible' interactions between soft Lewis bases and hard Lewis acids (and *vice versa*) [22]. Further to this, full structural analyses have allowed the identification of trends and comparisons in bond distances and angles as well as investigating the different macrocyclic conformations present.

Despite its advantages, the technique is limited by the necessity for growing suitable single crystals for the X-ray experiment, which for certain systems can either be very difficult or impossible. That being said, alongside improvements in diffraction technology, metal complexes which contain heavy atoms such as Sn, Sb, I, Pb etc. diffract strongly and smaller crystals can give good data sets in these systems. Good data sets generally have an R_{int} (internal residual factor) of <0.1.

The most serious challenge in crystallographic analysis of macrocyclic complexes is molecular disorder which can be commonly present in these systems [54]. This is a consequence of the ring-like structure (even in puckered rings), where more than one ring orientation has a packing energy minimum. This can lead to high residual factors such as R and R_w (weighted R-factor). It is these factors which offer an indication to the quality of the solution, low values of <0.1 are indicative of a good solution.

Other less general crystallographic problems are discussed on a case by case basis in the relevant chapters.

1.3.2 NMR spectroscopy

^{1}H NMR spectroscopy was used extensively in these studies to examine the behaviour of the coordinated macrocycles in solution. In certain cases variable temperature studies were conducted to allow observation of the dynamic processes occurring.

^{13}C NMR spectroscopy was only used in the positive identification of the 'free' macrocycles.

^{19}F and ^{31}P NMR spectroscopy [55] allowed obervation of the solution behaviour of the few fluoride, tetrafluoroborate and hexafluorophosphate complexes which were investigated. In kinetically labile systems the speciation may differ significantly between the solid and solution phases.

^{19}F{^{1}H} NMR spectroscopy has identified coordinated tetrafluoroborate in kinetically inert tetrafluoroborate organometallic complexes such as [CpFe(C_6H_8)(FBF_3)] and[$CpM(CO)_2(L)(FBF_3)$] (M= W or Mo; L= CO, PPh_3 or $P(OPh)_3$). The spectroscopic features are a doublet around δ= -150 and a quartet around δ= -370 which corresponds to M***F***BF_3 (CD_2Cl_2, 193 K); at elevated temperatures or in stronger donating solvents only free $[BF_4]^-$ was observed [56 57].

^{77}Se and ^{125}Te NMR [58] spectroscopy were useful when investigating the selenoether and telluroether compounds. Typical selenoethers have δ(^{77}Se) 0-~500 ppm and telluroethers δ(^{125}Te) 0-~800 ppm. The free macrocycles had distinctive chemical shifts for the respective nuclei. Obtaining a spectrum of the complexes depended on how dynamic the exchange processes were for the complexes in solution. In general coordination to a metal results in an increase of δ(E) (E= ^{77}Se or ^{125}Te), although exceptions to this exist such as in [$CpW(CO)_3(P(Se)Ph_2)$] and [$Cp_2M(SePh_2)_2$] (M= Ti, Zr or Hf); the former is due to the formation of a three-membered M–P–Se ring and the latter due to a greater diamagnetic circulation on the bulkier metal atoms [59 60]. The shifts observed in the present study were useful for further identifying coordination of the soft chalcogenoether donors.

^{45}Sc NMR spectroscopy [61] was a powerful spectroscopic technique in understanding the scandium macrocycle complexes synthesised.

The NMR active nucleus is one of the most sensitive nuclei (0.3 relative to ^{1}H) with only a modest quadrupole moment coupled with it being 100% abundant makes spectra relatively easy to obtain [61] [62]. Problems can arise through line broadening. In general the more concentrated a solution the greater the linewidth observed [61]. Other factors include, the labile nature of Sc(III) complexes in solution which can also broaden the signals observed.

The ^{45}Sc nucleus is very sensitive to the ligand donor environment. Studies on scandium(III) complexes with monodentate O- and N- donor ligands show the latter give a more enhanced high frequency shift [62]. The effect has also been investigated for the different scandium(III) halides, $[ScF_6]^{3-}$, $[ScCl_6]^{3-}$ and $[ScBr_6]^{3-}$ which have chemical shifts δ= 2.3, 249 and 288 respectively.

The coordination environment also has an effect on the relative line broadening and in extreme cases where there is a large electric field gradient around the metal centre no signal may be observed. An example of the correlation in chemical shift due to the coordination environment and line broadening due to an increasing electric field gradient can be seen in a series of $[ScX_2(Ph_3PO)_4][X]$ (X= Cl, Br or I) complexes, (see Table 1.1) [63].

Table 1.1 ^{45}Sc NMR spectroscopic data for scandium(III) halides with triphenylphosphine oxide [63]

Complex [63]	δ (^{45}Sc)	$W_{1/2}$ (Hz)
$[ScCl_2(Ph_3PO)_4][Cl]$	75	850
$[ScBr_2(Ph_3PO)_4][Br]$	108	4500
$[ScI_2(Ph_3PO)_4][I]$	~200	~20000

Another difficulty with Sc(III) chemistry is its very high sensitivity to moisture and hence there has to be no doubt in the integrity of both the

sample and the deuterated solvents used, $[ScCl_3(H_2O)_3]$ is easily recognisable as it has a chemical shift of $\delta(^{45}Sc)$= ~152.

To date the major focus has been on hard donors to Sc(III), and as yet there are few data on the effect of soft donors to Sc(III), although recently published data give values of $\delta(^{45}Sc)$= ~220-260 with fairly broad line widths for a S_2NCl_3 coordination environment in $[ScCl_3(R\text{-}SNS)]$ (R= ^{t}Bu, decyl) [64]. The relevant macrocyclic Sc(III) complexes are discussed in Chapter 4.

The techniques of ^{119}Sn and ^{207}Pb NMR spectroscopy [65] were only used in characterising the starting Lewis acidic reagents ($M(BF_4)_2$ and $M(PF_6)_2$; M= Sn or Pb).

One of the biggest influencing factors on $\delta(^{119}Sn)$ is coordination number. There is a stepwise shielding increase of ~150 ppm per addition of donor atoms to the metal centre from 4 to 6 with a subsequent addition of a 7th donor leading to an increase of ~100 ppm. This is important in tin systems which can autoassociate, such as the formation of halide-bridges, which will also have temperature and concentration-dependant chemical shifts [66] [67] [68]. Lead compounds have been less studied but are likely to exhibit the same behaviour but with larger $\delta(^{207}Pb)$.

Table 1.2 Magnetic properties of relevant NMR active nuclei [62].

Nucleus	Spin	Abundance	Ξ (MHz)	Q (m^2)	Receptivity (relative to ^{13}C)
^{19}F	1/2	100.00%	94.1	-	4716
^{31}P	1/2	100.00%	40.5	-	37.7
^{77}Se	1/2	7.63%	19.1	-	2.98
^{125}Te	1/2	7.07%	31.5	-	12.5
^{45}Sc	7/2	100.00%	24.5	-0.22×10^{-28}	1780
^{119}Sn	1/2	8.56%	37.3	-	25.2
^{207}Pb	1/2	22.1%	20.9	-	11.7

1.3.3 IR Spectroscopy

Infrared (IR) spectroscopy proved useful in confirming the presence of various functional groups present in the counter anions used in this study, it has also positively characterised metal chloride bonds when they have been a constituent of the complexes.

Discussed are also examples where the technique allowed us to distinguish the nature of the anion in the respective complexes (in the solid state). Unresolved splitting and broadening of the $[NO_3]^-$, $[PF_6]^-$ and $[BF_4]^-$ vibrational bands allowed us to infer coordination of these anions to the metal as opposed to their anionic uncoordinated state. By coordinating to metal centres, IR active ligands can undergo a lowering of their stretching frequencies (from the free ligand). In general this is due to a weakening of the intra-ligand bonds and a strengthening of the metal to ligand bond. Other factors can include packing or H-bonding interactions which will also have an effect on the stretching frequencies. Coordination to a heteroleptic metal complex also lowers the symmetry of

the newly coordinated ligand and hence it will cause its vibrations to undergo splitting. If these are properly resolved then the coordination mode for the ligand can be identified [69].

The other important role of IR was to monitor and identify the level of hydration of the complexes. Ingress of water, partial-hydrolysis and solvolytic effects (incorporation of THF or MeCN) were easily identified in the IR spectrum of the isolated solids.

1.3.4 Mass spectrometry

The technique was used solely in the identification of the synthesised macrocycles. The complexes in this study in general do not survive the sampling conditions required by the technique, the macrocycle readily dissociating from the metal.

1.3.5 Conductivity studies

In this thesus acetonitrile was the medium of choice for obtaining and analysing the coordination complexes.

Acetonitrile has some favourable properties as a solvent for conductance studies in that it has a low viscosity and high dielectric constant ($0.325\ g^{-1}\ sec^{-1}$, 36.2), although it has a relatively high coordinating power which can interfere with studies *via* dissociative and solvolytic effects. Nevertheless, acknowledgment of these issues has led to a higher proportion of definitive examples and acceptable conductance ranges are shown in Table 1.3.

Table 1.3 Conductivity ranges for common electrolyte ratios in MeCN [70]

Electrolyte Ratio	Λ_M ($ohm^{-1}\ cm^2\ mol^{-1}$)
1:1	120-160
2:1	220-300
3:1	340-420

A final note, the ranges above are obtained by not including remarkably high or low results for various complexes. Other factors lead to conductivity results outside the ranges given above [70].

1.4 Aims

The underlying aim of this project is to investigate highly "incompatible" Lewis acid and Lewis base interactions. In doing this, the extents of HSAB theory will be further evaluated and thus allow for a greater understanding of the limits within coordination chemistry.

To accomplish this aim, a family of macrocycles containing both soft and hard Lewis base Group 16 donors will allow for competitive coordination studies to be conducted on Lewis acids from the s-, d- and p-block.

Due to the academic nature of the project, other novel and interesting phenomena will be encountered and investigated in parallel.

- Optimisation of macrocycle syntheses.
- The importance of considering lattice energies in accessing coordination complexes.
- The unusual coordination behaviours for the weakly coordinating fluoroanions $[BF_4]^-$ and $[PF_6]^-$.
- The susceptibility of the saturated macrocycles to undergo ring-opening in the presence of certain Lewis acids.
- The effect co-ligands can have on the Lewis acidity of a metal centre.

1.5 References

1. P. L. Arnold, A. F. Pecharman and J. B. Love, *Angew. Chem. Int. Ed.*, 2011, **50**, 9456

2. B. T. Kilbourn, J. D. Dunitz, L. A. R. Pioda and W. Simon, *J. Mol. Biol.*, 1967, **30**, 559

3. R. R. Eady, *Chem. Rev.*, 1996, **96**, 3013

4. D. K. Cabbiness and D. W. Margerum, *J. Am. Chem. Soc.*, 1969, **91**, 2

5. D. H. Busch, K. Farmery, V. Goedken, V. Katovic, A. C. Melnyk, C. R. Sperati and N. Tokel, *Adv. Chem. Ser.*, 1971, 44

6. R. M. Clay, M. Micheloni, P. Paoletti and W. V. Steele, *J. Am. Chem. Soc.*, 1979, **101**, 4119

7. E. Stephen, A. J. Blake, E. S. Davies, J. McMaster and M. Schroder, *Chem. Commun.*, 2008, 5707

8. A. J. Doheny and B. Ganem, *J. Chem. Educ.*, 1980, **57**, 308

9. E. Stephen, A. J. Blake, E. Carter, D. Collison, E. S. Davies, R. Edge, W. Lewis, D. M. Murphy, C. Wilson, R. O. Gould, A. J. Holder, J. McMaster and M. Schröder, *Inorg. Chem.*, 2012, **51**, 1450

10. A. J. Blake, J. A. Greig, A. J. Holder, T. I. Hyde, A. Taylor and M. Schröder, *Angew. Chem. Int. Ed. Engl.*, 1990, **29**, 197

11. R. G. Pearson, *C. C./ Eng. Tech. Appl. Sci.*, 1986, 18

12. I.-H. Park, K.-M. Park and S. S. Lee, *Dalton Trans.*, 2010, **39**, 9696-9704.

13. C. D. Beard, L. Carr, M. F. Davis, J. Evans, W. Levason, L. D. Norman, G. Reid and M. Webster, *Eur. J. Inorg. Chem.*, 2006, 4399

14. W. Levason, M. C. Popham, G. Reid and M. Webster, *Dalton Trans.*, 2003, 291

15. L. F. Lindoy, *The Chemistry of Macrocyclic Ligand Complexes*, Cambridge University Press, Cambridge, UK, 1989

16. R. D. Rogers and C. B. Bauer, in *Molecular Recognition: Receptors for Cationic Guests*, ed. G. W. Gokel, Elsevier Science, 1999, vol. 1, pp. 315

17. F. Allen, *Acta Crystallogr. Sect. B*, 2002, **58**, 380

18. M. D. Brown, W. Levason, D. C. Murray, M. C. Popham, G. Reid and M. Webster, *Dalton Trans.*, 2003, 857

19. T. S. Cameron, A. Decken, Evgeny G. Ilyin, Grigori B. Nikiforov and J. Passmore, *Eur. J. Inorg. Chem.*, 2004, 3865

20. S. B. Larson, S. H. Simonsen, J. N. Ramsden and J. J. Lagowski, *Acta Crystallogr. Sect. C*, 1989, **45**, 161

21. A. Nieland, A. Mix, B. Neumann, H.-G. Stammler and N. W. Mitzel, *Dalton Trans.*, 2010, **39**, 6753

22. W. Levason and G. Reid, in *Supramol. Chem.*, John Wiley & Sons, Ltd, 2012

23. W. Levason and G. Reid, in *Comprehensive Coord. Chem. II*, eds. J. A. M. Editors-in-Chief: T. J. Meyer, Pergamon, Oxford, 2003, pp. 399

24. T. Röttgers and W. S. Sheldrick, *Z. Anorg. Allg. Chem.*, 2001, **627**, 1976

25. T. Röttgers and W. S. Sheldrick, *J. Solid State Chem.*, 2000, **152**, 271

26. R. Shannon, *Acta Crystallogr. Sect. A*, 1976, **32**, 751

27. B. Cordero, V. Gomez, A. E. Platero-Prats, M. Reves, J. Echeverria, E. Cremades, F. Barragan and S. Alvarez, *Dalton Trans.*, 2008, 2832

28. M. J. D. Champion, P. Farina, W. Levason and G. Reid, *Dalton Trans.*, 2013, **42**, 13179

29. A. L. Hector, W. Levason, G. Reid, M. Webster and W. Zhang, *Dalton Trans.*, 2011, **40**, 694

30. H. J. Drexler, I. Starke, M. Grotjahn, H. Reinke, E. Kleinpeter and H. J. Holdt, *Z. Naturforsch. B: Chem. Sci.*, 1999, **54**, 799

31. B. Metz, D. Moras and R. Weiss, *J. Inorg. Nucl. Chem.*, 1974, **36**, 785

32. C. R. Lucas, S. Liu and J. N. Bridson, *Can. J. Chem.*, 1995, **73**, 1023

33. G. J. Grant, D. F. Galas, M. W. Jones, K. D. Loveday, W. T. Pennington, G. L. Schimek, C. T. Eagle and D. G. VanDerveer, *Inorg. Chem.*, 1998, **37**, 5299

34. G. J. Grant, M. W. Jones, K. D. Loveday, D. G. VanDerveer, W. T. Pennington, C. T. Eagle and L. F. Mehne, *Inorg. Chim. Acta*, 2000, **300**, 250

35. A. J. Blake, G. Reid and M. Schroder, *J. Chem. Soc., Dalton Trans.*, 1990, 3849

36. C. R. Lucas, W. Liang, D. O. Miller and J. N. Bridson, *Inorg. Chem.*, 1997, **36**, 4508

37. M. J. Hesford, W. Levason, M. L. Matthews and G. Reid, *Dalton Trans.*, 2003, 2852

38. W.-P. Li, X.-F. Liu, H.-S. Xu, Y.-Q. Huang and S.-Z. Hu, *Chin. J. Chem .* 1995, **13**, 47

39. C. Bornet, R. Amardeil, P. Meunier and J. C. Daran, *J. Chem. Soc. Dalton Trans.*, 1999, 1039

40. G. Chaka, A. Kandegedara, M. J. Heeg and D. B. Rorabacher, *Dalton Trans.*, 2007, 449

41. K. M. Park, I. Yoon, J. Seo, J. E. Lee, J. Kim, K. S. Choi, O. S. Jung and S. S. Lee, *Cryst. Growth Des.*, 2005, **5**, 1707

42. M. Jo, J. Seo, M. L. Seo, K. S. Choi, S. K. Cha, L. F. Lindoy and S. S. Lee, *Inorg. Chem.*, 2009, **48**, 8186

43. H. J. Kim, M. R. Song, S. Y. Lee, J. Y. Lee and S. S. Lee, *Eur. J. Inorg. Chem.*, 2008, 3532

44. A. J. Blake, G. Reid and M. Schroder, *J. Chem. Soc. Chem. Comm.*, 1992, 1074

45. D. Huang, A. J. Blake, E. J. L. McInnes, J. McMaster, E. S. Davies, C. Wilson, J. Wolowska and M. Schroder, *Chem. Commun.*, 2008, 1305

46. D. Huang, X. Zhang, E. J. L. McInnes, J. McMaster, A. J. Blake, E. S. Davies, J. Wolowska, C. Wilson and M. Schröder, *Inorg. Chem.*, 2008, **47**, 9919

47. A. A. Dvorkin, E. V. Fesenko, L. I. Budarin, I. A. Simonov and T. I. Malinovskii, *Doklady Akademii Nauk Sssr*, 1990, **311**, 1126

48. G. J. Grant, M. E. Botros, J. S. Hassler, D. E. Janzen, C. A. Grapperhaus, M. G. O'Toole and D. G. VanDerveer, *Polyhedron*, 2008, **27**, 3097

.

49. H. J. Holdt, H. Muller, A. Kelling, H. J. Drexler, T. Muller, T. Schwarze, U. Schilde and I. Starke, *Z. Anorg. Allg. Chem.*, 2006, **632**, 114

50. S. C. Davies, M. C. Durrant, D. L. Hughes, C. Le Floch, S. J. A. Pope, G. Reid, R. L. Richards and J. R. Sanders, *J. Chem. Soc. Dalton Trans.*, 1998, 2191

51. M. C. Durrant, S. C. Davies, D. L. Hughes, C. Le Floch, R. L. Richards, J. R. Sanders, N. R. Champness, S. J. Pope and G. Reid, *Inorg. Chim. Acta*, 1996, **251**, 13

52. G. R. Willey, M. T. Lakin and N. W. Alcock, *J. Chem. Soc. Chem. Comm.*, 1991, 1414

53. S. J. A. Pope, N. R. Champness and G. Reid, *J. Chem. Soc. Dalton Trans.*, 1997, 1639

54. J. C. A. B. S. M. Dobson, *Volume 2: Stereochemical and Stereophysical Behaviour of Macrocycles*, Elsevier, 1987

55. K. Dixon, in *Multinuclear NMR*, ed. J. Mason, Springer US, 1987, ch. 13, pp. 369

56. W. Beck and K. Sunkel, *Chem. Rev.*, 1988, **88**, 1405

57. K. Sunkel, G. Urban and W. Beck, *J. Organomet. Chem.*, 1983, **252**, 187

58. H. C. E. McFarlane and W. McFarlane, in *Multinuclear NMR*, ed. J. Mason, Springer US, 1987, ch. 15, pp. 417

59. W. Malisch, R. Maisch, A. Meyer, D. Greissinger, E. Gross, I. J. Colquhoun and W. McFarlane, *Phosphorus Sulfur*, 1983, **18**, 299

60. P. Granger, B. Gautheron, G. Tainturier and S. Pouly, *Org. Magn. Resonance*, 1984, **22**, 701

61. D. Rehder, in *Multinuclear NMR*, ed. J. Mason, Springer US, 1987, ch. 19, pp. 479

62. E. Mann, *NMR and the Periodic Table*, Academic Press, London, 1978

63. N. J. Hill, W. Levason, M. C. Popham, G. Reid and M. Webster, *Polyhedron*, 2002, **21**, 1579

64. S. A. Bartlett, G. Cibin, A. J. Dent, J. Evans, M. J. Hanton, G. Reid, R. P. Tooze and M. Tromp, *Dalton Trans.*, 2013, **42**, 2213

65. J. Kennedy and W. McFarlane, in *Multinuclear NMR*, ed. J. Mason, Springer US, 1987, ch. 11, pp. 305

66. P. G. Harrison and J. J. Zuckerman, *J. Am. Chem. Soc.*, 1969, **91**, 6885

67. J. Otera, T. Hinoishi and R. Okawara, *J. Organomet. Chem.*, 1980, **202**, 93

68. J. D. Kennedy, P. J. Smith, R. F. M. White and L. Smith, *J. Chem. Soc. Perkin Trans. 2*, 1973, 1785

69. K. Nakamoto, in *Handbook of Vibrational Spectroscopy*, John Wiley & Sons, Ltd, 2006

70. W. J. Geary, *Coord. Chem. Rev.*, 1971, **7**, 81

2. Mixed Donor Chalcogenoether Macrocycle Synthesis

2.1 Introduction

Due to the advantageous attributes macrocycles afford a coordination chemist it is not surprising that their synthesis has been a subject of interest. There are generally two main methods towards the synthesis of macrocycles, direct cyclisation and metal ion template cyclisation. Both methods favour the formation of target macrocycle over inevitable oligomeric by-products.

An example of the positive effect high dilution conditions confer to macrocycle synthesis is in the formation of [14]aneS_4 (Figure 2.1) where the yield is increased from 7.5% [1] to 55% [2] as the reaction dilution is increased.

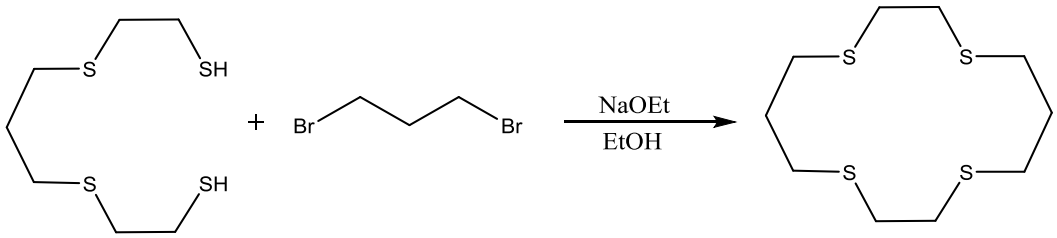

Figure 2.1 Reaction scheme for the synthesis of [14]aneS_4 [1 2].

In a few specific cases high yields (>70%) of macrocyclic product can be obtained without the need for high dilution conditions [3], but this is usually due to other factors intrinsic to the molecules being used; when making N_4 macrocycles with Schiff base-nitrogen atoms (Figure 2.2) [4], H-bonds can form between the nitrogen donors. These H-bonds help overcome the repulsion effect of the lone pairs and can even be compared to metal cations with respect to their promoting ring formation and having a stabilising effect once the ring forms.

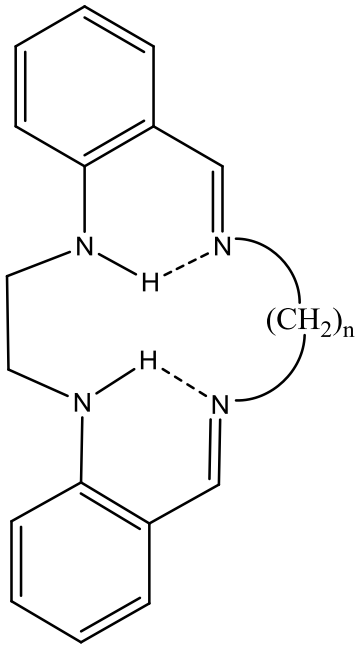

Figure 2.2 N_4 macrocycle with Schiff base-nitrogens showing H-bonding [4].

Metal ion template cyclisation results in the target macrocycles by the judicious choice of a metal centre. The metal coordinates to the reagents and then arranges them in a way favourable to cyclisation *viz* it templates the macrocycle. The metal can also bind preferentially to the cyclic product in a mixture where there is an equilibrium between the reactants and product thereby shifting the equilibrium in favour of the macrocycle. These two processes are known respectively as the kinetic and thermodynamic template effects [5]. Additionally, the metal centre is also capable of activating or masking the effect of functional groups which can also help facilitate macrocycle formation. There are many examples as would be expected from such a bespoke method. A few examples are mentioned, the first (Figure 2.3) shows ring closing condensation at an atom not coordinated to the metal centre. In this case the O atom is initially bound to the Ni(II) centre but dissociates to cyclise with the alkyl bromide 'half-bridge' [6].

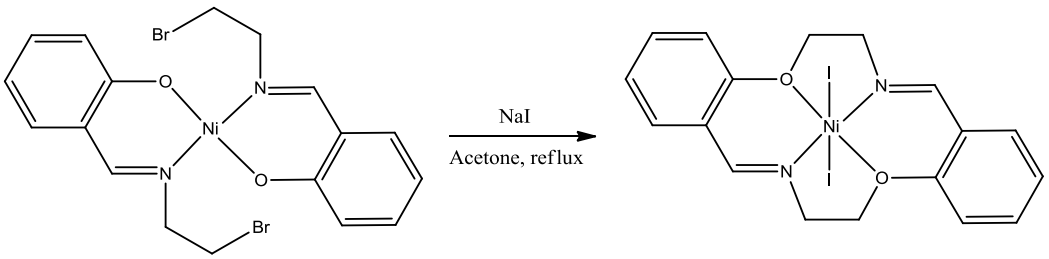

Figure 2.3 Ring closing condensation to form [NiI_2(dibenzo-14-N_2O_2)] [6]

For ring closing condensation reactions at a coordinated donor atom the general requirement is that there has to be a pair of non-bonding electrons in the correct orientation to react with the incoming electrophile; donors not completely bound to the metal cannot be discounted as they may also be involved in the ring closure mechanism [3].

As already mentioned the choice of metal is integral to template formation of macrocycles. Studies by Nelson *et al.* helped illustrate the roles different metal ions play in the template mechanism by using an extensive range of metals from Groups 2,3 and 7-14 exhibiting a range of effective ionic radii, 0.54-1.36 Å (equivalent covalent radii: 1.21-2.15 Å), in the formation of 15-,16- and 17-membered N_5-systems (Figure 2.4) [7]. It is important to note that without the presence of the metal ions only polymeric oils were formed. The initial function of the metal ion is the activation of the carbonyl groups in the starting reagent, 2,6-diacetylpyridine (Figure 2.5) towards nucleophillic attack, which subsequently leads to the ring closure.

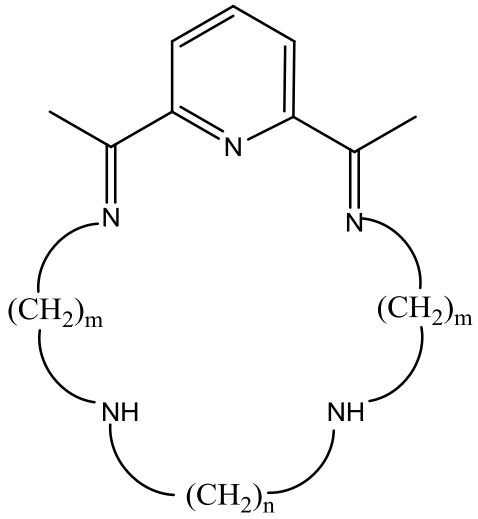

Figure 2.4 N_5 macrocyclic systems (m= 2, 3 n= 3, 2) [7]

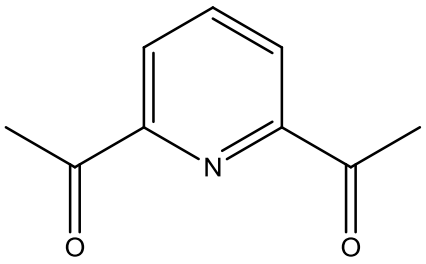

Figure 2.5 2,6-diacetylpyridine

Not all the metal ions were able to template all three N_5-macrocycles, some were only useful for certain ring sizes and some were completely ineffective at templating any of the macrocycles. A major factor was the size of the ion with respect to the hole-size in the target macrocycle, ions with a radius greater than ~0.8 Å (effective ionic radius) were able to template the 17-membered ring whereas the smaller ions were ineffectual; Ni(II) and Cu(II) were not able to act as templates for any of the three N_5-systems. Another factor is that transition metals tend to stabilise more orthogonal coordination geometries, in contrast the N_5-macrocycles are pre-organised for a more pentagonal-planar coordination, as seen in their main group metal complexes. An observation of note was that the relatively small rings were also able to be templated by the larger metal ions, in these cases the metal was positioned out of place in relation to the plane of the ring so that its effective presence was smaller than its true size. Although this set of

studies, amongst others [8], has proven useful in elucidating the template mechanism, new macrocycle synthesis remains difficult and exacting [3].

2.1.1 Mixed Donor Group 16 Macrocycles

The Group 16 donor macrocycles include the well investigated crown and thiacrown ethers e.g. 18-crown-6 (Figure 2.6) and [9]aneS_3 [9 10 11 12]. A sub-set are those that incorporate more than one type of E-donor (E= O, S, Se, Te) [12]. Studies by Frensdorff showed that mixed donor macrocycles were more flexible than their homoleptic analogues in coordinating both hard and soft Lewis acids [13]. In recent years mixed chalcogenoether macrocycles have begun to receive a greater amount of attention [12 14 15].

A series of mixed oxa-thia macrocycles was successfully synthesised in the 70's by Izatt *et al*. using polyether chlorides and thiols under high dilution conditions. The macrocycles synthesised included [18]aneO_4S_2 (Figure 2.7), [18]aneO_2S_4 (Figure 2.8), [15]aneO_3S_2 (Figure 2.10), [9]aneS_2O and were isolated in fairly low yields (Table 2.1) [16 17].

More recently the heavier mixed chalcogenoether macrocycles, [18]aneO_4Se_2 (Figure 2.12) and [18]aneO_4Te_2 (Figure 2.13) have also been synthesised [18].

Due to the reported low isolated yields and resource intensive nature of these high dilution macrocyclisations (in particular the oxa-thia macrocycles), optimising the synthesis of these macrocycles was a key objective to increasing the ease and accessibility towards studying their coordination chemistry. Discussed will be the modifications applied to the methods proposed by Izatt *et al* [16 17].

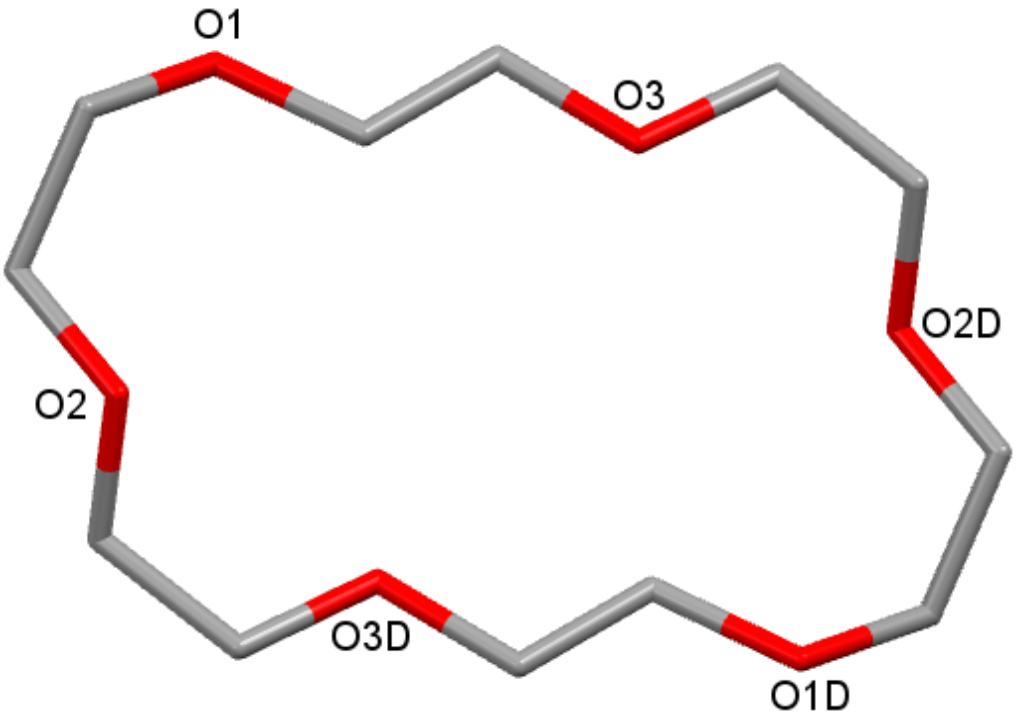

Figure 2.6 Structure of 18-crown-6. H atoms are omitted for clarity [19].

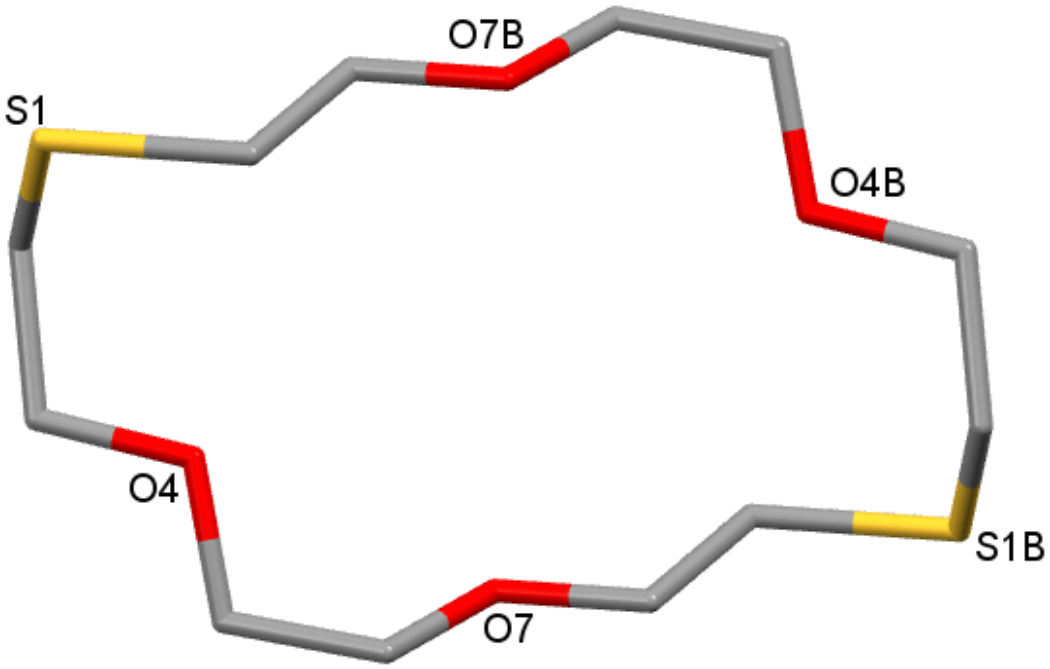

Figure 2.7 Structure of [18]aneO$_4$S$_2$. H atoms are omitted for clarity [20].

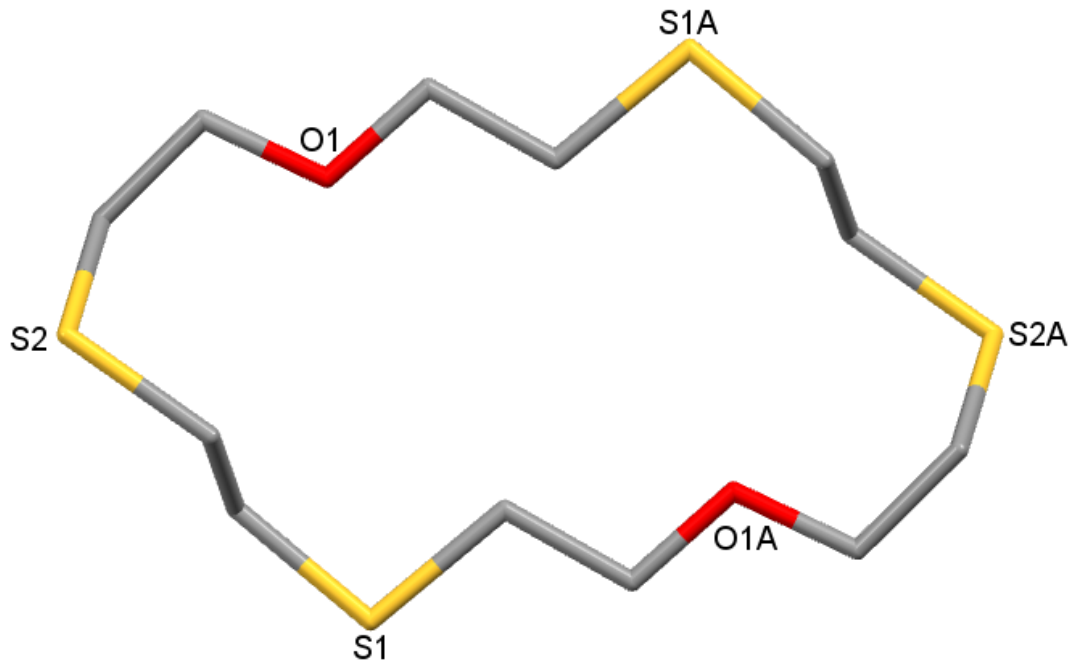

Figure 2.8 Structure of [18]aneO_2S_4. H atoms are omitted for clarity [21].

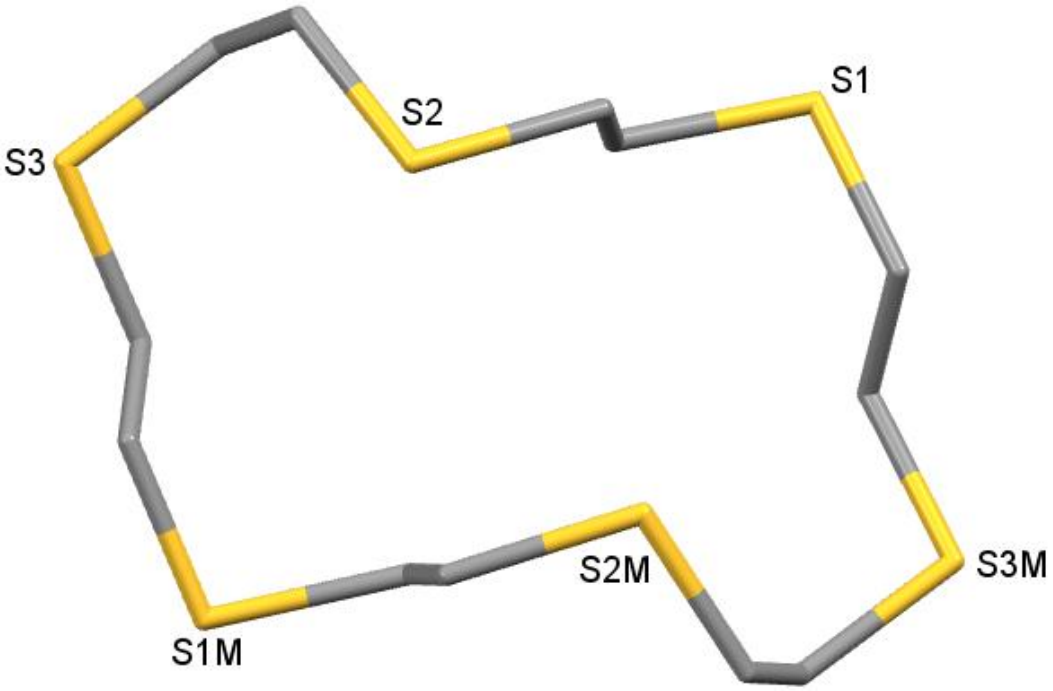

Figure 2.9 Structure of [18]aneS_6. H atoms are omitted for clarity [22].

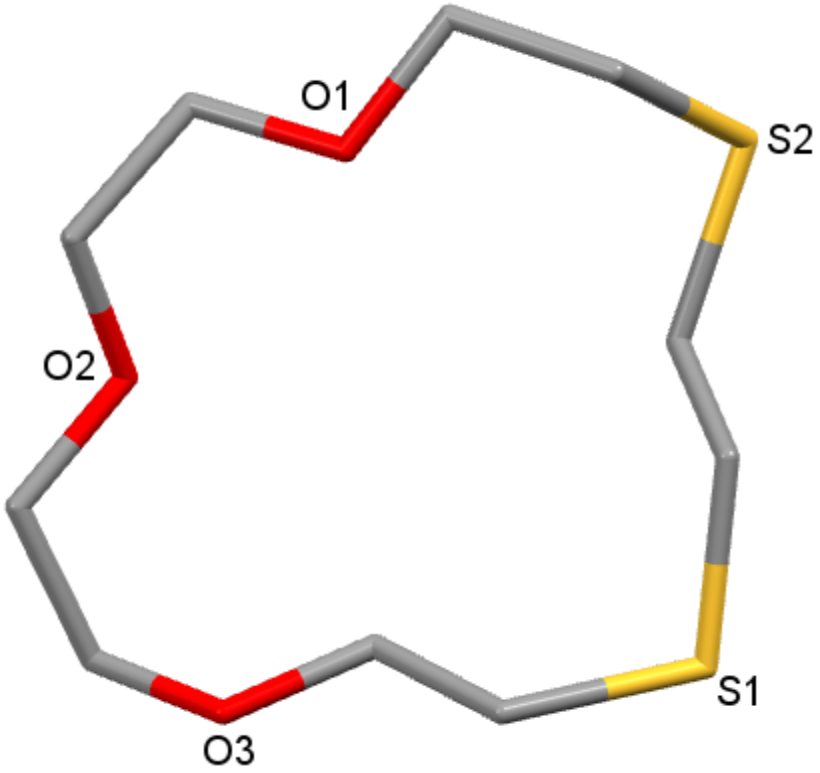

Figure 2.10 Structure of [15]aneO_3S_2. H atoms are omitted for clarity [20].

2.1.2 Ligand preorganisation

Preorganisation of the macrocyclic donors can be used to explain or tentatively predict the geometries observed for metal coordination complexes.

By looking at the crystal structures of the 'free' macrocyclic ligands the positioning and direction of the lone pairs of electrons gives an indication of whether the macrocycle will prefer to coordinate in an *exodentate* or *endodentate* fashion whilst in the idealised ring conformation.

Other factors such as the macrocyclic effect [23] and whether the Lewis acid centre has a strong stereochemical preference [3] will work antagonistically or synergistically with how the macrocycle is preorganised. This can give rise to a greater variety of macrocycle conformations and coordination modes seen for the complexes of a particular macrocyclic ligand.

Regarding the relevant macrocyclic ligands in this study; 18-crown-6 (Figure 2.6) [19] has a centrosymmetric structure with four O-donors pointing into the macrocyclic cavity (preorganised for *endodentate* coordination)

with the other two pointing out (preorganised for *exodentate* coordination).

Similarly [18]aneO_4S_2 (Figure 2.7) [20] has four crown ether moieties preorganised *endo* with two *exo* sulfur donors. The macrocycle is folded in a more sigmoidal fashion to the more planar 18-crown-6, a consequence of having to accommodate the larger sulfur atoms within the ring framework. The comparable preorganisation of [18]aneO_4S_2 to that of 18-crown-6 should result in the oxa-thia macrocycle having as an extensive coordination chemistry as the much more commonplace 18-crown-6.

Increasing the number of sulfur atoms relative to oxygen atoms leads to a switch in the preorganisation of the donors. In [18]aneO_2S_4 (Figure 2.8) [21] there are four donors preorganised *exo* (S_4) and only two *endo* (O_2). The macrocycle has similar s-folding to [18]aneO_4S_2. [18]aneS_6 (Figure 2.9) has the same preorganisation as [18]aneO_2S_4 with two *endo* S-donors replacing the oxygen atoms, and is more folded giving a more concave conformation [22]. The similar preorganisation of [18]aneO_2S_4 and [18]aneS_6 would suggest its coordination behaviour should be more akin to that of the thiacrown.

A point of note is that for medium to large, saturated macrocycles the barrier to conformational change is considered to be relatively small, and hence a greater variety of macrocyclic conformations can be seen, e.g metal complexes of [18]aneO_4S_2.

The smaller macrocycle [15]aneO_3S_2 (Figure 2.10) has three donors *exo* (OS_2) and two *endo* (O_2), one of the sulfur donors in puckered out of the plane of the ring [20].

Although the chemistry of these mixed donor chalcogenoether has begun to be explored more in-depth, the area remains relatively little developed [12]. The majority of reported complexes are with middle to late, low to medium oxidation state d-block metals (see Chapter 1).

2.2 Results and Discussion

The Izatt *et al.* methods for the syntheses of oxa-thia macrocycles use high dilution conditions, reacting thiols and chloro-polyethers in ethanol with stoichiometric amounts of NaOH [16] [17].

The sodium thiolate salt formed by the deprotonation of the thiol is highly sensitive to hydrolysis (reforming the thiol). For this reason all the ethanol solvent used for the high dilution setup was dried prior to use, to diminish this competing reverse reaction. Additionally the macrocyclisations were conducted under a N_2 environment to prevent oxidation of the thiolate to disulfide.

The sodium thiolate reacts with the polar $C^{\delta+}$–$Cl^{\delta-}$ bond eliminating NaCl. Replacing chloride for bromide makes the C–X species more nucleophillic reacting far more readily with the sodium thiolate. The macrocyclisation step is quicker and more efficient.

In the synthesis of [18]aneO_4S_2 the higher excess of NaOH in the ethanol reservoir increases the amount of free Na^+; the metal cation likely has a templating effect. This is consistent with the [2+2] addition macrocycle being favoured in this reaction over the [1+1] product (the 9-membered ring), the other macrocycles with a higher ratio of sulfur donors do not exhibit this effect. In the ESI^+ MS the ion observed for [18]aneO_4E_2 solutions (E= O, S, Se, Te) is the sodium complex.

Excess Na^+ also increases the relative amount of the sodium thiolate.

Other less general modifications are reported in 2.4 Experimental.

A comparison of the substantially elevated yields obtained is presented in Table 2.1. The general reaction scheme for making these oxa-thia macrocycles is shown in Figure 2.11.

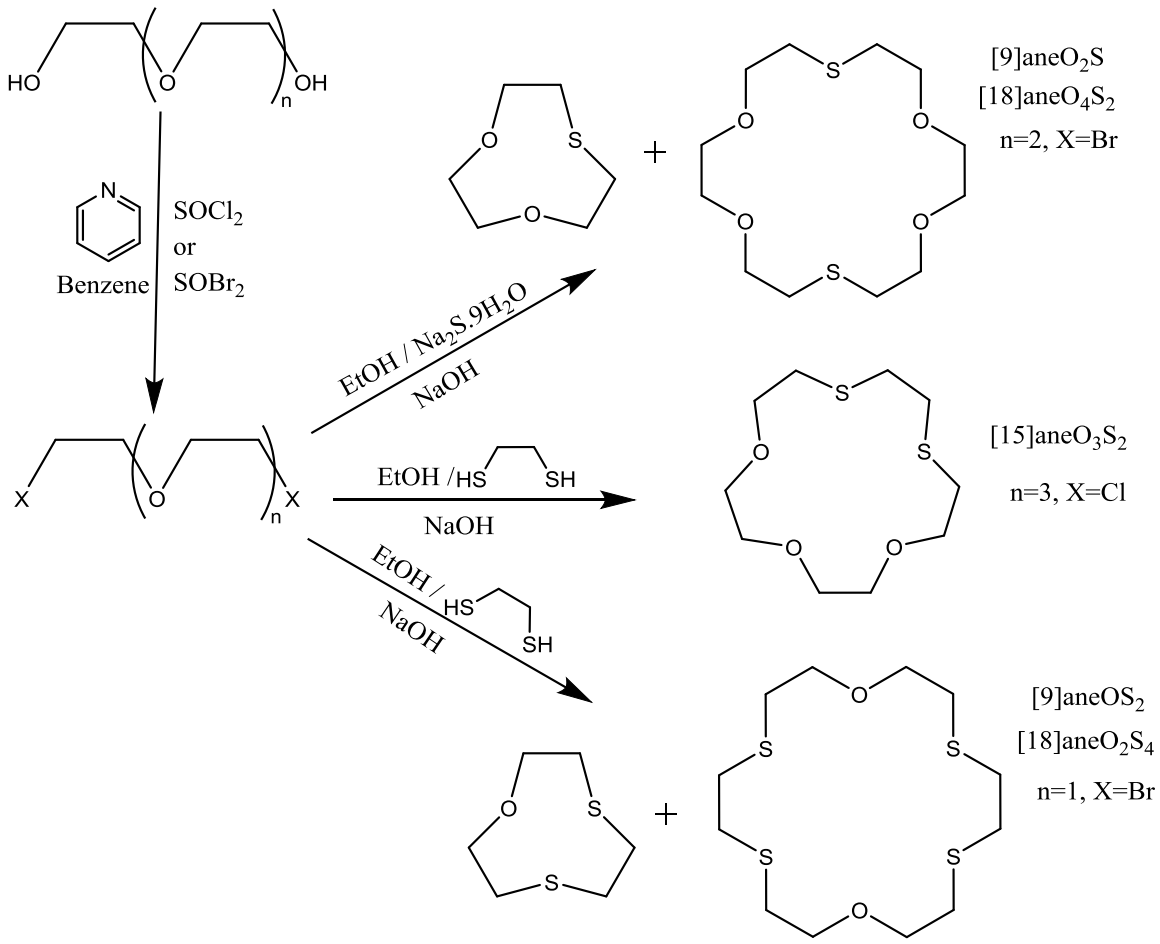

Figure 2.11 Reaction scheme towards oxa-thia macrocycles.

The synthesis of the oxa-selena and oxa-tellura macrocycles [18]aneO_4Se_2 and [18]aneO_4Te_2 were reported more recently [18]. Their synthesis required reduction of elemental selenium or tellurium by sodium in liquid ammonia initially. The crude Na_2E (E= Se, Te) thus formed was then reacted with the polyether chloride under medium dilution conditions.

In this study [18]aneO_4Se_2 (Figure 2.12) was made by reducing Se to Na_2Se, then dissolving it in ethanol and transferring it to an addition funnel to be added and reacted with the respective polyether bromide under high dilution and at equimolar concentrations. An excess of NaOH was also placed in the EtOH reservoir to take advantage of the templating effect. No formation of the small ring was observed ([9]aneO_2Se).

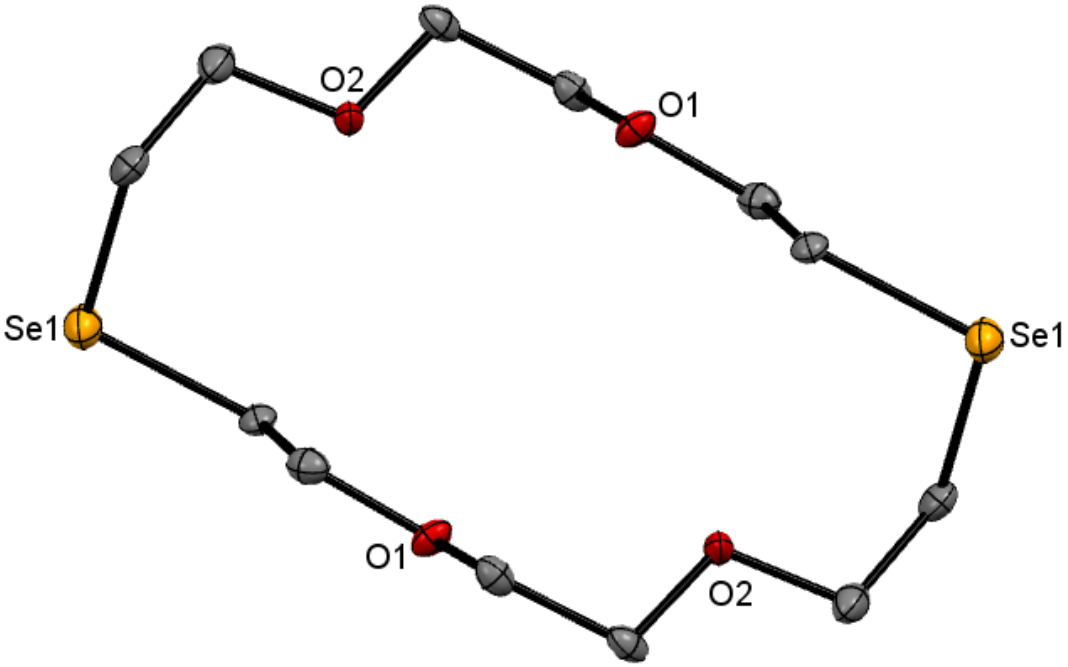

Figure 2.12 Crystal structure of the centrosymmetric [18]anO$_4$Se$_2$ showing the atom numbering scheme. Atomic displacement ellipsoids are drawn at the 50% probability level and hydrogen atoms have been omitted for clarity.
Symmetry operation: a = 1 – x, 1 – y, –z.

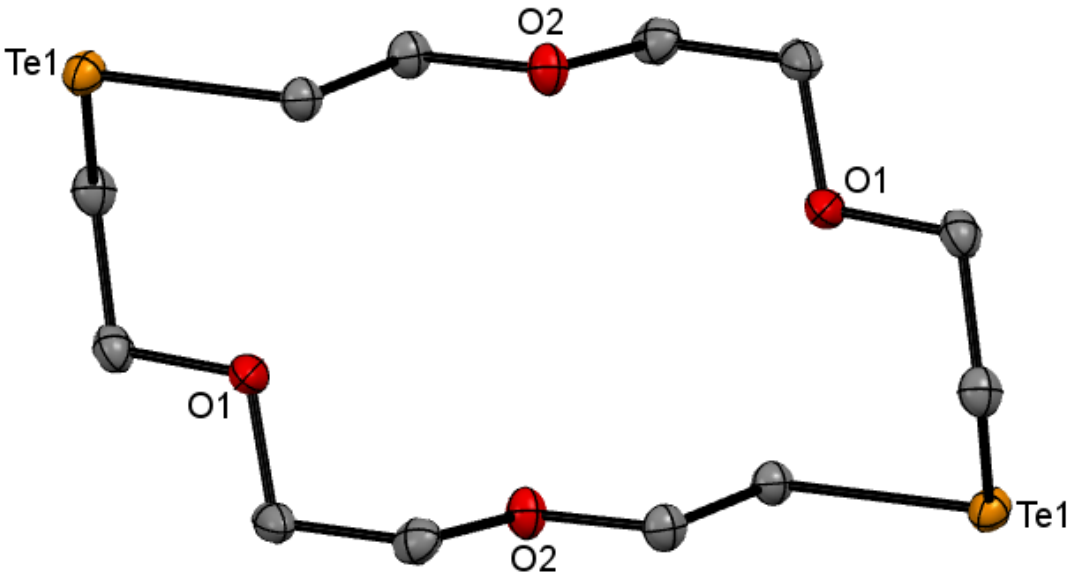

Figure 2.13 Crystal structure of the centrosymmetric [18]anO$_4$Te$_2$ showing the atom numbering scheme. Atomic displacement ellipsoids are drawn at the 50% probability level and hydrogen atoms have been omitted for clarity.
Symmetry operation: a = 2 – x, 1 – y, 1 – z.

The crystal structure of the free ligand was elucidated for the first time. It is isostructural to the structure for [18]aneO$_4$S$_2$ (Figure 2.7). The bulk material isolated was pure; the ^{1}H, ^{13}C and ^{77}Se NMR spectroscopic data was consistent with the measurements reported.

The reaction with Na$_2$Te and bis(2-bromoethoxy)ethane was performed under medium dilution conditions. This gave an orange powder that was identified by ^{125}Te{^{1}H} NMR spectroscopy as the small ring ([9]aneO$_2$Te). Little initial evidence for the larger ring was seen although attempts to get a crystal of the small ring only crystallised [18]aneO$_4$Te$_2$ (Figure 2.13). ^{125}Te{^{1}H} NMR spectroscopy on the recrystallised solid still showed predominantly the small ring and ESI$^+$ MS showed both ring species present. A possible explanation is the weak C–Te bond which could lead to an interconversion between the two ring species. Using the bromide over the chloride reagent seems to preferentially form the [1+1] addition product, Na$_2$Te and the C$^{\delta+}$–Br$^{\delta-}$ bond are very reactive and probably undergo the macrocyclisation rapidly. The Na$^+$ templating effect is also diminished due to the lower affinity of the tellurium for the alkali metal cation (see Chapter 3).

It was essential to store these macrocyclic telluroethers under nitrogen and at 5°C as the weak C–Te bond was prone to decomposition in the presence of oxygen and at room temperature.

The crystal structure of [18]aneO$_4$Te$_2$ was determined for comparison with the Se and S analogies. It has a similar centrosymmetric structure to [18]aneO$_4$E$_2$ (E= S, Se).

The [2+2] addition product [18]aneO$_4$Te$_2$ was obtained exclusively by following the original preparation and using bis(2-chloroethoxy)ethane. The reduction step was held at reflux (-33°C) until all the Te (black) had been consumed. The spectroscopic data on the bulk material was consistent from the reported values.

Only one structurally authenticated complex of [18]aneO$_4$Se$_2$ was known before the complexes reported in this study, [PtCl$_2$([18]aneO$_4$Se$_2$)]. Similarly [18]aneO$_4$Te$_2$ had only been coordinated to PdCl$_2$ or PtCl$_2$ [18]. In all three complexes the Lewis acid coordinates exclusively *via* both the soft donors (Se or Te).

Table 2.1 Comparison of macrocycle yields [16] [17] [18].

Macrocycle	Literature	This work
[9]aneO$_2$S	5%	15%
[9]aneOS$_2$	6%	41%
[9]aneO$_2$Te	4%	*37%
[15]aneO$_3$S$_2$	27%	*17%
[18]aneO$_4$S$_2$	12%	23%
[18]aneO$_2$S$_4$	4%	13%
[18]aneO$_4$Se$_2$	18%	26%
[18]aneO$_4$Te$_2$	54%	92%

* See discussion

Although a lower yield is reported for [15]aneO$_3$S$_2$ the product was isolated as a mass of large clear crystals at room temperature. The literature preparation reported it as a viscous oil.

2.3 Conclusions

Significant improvements to the original methods synthesising mixed chalcogenoether macrocycles have been developed. This has helped enable subsequent studies of their coordination chemistry by making larger quantities available for study.

The crystal structures for [18]aneO_4Se_2 and [18]aneO_4Te_2 have been determined for the first time.

2.4 Experimental

2.4.1 1,4,7-dioxathiacyclononane ([9]aneO$_2$S) and 1,4,10,13-tetraoxa-7,16-dithiacyclooctadecane ([18]aneO$_4$S$_2$):

In two separate graduated addition funnels, ethanolic solutions (2 x 300 mL) of 1,2 bis(2-bromoethoxy)ethane (33.10 g, 0.121 mol) and ground $Na_2S.9H_2O$ (28.80 g, 0.120 mol) were placed. They were added dropwise to a stirring reservoir of NaOH (2.00 g, 0.055 mol) in dry ethanol (700mL) over 24 h. The yellow/orange mixture was neutralised using HCl in water (100mL). The ethanol was boiled away. The organic components were extracted using diethyl ether (2 x 200mL) and dried over $MgSO_4$. The ether was removed leaving behind a white solid and an off-colour oil. The oil and solid were separated *via* Buchner filtration and subsequent washings of cold hexane. The oil was distilled under vacuum (80°C/0.05 mmHg) giving the smaller ring. Yield: 2.60 g, 15 %. ^{1}H NMR ($CDCl_3$, 293 K): δ 2.80 (t, [4H], SC***H***$_2$), 3.60 (s, [4H], OC***H***$_2$), 3.89 (t, [4H], SCH_2C***H***$_2$O). ^{13}C{^{1}H} NMR ($CDCl_3$, 293 K): δ 31.8, 71.3, 74.9.

The larger ring, a white solid. Yield: 4.00 g, 23 %. ^{1}H NMR ($CDCl_3$, 293 K): δ 2.84 (t, [8H], SC***H***$_2$), 3.63 (s, [8H], OC***H***$_2$), 3.72 (t, [8H], SCH_2C***H***$_2$O); (CD_3CN, 293K): δ 2.76 (t, [8H], SC***H***$_2$), 3.55 (s, [8H], OC***H***$_2$), 3.64 (t, [8H], SCH_2C***H***$_2$O). ^{13}C{^{1}H} NMR ($CDCl_3$, 293 K): δ 31.5, 70.5, 72.1.

2.4.2 1,4,7-oxadithiacyclononane ([9]aneOS$_2$) and 1,10-dioxa-4,7,13,16-tetrathiacyclooctadecane ([18]aneO$_2$S$_4$): In two separate graduated addition funnels, ethanolic solutions (2 x 300 mL) of bis(2-bromoethyl)ether (22.30 g, 0.096 mol) and ethane dithiol (8 mL, 0.096 mol), were placed. Dropwise they were added to a stirring reservoir of dry ethanol (350 mL) and NaOH (10.00 g, 0.250 mol). This was done over 24 h, the reservoir became cloudy after 4 h. It was left to stir for an extra day, a substantial amount of white solid deposited. HCl in water (100 mL) was added to neutralise the reaction mixture. The solid was filtered. The ethanol was removed under vacuum leaving behind a clear oil that was taken up in diethyl ether (2 x 100mL). The ethereal fractions were dried over $MgSO_4$ and filtered. The ether was removed and the remaining oil was distilled under vacuum (70˚C/0.05 mmHg) giving the smaller ring. Yield: 6.40 g, 41%. ^{1}H NMR ($CDCl_3$, 293 K): δ 2.64 (t, [4H], SC***H***$_2$CH$_2$O), 2.90 (s, [4H], SC***H***$_2$), 3.78 (t, [4H], OC***H***$_2$). ^{13}C{^{1}H} NMR ($CDCl_3$, 293 K): δ 32.7, 34.6, 73.6.

The solid retained from the filtration was suspended in CH_2Cl_2 and then filtered and dried *in vacuo* leaving behind a large amount of white powder which was recrystallised from chloroform:hexane at 5˚C giving pure large macrocycle. Yield: 2.00 g, 13%. ^{1}H NMR ($CDCl_3$, 293 K): δ 2.76 (t, [8H] SC***H***$_2$CH$_2$O), 2.88 (s, [8H], SC***H***$_2$), 3.69 (t, [8H], OC***H***$_2$). ^{13}C{^{1}H} NMR ($CDCl_3$, 293 K): δ 31.2, 32.5, 72.0.

2.4.3 1,4,7-trioxa-10,13-dithiacyclopentadecane ([15]aneO$_3$S$_2$): In two separate graduated addition funnels, ethanolic solutions (2 x 300 mL) of 1,5 bis(2-chloroethoxy)diethylether (22.30 g, 0.096 mol) and ethane dithiol (8 mL, 0.096 mol) were placed. They were added dropwise to a refluxing reservoir of NaOH (44.50 g, 1.113 mol) in dry ethanol (700 mL). The reaction began to opalesce very quickly. The addition was completed over 16 h and the reaction allowed a further 12 h at reflux. HCl in water (100 mL) was added and the EtOH removed *in vacuo* leaving behind some solid and a yellow oil. Diethyl ether was used to extract the organic residues until no more colour was observed in the ethereal fractions. The combined ether fractions were dried over $MgSO_4$ and after filtering, left under vacuum until the volatiles had been removed. The remaining crude yellow oil was shown to be predominantly the product, the oil was distilled (170°C/0.05 mmHg) using a Kugelrohr leaving a light yellow oil. This oil was left under vacuum and large clear crystals of macrocycle formed. The crystals were filtered and washed with cold hexane. Yield: 4.00 g, 17%. ^{1}H NMR ($CDCl_3$, 293 K): δ 2.72 (t, [4H], SC***H***$_2$CH$_2$O), 2.87 (s, [4H], SC***H***$_2$), 3.65 (s, [8H], OC***H***$_2$), 3.75 (t, [4H], SCH$_2$C***H***$_2$O). ^{13}C{^{1}H} NMR ($CDCl_3$, 293 K): δ 31.7, 33.1, 70.2, 71.3, 72.8.

2.4.4 1,4,10,13-tetraoxa-7,16-diselenacyclooctadecane ([18]aneO$_4$Se$_2$):

Sodium (2.50 g, 0.054 mol) was dissolved in liquid NH_3 (400 mL) and selenium powder (4.29 g, 0.054 mol) added. The suspension was allowed to stir and warm up to room temperature. Upon warming a white solid immediately began to form, the blue colour of the solution persisted. The ammonia was allowed to evaporate off over 18 h, the reaction was maintained under N_2 at all times. The white solid was then taken up in previously dried ethanol (300 mL) and transferred to a graduated dropping funnel. In a separate graduated dropping funnel an ethanolic solution (300 mL) of bis(2-bromoethoxy)ethane (15.00 g, 0.054 mol) was made up. Both solutions were allowed to add simultaneously to a stirring reservoir of dry ethanol (700 mL) and NaOH (4.20 g, 0.105 mol) over 3 d. Colour changes were observed ranging from yellow to orange as the addition rates for the two solutions were equilibrated, the solution going more orange as the Na_2Se solution became more concentrated in the final reaction mixture. After complete addition the reaction was left to stir for a further 2 days. Some precipitate had formed and the solution paled to a light yellow. The mixture was neutralised using HCl in water (200 mL) and then filtered. The ethanol was removed leaving behind a yellow oil. The oil was extracted using CH_2Cl_2 (2 x 200 mL) and dried over $MgSO_4$. The volatiles were removed *in vacuo* and the yellow oil dissolved in the minimum amount of CH_2Cl_2 and layered with hexane. At room temperature a fine white solid formed upon agitation of the two layers, the crystalisation mixture was left at 5°C and large colourless single crystals formed. These were filtered. Subsequent recrystalisations using just the minimum amount of CH_2Cl_2 and placement at 5°C yielded further crops of the pure large ring. Yield: 2.77 g, 26%. ^{1}H NMR ($CDCl_3$, 293 K): δ 2.86 (t, [8H], SeC***H***$_2$), 3.63 (s, [8H], OC***H***$_2$), 3.79 (t, [8H], SeCH$_2$C***H***$_2$O); (CD_3CN, 293 K): δ 2.80 (t, [8H], SeC***H***$_2$), 3.56 (s, [8H], OC***H***$_2$), 3.72 (t, [8H], SeCH$_2$C***H***$_2$O). ^{13}C{^{1}H} NMR ($CDCl_3$, 293

K): δ 22.8, 70.4, 72.5. $^{77}Se\{^{1}H\}$ NMR ($CDCl_3/CH_2Cl_2$, 293 K): δ 143.

2.4.5 1,4,7-dioxatelluracyclononane ([9]aneO_2Te): Sodium (2.14 g, 0.093 mol) was dissolved in liquid NH_3 (500 mL) and left to stir for 15 min, then freshly ground tellurium (5.92 g, 0.046 mol) was added. The suspension was allowed to stir and reflux at -33˚C until all the black tellurium had been converted to white Na_2Te. The ammonia was cooled back down to -78˚C and a THF (150 mL) solution of bis(2-bromoethoxy)ethane (12.80 g, 0.046 mol) added drop wise over 1.5 h. The reaction mixture slowly turned from a blue colour to a deep red and the ammonia was allowed to evaporate off over 16 h. The now murky yellow suspension was hydrolysed with degassed water (200 mL) and the organic residues extracted with degassed CH_2Cl_2 (2 x 100 mL). The fractions were dried over $MgSO_4$ and filtered. Removal of the volatiles under vacuum left an oil and an orange precipitate. A pure orange solid was obtained from multiple crystalisations using diethyl ether and CH_2Cl_2. Yield: 4.20 g, 37%. ^{1}H NMR ($CDCl_3$, 293 K): δ 2.91 (t, [4H], $TeC\boldsymbol{H}_2$), 3.64 (s, [4H], $OC\boldsymbol{H}_2$), 3.89 (t, [4H], $TeCH_2C\boldsymbol{H}_2O$). $^{13}C\{^{1}H\}$ NMR ($CDCl_3$, 293 K): δ 2.0, 70.2, 73.9. $^{125}Te\{^{1}H\}$ NMR ($CDCl_3/CH_2Cl_2$, 293 K): δ 200.

$^{125}Te\{^{1}H\}$ NMR showed only one species corresponding to the small ring, although spurious crystals of the larger ring ([18]aneO_4Te_2) were also found.

2.4.6 1,4,10,13-tetraoxa-7,16-ditelluracyclooctadecane ([18]aneO$_4$Te$_2$):

Sodium (3.40 g, 0.148 mol) was dissolved in liquid NH_3 (500 mL) and left to stir for 15 min, then freshly ground tellurium (8.50 g, 0.067 mol) was added. The suspension was allowed to stir and reflux at -33°C until all the black tellurium had been converted to white Na_2Te. The ammonia was cooled back down to -78°C and a THF (150 mL) solution of bis(2-chloroethoxy)ethane (12.46 g, 0.067 mol) added drop wise over 1.5 h. The reaction mixture slowly turned from blue to mint green and the ammonia was allowed to evaporate off over 16 h, the solution turned to a pale yellow and deposited a white precipitate. The reaction was hydrolysed with degassed water (200 mL) and the organic residues extracted with degassed CH_2Cl_2 (2 x 200 mL). The fractions were dried over $MgSO_4$ and filtered. Removal of the volatiles under vacuum left a crude solid. Pure large ring was obtained by crystalisation from diethyl ether and CH_2Cl_2 at 5°C. Yield: 15.00 g, 92%. ^{1}H NMR ($CDCl_3$, 293 K): δ 2.77 (t, [8H], TeC***H***$_2$), 3.53 (s, [8H], OC***H***$_2$), 3.71 (t, [8H], TeCH$_2$C***H***$_2$O). ^{13}C{^{1}H} NMR (CD_2Cl_2, 293 K): δ 2.9, 70.5, 73.8. ^{125}Te{^{1}H} NMR (CD_2Cl_2/CH_2Cl_2, 293 K): δ 176.

2.5 Structural Data

Compound	[18]aneO$_4$Se$_2$	[18]aneO$_4$Te$_2$
Formula	$C_{12}H_{24}O_4Se_2$	$C_{12}H_{24}O_4Te_2$
mwt.	390.23	487.51
crystal system	Monoclinic	Triclinic
space group	$P2_1/n$ (14)	P-1 (2)
a (Å)	6.933(4)	4.772(2)
b (Å)	13.419(7)	7.805(4)
c (Å)	8.573(4)	11.515(6)
α (°)	90	76.008(5)
β (°)	102.489(7)	86.854(6)
γ (°)	90	79.925(6)
U (Å^3)	778.7(7)	409.7(3)
Z	2	1
μ(Mo Kα) (mm^{-1})	4.752	3.564
F(000)	392	232
total no. reflns	7115	3529
unique reflns	1775	3456
R_{int}	0.118	0.0225
no. of params, restraints	82, 0	82, 0
R_1[a] [$I_o > 2\sigma(I_o)$]	0.0349	0.0160
R_1 (all data)	0.084	0.0170
wR_2[a] [$I_o > 2\sigma(I_o)$]	0.055	0.0384
wR_2(all data)	0.059	0.0388

[a] $R_1 = \Sigma||F_o| - |F_c||/\Sigma|F_o|$. $wR_2 = [\Sigma w(F_o^2 - F_c^2)^2/\Sigma wF_o^4]^{1/2}$

Common items: temperature = 100K; wavelength (Mo Kα)= 0.71073 Å; θ_{max}= 7.5°

2.6 References

1. W. Rosen and D. H. Busch, *J. Am. Chem. Soc.*, 1969, **91**, 4

2. K. Travis and D. H. Busch, *Inorg. Chem.*, 1974, **13**, 2591

3. L. F. Lindoy, *The Chemistry of Macrocyclic Ligand Complexes*, Cambridge University Press, Cambridge, UK, 1989

4. P. G. Owston, R. Peters, E. Ramsammy, P. A. Tasker and J. Trotter, *J. Chem. Soc. Chem. Comm.*, 1980, 1218

5. M. C. Thompson and D. H. Busch, *J. Am. Chem. Soc.*, 1964, **86**, 6

6. R. W. Kluiber and G. Sasso, *Inorg. Chim. Acta*, 1970, **4**, 4

7. S. M. Nelson, *Pure Appl. Chem.*, 1980, **52**, 2461

8. M. G. B. Drew, F. S. Esho and S. M. Nelson, *J. Chem. Soc. Dalton Trans.*, 1983, 1653

9. P. C. Junk and J. W. Steed, *J. Coord. Chem.*, 2007, **60**, 1017

10. R. D. Rogers and C. B. Bauer, in *Molecular Recognition: Receptors for Cationic Guests*, ed. G. W. Gokel, Elsevier Science, 1999, vol. 1, pp. 315

11. W. Levason and G. Reid, in *Comprehensive Coord. Chem. II*, eds. J. A. M. Editors-in-Chief: T. J. Meyer, Pergamon, Oxford, 2003, pp. 399

12. W. Levason and G. Reid, in *Supramol. Chem.*, John Wiley & Sons, Ltd, 2012

13. Frensdor.Hk, *J. Am. Chem. Soc.*, 1971, **93**, 600

14. I.H. Park, K.M. Park and S. S. Lee, *Dalton Trans.*, 2010, **39**, 9696

15. M. Ciampolini, C. Mealli and N. Nardi, *J. Chem. Soc. Dalton Trans.*, 1980, 376

16. J. S. Bradshaw, J. Y. Hui, Y. Chan, B. L. Haymore, R. M. Izatt and J. J. Christensen, *J. Heterocycl. Chem.*, 1974, **11**, 45

17. J. S. Bradshaw, J. Y. Hui, B. L. Haymore, J. J. Christensen and R. M. Izatt, *J. Heterocycl. Chem.*, 1973, **10**, 1

18. M. J. Hesford, W. Levason, M. L. Matthews and G. Reid, *Dalton Trans.*, 2003, 2852

19. E. Maverick, P. Seiler, W. B. Schweizer and J. D. Dunitz, *Acta Crystallogr. Sect. B*, 1980, **36**, 615

20. A. J. Blake, C. Radek and M. Schroder, *Acta Crystallogr. Sect. C: Cryst. Struct. Commun.*, 1995, **51**, 2668

21. G. J. Grant, D. F. Galas, M. W. Jones, K. D. Loveday, W. T. Pennington, G. L. Schimek, C. T. Eagle and D. G. VanDerveer, *Inorg. Chem.*, 1998, **37**, 5299

22. J. R. Hartman, R. E. Wolf, B. M. Foxman and S. R. Cooper, *J. Am. Chem. Soc.*, 1983, **105**, 131

23. D. K. Cabbiness and D. W. Margerum, *J. Am. Chem. Soc.*, 1969, **91**, 2.

3. Mixed Chalcogenoether Donor Macrocyclic Complexes of Divalent Calcium and Strontium

3.1 Introduction

Both calcium and strontium form part of the alkaline earth group. Calcium is the 5th most abundant element found in the Earth's crust (3.4% wt. abundance), and is a biologically essential metal [1]. $CaCO_3$ is the major constituent of shells and corals, likewise calcium phosphate (in the form of apatite) makes up a large component of mammalian bone [2]. Ca^{2+} is also important in signal transduction in living systems [3]. In terms of society, calcium salts have seen major roles as engineering materials throughout history, marble/limestone ($CaCO_3$), construction-cements ($Ca(OH)_2$, $CaSO_4$) and glasses/fluxes (CaO, CaF_2) [1]. Strontium has seen applications in medicine, Sr^{2+} acts much like Ca^{2+} *in vivo*, and therefore it has been used in many bone related therapeutics. The radiopharmaceutical $^{89}SrCl_2$ is used in metastatic bone cancers and the complex strontium ranelate is a registered treatment for osteoporosis [4] [5]. ^{90}Sr, another radioisotope of strontium, is used in radiotherapy for surface cancers and tumours [6]. The radio-toxicity of ^{90}Sr coupled with its wide distribution due to nuclear weaponry and isolated incidents such as Chernobyl have led to concerted efforts to develop extraction procedures based upon crown ether derivatives [7] [8].

Calcium has a covalent radius of 1.76 Å and a Pauling electronegativity of 1.00. Strontium is a heavier analogue in Group 2 and has a covalent radius of 1.95 Å and a Pauling electronegativity of 0.95 [9] . The chemistry of the heavier Group 2 M^{2+} ions (Ca, Sr, Ba) has been dominated by their halide or oxo-anion salts. The different strengths of the largely electrostatic interactions with anions or hard ligands such as water are put down to the increasing ionic radii down the group (decreasing charge/radius ratio) [7]. The known coordination chemistry of calcium and strontium is limited receiving less study than that of the alkali metals [10]. The ligands tend to be exclusively hard oxygen donors

such as β-diketonates, alkoxides, crown ethers, as well as water featuring many hydrated salts. A range of less stable N-donor adducts has also been developed in amide, diamine, diimine and acetonitrile complexes [11].

Recent interest in the coordination chemistry of Group 2 dications, in particular Ca^{2+}, stem from its cheapness and relatively ubiquitous availability; Ca(II) is "biocompatible" expressing a low toxicity and is easy to convert into limestone ($CaCO_3$) or slaked lime ($Ca(OH)_2$) for disposal, making it attractive for developing 'green' catalysts and in the production of biodegradable polymers or those for medical applications [10 12]. Recently, calcium alkoxide catalysts have been used in the polymerisation of lactides or ε-caprolactone towards making medicinal biopolymers [13]. Further to this, organocalcium reagents have been shown to catalyse many other industrially important processes such as hydrogenation, hydroamination, hydrosilylation, hydrophosphination and alkene polymerisation [12]. As already stated, this area of chemistry is little developed and would benefit from further study of the coordinative flexibility of Ca(II) complexes and of their structures.

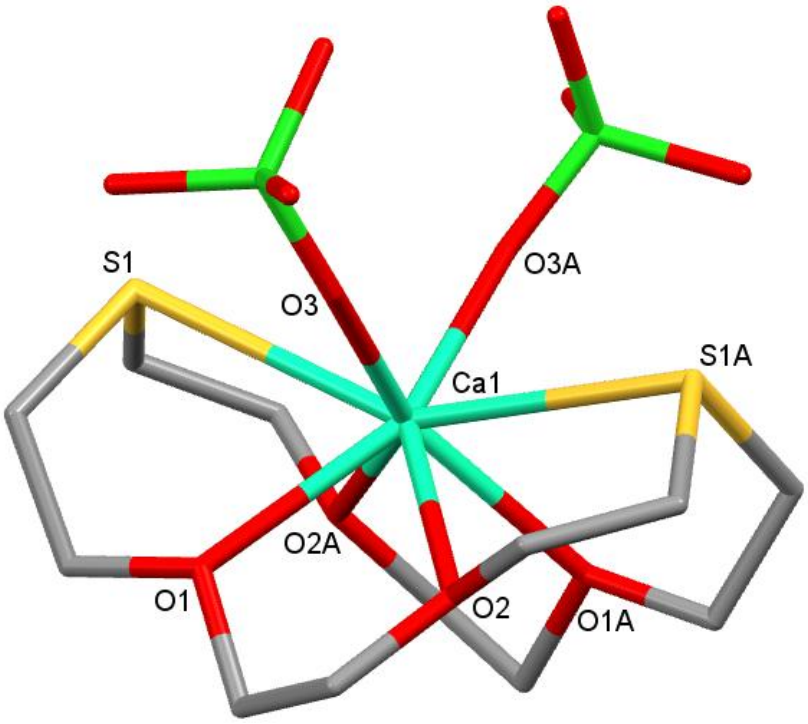

Figure 3.1 Structure of $[Ca(ClO_4)_2([18]aneO_4S_2)]$. H atoms omitted for clarity. [14]

Macrocycles are an incredibly versatile ligand archetype [15] [16] [17]. Recently an oxa-thia macrocycle complex of Ca(II) has been isolated, $[Ca(ClO_4)_2([18]aneO_4S_2)]$ (Figure 3.1) [14]. It exhibits unexpected soft S-donor coordination to the hard Ca(II) centre. The only other examples of Group 16 donors with Ca(II) or Sr(II) are very water and oxygen sensitive compounds with anionic chalcogenolates (ER^-, E= S, Se, Te) [11].

3.2 Results and Discussion

3.2.1 Ca(II) coordination chemistry

The chemistry of Ca^{2+} with soft donors has been considered limited and highly 'incompatible' and this attitude has been based substantially on the qualitative principles proposed by Pearson's HSAB Theory [18]. With these concerns in mind a few Ca(II) 18-crown-6 complexes were investigated initially to help guide the synthetic conditions necessary for thioether and selenoether coordination; 18-crown-6 being directly analogous to the mixed donor chalcogenoether macrocycles focussed on in this study.

Using the halide abstractor $SbCl_5$ to solubilise poorly soluble metal halides and thereby providing an entry into the metal's coordination chemistry has previously been a successful strategy, examples being the formation of the Pb(II) complex [PbCl(18-crown-6)][$SbCl_6$] (see Chapter 5), accessing Sc(III) crown ether complexes (see Chapter 4) and within Group 2 for accessing alkaline earth phosphine oxide coordination compounds [19] [20] [21].

The reaction between $CaCl_2$, $SbCl_5$ and 18-crown-6 in acetonitrile gives the ionic complex [Ca(18-crown-6)$(MeCN)_2$][$SbCl_6$]$_2$ (Figure 3.2). The Ca(II) cation lies in the plane of the crown, coordinated to all six O-donors and two acetonitrile groups giving a coordination number of 8. The two MeCN groups are arranged *trans* to each other and the macrocycle is appreciably buckled, two hexachloroantimonate(V) anions provide charge balance.

The spectroscopic measurements are all in agreement with the crystal structure. The IR band at 341 cm^{-1} is indicative of the presence of $[SbCl_6]^-$, two bands at 2302 and 2274 cm^{-1} correspond to coordinated MeCN and peaks associated with the macrocycle are all seen in the IR spectrum. The ^1H NMR spectrum showed a broadened resonance for MeCN and a singlet substantially shifted from free ligand showing coordinated 18-crown-6.

Using freshly distilled $SbCl_5$ as a halide abstractor proved a successful approach in accessing the coordination chemistry of Ca(II)

crown ethers. The analogous reactions with the oxa-thia macrocycles [18]aneO_4S_2 and [15]aneO_3S_2 did not result in the desired complexes, instead redox chemistry with the reduction of Sb(V) to Sb(III) proceeded, resulting in the latter coordinating to the oxa-thia macrocycles preferentially, (leading to the results discussed in Chapter 7; see also Chapter 4).

Renewed efforts in finding alternative Ca(II) precursors led to the use of calcium(II) triflate which has an appreciable solubility in acetonitrile (the medium of choice for accessing the complexes in this study). Experiments with both 18-crown-6 and [18]aneO_4S_2 were attempted, proving successful.

[$Ca(CF_3SO_3)_2$(18-crown-6)(H_2O)] (Figure 3.3) differs from the previous Ca(II) crown complex, it is 9-coordinate and neutral with the κ^1-triflate anions coordinated mutually *cis*. The Ca(II) ion is again bound *endocyclic* to all the macrocycle donors, the macrocycle folds away slightly from the bulkier triflate groups and a water molecule *trans* to the coordinated $[CF_3SO_3]^-$ anions completes the primary coordination sphere.

Both the IR and ^{1}H NMR spectra showed evidence for coordinated water, especially with a sharpening of the OH stretching vibration at 3479 cm^{-1} relative to free water. The crown C***H***$_2$ protons are shifted by 0.4 ppm to high frequency from the free ligand. All other expected spectroscopic markers were also present and consistent with the stated formulation. The unintended ingress of water highlights one of the major synthetic challenges with exploring the coordination chemistry of soft chalcogenoethers in this area of the periodic table. Ca(II) has a much higher affinity for hard Lewis bases and thus competition from water and other protic/strongly donating solvents can severely hinder the formation of thio- and selenoether complexes [10]. Maintaining rigorously anhydrous conditions was a priority.

The complex [$Ca(CF_3SO_3)_2$([18]aneO_4S_2)] (Figure 3.6) will be discussed later.

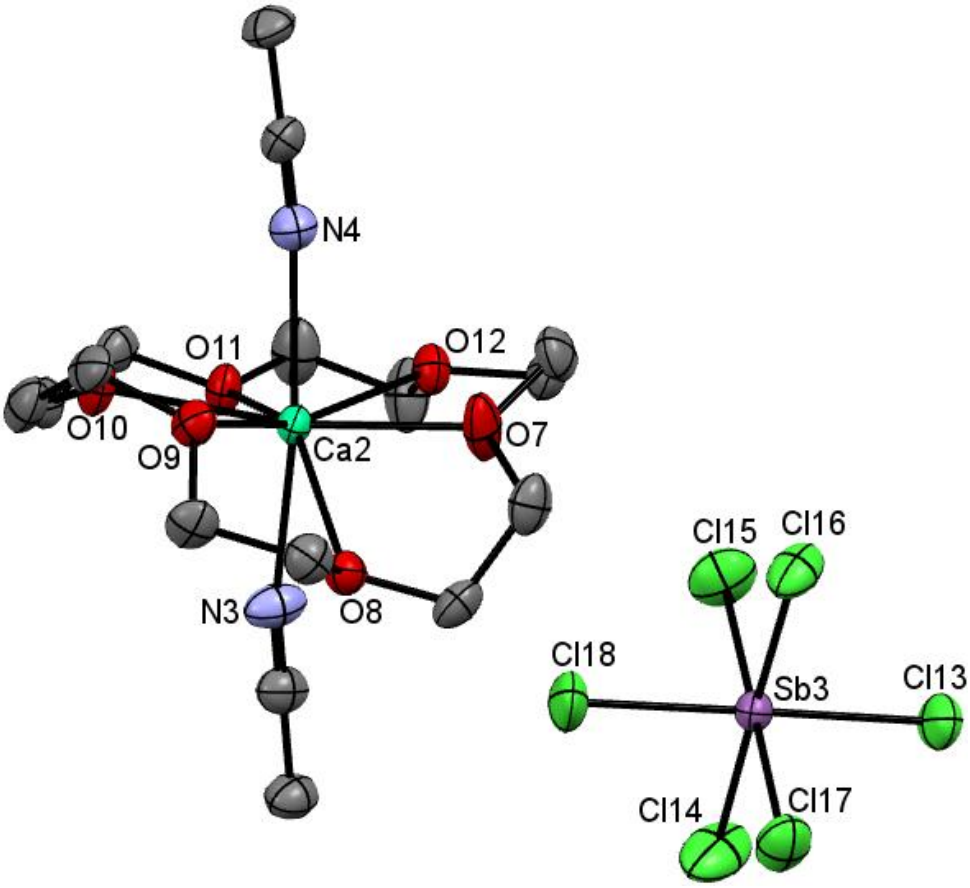

Figure 3.2 Crystal structure of the crystallographically independent Ca2 centred cation and Sb3 centred anion in $[Ca(18\text{-crown-6})(MeCN)_2][SbCl_6]_2$ showing the atom numbering scheme. Ellipsoids are drawn at the 50% probability level and H atoms are omitted for clarity.

Table 3.1 Selected bond lengths (Å) and angles (°) for $[Ca(18\text{-crown-6})(MeCN)_2][SbCl_6]_2$

Ca2–O7	2.418(5)	N3–Ca2–N4	165.7(2)
Ca2–O8	2.560(5)	O7–Ca2–O8	63.7(2)
Ca2–O9	2.498(5)	O8–Ca2–O9	63.3(2)
Ca2–O10	2.472(5)	O9–Ca2–O10	65.7(2)
Ca2–O11	2.504(4)	O10–Ca2–O11	63.6(2)
Ca2–O12	2.483(6)	O11–Ca2–O12	63.6(2)
Ca2–N3	2.473(7)	O12–Ca2–O7	64.5(2)
Ca2–N4	2.472(7)		

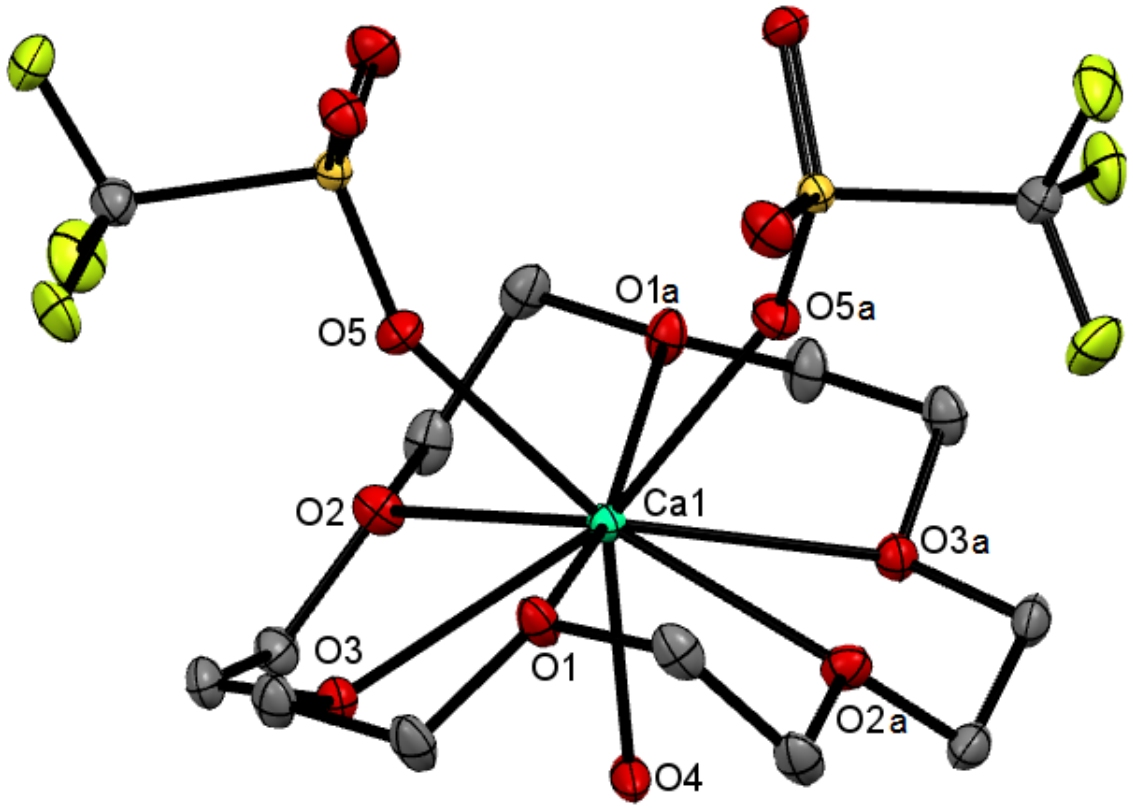

Figure 3.3 Crystal structure of [Ca(CF_3SO_3)$_2$(18-crown-6)(H_2O)] showing the atom numbering scheme. Ellipsoids are drawn at the 50% probability level and H atoms are omitted for clarity. Symmetry operation: a = – x, y, 1/2 – z.

Table 3.2 Selected bond lengths (Å) and angles (°) for [Ca(CF_3SO_3)$_2$(18-crown-6)(H_2O)]

Ca1–O1	2.5551)	O1–Ca1–O2	63.59(4)
Ca1–O2	2.647(2)	O1–Ca1–O3	61.01(4)
Ca1–O3	2.657(1)	O2–Ca1–O3	63.12(4)
Ca1–O4	2.348(2)	O4–Ca1–O5	139.75(5)
Ca1–O5	2.392(1)	O5–Ca1–O5a	80.50(4)
O4a···O6	2.804(2)		

Parallel investigations using $CaCl_2$ as a synthon resulted in the complex $[CaCl_2(18\text{-crown-6})]$ (Figure 3.4). $CaCl_2$ is insoluble in acetonitrile and therefore does not present itself as an immediate choice as a precursor to the coordination complexes in this study. Nevertheless crown ethers and macrocycles in general have shown to be useful in aiding the dissolution of various insoluble metal salts due in part to the macrocyclic effect.

A similar situation was observed by suspending $CaCl_2$ in hot acetonitrile for 9 d in the presence of 18-crown-6. The crown was able to sequester molecular calcium(II) chloride as the adduct $[CaCl_2(18\text{-crown-6})]$. The reaction did not go to completion, highlighting the strong lattice energy associated with $CaCl_2$ (2271 kJ mol^{-1}) [22]. Using the much more strongly donating solvent methanol (to completely dissolve the metal chloride) provided a more reliable method towards obtaining large quantities of the product.

Spectroscopically the large colourless crystals obtained analyse as the anhydrous complex. The IR spectrum has absorptions due to the crown and a single νCa–Cl 272 cm^{-1} which is consistent with *trans* chlorides. The ^1H NMR shows a high frequency shift from the free ligand (+0.35 ppm). Examination of the crystal structure (Figure 3.4) shows clear rotational disorder of the macrocycle, all the atoms are still identifiable but a detailed comparison of the bond distances is precluded. The Ca(II) centre sits within the plane of the macrocycle and the two chlorides are bound *trans* across the metal, in accordance with the IR data, giving 8-coordinate Ca(II).

Despite the high lattice energy associated with $CaCl_2$, 18-crown-6 was still able to overcome this energy barrier (in acetonitrile) and form the adduct $[CaCl_2(18\text{-crown-6})]$. The analogous reactions with the oxa-thia crowns [18]aneO_4S_2 and [15]aneO_3S_2 resulted in white powders (again the reactions did not go to completion leaving behind large amounts of unreacted starting material), but analysis of the isolated solids showed no evidence for there being any macrocycle present, instead the results from the elemental analysis showed a high percentage of N content. Although alkaline earth chloride adducts of acetonitrile have not yet been identified, the heavier halides have been structurally characterised $[Mg(MeCN)_6][MgBr_4]$, $[CaBr_2(MeCN)_2]_\infty$, $[MI_2(MeCN)_5]$ etc. (M= Ca, Sr) [23]. It is

highly likely that the white powders obtained could be products of the type $CaCl_2 \cdot n$MeCN. With respect to accessing soft chalcogenoether coordination to $CaCl_2$, the oxa-thia macrocycles proved unable to overcome the energy requirements in breaking the metal chloride salt lattice and form the desired complexes.

To further test this observation calcium(II) chloride was replaced by calcium(II) iodide. The iodide is soluble in acetonitrile (the pentakis-acetonitrile solvate being already known [23]) and importantly has a lower associated lattice energy ($CaCl_2$ 2271 kJ mol^{-1} *vs.* CaI_2 ~2087 kJ mol^{-1}) [22]. CaI_2 would prove to be the reagent of choice and a resultant series of calcium(II) iodide adducts with both oxa-thia and oxa-selena crowns were successfully synthesised.

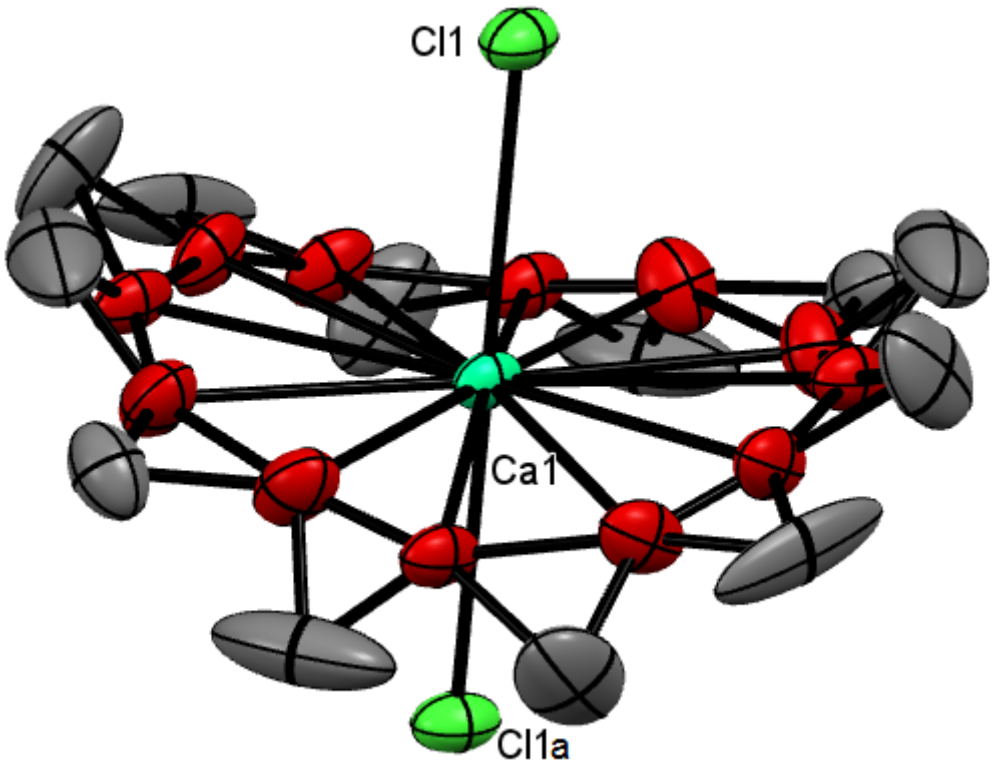

Figure 3.4 Disordered structure of [$CaCl_2$(18-crown-6)], showing the rotational disorder of the macrocycle and *trans* chlorides.

A fourth route attempted was the metathesis of $CaCl_2$ to $Ca(PF_6)_2$ by thallium(I) hexafluorophosphate with the macrocycle *in situ*, (a two-step reaction proved ineffective). The isolated solids were extremely moisture sensitive and difficult to handle. Crystals obtained from the reactions with 18-crown-6 and [18]aneO_4S_2 readily decomposed even when handled

using Fomblin™ and under a stream of N_2, resultantly the reactions were abandoned.

Due to the limited spectroscopic techniques available for positively analysing the Group II complexes, single crystal X-ray diffraction analysis remains the most powerful and key characterisation technique for proving the formation of these complexes without reasonable doubt.

The reaction between CaI_2 and [18]aneO_4S_2 in acetonitrile gave a white solid with all the spectroscopic measurements expected for the target complex [CaI_2([18]aneO_4S_2)]. Both the IR and ^{1}H NMR spectra confirmed the product was anhydrous. Examination of the resonances showed all three ligand environments substantially shifted to high frequency from the free ligand, the C***H***$_2$ groups adjacent to the oxygen donors experienced the most pronounced shifts (+0.33 and 0.24 ppm) compared to the protons associated to the thioether (+0.16 ppm). This is as expected, the O-donors being coordinated more strongly over the softer S-donors in the macrocycle to the hard Ca(II) centre. Attempts to grow crystals suitable for an X-ray analysis only resulted in poor, small and weakly diffracting crystals that precluded a complete structure analysis. Data collected from one such crystal (Figure 3.5), clearly showed the macrocycle beginning to encapsulate the metal centre in a folded conformation, with *cis*-iodo ligands and hexadentate coordination of all the macrocycle donors.

Further attempts to obtain better quality crystals (cooling a CH_2Cl_2 solution in the freezer) resulted in the same mass of inferior crystals of the parent complex as well as a few larger and well-formed crystals which were subsequently identified as the dihydrate [Ca([18]aneO_4S_2)$(H_2O)_2$][I]$_2$ (Figure 3.7).

The complex [Ca$(CF_3SO_3)_2$([18]aneO_4S_2)] was successfully made, albeit in a low yield, by reacting Ca$(CF_3SO_3)_2$ and [18]aneO_4S_2 in acetonitrile. Like the iodide analogue, both the IR spectrum and ^{1}H NMR spectrum confirmed the solid was anhydrous and the expected spectroscopic features were present.

Crystals readily grew from the filtrate obtained. The crystals had the titular composition and were of sufficient quality to allow a full structural analysis (Figure 3.6). The structure has a discrete 8-coordinate Ca(II) centre,

with all the macrocycle donors coordinated and the two triflate groups bound mutually *cis*. This arrangement closely matches that of the partial structure in $[CaI_2([18]aneO_4S_2)]$ and the literature complex $[Ca(ClO_4)_2([18]aneO_4S_2)]$ (Figure 3.1) [14]. The ionic complex $[Ca([18]aneO_4S_2)(H_2O)_2][I]_2$ (Figure 3.7) also has the same folded conformation of the macrocycle but in this case the two anions have been displaced by two coordinated water ligands which remain *cisoidal*; there are significant H-bonding interactions between the aqua ligands and adjacent iodide anions forming a chain network ($I\cdots O_{water}$ 3.432(6)-3.548(6) Å), (Figure 3.12).

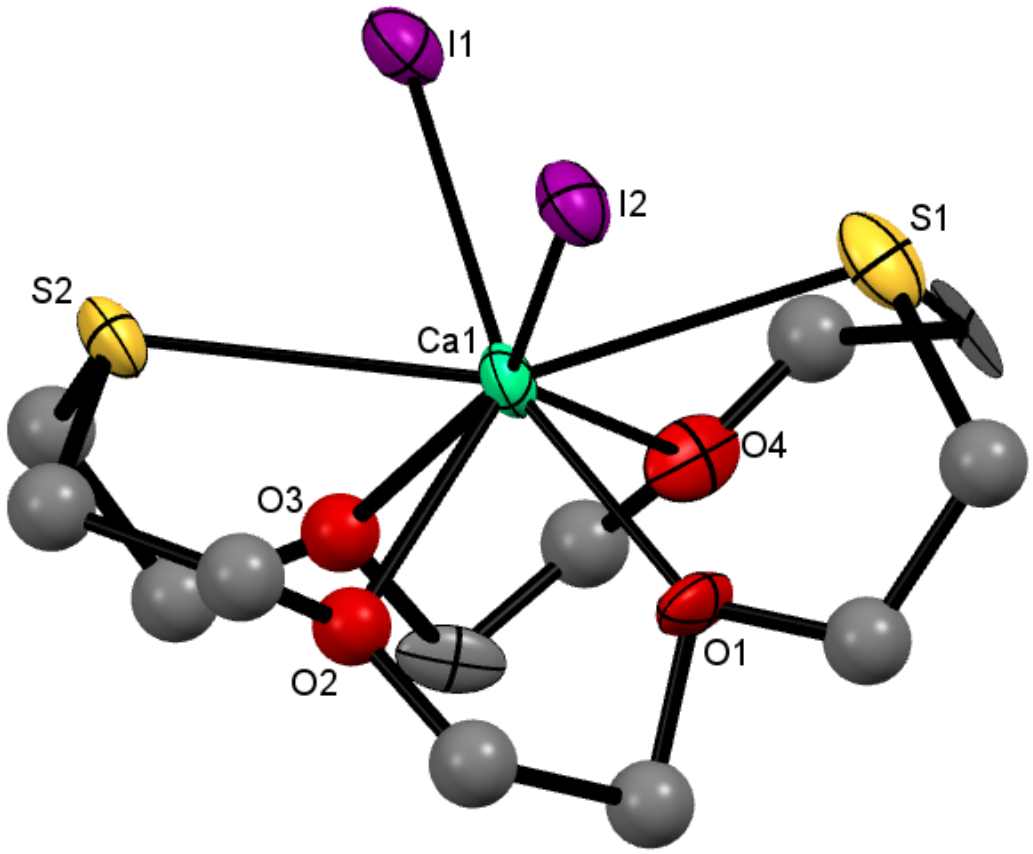

Figure 3.5 Partial structure of $[CaI_2([18]aneO_4S_2)]$.

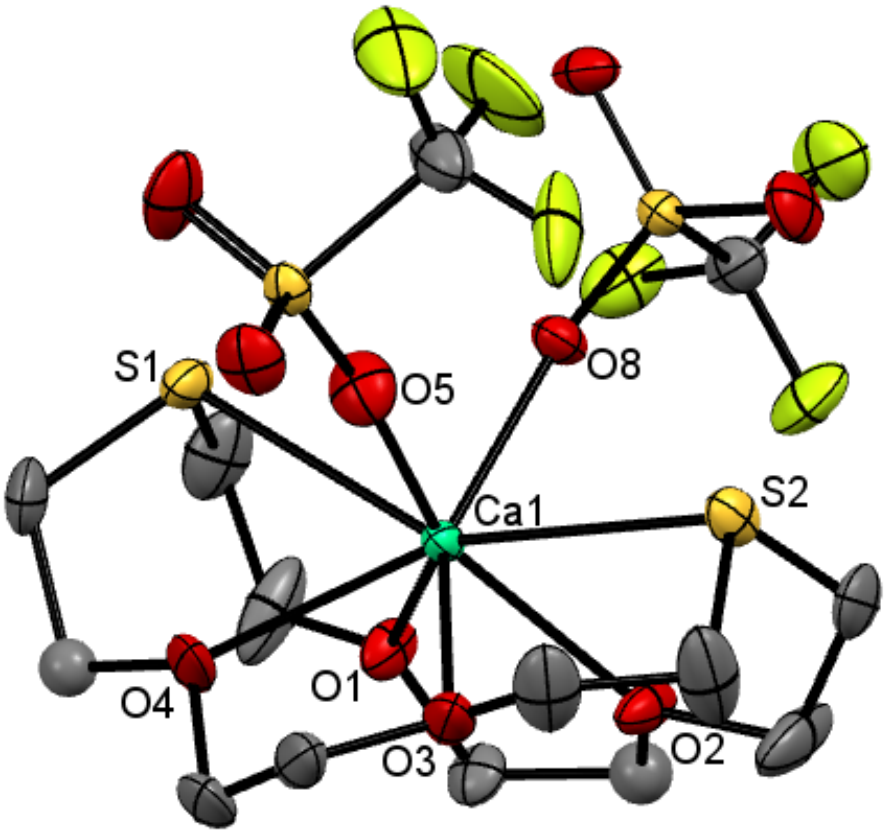

Figure 3.6 Crystal structure of [Ca(CF_3SO_3)$_2$([18]aneO_4S_2)] showing the atom numbering scheme. Ellipsoids are drawn at the 40% probability level and H atoms are omitted for clarity.

Table 3.3 Selected bond lengths (Å) and angles (°) for [Ca(CF_3SO_3)$_2$([18]aneO_4S_2)]

Ca1–S1	2.949(1)	S1–Ca1–S2	147.76(4)
Ca1–S2	2.961(2)	S1–Ca1–O1	68.23(7)
Ca1–O1	2.461(3)	O1–Ca1–O2	65.8(1)
Ca1–O2	2.458(3)	O2–Ca1–S2	66.96(8)
Ca1–O3	2.533(3)	S2–Ca1–O3	67.84(7)
Ca1–O4	2.490(4)	O3–Ca1–O4	67.3(1)
Ca1–O5	2.292(3)	S1–Ca1–O4	66.9(1)
Ca1–O8	2.307(3)	O5–Ca1–O8	92.1(1)

The three analogous [18]aneO$_4$S$_2$ structures can be compared. Examination of all the bond lengths show only minor differences in the metal to donor distances (Ca–S and Ca–O); Table 3.4. The dicationic charge has little effect on the structural parameters in [Ca([18]aneO$_4$S$_2$)(H$_2$O)$_2$][I]$_2$ (Figure 3.7) and the small differences are more a consequence of the individual electronic and steric requirements of the interchangeable oxo-ligands. More importantly these three complexes represent the first structurally authenticated neutral thioether coordination bonds to Ca(II), an interaction not immediately predictable from the known coordination chemistry of the alkaline earth dications nor from HSAB Theory. All the calcium(II) macrocycle donor distances are substantially within the respective ΣVdW radii (Ca+O= 3.83 Å; Ca+S= 4.11 Å) [24]. A more detailed inspection of the bond distances shows there is a preference for the ether oxygens over the sulfur donors within the macrocycle. Taking [Ca(CF$_3$SO$_3$)$_2$([18]aneO$_4$S$_2$)] (Figure 3.6) as the example, the difference between the Ca–S$_{macrocycle}$ and Ca–O$_{macrocycle}$ distances (2.955 and 2.486 Å (ave) respectively; $\Delta_{Ca\text{-}S/Ca\text{-}O}$= 0.47 Å) shows the Ca–O interaction is significantly shorter when comparing the difference in the covalent radii for S *vs.* O (1.05 and 0.66 Å respectively; Δ_{radii}= 0.39 Å) [9]. This is as expected for the hard Ca(II) Lewis acid and also is in agreement with the ^{1}H NMR data collected for the systems.

Table 3.4 Comparison of the mean bond distances (Å) for three Ca(II) [18]aneO$_4$S$_2$ complexes

Average Bond Length (Å)	Perchlorate[a] [14]	Triflate[b]	Iodide Dihydrate[c]
Ca–S$_{macrocycle}$	3.007	2.955	2.996
Ca–O$_{macrocycle}$	2.471	2.486	2.469
Ca–O$_{co\text{-}ligand}$	2.320	2.300	2.344

[a] [Ca(ClO$_4$)$_2$([18]aneO$_4$S$_2$)], [b] [Ca(CF$_3$SO$_3$)$_2$([18]aneO$_4$S$_2$)], [c] [Ca([18]aneO$_4$S$_2$)(H$_2$O)$_2$][I]$_2$

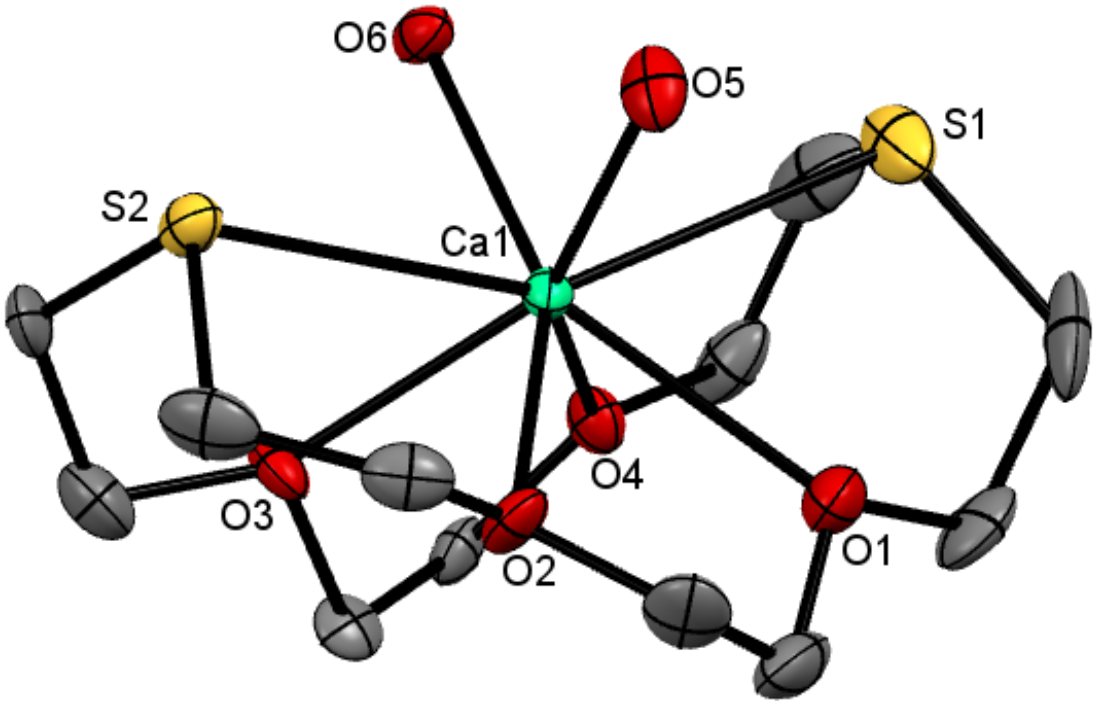

Figure 3.7 Crystal structure of the cation in $[Ca([18]aneO_4S_2)(H_2O)_2][I]_2$ showing the atom numbering scheme. Ellipsoids are drawn at the 50% probability level and H atoms are omitted for clarity.

Table 3.5 Selected bond lengths (Å) and angles (°) for $[Ca([18]aneO_4S_2)(H_2O)_2][I]_2$

Ca1–S1	2.971(3)	S1–Ca1–S2	149.69(9)
Ca1–S2	3.021(3)	S1–Ca1–O1	65.8(1)
Ca1–O1	2.505(5)	O1–Ca1–O2	66.8(2)
Ca1–O2	2.487(6)	O2–Ca1–S2	67.9(1)
Ca1–O3	2.424(5)	S2–Ca1–O3	67.7(1)
Ca1–O4	2.461(5)	O3–Ca1–O4	65.7(2)
Ca1–O5	2.317(6)	S1–Ca1–O4	67.5(1)
Ca1–O6	2.370(6)	O5–Ca1–O6	90.8(2)
O5···I1	3.479(6)		
O5···I2	3.433(6)		
O6···I1	3.548(4)		
O6···I2	3.490(4)		

Attempts to increase the ratio of neutral sulfur coordination relative to the number of neutral oxygen donors by reacting calcium(II) triflate and the dioxa-tetrathia macrocycle [18]aneO_2S_4, resulted in only recovery of the starting materials.

Calcium(II) iodide on the other hand did form complexes of the type [CaI_2([15]aneO_3S_2)] and [CaI_2([18]aneO_2S_4)]. Both complexes achieved an increment in the proportion of thioether donors at Ca(II).

Reacting CaI_2 and [15]aneO_3S_2 in acetonitrile gave an unexpectedly light yellow complex, [CaI_2([15]aneO_3S_2)] (Figure 3.8). The spectroscopic measurements all confirm the stated composition, the ^{1}H NMR showing only small shifts to high frequency from the free ligand. The crystal structure shows the metal situated above the plane of the macrocycle coordinated to all the available donors giving 7-coordinate calcium(II). At the time this complex was only the third example of rare *endo*-coordination by this ligand, the others being [Ag([15]aneO_3S_2)]$^+$ and [GeCl([15]aneO_3S_2)]$^+$ [25] [26]. Examination of the bond distances show a similar range to those reported so far for Ca(II) oxa-thia macrocycle complexes.

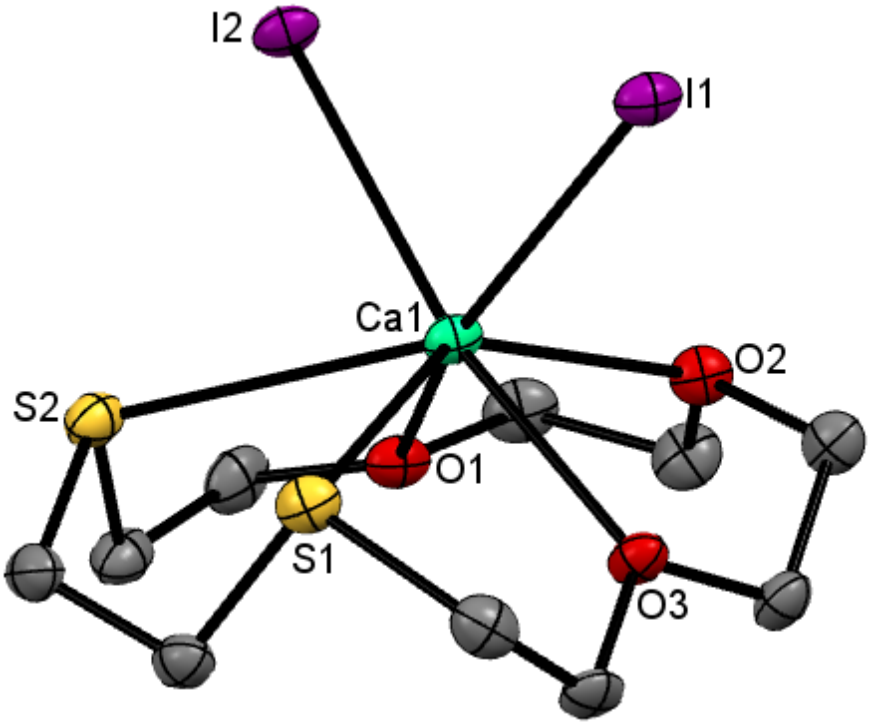

Figure 3.8 Crystal structure of [CaI_2([15]aneO_3S_2)] showing the atom numbering scheme. Ellipsoids are drawn at the 50% probability level and H atoms are omitted for clarity.

Table 3.6 Selected bond lengths (Å) and angles (°) for $[CaI_2([15]aneO_3S_2)]$

Ca1–S1	2.983(2)	S1–Ca1–S2	66.97(5)
Ca1–S2	2.975(2)	S1–Ca1–O3	68.9(1)
Ca1–O1	2.431(5)	S2–Ca1–O1	67.5(1)
Ca1–O2	2.400(4)	O1–Ca1–O2	68.3(1)
Ca1–O3	2.502(4)	O2–Ca1–O3	66.9(1)
Ca1–I1	3.081(2)	I1–Ca1–I2	90.19(3)
Ca1–I2	3.175(2)		

Under similar experimental conditions the complex $[CaI_2([18]aneO_2S_4)]$ (Figure 3.9) was isolated as a yellow solid. Both the colour and the ratio of soft thioether donors coordinated is unprecedented, the complex marks a milestone in achieving a softer coordination sphere around the very hard calcium(II) centre. The macrocycle is folded similarly to the $[18]aneO_4S_2$ complexes and the two bound iodides are mutually *cis*. The ^1H NMR spectrum shows negligible differences (CD_3CN) to the parent macrocycle, indicative of the expected dissociation of the complex in solution. Authentication of the complex came from determination of its crystal structure. The structure clearly shows all four S-donors coordinated and the Ca–S distances (2.905(2)-2.966(3) Å) are well within the ΣVdW radii (4.11 Å) [24]. Interestingly the Ca–O bonds are longer than in the previous oxa-thia macrocycle complexes by ~0.2 Å, they are still just significantly shorter but the difference is diminished.

The unusual yellow colour of the latter two complexes was surprising, Ca(II) complexes tend to be colourless solids (CaI_2 is a white solid) and the oxa-thia macrocycles are also colourless. $[CaI_2([18]aneO_4S_2)]$ is a white solid, but increasing the ratio of soft neutral thioether coordination around the Ca(II) centre such as in $[CaI_2([15]aneO_3S_2)]$ and $[CaI_2([18]aneO_2S_4)]$ gives compounds which are pale yellow and yellow respectively. This increase in colour intensity seems to be an indicator for the increasing charge transfer to the metal centre by the heavier S-donors (see also Chapter 4).

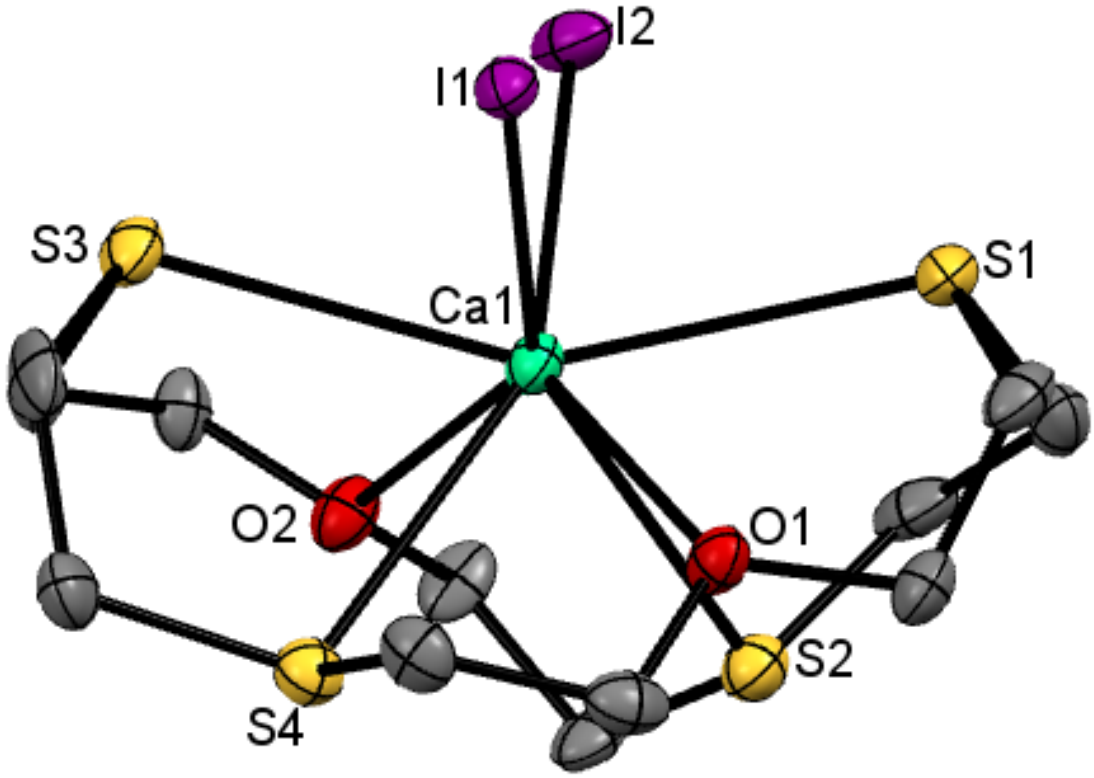

Figure 3.9 Crystal structure of $[CaI_2([18]aneO_2S_4)]\cdot\frac{1}{2}CH_2Cl_2$ showing the atom numbering scheme. Ellipsoids are drawn at the 50% probability level. The solvate and H atoms are omitted for clarity.

Table 3.7 Selected bond lengths (Å) and angles (°) for $[CaI_2([18]aneO_2S_4)]\cdot\frac{1}{2}CH_2Cl_2$

Ca1–S1	2.951(2)	S1–Ca1–S2	69.15(6)
Ca1–S2	2.966(2)	S2–Ca1–O2	67.5(9)
Ca1–S3	2.924(2)	O2–Ca1–S3	67.3(1)
Ca1–S4	2.905(2)	S3–Ca1–S4	71.48(6)
Ca1–O1	2.621(5)	S4–Ca1–O1	66.5(1)
Ca1–O2	2.654(5)	S1–Ca1–O1	68.2(1)
Ca1–I1	3.118(2)	I1–Ca1–I2	95.24(4)
Ca1–I2	3.116(2)		

Further attempts to increase the ratio of thioether donation to Ca(II) by using [18]aneS$_6$ under analogous conditions did not result in the formation of [CaI$_2$[18]aneS$_6$], with only the starting reagents isolated.

Attempts to isolate complexes with the smaller, tridentate macrocycles [9]aneO$_2$S and [9]aneOS$_2$ were unsuccessful. Ca(II) complexes tend to exhibit coordination numbers between 7 to 9, and it is highly likely the nine-membered oxa-thia macrocycles are too small to be suitable for coordination to calcium(II).

Selenoethers are even softer Lewis bases than their analogous thioethers. Using the related oxa-selena crown [18]aneO$_4$Se$_2$ the Ca(II) complex [CaI$_2$([18]aneO$_4$Se$_2$)] (Figure 3.10) was isolated. Selenoether coordination complexes at the time were unknown for the first three Groups in the Periodic table, therefore it was paramount to authenticate the Ca–Se interaction. All the spectroscopic measurements were in accordance to the formulation stated and the ^{1}H NMR spectrum was typical of coordinated [18]aneO$_4$Se$_2$. The crystal structure unambiguously identified the complex, the first example of selenoether coordination to an element in Groups 1, 2 and 3 and what was at the time only the second known coordination complex of [18]aneO$_4$Se$_2$. Like the analogous [18]aneO$_4$S$_2$ complexes the macrocycle adopts a very folded conformation around the Ca(II) centre and the two coordinated iodides are *cisoidal*. Analysis of the distances shows the Ca–O bonds are little different to the previous complexes in this study, but the Ca–Se interaction is longer (3.106(1) Å). This increase is almost exactly that expected from the difference in covalent radii for Se and S (Se being larger by 0.15 Å)[9].

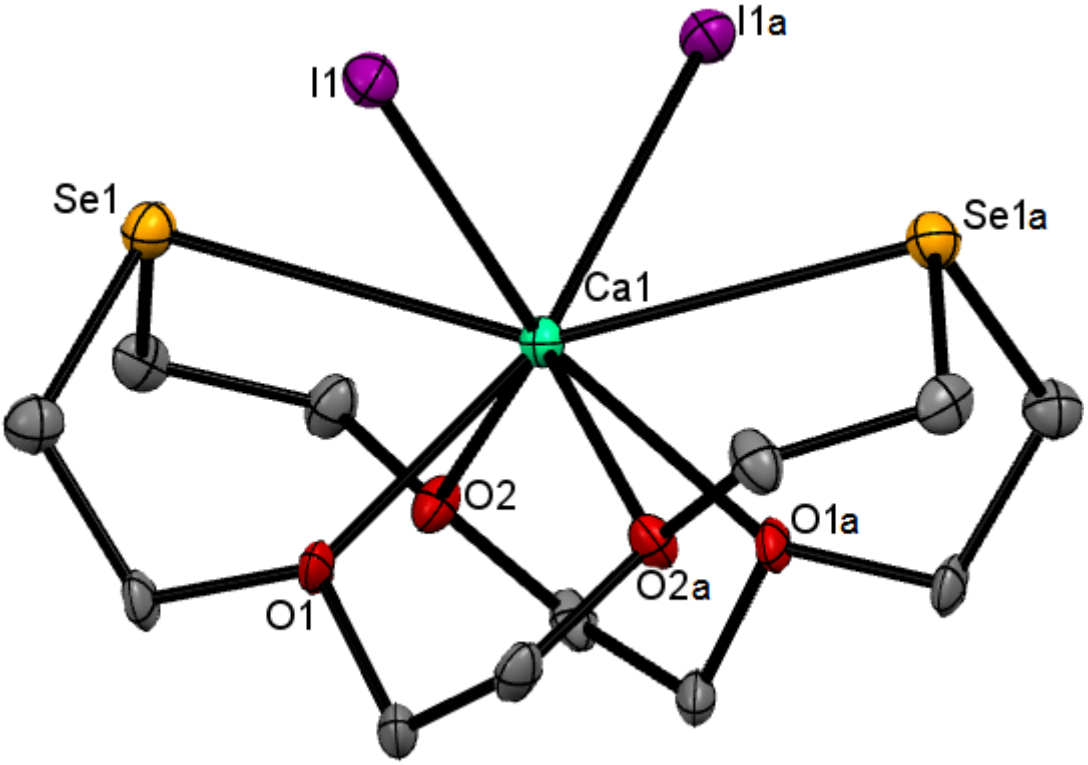

Figure 3.10 Crystal structure of $[CaI_2([18]aneO_4Se_2)]$ showing the atom numbering scheme. Ellipsoids are drawn at the 50% probability level and H atoms are omitted for clarity. Symmetry operation: a = 1 – x, y, 1/2 – z.

Table 3.8 Selected bond lengths (Å) and angles (°) for $[CaI_2([18]aneO_4Se_2)]$

Ca1–Se1	3.106(1)	Se1–Ca1–Se1a	151.34(9)
Ca1–O1	2.433(6)	Se1–Ca1–O1	70.5(1)
Ca1–O2	2.599(6)	Se1–Ca1–O2	65.2(1)
Ca1–I2	3.174(2)	O1–Ca1–O2	65.4(2)
		I1–Ca1–I1a	99.53(7)

To further push the limits of very soft chalcogenoether coordination to Ca(II), the analogous reaction with the tellura-oxa macrocycle $[18]aneO_4Te_2$ was attempted. Unlike its lighter chalcogenoether analogues (Se, S, O) the reaction did not result in a desired complex. Instead intractable powders were isolated and the reaction was not pursued further. The failure to isolate a telluroether complex of calcium(II) adds

further credence to the importance of the Ca–Se and Ca–S interactions for isolating the complexes $[CaI_2([18]aneO_4E_2)]$ (E= S, Se) *viz* the Ca(II) has an integral affinity for the softer donor and the four crown ether O-donor atoms alone are not sufficient enough to allow coordination of these mixed donor macrocycles to the Group 2 dications.

3.2.2 Sr(II) coordination chemistry

The coordination chemistry of Sr(II) is even less developed than that of calcium. Comparable investigations with SrI_2 and mixed donor chalcogenoether macrocycles were undertaken in parallel.

The complex $[SrI_2([15]aneO_3S_2)]$ was isolated as a fine white anhydrous solid. All the spectroscopic measurements were in accordance with the above formulation and the resonances in both the IR spectrum and ^1H NMR spectrum closely resembled those obtained for the calcium(II) complex. The microanalytical data was slightly inconsistent in that it fits better as the monohydrate, it has already been stated these solids are highly deliquescent and therefore even trace amounts of water can be incorporated into the composition of the solids, especially after sequential handlings.

Crystals were grown by storing a Schlenk containing the filtrate from the reaction at -18°C. After a few days colourless crystals of $[Sr([15]aneO_3S_2)(H_2O)_3][I_2]$ (Figure 3.11) were collected. Again this is evidence that the complex undergoes partial hydrolysis. The structure bears a close similarity to the Ca(II) analogue, the Sr^{2+} cation sits above the plane of the macrocycle which binds *pseudo*-facially and *trans* to three aquo ligands that have a mutually *fac* arrangement. The displaced iodides form interactions *via* hydrogen bonds to the coordinated water molecules. The Sr–E (E= S (Se), O) bond lengths are longer as expected, calcium(II) is smaller than strontium(II) ($\Delta_{\text{covalent radii}}$= 0.19 Å).

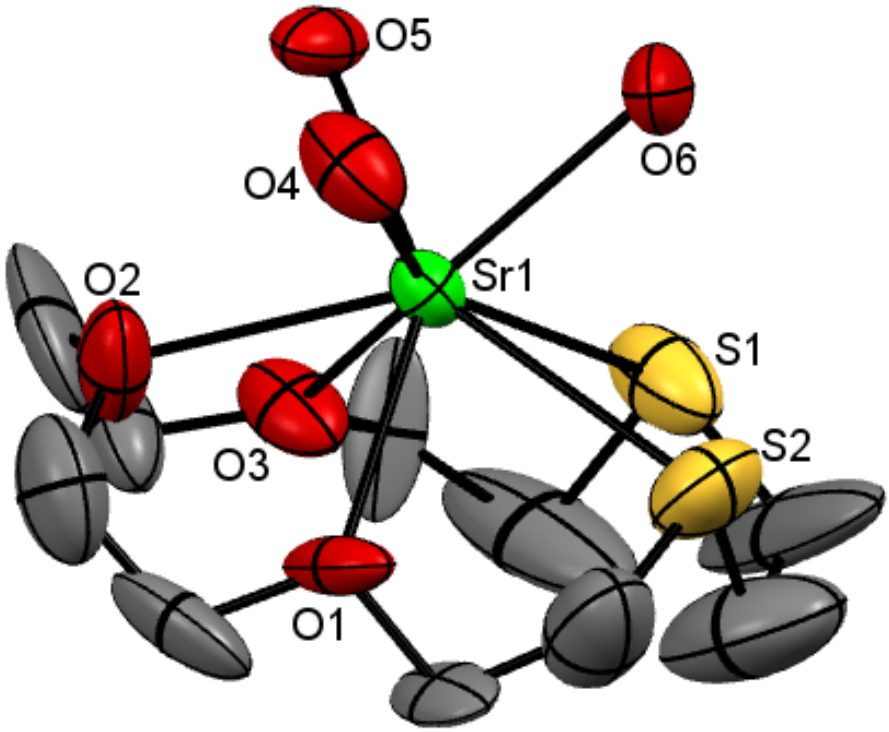

Figure 3.11 Crystal structure of the cation in $[Sr([15]aneO_3S_2)(H_2O)_3][I]_2$ showing the atom numbering scheme. Ellipsoids are drawn at the 35% probability level and H atoms are omitted for clarity.

Table 3.9 Selected bond lengths (Å) and angles (°) for $[Sr([15]aneO_3S_2)(H_2O)_3][I]_2$

Sr1–S1	3.062(6)	S1–Sr1–S2	69.02)
Sr1–S2	3.036(7)	S1–Sr1–O3	64.7(3)
Sr1–O1	2.73(1)	S2–Sr1–O1	64.5(4)
Sr1–O2	2.65(1)	O1–Sr1–O2	63.0(4)
Sr1–O3	2.65(1)	O2–Sr1–O3	61.5(3)
Sr1–O4	2.52(1)	O4–Sr1–O5	90.9(4)
Sr1–O5	2.53(1)	O4–Sr1–O6	78.6(4)
Sr1–O6	2.54(1)	O5–Sr1–O6	78.9(4)
O5···I1	3.42(1)		
O5···I2	3.46(1)		

Reacting SrI_2 with the larger oxa-thia macrocycle [18]aneO_4S_2 gave [SrI_2([18]aneO_4S_2)]. Also a fine white anhydrous solid, it proved to be moderately insoluble immediately dropping out of the reaction solution. All the spectroscopic data, including the elemental analysis, confirmed the solid as anhydrous. Interestingly, in the ^{1}H NMR spectrum the OC$\boldsymbol{H}_2$ environment experiences a much larger deshielding effect at Sr(II) (+0.31 ppm) than the other two C$\boldsymbol{H}_2$ environments (SC$\boldsymbol{H}_2$ and $SCH_2C\boldsymbol{H}_2O$; ~+0.15 ppm). As expected strontium(II) binds preferentially to the harder donor but Sr(II) seems to also bind more strongly to the centre of the macrocyclic pore coordinated to the four central crown ether O-donors.

The crystal structure of the dihydrate, [Sr([18]aneO_4S_2)$(H_2O)_2$][I]$_2$ (Figure 3.13) showed a different conformation for the oxa-thia macrocycle, which may help explain the observations in the ^{1}H NMR spectrum. The macrocycle is far more planar although the "terminal" S-donors are still puckered *syn*. The Sr(II) centre sits more in the plane of the macrocycle rather than being encapsulated. Again the iodide anions have been displaced from the primary coordination sphere and three water molecules are coordinated forming a *meridian* at Sr^{2+}. The absolute configuration of the primary ligands is more akin to the [18]aneO_4S_2 Group 14 complexes in Chapters 5 & 6 and that of La(III), than the other Group 2 [18]aneO_4E_2 (E= S, Se) complexes present in this study [14, 27]. The bond distances are all within ΣVdW radii and comparison of the average Sr–E (E= O, S) distances show there is only a marginal difference in the bond lengths relative to the difference in covalent radii for O *vs*. S (2.708 *vs*. 3.103 Å; 0.66 *vs*. 1.05 Å) [9]. Sr(II) is larger than Ca(II) also making it relatively softer, the constraints of the macrocycle are the same for the analogous alkaline earth complexes and it is these factors that explain why a larger difference in seen for Ca–$E_{macrocycle}$ distances than for the analogous strontium(II) interactions. The small-scale, adventitious hydrolysis of the strontium complexes (and [CaI_2([18]aneO_4S_2)] (Figure 3.5)), shows the ease at which water can be introduced in these systems. More surprising is that instead of disrupting the M–S/Se (M= Ca, Sr) bond it displaces the coordinated iodides, demonstrating the preference for retention of the soft chalcogenoether interaction. Further to this, examination of the respective lattice structures show all the complexes form a network with several O···I contacts *ca*. 3.5 Å. This H-bonding

network helps stabalise the partially hydrated structures and most likely is the driving force for the formation of the few well-formed and defined crystals found amongst the bulk of the products that are anhydrous.

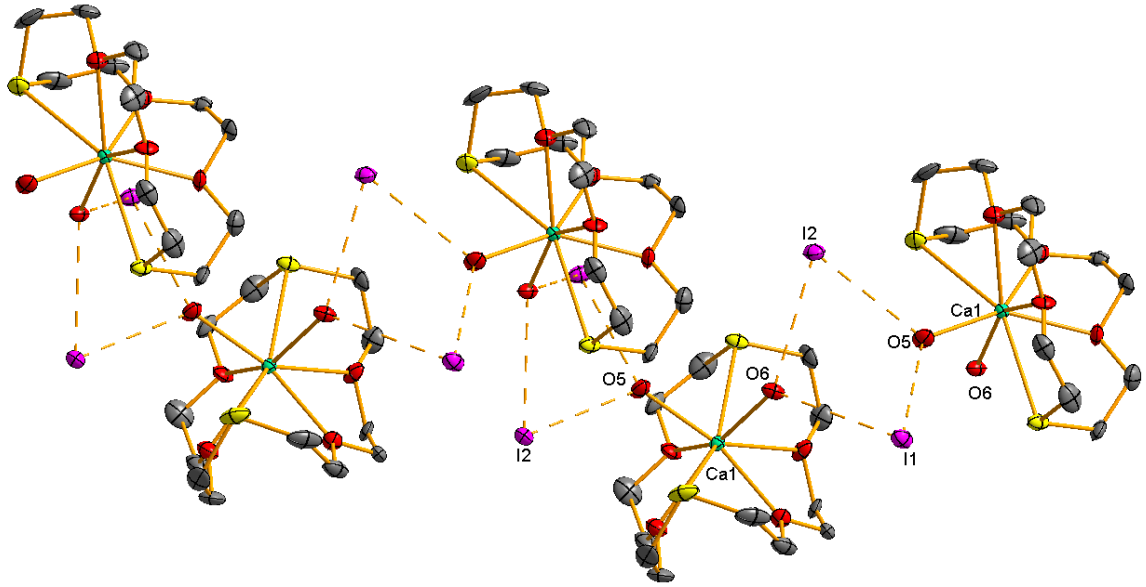

Figure 3.12 Repeating chain network in $[Ca([18]aneO_4S_2)(H_2O)_2][I]_2$ showing the H-bonds between the aquo ligands and ionic iodides.

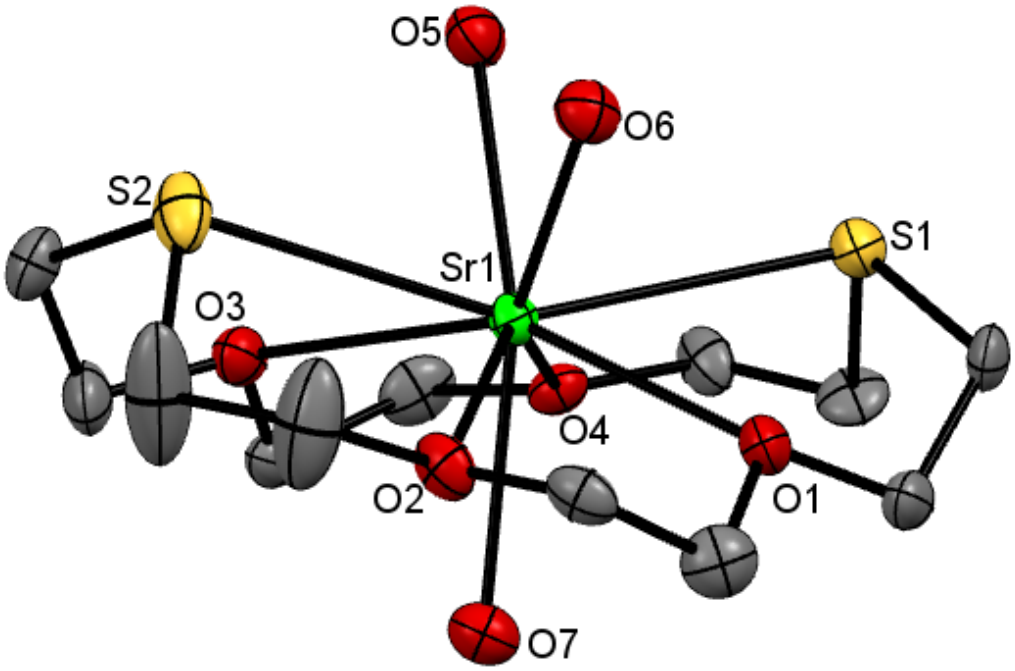

Figure 3.13 Crystal structure of the cation in $[Sr([18]aneO_4S_2)(H_2O)_3][I]_2 \cdot H_2O$ showing the atom numbering scheme. Ellipsoids are drawn at the 50% probability level and H atoms are omitted for clarity.

Table 3.10 Selected bond lengths (Å) and angles (°) for $[Sr([18]aneO_4S_2)(H_2O)_3][I]_2 \cdot H_2O$

Sr1–S1	3.095(3)	S1–Sr1–S2	153.02(8)
Sr1–S2	3.111(3)	S1–Sr1–O1	64.7(2)
Sr1–O1	2.692(9)	O1–Sr1–O2	62.2(2)
Sr1–O2	2.707(7)	S2–Sr1–O2	65.7(2)
Sr1–O3	2.749(9)	S2–Sr1–O3	63.5(2)
Sr1–O4	2.685(7)	O3–Sr1–O4	62.3(2)
Sr1–O5	2.591(8)	S1–Sr1–O4	63.6(2)
Sr1–O6	2.547(8)	O5–Sr1–O6	75.8(2)
Sr1–O7	2.588(8)	O6–Sr1–O7	138.2(2)
O7···I1	3.470(7)	O5–Sr1–O7	145.8(2)
O6···O8	2.77(1)		

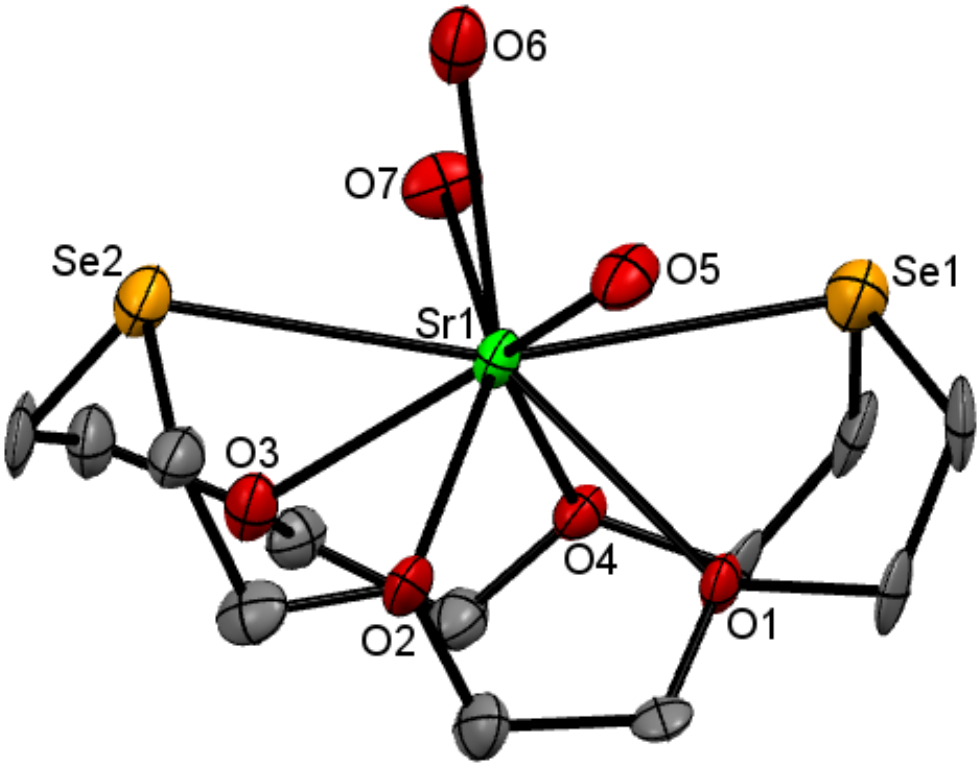

Figure 3.14 Crystal structure of the cation in $[Sr([18]aneO_4Se_2)(H_2O)_3][I]_2$ showing the atom numbering scheme. Ellipsoids are drawn at the 50% probability level and H atoms are omitted for clarity.

Table 3.11 Selected bond lengths (Å) and angles (°) for $[Sr([18]aneO_4Se_2)(H_2O)_3][I]_2$

Sr1–Se1	3.167(2)	Se1–Sr1–Se2	161.32(7)
Sr1–Se2	3.224(2)	Se1–Sr1–O1	63.6(2)
Sr1–O1	2.72(1)	O1–Sr1–O2	62.0(3)
Sr1–O2	2.65(1)	Se2–Sr1–O2	66.6(2)
Sr1–O3	2.76(1)	Se2–Sr1–O3	65.4(2)
Sr1–O4	2.67(1)	O3–Sr1–O4	63.5(3)
Sr1–O5	2.57(1)	Se1–Sr1–O4	65.6(2)
Sr1–O6	2.69(1)	O5–Sr1–O6	66.6(4)
Sr1–O7	2.57(1)	O6–Sr1–O7	67.3(4)
O5···I1	3.49(1)	O5–Sr1–O7	129.2(3)
O5···I2	3.49(1)		
O7···I1	3.47(1)		
O7···I2	3.45(1)		

The analogous reaction with the oxa-selena crown gave $[SrI_2([18]aneO_4Se_2)]$, a similarly insoluble white anhydrous powder with all the attributable spectroscopic measurements. The crystal structure shows the complex has undergone partial hydrolysis, the crystals having the constitution $[Sr([18]aneO_4Se_2)(H_2O)_3][I_2]$ (Figure 3.14). In this complex the macrocycle adopts the more folded conformation beginning to encapsulate the Sr^{2+} cation. The three aquo ligands are in an unusual adjacent arrangement on one side of the strontium(II) centre. Examination of the bond distances between the metal and the macrocyclic donors showed only a small preference for the O-donors over the Se- donors (Sr–O= 2.698, Sr–Se= 3.195 Å).

The three complexes presented represent the first examples of strontium-thio/selenoether coordination.

Further attempts to increase the degree of soft coordination at Sr(II) were unsuccessful. SrI_2 did not react with [18]aneO_4Te_2 under the conditions employed, the same outcome as the analogous CaI_2 reaction. The attempted reaction with [18]anO_2S_4 also failed to isolate the desired complex. Instead a white, highly insoluble powder formed. Multiple attempts to grow a crystal were also unsuccessful; in light of the limited data obtained the reaction was abandoned. Under the same reaction conditions (MeCN/CH_2Cl_2), [18]anO_2S_4 has failed to coordinate other Lewis acids such as Pb(II), Sn(II) and $SbCl_3$ (see Chapters 5,6 and 7). A possible reason could be the different steric constraints of the macrocycle compared to the other 18-membered Group 16 crowns (see Chapter 2), make it unsuitable for coordination to Sr(II).

3.3 Conclusions

A series of widely unexpected and unusual coordination complexes exhibiting the soft coordination of thioether and selenoether groups to the hard alkaline earth dications Ca^{2+} and Sr^{2+} have been synthesised. They challenge the established views relating to HSAB theory and more importantly highlight a much broader coordination chemistry of the Group 2 metals than once thought. Due to the biological importance of calcium and the emerging attention of alkaline earth metals in mediating 'green' catalysis, the results of this study represent notable findings.

A key finding was demonstrating that a significantly greater amount of S-donor coordination can be achieved in the presence of relatively harder donors such as intramolecular crown ether donors and acetonitrile solvent. The compound $[CaI_2([18]aneO_2S_4]$ is representative of this. Although attempts to coordinate more thioether groups and softer ligands were unsuccessful (the reactions with $[18]aneS_6$ and $[18]aneO_4Te_2$), it has helped to quantify the extent of the coordination chemistry accessible and presented a set of more definitive boundary lines in the sense of what is possible with the Group 2 dications.

The first examples of thioether and selenoether coordination to Sr(II) and selenoether coordination to Ca(II) has been presented and characterised. The calcium(II) complexes show a preference for the harder O-donors over the S-donor which is in accordance with the accepted view it is a hard Lewis acid. The case with Sr(II) is a little less defined, with a diminished significant difference in the mean bond distances Sr–E (E= O, S (Se)), as has been the case for research undertaken with the alkaline earth metals the change is ascribed to the variation in radii, strontium(II) being larger than calcium(II).

The soft donor interaction is essential towards the formation of the complexes in these systems. Macrocyclic complexes of the type $[M([18]aneO_4E_2)]^{2+}$ (M= Ca, Sr) only form for E= S and Se, when the soft donor is tellurium the complex does not form highlighting that the four ether donors and macrocyclic framework are not sufficient alone. Further to this the soft donor metal interaction survives the initial stages of hydrolysis, water displacing the iodide co-ligand preferentially. In the ionic systems extensive packing interaction and/or H-bonding networks are observed.

3.4 Experimental

3.4.1 **[Ca(18-crown-6)(MeCN)$_2$][SbCl$_6$]$_2$:** $CaCl_2$ (0.150 g, 1.35 x 10^{-3} mol) and a freshly prepared acetonitrile solution of $SbCl_5$ (13.6 mL, 0.2 mol dm^{-3}, 2.70 x 10^{-3} mol) was left to stir for 40 min with gentle warming before 18-crown-6 (0.357 g, 1.35 x 10^{-3} mol) was added and left to stir overnight. The solution turned a pale straw colour. Concentrating the solution *in vacuo* to ~4 mL gave an orange solution. Since no solid formed at -20˚C the MeCN was completely removed under vacuum and the remaining solid taken up in CH_2Cl_2 and layered with hexane. A large mass of big colourless crystals formed, which were collected by filtration and dried *in vacuo*. Yield: 0.546 g, 70%. Required for $C_{16}H_{30}CaCl_{12}O_6N_2Sb_2$ (1055.22) C, 18.21; H, 2.86; N, 2.65. Found: C, 18.22; H, 2.84; N, 2.46%. IR (Nujol cm^{-1}): 2302, 2274 (MeCN), 341 ($SbCl_6$). ^{1}H NMR (CD_3CN, 298K): δ 3.77 (s, crown C***H***$_2$).

3.4.2 **[Ca(CF$_3$SO$_3$)$_2$(18-crown-6)(H$_2$O)]:** $Ca(CF_3SO_3)_2$ (0.080 g, 2.37 x 10^{-4} mol) and 18-crown-6 (0.063 g, 2.37 x 10^{-4} mol) were dissolved together and left to stir at room temperature overnight in MeCN (15 mL). $Ca(CF_3SO_3)_2$ itself has only partial solubility in MeCN but dissolves completely upon addition of the crown. The solvent was removed *in vacuo* and the white powder taken up in CH_2Cl_2 layered with hexane and then placed in the fridge. A white precipitate formed which was filtered and dried under vacuum. X-ray quality crystals were grown from the filtrate. Yield: 0.112 g, 72%. Required for $C_{14}H_{26}CaF_6O_{13}S_2$ (620.15): C, 27.07; H, 4.22. Found: C, 27.72 H, 4.17%. IR (Nujol cm^{-1}): 3479, 1648 (H_2O). ^{1}H NMR (CD_3CN, 298K): δ 2.38-2.57 (m, ***H***$_2$O), 3.81 (s, [24H], crown C***H***$_2$).

3.4.3 **[$CaCl_2$(18-crown-6)]:** METHOD 1: $CaCl_2$ (0.082 g, 7.39 x 10^{-4} mol) and 18-crown-6 (0.195 g, 7.39 x 10^{-4} mol) were combined and left to stir in MeCN (40 mL) at 70˚C for 9 d. The solution was allowed to cool and filtered to remove the modest amount of residual unreacted solid. The filtrate was concentrated to ~15 mL and left to stand at room temperature, a few very large colourless crystals grew. The mother liquor was isolated and placed at 5˚C, a second small crop formed. Required for $C_{12}H_{24}CaCl_2O_6$ (375.14): C, 38.40; H, 6.45. Found: C, 38.41; H, 6.90%. IR (Nujol cm^{-1}): 272 (CaCl). ^{1}H NMR (CD_3CN, 298K): δ 3.78 (s, crown C***H***$_2$). Yield not recorded.

METHOD 2: $CaCl_2$ (0.100 g, 9.01 x 10^{-4} mol) and 18-crown-6 (0.238 g, 9.01 x 10^{-4} mol) were dissolved fully in anhydrous MeOH (70 mL) and left to stir at 65˚C for 3 d. The solvent was completely removed and the remaining solid washed with CH_2Cl_2. The white solid had identical spectra. Yield: 0.170 g, 50%.

3.4.4 **[CaI_2([18]aneO$_4$S$_2$)]:** CaI_2 (0.065 g, 2.21 x 10^{-4} mol) was dissolved in MeCN (10 mL), [18]aneO$_4$S$_2$ (0.065 g, 2.21 x 10^{-4} mol) was added and left to stir. After a few minutes a white solid began to form. The solid was filtered. Weakly diffracting crystals were grown from the filtrate at room temperature. Yield: 0.040 g, 40%. Required for $C_{12}H_{24}CaI_2O_4S_2$ (590.00): C, 24.42; H, 4.10. Found: C, 23.70; H, 3.88%. ^{1}H NMR (CD_3CN, 298K): δ 3.12-3.32 (t, [8H], SC***H***$_2$), 3.88 (m, [16H], OC***H***$_2$).

A subsequent attempt to grow X-ray quality crystals resulted in the formation of large strongly diffracting crystals of the dihydrate, [Ca([18]aneO$_4$S$_2$)(H$_2$O)$_2$][I]$_2$, along with the smaller, poorer quality, neutral complex which were identified from the unit cell.

3.4.5 **[Ca(CF_3SO_3)$_2$([18]aneO_4S_2)]:** Ca(CF_3SO_3)$_2$ (0.152 g, 4.51 x 10^{-4} mol) and [18]aneO_4S_2 (0.133 g, 4.51 x 10^{-4} mol) were co-dissolved and left to stir overnight in MeCN (15 mL). Ca(CF_3SO_3)$_2$ has only partial solubility in MeCN but dissolves completely upon addition of the macrocycle. The MeCN was removed *in vacuo* leaving a white powder which was taken up in CH_2Cl_2. This was filtered and concentration afforded a white solid, which was further filtered. X-Ray quality crystals were grown from the filtrate. Yield: 0.043 g, 15%. ^{1}H NMR (CD_3CN, 298K): δ 2.91 (t, [8H], SC***H***$_2$), 3.80 (t, [8H], SCH_2C***H***$_2$O), 3.89(s, [8H], OC***H***$_2$).

3.4.6 **[CaI_2([15]aneO_3S_2)]:** CaI_2 (0.080 g, 2.72 x 10^{-4} mol) and [15]aneO_3S_2 (0.069 g, 2.72 x 10^{-4} mol) were dissolved in MeCN (10 mL) and left to stir overnight. The solution took on a pale yellow tinge with some solid beginning to form. Concentration did not cause any additional solid to precipitate, hence the solvent was completely removed *in vacuo* and the residues taken up in CH_2Cl_2. A large amount of pale yellow solid was deposited. This was collected by filtration and dried under vacuum. From the filtrate X-ray quality crystals were grown. Yield: 0.090 g, 61%. Required for $C_{10}H_{20}CaI_2O_3S_2$ (545.97): C, 21.99; H, 3.69. Found: C, 21.82; H, 3.71%. ^{1}H NMR (CD_3CN, 298K): δ 2.79 (t, [4H], SC***H***$_2$$CH_2$O), 2.90 (s, [4H], SC***H***$_2$), 3.70 (s, [8H], OC***H***$_2$), 3.77 (t, [4H], SCH_2C***H***$_2$O).

3.4.7 **[CaI_2([18]aneO_2S_4)]:** [18]aneO_2S_4 (0.090 g, 2.72 x 10^{-4} mol) was dissolved in CH_2Cl_2 (10 mL) and added to an MeCN (10 mL) solution of CaI_2 (0.080 g, 2.72 x 10^{-4} mol). The reaction was left to stir at room temperature for 16 h, a light yellow solid formed. The solid was filtered. From the filtrate small yellow crystals were grown. Yield: 0.060 g, 35%. Required for $C_{12}H_{24}CaI_2O_2S_4 \cdot CH_2Cl_2$ (706.87): C, 22.07; H, 3.71. Found: C, 21.51; H, 3.63%. ^{1}H NMR (CD_3CN, 298K): δ 2.72 (t, [8H], SC***H***$_2$$CH_2$O), 2.82 (s, [8H], SC***H***$_2$), 3.64 (t, [8H], OC***H***$_2$).

3.4.8 **[CaI_2([18]aneO_4Se_2)]:** CaI_2 (0.045 g, 1.539 x 10^{-4} mol) and [18]aneO_4Se_2 (0.060 g, 1.539 x 10^{-4} mol) were dissolved in MeCN (20 mL) and left to stir overnight. A white precipitate crashed out which was collected *via* filtration and washed with CH_2Cl_2. X-Ray quality crystals grew at 5˚C upon concentration of the filtrate. Yield: 0.080 g, 76%. Required for $C_{12}H_{24}CaI_2O_4Se_2$ (683.97): C, 21.07; H, 3.54. Found: C, 21.25; H, 3.52%. ^{1}H NMR (CD_3CN, 298K): δ 2.85 (t, SeCH_2, [8H]), 2.76 (s, [8H], OCH_2), 3.87 (t, [8H], $SeCH_2CH_2O$).

3.4.9 **[SrI_2([15]aneO_3S_2)]:** SrI_2 (0.080 g, 2.72 x 10^{-4} mol) and [15]aneO_3S_2 (0.069 g, 2.72 x 10^{-4} mol) were dissolved in MeCN (20 mL) and left to stir overnight at room temperature. The solution was concentrated to ~3 mL, yielding a colourless microcrystalline solid. Yield: 0.060 g, 40%. Required for $C_{10}H_{20}I_2O_4S_2Sr$ (593.51): C, 20.20; H, 3.40. Found: C, 19.50; H, 3.40%. ^{1}H NMR (CD_3CN, 298K): δ 2.79 (t, [4H], SCH_2CH_2O), 2.90 (s, [4H], OCH_2), 3.70 (s, [8H], SCH_2), 3.77 (t, [4H], SCH_2CH_2O)

Placing the filtrate in the freezer afforded small colourless crystals of [Sr([15]aneO_3S_2)$(H_2O)_3$][I]$_2$.

3.4.10 **[SrI_2([18]aneO_4S_2)]:** SrI_2 (0.080 g, 2.343 x 10^{-4} mol) and [18]aneO_4S_2 (0.070 g, 2.343 x 10^{-4} mol) were dissolved in MeCN (20 mL) and stirred. A fine white powder crashed out almost instantaneously. The reaction was left to stir at room temperature for 4 h. The solid was collected *via* filtration, washed with CH_2Cl_2, and dried *in vacuo*. Yield: 0.030 g, 20%. Required for $C_{12}H_{24}I_2O_4S_2Sr$ (637.54): C, 22.60; H, 3.79. Found: C, 22.49; H, 3.91%. ^{1}H NMR (CD_3CN, 298K): δ 2.91 (t, [8H], SCH_2), 3.80 (t, [8H], SCH_2CH_2O), 3.86 (s, [8H], OCH_2).

Large X-ray quality crystals were grown by repeating the experiment on a small scale (~2 mL) and by layering two stoichiometric solutions of the starting reagents. The crystals had the formulation [Sr([18]aneO_4S_2)$(H_2O)_3$][I]$_2$. This was performed at room temperature in a glove box with an atmosphere of N_2.

3.4.11 **[SrI_2([18]aneO_4Se_2)]:** SrI_2 (0.080 g, 2.343 x 10^{-4} mol) and [18]aneO_4Se_2 (0.091 g, 2.343 x 10^{-4} mol) were dissolved in MeCN (20 mL) and stirred. Almost immediately a fine white powder crashed out. Left to stir overnight and then filtered. The filtrate was kept to grow crystals. Yield: 0.040 g, 40%. Required for $C_{12}H_{24}I_2O_4Se_2Sr$ (731.52): C, 19.70; H, 3.31. Found: C, 19.84; H, 3.34%. ^{1}H NMR (CD_3CN, 298K): δ 2.83. (t, [8H], SeC***H***$_2$), 3.67 (s, [8H], OC***H***$_2$), 3.77 (t, [8H], $SeCH_2C$***H***$_2$O).

Placing the filtrate in the freezer afforded small colourless crystals of [Sr([18]aneO_4Se_2)$(H_2O)_3$][I]$_2$.

3.5 Structural Data

Compound	[Ca(18-crown-6)(MeCN)$_2$][SbCl$_6$]	[Ca(CF$_3$SO$_3$)$_2$-(18-crown-6)(H$_2$O)]	[Ca([18]aneO$_4$S$_2$)(H$_2$O)$_2$][I]$_2$
Formula	$C_{16}H_{30}CaCl_{12}N_2O_6Sb$	$C_{14}H_{26}CaF_6O_{13}S_2$	$C_{12}H_{28}CaIO_6S_2$
mwt.	1055.40	620.55	626.34
Crystal system	Monoclinic	Monoclinic	Orthorhombic
Space group	$P2_1/c$ (14)	$C2/c$ (15)	$P2_12_12_1$ (19)
a (Å)	26.561(6)	14.570(4)	9.313(3)
b (Å)	13.365(2)	8.595(2)	11.947(4)
c (Å)	23.205(7)	19.596(8)	19.736(7)
α (°)	90	90	90
β (°)	115.331(10)	103.51(3)	90
γ (°)	90	90	90
U (Å^3)	7445(3)	2386.2(12)	2195.9(11)
Z	8	4	4
μ(Mo Kα) (mm^{-1})	2.482	0.547	3.309
F(000)	4112	1280	1224
total no. reflns	40678	8352	10240
unique reflns	15579	2710	4991
R_{int}	0.053	0.0359	0.072
no. of params, restraints	703, 0	167, 1	217, 2
R_1[a] [$I_o > 2\sigma(I_o)$]	0.062	0.031	0.052
R_1 (all data)	0.079	0.039	0.110
wR_2[a] [$I_o > 2\sigma(I_o)$]	0.157	0.068	0.068
wR_2(all data)	0.178	0.071	0.078

Compound	$[Ca(CF_3SO_3)_2([18]aneO_4S_2)]$	$[CaI_2([15]aneO_3S_2)]$	$[CaI_2([18]aneO_2S_4)] \cdot ½CH_2Cl_2$
Formula	$C_{14}H_{24}CaF_6O_{10}S_4$	$C_{10}H_{20}CaI_2O_3S_2$	$C_{12}H_{24}CaI_2O_2S_4 \cdot 0.5CH_2Cl_2$
mwt.	634.65	546.26	664.90
crystal system	Orthorhombic	Monoclinic	Monoclinic
space group	$Pca2_1$ (29)	$P2_1/n$ (14)	$P2_1/c$ (14)
a (Å)	14.855(4)	10.027(4)	17.076(4)
b (Å)	9.400(3)	13.924(5)	8.2970(18)
c (Å)	17.855(6)	12.848(5)	15.745(4)
α (°)	90	90	90
β (°)	90	101.82(4)	91.464(12)
γ (°)	90	90	90
U (Å^3)	2493.2(13)	1755.8(12)	2230.0(9)
Z	4	4	4
μ(Mo Kα) (mm^{-1})	0.678	4.110	3.548
F(000)	1304	1048	1292
total no. reflns	12107	8699	10627
unique reflns	5639	4003	5065
R_{int}	0.049	0.041	0.059
no. of params, restraints	317, 9	163, 0	208, 2
R_1[a] [$I_o > 2\sigma(I_o)$]	0.047	0.044	0.052
R_1 (all data)	0.069	0.054	0.088
wR_2[a] [$I_o > 2\sigma(I_o)$]	0.091	0.110	0.099
wR_2(all data)	0.101	0.119	0.114

Compound	$[CaI_2([18]aneO_4Se_2)]$	$[Sr([18]aneO_4S_2)(H_2O)_3][I]_2 \cdot H_2O$	$[Sr([15]aneO_3S_2)(H_2O)_3][I]_2$
Formula	$C_{12}H_{24}CaI_2O_4Se_2$	$C_{12}H_{32}I_2O_8S_2Sr$	$C_{10}H_{28}I_2O_6S_2Sr$
mwt.	684.11	709.92	647.85
Crystal system	Monoclinic	Monoclinic	Monoclinic
Space group	*C*2/*c* (15)	$P2_1/c$ (14)	*Cc* (9)
a (Å)	10.808(3)	10.452(4)	9.506(4)
b (Å)	11.798(3)	18.580(7)	17.630(7)
c (Å)	15.203(4)	13.866(5)	12.782(5)
α (°)	90	90	90
β (°)	93.040(7)	112.182(6)	92.101(7)
γ (°)	90	90	90
U (Å^3)	1935.9(9)	2493.5(15)	2140.7(15)
Z	4	4	4
μ(Mo Kα) (mm^{-1})	7.284	4.835	5.615
F(000)	1288	1376	1240
total no. reflns	4452	23787	9930
unique reflns	2202	5671	3986
R_{int}	0.057	0.129	0.061
no. of params, restraints	96, 0	226, 0	190, 17
R_1[a] [$I_o > 2\sigma(I_o)$]	0.057	0.066	0.062
R_1 (all data)	0.088	0.123	0.101
wR_2[a] [$I_o > 2\sigma(I_o)$]	0.105	0.136	0.132
wR_2(all data)	0.120	0.158	0.150

Compound	$[Sr([18]aneO_4Se_2)(H_2O)_3][I]_2$
Formula	$C_{12}H_{30}I_2O_7Se_2Sr$
mwt.	785.70
crystal system	Monoclinic
space group	$P2_1/n$ (14)
a (Å)	10.230(2)
b (Å)	14.005(2)
c (Å)	16.244(3)
α (°)	90
β (°)	91.305(6)
γ (°)	90
U (Å^3)	2326.7(7)
Z	4
μ(Mo Kα) [mm^{-1}]	8.125
F(000)	1480
total no. reflns	19785
unique reflns	5295
R_{int}	0.148
no. of params, restraints	217, 36
R_1[a] [$I_o > 2\sigma(I_o)$]	0.087
R_1 (all data)	0.153
wR_2[a] [$I_o > 2\sigma(I_o)$]	0.204
wR_2(all data)	0.239

[a] $R_1 = \Sigma||F_o| - |F_c||/\Sigma|F_o|$. $wR_2 = [\Sigma w(F_o^2 - F_c^2)^2/\Sigma wF_o^4]^{1/2}$

Common items: temperature = 100K; wavelength (Mo Kα)= 0.71073 Å; θ_{max}= 27.5°

3.6 References

1. A. Earnshaw and N. N. Greenwood, in *Chemistry of the Elements (Second Edition)*, Butterworth-Heinemann, Oxford, 1984, pp. 107

2. S. Mann, *Biomineralisation*, OUP, Oxford, 2001

3. J. Krebs, in *Encyclopedia of Molecular Cell Biology and Molecular Medicine*, Wiley-VCH Verlag GmbH & Co. KGaA, 2006

4. R. G. Robinson, D. F. Preston, M. Schiefelbein and K. G. Baxter, *JAMA*, 1995, **274**, 420

5. P. J. Meunier, C. Roux, E. Seeman, S. Ortolani, J. E. Badurski, T. D. Spector, J. Cannata, A. Balogh, E.-M. Lemmel, S. Pors-Nielsen, R. Rizzoli, H. K. Genant and J.-Y. Reginster, *New Engl. J. Med.*, 2004, **350**, 459

6. S. Fukushima, T. Inoue, T. Inoue and S. Ozeki, *Int. J. Radiat. Oncol.*, 1999, **43**, 597

7. F. A. Cotton, C. Wilikinson, C. A. Murillo and M. Bochmann, *Advanced Inorganic Chemistry, 6th Edition*, Wiley-Interscience, 1999

8. R. D. Rogers, M. L. Jezl and C. B. Bauer, *Inorg. Chem.*, 1994, **33**, 5682

9. B. Cordero, V. Gomez, A. E. Platero-Prats, M. Reves, J. Echeverria, E. Cremades, F. Barragan and S. Alvarez, *Dalton Trans.*, 2008, 2832

10. M. Westerhausen, *Z. Anorg. Allg. Chem.*, 2009, **635**, 13

11. T. P. Hanusa, in *Comprehensive Coord. Chem. II*, eds. J. A. M. Editors-in-Chief: T. J. Meyer, Pergamon, Oxford, 2003, pp. 1

12. S. Harder, *Chem. Rev.*, 2010, **110**, 3852

13. Z. Zhong, S. Schneiderbauer, P. Dijkstra, M. Westerhausen and J. Feijen, *Polym. Bull.*, 2003, **51**, 175

14. I.-H. Park, K.-M. Park and S. S. Lee, *Dalton Trans.*, 2010, **39**, 9696

15. L. F. Lindoy, *The Chemistry of Macrocyclic Ligand Complexes*, Cambridge University Press, Cambridge, UK, 1989

16. W. Levason and G. Reid, in *Comprehensive Coord. Chem. II*, eds. J. A. M. Editors-in-Chief: T. J. Meyer, Pergamon, Oxford, 2003, pp. 399

17. W. Levason and G. Reid, in *Supramol. Chem.*, John Wiley & Sons, Ltd, 2012

18. R. G. Pearson, *C. C./Eng. Tech. Appl. Sci.*, 1986, 18

19. H. Von Arnim, K. Dehnicke, K. Maczek and D. Fenske, *Z. Anorg. Allg. Chem.*, 1993, **619**, 1704

20. M. D. Brown, W. Levason, D. C. Murray, M. C. Popham, G. Reid and M. Webster, *Dalton Trans.*, 2003, 857

21. M. B. Hursthouse, W. Levason, R. Ratnani, G. Reid, H. Stainer and M. Webster, *Polyhedron*, 2005, **24**, 121

22. W. M. Haynes, *CRC Handbook of Chemistry and Physics, 94th Edition (CRC Handbook of Chemistry & Physics)*, CRC Press, 2013

23. A. F. Waters and A. H. White, *Aust. J. Chem.*, 1996, **49**, 27

24. M. Mantina, A. C. Chamberlin, R. Valero, C. J. Cramer and D. G. Truhlar, *J. Phys. Chem. A*, 2009, **113**, 5806

25. A. J. Blake, G. Reid and M. Schroder, *J. Chem. Soc. Chem. Commun.*, 1992, 1074

26. A. L. Hector, W. Levason, G. Reid, M. Webster and W. Zhang, *Dalton Trans.*, 2011, **40**, 694

27. M. J. D. Champion, P. Farina, W. Levason and G. Reid, *Dalton Trans.*, 2013, **42**, 13179

4. Mixed Chalcogenoether Donor Macrocyclic Complexes of Trivalent Scandium and Yttrium

4.1 Introduction

Scandium and yttrium represent the largest d-block metals in their respective Periods. Scandium has a covalent radius of 1.70 Å and a Pauling electronegativity of 1.36, yttrium is heavier and has a radius of 1.90 Å and an electronegativity of 1.20 [1]. In solution they exclusively exhibit only one oxidation state (3+) unlike some of the other heavier rare earth metals [2 3].

With respect to the other d-block elements the coordination chemistry of the two lighter rare earth metals remain the least researched [2 4]. The known complexes tend to stem from the hard and electropositive properties assigned to the two metals i.e. complexes with small hard donors (usually charged) such as F^-, O^{2-}, OH^-, OR^- or NO_3^-, or polydentate nitrogen or oxygen donor ligands [2 4].

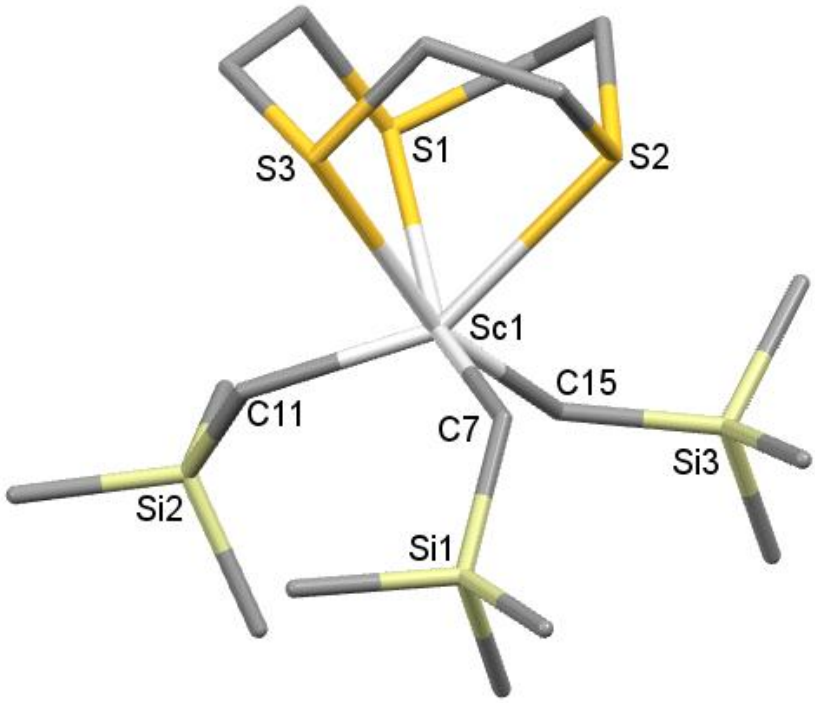

Figure 4.1 Structure of $[Sc(CH_2SiMe_3)_3([9]aneS_3)]$. H atoms are omitted for clarity [5].

Considering the known chemistry and the precepts of HSAB theory it was unlikely that the 3d and 4d rare earth metals [3] would support coordination complexes with neutral soft chalcogenoether donors [6]. Nevertheless in the past 10 years structural authentication of softthioether coordination to Sc(III) has been reported in a family of bis-phenolato thioether linked open-chain ligands (Figure 4.2) [7]. The first sulfur-donor ligand complexes of organoscandium have also been synthesised, $[Sc(CH_2SiMe_3)_3([9]aneS_3)]$ (Figure 4.1) and $[Sc(CH_2SiMe_3)_2([9]aneS_3)(THF)][BPh_4]$ [5] [8]. A comparison of the Sc–S bond distances exhibited is discussed (*vide infra*). More importantly the latter and the open-chain-OSSO scandium complexes are, respectively, active catalysts for olefin polymerisation and ring opening polymerisation of *rac*-lactide [7] [5] [8] [9] [10] [11].

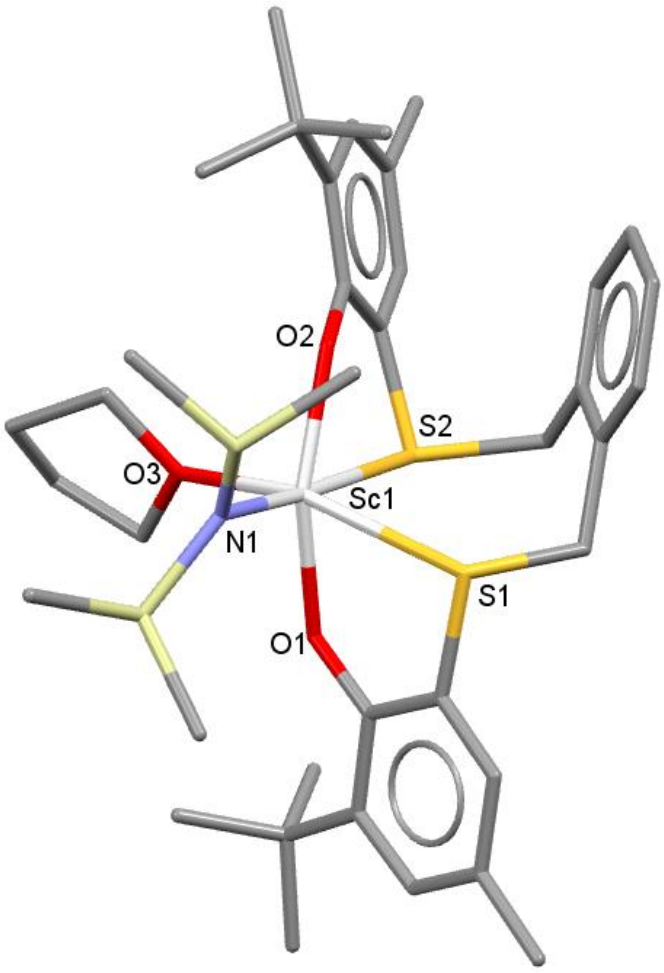

Figure 4.2 Structure of $[Sc(N(SiMe_2)_2)\{(3\text{-}^tBu\text{-}5\text{-}Me\text{-}2\text{-}O\text{-}PhSMe)_2\text{-}benzene\text{-}O,O',S,S'\}(THF)]$. H atoms are omitted for clarity [7].

Also recently published are complexes of the type $[ScCl_3(R\text{-}SNS)]$ (R= ^{t}Bu or ^{n}decyl), the open-chain ligand is tridentate with neutral NS_2 donor atoms coordinated to the scandium(III) chloride. The complexes lack structural authentication but their identities are not in doubt from the spectroscopic and analytical characterisation.

The coordination chemistry of the scandium(III) halides with soft neutral donor ligands has been even less explored and there exist few structural examples of complexes with soft Lewis basic ligands (mainly phosphines) and none with soft chalcogenoethers (despite strong spectroscopic evidence for Sc–S coordination in complexes such as $[ScCl_3(^n\text{decyl-SNS})]$ or $[ScCl_2([18]aneO_4S_2)][FeCl_4]$) [2] [12] [13] [14]. Other complexes include $[ScCl_3(THF)_3]$ (Figure 4.3) [15] which is an incredibly versatile synthon. Scandium(III) chloride complexes such as $[ScCl_2(18\text{-crown-6})][FeCl_4]$ (Figure 4.4) can be accessed through the use of a halide abstractor such as $FeCl_3$ and $[ScCl_3(THF)_3]$ [14]. Neutral $ScCl_3$ complexes can also be accessed by displacement of the THF molecules, readily achieved by multidentate ligands such as R-SNS (R= ^{t}Bu or ^{n}decyl) or Me_3-tacn in acetonitrile [13] [16]. Phophine oxide coordination compounds of $ScCl_3$ have also been made this way [17].

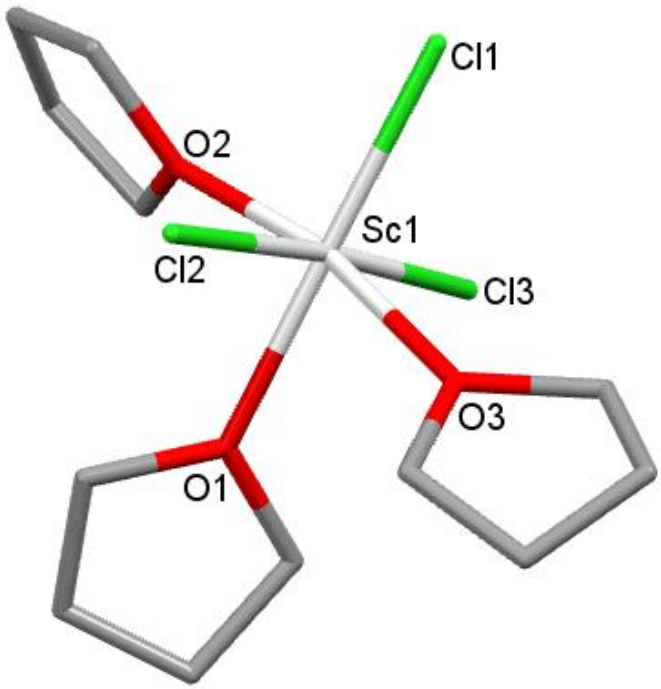

Figure 4.3 Structure of $[ScCl_3(THF)_3]$. H atoms are omitted for clarity [15].

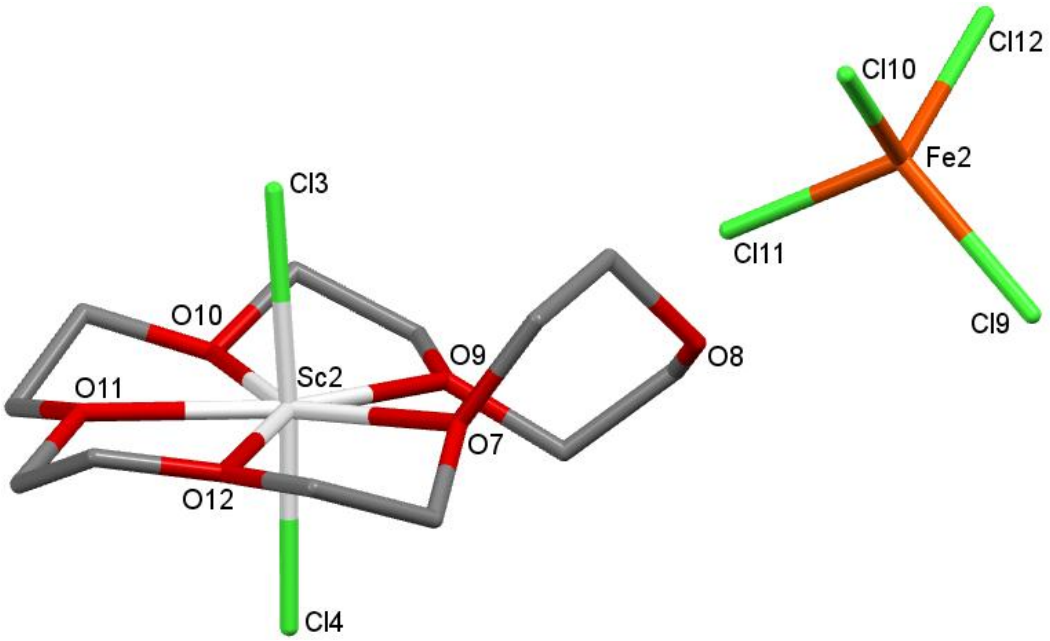

Figure 4.4 Structure of $[ScCl_2(18\text{-crown-6})][FeCl_4]$. H atoms have been omitted for clarity [14].

Examples of thioether coordination to yttrium(III) are more plentiful than for scandium but the area remains equally underdeveloped. Structurally authenticated examples include the analogous (Figure 4.2) bis-phenolato open-chain-OSSO yttrium complexes by Okuda *et al*. and dimeric Y(III) thiolates where the $RSY(X)_2$ units (R= pentyl, phenyl; X= cyclopentadienyl derivatives or functionalised guanadinates) interact with eachother *via* the S-donor atoms [9 18 19 20 21 22 23]. In the latter type the Y–S distances are very similar and it is unclear in the individual systems which is the thiolate-yttrium bond as opposed to the S-coordination interaction. Similar dimers have also been reported with thiophene or isothiocyante groups coordinated and bonded to the Y(III) centres [24 25 26].

An interesting monomeric example of an yttrium(III) monochloride complex with neutral thioether coordination is $[YCl(\eta^5\text{-}CpC_2H_4SC_2H_5)_2]$, this so far represents the only example of soft chalcogenoether coordination to an yttrium(III) halide species [27]. A further discussion on the Y–S bond distances is included below.

4.2 Results and Discussion

4.2.1 Sc(III) coordination chemistry

Anhydrous $ScCl_3$ is a polymeric white powder with a very high associated lattice energy (4901 kJ mol^{-1}) [28]. The compound $[ScCl_3(THF)_3]$ (Figure 4.3) provides a soluble source of monomeric $ScCl_3$ making its coordination chemistry more easily accessible [15]. Using the halide abstractors $SbCl_5$, $FeCl_3$ and $CuCl_2$ is a proven route towards Sc(III) crown ether complexes although the complexes are extremely moisture sensitive, water readily displacing the crown from the primary coordination sphere of the scandium metal [14 29 30 31]. Rigorously anhydrous conditions were essential in the work with the Group 3 complexes.

The first example of a coordinated thioether scandium(III) complex $[ScCl_2([15]aneO_3S_2)][FeCl_4]$ had been made 10 years ago, but lacked structural authentication [14]. The coordination complex's relevance to the present study meant it was remade with the aim to grow X-ray quality single crystals. The yellow compound obtained had the same spectroscopic measurements and seemingly good quality crystals were grown.

The crystal data obtained confirmed the gross structure of the complex, the Sc^{3+} centre is coordinated to all the donors in the plane of the oxa-thia macrocycle with the chlorides mutually *trans* (Figure 4.5). Crystallographic problems were encountered and R_1 failed to give a satisfactory fit (~15%) despite R_{int} being fairly good (~7%). The cause of the poor fit resulted from the number of atoms that lie on the mirror plane, a consequence of the packing intrinsic to the complex. Multiple attempts to grow better crystals resulted in data sets with the same problem.

The same reaction was performed using the larger oxa-thia macrocycle, giving the desired complex, $[ScCl_2([18]aneO_4S_2)][FeCl_4]$. The complex was isolated as a yellow powder. The IR spectrum confirmed the solid was anhydrous and absorptions at 381 and 316 cm^{-1} were assigned to $[FeCl_4]^-$ and Sc–Cl respectively [32]. The ^1H NMR spectrum showed extensively broadened signals all shifted to high frequency and indicative of the macrocycle coordinated to a quadrupolar nucleus (see Chapter 1). Using

different solvents (CD_3CN or d_6-acetone) and variable temperature conditions failed to substantially sharpen the resonances, which can also be indicative of dynamic processes, in the case of the Sc(III) complexes it is unclear whether both or either (the quadrupolar nucleus or dynamic processes) is the causal factor for the substantial line broadening. The results from the ^{45}Sc NMR spectrum are discussed below.

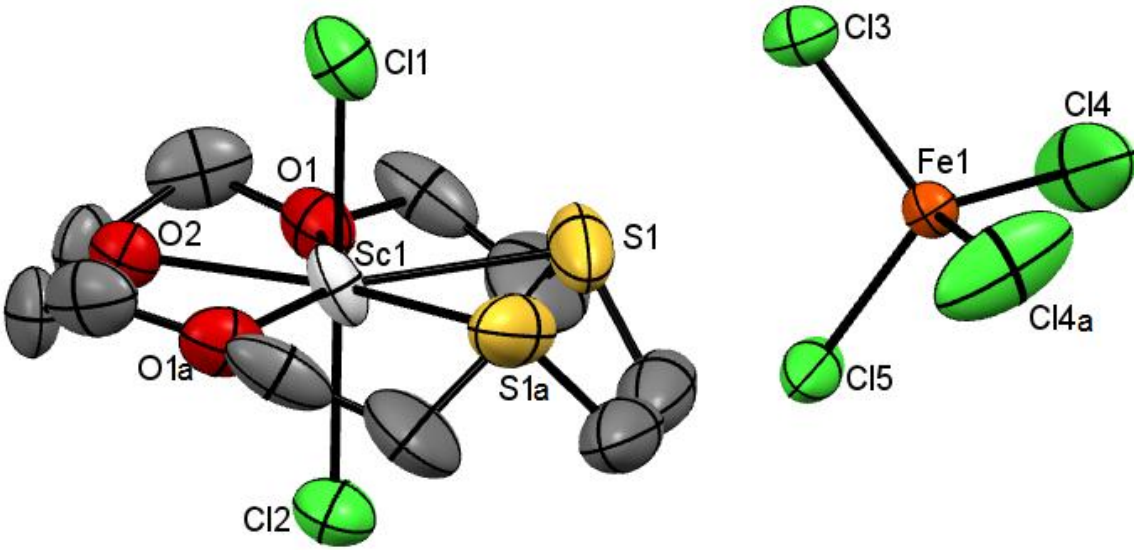

Figure 4.5 Partial structure of $[ScCl_2([15]aneO_3S_2)][FeCl_4]$ showing the atom labelling scheme, (see the discussion regarding data quality). The displacement ellipsoids are drawn at the 40% probability level and H atoms are omitted for clarity. Symmetry operation: a = x, 3/2 – y, z.

Yellow crystals of $[ScCl_2([18]aneO_4S_2)][FeCl_4]$ (Figure 4.6) were grown at 5˚C from $MeCN/CH_2Cl_2$. The structure showed the metal centre encapsulated by the macrocycle, coordinating to all six donors and in further contrast to the 18-crown-6 (Figure 4.4) and $[15]aneO_3S_2$ complex (Figure 4.5) the two chlorides were mutually *cis*. In both oxa-thia structures the R factors were unusually high compared to their R_{int}. In light of this, other related oxa-thia Sc(III) systems were investigated to obtain better quality structural data.

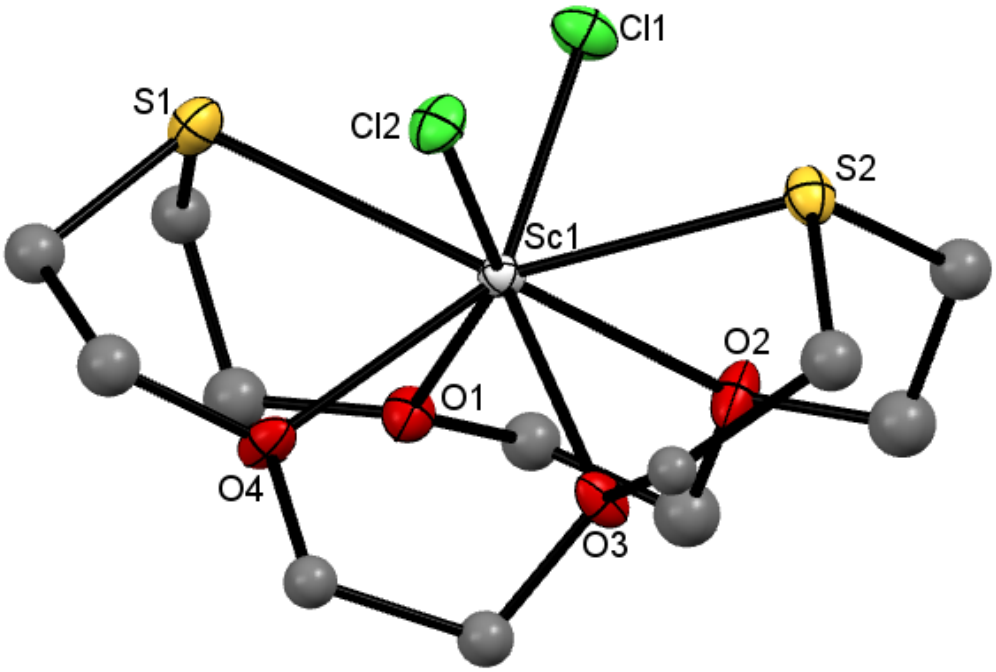

Figure 4.6 Crystal structure of the Sc1 centred cation in $[ScCl_2([18]aneO_4S_2)][FeCl_4]$ showing the atom labelling scheme (see the discussion regarding data quality). The displacement ellipsoids are drawn at the 50% probability level and H atoms are omitted for clarity.

Table 4.1 Selected bond lengths (Å) and angles (°) for $[ScCl_2([18]aneO_4S_2)][FeCl_4]$

Sc1–S1	2.753(3)	S1–Sc1–S2	140.0(1)
Sc1–S2	2.734(3)	S1–Sc1–O1	74.5(2)
Sc1–O1	2.247(8)	O1–Sc1–O2	67.8(3)
Sc1–O2	2.436(8)	S2–Sc1–O2	69.3(2)
Sc1–O3	2.255(8)	S2–Sc1–O3	70.3(2)
Sc1–O4	2.389(8)	O3–Sc1–O4	70.7(3)
Sc1–Cl1	2.422(3)	S1–Sc1–O4	69.2(2)
Sc1–Cl2	2.466(3)	Cl1–Sc1–Cl2	97.7(1)

Using $SbCl_5$ instead as the halide abstractor concluded in an analogous situation to that described in Chapter 3, where reduction of Sb(V) resulted in isolation of $[SbCl_2([18]aneO_4S_2)][SbCl_6]$ (see Chapter 7).

The strategy described in Chapter 3 of moving from metal chlorides to metal iodides to take advantage of the lower associated lattice energies allowed for an entry into the oxa-thia/selena macrocycle coordination chemistry of Ca(II) and Sr(II). The same strategy was therefore employed for Sc(III). ScI_3 is a yellow crystalline solid that is insoluble in acetonitrile at room temperature (unlike CaI_2) and it has an associated lattice energy of 4640 kJ mol^{-1} (calculated) [28]. ScI_3 was dissolved in MeCN in the presence of the dissolved oxa-thia macrocycles and, upon working up the reactions, the respective scandium(III) macrocycle complexes were isolated, in good yield as yellow solids.

$[ScI_2([18]aneO_4S_2)][I]$ (Figure 4.7) had comparable spectroscopic measurements to $[ScCl_2([18]aneO_4S_2)][FeCl_4]$ (Figure 4.6), both yellow solids were anhydrous and had broadened ^1H NMR resonances shifted to high frequency. X-ray quality crystals of the iodide complex were grown by slow evaporation of the acetonitrile solvent under N_2.

The structure identified a very similar cation $[ScX_2([18]aneO_4S_2)]^+$ (X= I or Cl), making a definitive case for the chloride analogue being a scandium(III) oxa-thia macrocycle coordination complex rather than an iron complex, an uncertainty that would not have arisen had the quality of the previous structures been better. Analysis of the yttrium(III) complex, $[YCl_2([18]aneO_4S_2)][FeCl_4]$ (Figure 4.9) discussed below, gives further credence to this determination. The difference between the M–S bonds (M= Sc, Y; Sc–S= 2.743 and Y–S= 2.905 Å) is close to the difference in covalent radii for Sc and Y (0.2 Å). The Sc–S coordination bond is also just within the sum of the covalent radii for Sc and S (2.75 Å) [1] which further highlights the validity of the hard scandium(III) to soft neutral sulfur donor coordination bond. A calculated Van der Waals radius for Sc is not available, but it can be assumed the mean bond lengths are substantially within the ΣVdW radii for Sc and S; (the ΣVdW radii for Ca and S is 4.11 Å, Ca being in the adjacent Group and same Period) [33].

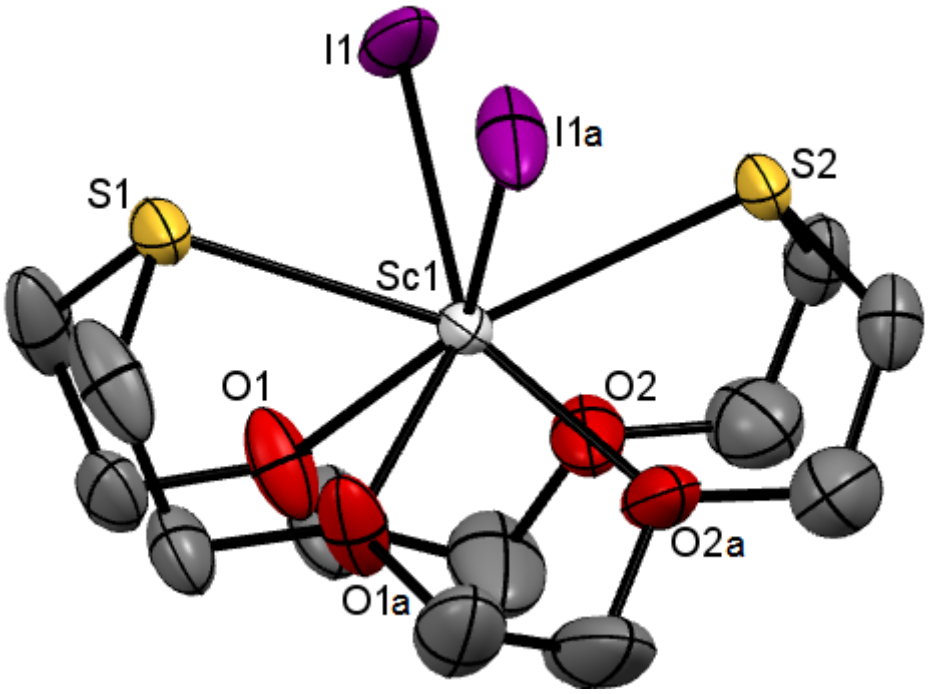

Figure 4.7 Crystal structure of the cation in $[ScI_2([18]aneO_4S_2)][I]\cdot MeCN$ showing the atom labelling scheme. The displacement ellipsoids are drawn at the 40% probability level and H atoms are omitted for clarity. Symmetry operation: a = x, 1/2 – y, z.

Table 4.2 Selected bond lengths (Å) and angles (°) for $[ScI_2([18]aneO_4S_2)][I]\cdot MeCN$

Sc1–S1	2.711(5)	S1–Sc1–S2	137.1(1)
Sc1–S2	2.715(4)	S1–Sc1–O1	71.8(2)
Sc1–O1	2.272(9)	O1–Sc1–O2	69.0(3)
Sc1–O2	2.263(9)	S2–Sc1–O2	70.6(3)
Sc1–I1	2.915(2)	I1–Sc1–I1a	94.03(8)

Since the initial synthesis of $[ScCl_2([15]aneO_3S_2)][FeCl_4]$ (Figure 4.5) there have been a few crystallographically authenticated examples of soft thioether donation to Sc(III), including the first example of a Sc catalyst supported by an all-sulfur macrocyclic donor set. Comparing the scandium(III) oxa-thia macrocycle structures from this study with the few other thioether scandium(III) complexes show the Sc–S bond lengths to be fairly similar. The average Sc–S distance in $[Sc(CH_2SiMe_3)_3([9]aneS_3)]$

(Figure 4.1) and in the benzene derivative of the bis-phenolate scandium(III) complex (open chain ligand with an OSSO donor set) are both similarly ~2.79 Å [5 7]. Moving to monocationic Sc(III) species such as the cations in the scandium complexes reported in this study and $[Sc(CH_2SiMe_3)_2([9]aneS_3)(THF)]^+$ have on average marginally shorter Sc-S interactions, 2.713 Å in the iodide (Figure 4.7) and ~2.74 Å for the other two.

Comparisons with the analogous 18-crown-6 complex $[ScCl_2(18\text{-crown-}6)][X]$ ([X]= $[SbCl_6]^-$ or $[FeCl_4]^-$) shows a different conformation of the $ScCl_2^+$ cation centre. In the crown ether complex the Sc(III) centre coordinates in a plane to only five of the available six O-donors in the macrocycle with the chlorides arranged mutually *trans* (Figure 4.4) [14]. There is a close likeness to the gross structure of $[ScCl_2([15]aneO_3S_2)]^+$ (Figure 4.5) and suggests the Sc prefers a pentagonal bipyramidal geometry with both of these macrocyclic ligands.

In contrast, the 18-membered oxa-thia macrocycle $[18]aneO_4S_2$ forms hexadentate complexes with Sc(III) where the co-ligands are arranged mutually *cis*. A possible reasoning for the difference is the longer Sc–S bond (~2.74 Å); (see Chapter 1 relating to $CrCl_3$ and VCl_3 thioether and crown ether complexes) [34]. In the scandium(III) oxa-thia macrocycle systems the longer Sc-E (E= S, O) distances compared to the Sc-O in the crown complex (oxa-thia crown complex= 2.247(8)-2.435(8); crown complex= 2.195(2)-2.264(2) Å) allows for all six macrocyclic donors to be accommodated by the small scandium centre (1.70 Å) [1].

For the remaining scandium(III) complexes crystallographic authentication was precluded by the difficulties in producing single X-ray quality crystals, there remains strong spectroscopic evidence for the formation of these complexes and the credibility of their reported soft donor interactions with Sc(III).

$[ScI_2([15]aneO_3S_2)][I]$ was made by suspending ScI_3 in acetonitrile and adding the ligand. The reaction resulted in a light yellow powder. The ^1H NMR spectrum showed complicated and very broad signals significantly shifted from the free ligand, some evidence for a small amount of the free ligand is present but the solid analyses with the stated composition and

the IR spectrum confirms it is anhydrous. Most likely trace water present in the deuterated solvent causes hydrolysis of some of the dissolved complex generating small amounts of free ligand.

Neutral selenoether coordination to scandium(III) is unknown in the literature. The reaction of $[ScCl_3(THF)_3]$, $FeCl_3$ and $[18]aneO_4Se_2$ in acetonitrile gave the extremely moisture sensitive and ochre solid, $[ScCl_2([18]aneO_4Se_2)][FeCl_4]$. Making the analogous iodide complex $[ScI_2([18]aneO_4Se_2)][I]$ was less straightforward. Unlike the oxa-thia crowns, the oxa-selena macrocycle was unable to solubilise ScI_3 (a large amount of unreacted starting material remained upon addition of the macrocycle). An alternative route involved heating the scandium(III) iodide/acetonitrile suspension under reflux at 83°C for a few hours, eventually a clear yellow solution remained which did not precipitate a solid on cooling to room temperature. Reacting this solution (presumed to be of a $ScI_3 \cdot (MeCN)_n$ adduct) with the oxa-selena crown gave the desired complex, an ochre solid with the constitution $[ScI_2([18]aneO_4Se_2)][I]$.

Both complexes represent the first evidence for Sc–Se coordination in a neutral ligand system. The ^1H NMR spectra had complicated and broadened resonances which were difficult to interpret, but clearly showed the ligand present and coordinated. Both solids were anhydrous and the respective bands for $[FeCl_4]^-$ and Sc–Cl (388 and 317 cm^{-1}) were present in the IR spectrum of the chloride complex. For the iodide $^{77}Se\{^1H\}$ NMR resonances were not observed (presumably due to exchange processes), but for the chloride a $^{77}Se\{^1H\}$ NMR resonance (CD_3CN) was seen at +150 ppm compared to the "free" ligand resonance at +140 ppm which is evidence the Sc–Se interactions are retained in solution. The ^{77}Se NMR data allows for the identification of a Sc–Se interaction in the absence of adequate structural data. The related Y(III) selenoether complexes are discussed below.

The reaction with the related oxa-tellura macrocycle gave a unique example of an $[18]aneO_4Te_2$ complex. The extremely sensitive brown solid had a composition corresponding to $[ScCl_2([18]aneO_4Te_2)][FeCl_4]$. The IR spectrum showed the presence of the ligand and the absence of THF or MeCN, also present were absorbances at 378 and 324 cm^{-1} which further support the formulation ($[FeCl_4]^-$ and vSc–Cl respectively). Monitoring of

the IR spectra from a freshly prepared sample left to stand in air showed the incremental presence of water and a diminishing of the $[FeCl_4]^-$ band, as expected the complex was extremely moisture sensitive and rapidly decomposed in air to a black solid. Further to this, a solution in CD_3CN rapidly darkens and deposits black tellurium (the same happens in CD_2Cl_2 but on a longer timescale, attributed to the complex's poor solubility in the halocarbon solvent). It was possible to obtain a ^1H NMR spectrum from a solution of CD_3CN made up at 240 K and recorded immediately, the features attributed to the methylene protons in the oxa-tellura macrocycle were evident (δ 3.74 [16H] and 4.19 [8H]) albeit substantially broadened. On standing, the solution deposited a black precipitate (elemental Te), and new resonances appeared, including a doublet at ~5.5 ppm which is in the region for vinyllic protons. [18]aneO_4Te_2 contains reactive Te–C bonds, present on the ethylene bridged Te donors, which have been shown to readily undergo elimination of ethene in other systems [35] [36]. Sc(III) seems to be borderline case in that a complex precipitates from the concentrated synthesis solution but decomposes in dilute solutions. This contrasts with the reactions with Group 2 acceptors were the macrocycle remains in solution unreacted (Chapter 3) and the Pb(II) and Sb(III) chemistry where the ring was immediately cleaved (Chapters 5 and 7).

An unusual characteristic of these complexes is the unexpected colours of the isolated solids. The oxa-thia macrocyclic complexes, $[ScCl_2([18]aneO_4S_2)][FeCl_4]$ and $[ScCl_2([15]aneO_3S_2)][FeCl_4]$, are both yellow and at first this colouration was attributed to the presence of the $[FeCl_4]^-$ anion; anions have been known to give coloured complexes with metals that lack incompletely filled d-orbitals (e.g. [Ca(2,6-^{i}PrC_6H_3-BIAN)$(THF)_4$] [37]), also Sc(III) complexes tend to be colourless due to the metal centre having an electronic configuration of $[Ar]3d^04s^0$ and hence no d-d transitions.

However, $[ScCl_2$(18-crown-6)$][FeCl_4]$ is a white solid, further to this, structural authentication of the Sc–S interaction and synthesis of the progressively darker coloured heavier mixed donor chalcogenoether macrocyclic scandium(III) complexes lead to a reassessment of the possible colour origins in these complexes.

The solids $[ScCl_2([18]aneO_4E_2)][FeCl_4]$ change colour depending on the nature of E (E= O, white; S, yellow; Se, ochre; Te, brown). The trend was ascribed to the increasing charge transfer to the metal by the exchanging of the Group 16 donor atoms. The starting macrocycles* and $[ScCl_3(THF)_3]$ are white solids (*apart from $[18]aneO_4Te_2$ which is orange) and $FeCl_3$ is a dark powder i.e. completely different to the end products. Similar colour changes were noticed for the iodide systems and the reported $[ScCl_3(R\text{-}SNS)]$ (R= ^{t}Bu or ^{n}decyl) complexes are yellow ($ScCl_3$ and the SNS-ligands are colourless; the related $[ScCl_3(Me_3\text{-}tacn)]$ complex is a white solid). Like in the Ca(II) systems (see Chapter 3) the observed colours provide a possible qualitative indication of increased soft chalcogenoether coordination to the hard Lewis acidic centres.

Attempts to increase the ratio of thioether donors at Sc(III) halides further was achieved in the complexes $[ScCl_2([18]aneO_2S_4)][FeCl_4]$ and $[ScI_3([9]aneS_3)]$.

$[ScCl_2([18]aneO_2S_4)][FeCl_4]$ was made similarly to the other related complexes. It is an extremely sensitive yellow solid which readily reacts with water as seen by the IR spectrum, also in the spectrum were bands for the $[FeCl_4]^-$ anion and Sc-Cl bond (379 and 328 cm^{-1}). The initially isolated solid is anhydrous and analyses with the given composition. The ^{1}H NMR spectrum shows a pair of resonances substantially broadened and modestly shifted to low frequency from the free ligand. Attempts to grow crystals only resulted in recovery of the free ligand.

Heating ScI_3 and $[9]aneS_3$ in acetonitrile gave a light orange powder that analysed as the complex $[ScI_3([9]aneS_3)]$. The ^{1}H NMR spectrum is more complicated, as well as a resonance at 3.09 ppm ($C\boldsymbol{H}_2$ in $[9]aneS_3$) there were two substantial signals between 6.5-6.9 ppm. It has been shown in $[M([9]aneS_3)_2]^{3+}$ (M= Co, Rh or Ir) systems that the metal is capable of deprotonating one of the methylene groups on a thiacrown producing a vinyl thioether; the complex $[Rh([9]aneS_3)(H_2C{=}CHS(CH_2)_2S(CH_2)_2S)]$ is structurally authenticated; the ^{1}H NMR spectra for these systems exhibit chemical shifts at δ 6.2 (m, [2H]) and 6.6 (dd, [1H]) in addition to the thioether methylene protons (2.8-4.0 ppm) [38]. In the present case the resonances do not fit the expected 1:2:20 ratio for an analogous Sc(III)

vinyl thioether complex and the origin of these high frequency shifts remains ambiguous. Attempts to grow a crystal for analysis resulted in only white crystals of [9]aneS_3.

Reactions attempted with other thiacrowns ([14]aneS_4 and [16]aneS_4) proved unsuccessful with some evidence that the iron (from $FeCl_3$) was binding preferentially.

4.2.1.1 ^{45}Sc NMR spectroscopic studies

A powerful technique for characterising scandium complexes is ^{45}Sc NMR spectroscopy due to the 100% abundance and high sensitivity of the nucleus (R_c= 0.302, Ξ= 24.5 MHz, Q= -0.22 x 10^{-28} m^2). The chemical shifts seen for the systems described above as well as those of relevant scandium(III) crown complexes are detailed in Table 4.3.

Table 4.3 Table showing ^{45}Sc NMR shifts (δ) for Sc(III)-macrocycle complexes.

Sc(III) Complex	^{45}Sc (δ)
$[Sc(12\text{-crown-}4)_2]^{3+}$ [39]	26
$[ScCl(MeCN)(15\text{-crown-}5)][SbCl_6]_2$ [14]	99.5
$[ScCl_2(15\text{-crown-}5)][SbCl_6]$ [40]	128
$[ScCl_2(18\text{-crown-}6)][FeCl_4]$ [30]	132
$[ScCl_2([15]aneO_3S_2)][FeCl_4]$ [14, 40]	200
$[ScCl_2([18]aneO_4S_2)][FeCl_4]$	204
$[ScCl_2([18]aneO_4Se_2)][FeCl_4]$	204
$[ScCl_2([18]aneO_4Te_2)][FeCl_4]$	*–
$[ScCl_2([18]aneO_2S_4)][FeCl_4]$	**256
$[ScI_2([15]aneO_3S_2)][I]$	297
$[ScI_2([18]aneO_4S_2)][I]$	*207
$[ScI_2([18]aneO_4Se_2)][I]$	n.o.
$[ScI_3([9]aneS_3]$	371

All samples run in CD_3CN/MeCN; n.o. not observed; * See Discussion; ** run in CD_2Cl_2/CH_2Cl_2

In the $[ScCl_2(S/O\text{-macrocycle})][FeCl_4]$ systems the replacement of oxygen donors for sulfur donors produces a high frequency shift (~70 ppm) from the analogous crown ether complexes. Comparing $[ScI_2([15]aneO_3S_2)][I]$ and $[ScCl_2([15]aneO_3S_2)][FeCl_4]$ (Figure 4.5) also shows a high frequency shift in the iodide, this is consistent with similar shifts that have been seen in corresponding scandium halide-phosphine oxide complexes.

Surprisingly, for $[ScI_2([18]aneO_4S_2)][I]$ (Figure 4.7) a shift at δ 207 was observed. This contrasts from an expected higher frequency shift due to the coordinated iodide. It is possible that in solution in this system the iodides are displaced by the acetonitrile solvent giving an $N_2O_4S_2$ donor environment around the scandium which would produce a significant low frequency shift. The oxa-selena complex $[ScCl_2([18]aneO_4Se_2)][FeCl_4]$ has a similar chemical shift to $[ScCl_2([18]aneO_4S_2)][FeCl_4]$ (Figure 4.6), indicating that the two related macrocycles have a similar effect on the ^{45}Sc nucleus.

Due to the instability of $[ScCl_2([18]aneO_4Te_2)][FeCl_4]$ system the data from the ^{45}Sc NMR spectroscopy was analysed more tentatively. Despite quickly making the sample and running the NMR experiment at 240 K a cogent spectrum was not obtained.

Increasing the ratio of sulfur donors at Sc(III) also produces a high frequency shift in the complex $[ScCl_2([18]aneO_2S_4)][FeCl_4]$ which is consistent with the previous ^{45}Sc data. For $[ScI_2([18]aneO_4Se_2)][I]$ a resonance was not observed and it is likely exchange processes are the cause; a ^{45}Sc NMR resonance was not observed for a solution of $ScI_3 \cdot (MeCN)_n$. The highest observed shift was for the half-sandwich complex $[ScI_3([9]aneS_3]$ (δ 371) which is consistent with an I_3S_3 scandium environment. Despite the promising results there are still few data for ^{45}Sc NMR shifts which limits the number of relevant comparisons that can be made.

4.2.1.2 $[ScCl_3(MeCN)_3]$

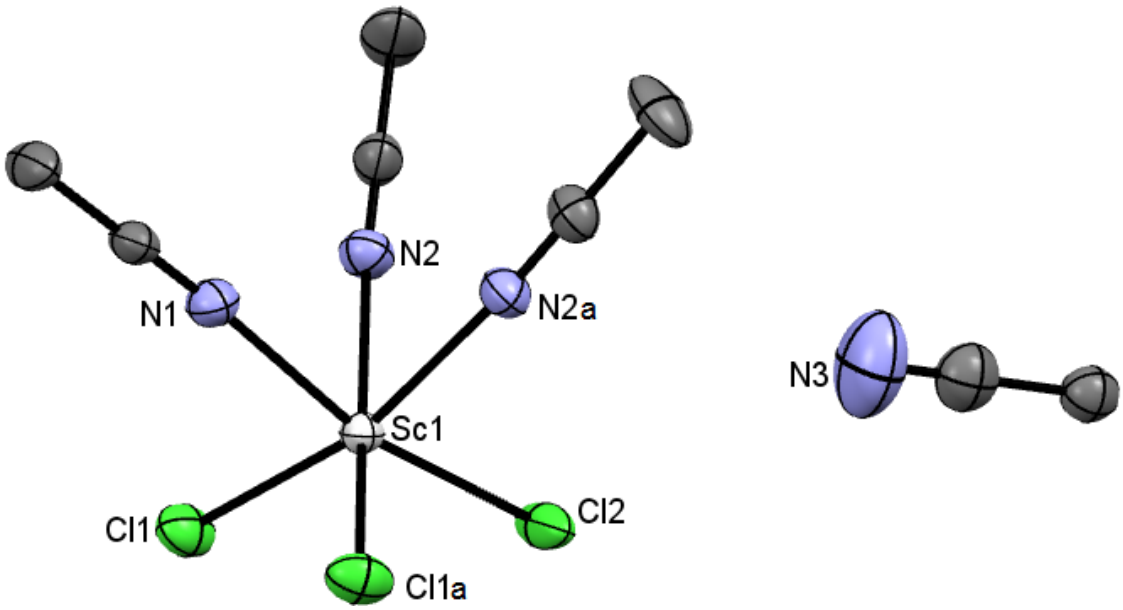

Figure 4.8 Crystal structure of $[ScCl_3(MeCN)_3]\cdot MeCN$ showing the atom labelling scheme. The displacement ellipsoids are drawn at the 50% probability level and H atoms are omitted for clarity. Symmetry operation: a = x, y, 1/2 – z.

Table 4.4 Selected bond lengths (Å) and angles (°) for $[ScCl_3(MeCN)_3]\cdot MeCN$

Sc1–Cl1	2.387(1)	N1–Sc1–N2	81.0(1)
Sc1–Cl2	2.393(2)	N2–Sc1–N2a	77.8(1)
Sc1–N1	2.265(4)	N1–Sc1–Cl1	89.1(1)
Sc1–N2	2.295(3)	Cl1–Sc1–Cl1a	98.44(4)
		Cl1–Sc1–Cl2	99.04(5)
		Cl2–Sc1–N2	89.23(8)

Crystals of the title complex (Figure 4.8) were serendipitously formed in the unsuccesful reaction of $[ScCl_3(THF)_3]$ and the open-chain ligand $MeS(CH_2)_2O(CH_2)_2SMe$ in acetonitrile. Direct attempts, (dissolving $[ScCl_3(THF)_3]$ in acetonitrile and concentrating), to obtain a bulk sample were unsuccessful in that there remained some THF in the isolated white solids. The crystals were extremely sensitive and readily decomposed to white powders even when handling under Fomblin™. The ^{45}Sc NMR of

$[ScCl_3(THF)_3]$ in CD_3CN shows more than one species present (only one is present in CD_2Cl_2 δ 204). In light of the structure these extra resonances (δ 210 and 197) can be attributed to the mixed acetonitrile/THF derivatives. The structure and in some part the ^{45}Sc NMR data are evidence for the species being formed *in situ*.

An interesting comparison between the two structures $[ScCl_3(THF)_3]$ (Figure 4.3) [15] and $[ScCl_3(MeCN)_3]$ (Figure 4.8), is in their arrangement of the ligands, the THF analogue is the *mer*-isomer whereas the acetonitrile analogue exists as the *fac*-complex. This rearrangement may reflect the reduced steric requirement of the linear MeCN relative to the bulkier THF, although the inter-ligand angles are more disparate from the idealised octahedral geometry in the acetonitrile adduct, crystal packing and the *trans* influence cannot be discounted either; alternatively the respective *fac*- and *mer*-complexes are the least soluble isomers which then crystallise out of the solutions.

4.2.2 Y(III) coordination complexes

As with the case of $[ScCl_3(THF)_3]$, the complex $[YCl_2(THF)_5][YCl_4(THF)_2]$ provided a soluble source of yttrium(III) chloride. Preliminary studies into the analogous yttrium(III) oxa-thia macrocycle complexes resulted in two new complexes, $[YCl_2([18]aneO_4S_2)][FeCl_4]$ and $[YCl_2([15]aneO_3S_2)][FeCl_4]$.

The spectroscopic data for both complexes closely match the respective scandium analogues. Both the IR and ^1H NMR spectra for $[YCl_2([15]aneO_3S_2)][FeCl_4]$ confirm the stated composition. In the IR spectrum a band at 381 cm^{-1} corresponds to $[FeCl_4]^-$ and one at 262 cm^{-1} to Y–Cl. The ^1H NMR spectrum shows very broadened resonances of the ligand. Attempts to grow crystals only gave amorphous yellow solids.

$[YCl_2([18]aneO_4S_2)][FeCl_4]$ (Figure 4.9) was made similarly. The IR spectrum had the expected bands (375 and 265 cm^{-1}) and the ^1H NMR spectrum showed the ligand resonances significantly shifted to high frequency and increasingly broadened. Yellow crystals were successfully grown by dissolving the solid in acetonitrile and slow evaporation of the solvent under N_2.

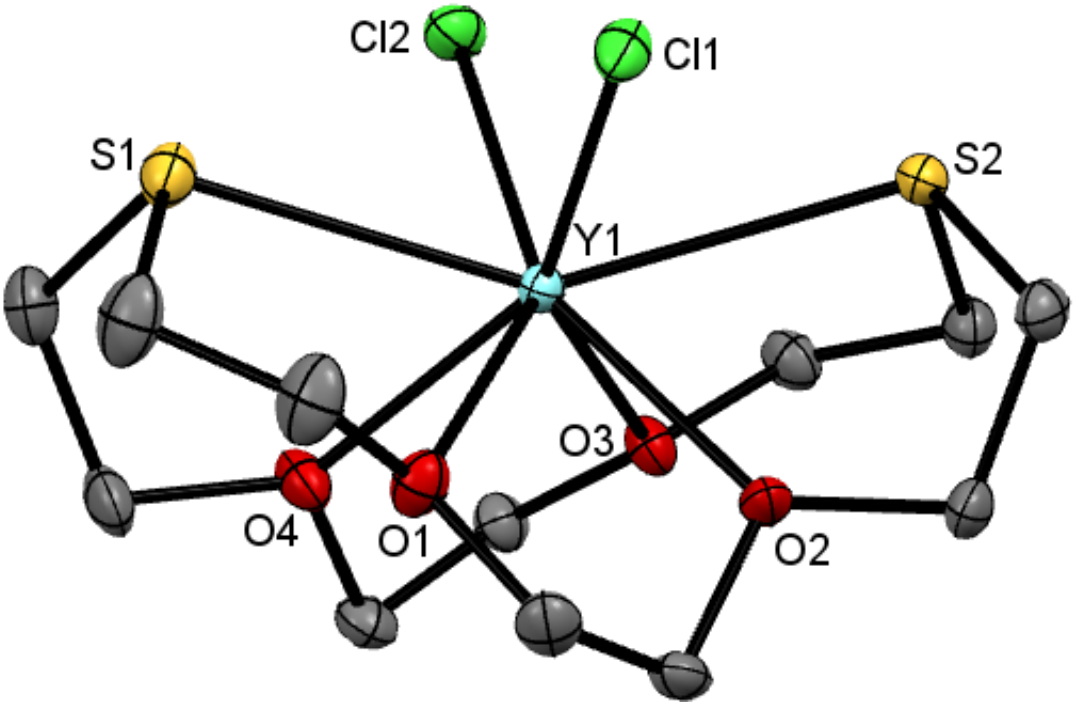

Figure 4.9 Crystal structure of the cation in $[YCl_2([18]aneO_4S_2)][FeCl_4]$ showing the atom labelling scheme. The displacement ellipsoids are drawn at the 50% probability level and H atoms are omitted for clarity.

Table 4.5 Selected bond lengths (Å) and angles (°) for $[YCl_2([18]aneO_4S_2)][FeCl_4]$

Y1–S1	2.9163(7)	S1–Y1–S2	148.33(2)
Y1–S2	2.8954(8)	S1–Y1–O1	66.58(4)
Y1–O1	2.491(2)	O1–Y1–O2	66.42(6)
Y1–O2	2.365(2)	S2–Y1–O2	68.09(4)
Y1–O3	2.470(2)	S2–Y1–O3	68.25(4)
Y1–O4	2.401(2)	O3–Y1–O4	67.14(6)
Y1–Cl1	2.5914(8)	S1–Y1–O4	69.20(4)
Y1–Cl2	2.5683(8)	Cl1–Y1–Cl2	94.64(2)

The analogous crown ether and oxa-selena crown yttrium(III) halide complexes were synthesised by M. Champion and serve as useful comparisons [41]. $[YCl_2(18\text{-crown-6})]_3[Y_2Cl_9]$ is an interesting complex in that it has two structural isomers for the $[YCl_2(18\text{-crown-6})]^+$ cation. Both

isomeric cations have similar O–Y–O and Y–O angles and distances. They differ mainly in the arrangement of the Cl^- co-ligands and the conformation of the macrocyclic framework. The *trans* chloride arrangement (Figure 4.11) has a very buckled crown where all the O-donors are bound to the Y(III) centre, this contrasts the smaller Sc(III) which only coordinates κ^5-18-crown-6 (Figure 4.4). The other isomer (Figure 4.10) has a very familiar motif (although unusual for 18-crown-6) with the metal centre being encapsulated by the folded-ring bound to all the macrocyclic donors and the co-ligands *cisoidal*. The Y(III) is large enough to stabilise both conformers and coordinate to all the ring donors.

In $[YCl_2([18]aneO_4S_2)][FeCl_4]$ (Figure 4.9) the Cl–Y–Cl angle is 94.6° and in *cis*-$[YCl_2(18\text{-crown-6})]^+$ (Figure 4.10) it is more acute 89.5°. The Y–O bond lengths in the crown ether complex are all very similar (2.413(4)-2.451(4) Å), but more disparate in the oxa-thia complex (2.365(2)-2.491(2) Å). The average Y–O distance is 2.41 Å and is significantly shorter than the average Y–S bonds (2.91 Å).

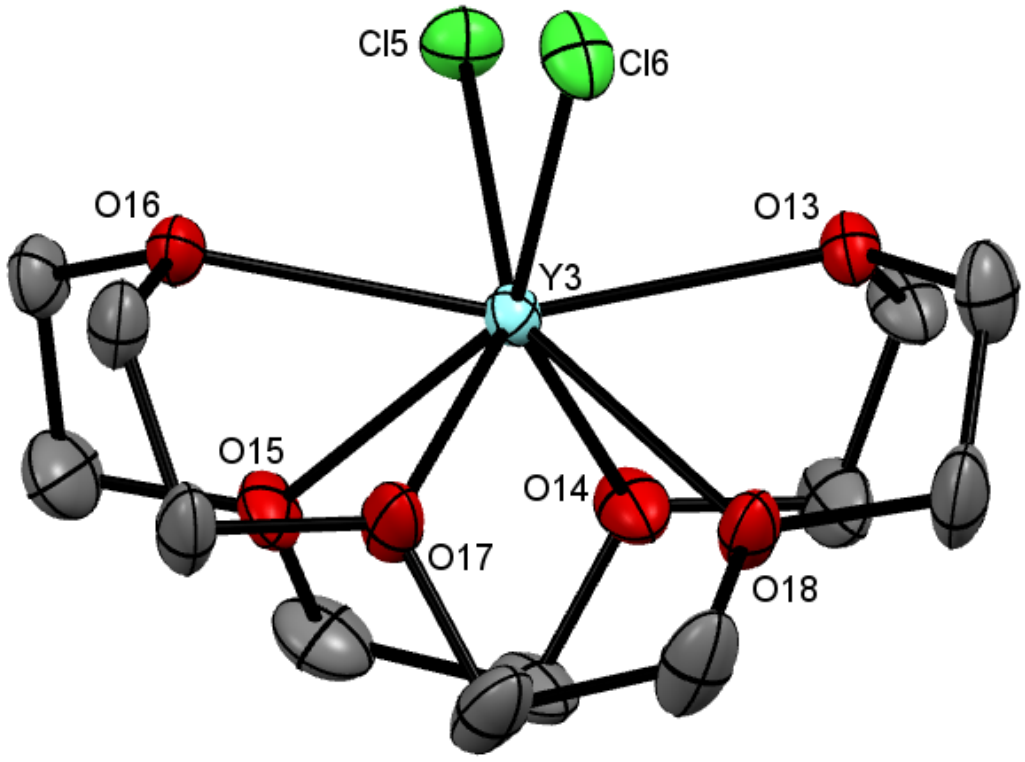

Figure 4.10 Crystal structure of *cis*-$[YCl_2(18\text{-crown-6})]^+$. H atoms omitted for clarity.

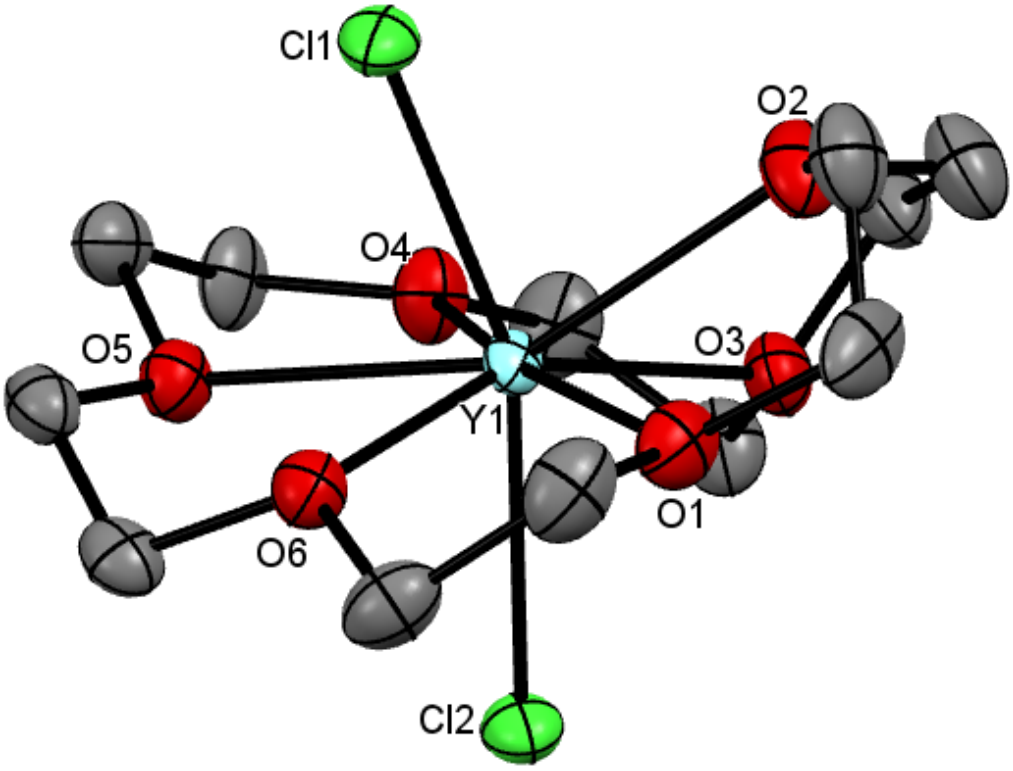

Figure 4.11 Crystal structure of *trans*-[YCl_2(18-crown-6)]$^+$. H atoms omitted for clarity.

The selenoether complexes [YCl_2([18]aneO$_4$Se$_2$)][$FeCl_4$] and [YI_2([18]aneO$_4$Se$_2$)][I] have not been structurally authenticated, but their identities are not in doubt from the spectroscopic and analytical characterisation. ^{77}Se NMR data have also been recorded. Both complexes exhibit low frequency coordination shifts from the free ligand (δ= 103 and 125, respectively), this contrasts the scandium analogues (see above).

Comparison of the Y–S bonds in [YCl_2([18]aneO$_4$S$_2$)][$FeCl_4$] with those in the literature show they are very similar. The closest structurally authenticated example is [YCl(η^5-Cp$C_2H_4SC_2H_5)_2$] where the Y–S bond distances are 2.938(7) and 2.957(6) Å which are marginally longer, the Y–Cl bond is also longer at 2.607(7) Å [27]. The bond lengths in the Okuda *et al* yttrium(III) OSSO-systems vary from 2.83 to 2.97 Å [9 18 19 20]. The dimeric yttrium(III) thiolate systems have Y–S interactions ranging from 2.74 to 2.90 Å but it is difficult to compare these data to the other neutral coordinated systems as the distinction between the yttrium thiolate function from the coordinated neutral sulfur bond is ambiguous in these systems [21 22 23]. In all the examples reported, the Y–S bonds are

within the sum of the covalent radii for Y and S (2.95 Å) indicating the Y(III) centre has a definitive affinity for the softer sulfur donor.

4.3 Conclusions

Rare examples of crystallographically authenticated soft neutral thioether coordination to the hard early rare earth metal trications Sc(III) and Y(III)[3] have been reported. Also the first evidence for possible selenoether and telluroether coordination to scandium(III) is presented, demonstrating the metal centre can likely accommodate (under the appropriate conditions) a much wider range of Lewis bases than previously thought.

The unusually coloured complexes are the first series of mixed chalcogenoether macrocycle complexes with the harder scandium(III) halides. $[ScCl_2([18]aneO_2S_4)][FeCl_4]$ is believed to contain four thioether donor groups coordinated to the scandium centre, although this still requires structural authentication; prior to this the maximum number of thioethers coordinated in any Sc(III) complex was three. Examination of the Sc–S and Y–S distances further suggests an evident affinity for the sulfur ligand, being within the sum of the covalent radii for S and the respective metal, which is at odds with HSAB theory [6]. The different colours of the isolated solids also proved to be a qualitative indicator for soft chalcogenoether coordination to Sc/Y(III).

The literature reports many of the scandium/yttrium-thioether complexes exhibit catalytic activity. The 18-membered oxa-thia macrocycles preorganise the co-ligands at scandium(III) in a *cisoidal* fashion. A prerequisite of many catalytic cycles is the presence of two mutually *cis* binding sites. The complexes presented could represent preliminary designs for future Sc/Y(III) catalysts.

A set of empirical data for ^{45}Sc NMR shifts has been catalogued and provide useful comparisons for a wider range of donor environments for Sc(III) in solution. Due to the limited range and comparable data in the literature this study has considerably increased the knowledge base in this area.

The species $[ScCl_3(MeCN)_3]$, with mutually *fac* Cl ligands, has been structurally authenticated, until now its formation was only presumed *in situ*.

4.4 Experimental

4.4.1 **[$ScCl_2$([15]aneO_3S_2)][$FeCl_4$]:** $ScCl_3(THF)_3$ (0.060 g, 1.63 x 10^{-4} mol) and $FeCl_3$ (0.027 g, 1.63 x 10^{-4} mol) were dissolved together in MeCN (15 mL) and left to stir for 1 h. [15]aneO_3S_2 (0.042 g, 1.63 x 10^{-4} mol) was then added, and the yellow solution was allowed to stir overnight at room temperature. The volatiles were removed and the remaining yellow solid washed with CH_2Cl_2, filtered and dried *in vacuo*. Yield: 0.038 g, 41%. Crystals grown by dissolving in MeCN and slow evaporation of the solvent. Required for $C_{10}H_{20}Cl_6FeO_3S_2Sc$ (565.61): C, 21.22; H, 3.56. Found: C, 21.56; H, 4.10%. IR (Nujol, cm^{-1}): 380 ($FeCl_4$), 293 (ScCl). ^{1}H NMR (CD_3CN, 293K): δ 3.55 (v.br, SC***H***$_2$), 3.77 (v.br, SC***H***$_2$), 4.34 (v.br, OC***H***$_2$), 4.48 (v.br, OC***H***$_2$). ^{45}Sc NMR (CD_3CN/MeCN, 298K): δ 201.

4.4.2 **[$ScCl_2$([18]aneO_4S_2)][$FeCl_4$]:** $ScCl_3(THF)_3$ (0.060 g, 1.63 x 10^{-4} mol) and $FeCl_3$ (0.027 g, 1.63 x 10^{-4} mol) were dissolved together in MeCN (15 mL) and left to stir for 1 h. [18]aneO_4S_2 (0.049 g, 1.63 x 10^{-4} mol) was then added and the yellow solution was allowed to stir overnight at room temperature. The volatiles were removed and the remaining yellow solid washed with CH_2Cl_2, filtered and dried *in vacuo*. Yield: 0.065 g, 65%. X-Ray quality crystals grown by dissolving in MeCN/CH_2Cl_2 and leaving at 5°C. Required for $C_{12}H_{24}Cl_6FeO_4S_2Sc$ (609.63): C, 23.63; H, 3.97. Found: C, 24.12; H, 4.75%. IR (Nujol, cm^{-1}): 381 ($FeCl_4$), 316 (ScCl). ^{1}H NMR (CD_3CN, 293K): δ 2.88-3.34 (v.br m, [8H], SC***H***$_2$), 3.82 (v.br, [8H], SCH_2C***H***$_2$O), 4.41 (v.br, [8H], OC***H***$_2$); (230K): δ 2.77 (v.br, SC***H***$_2$), 3.55 (v.br, SCH_2C***H***$_2$O), 4.34 (v.br, OC***H***$_2$); (d_6-acetone, 263K): δ 2.71 (br, [8H], SC***H***$_2$), 3.55 and 3.63 (br m, [16H], OC***H***$_2$); (183K): δ 2.77 (br, [8H], SC***H***$_2$), 3.53 (v.br m, [16H], OC***H***$_2$). ^{45}Sc NMR (CD_3CN/MeCN, 293K): δ 204.

4.4.3 **[ScI_2([18]aneO_4S_2)][I]:** ScI_3 (0.040 g, 9.40 x 10^{-5} mol) was suspended in MeCN (15 mL) and [18]aneO_4S_2 (0.028 g, 9.40 x 10^{-5} mol) added. The ligand dissolved and slowly the MeCN turned yellow as the reaction proceeded. Left stirring overnight at room temperature the ScI_3 fully dissolved. The yellow solution was exposed to vacuum conditions until all the volatiles had been removed, the remaining yellow powder was washed with CH_2Cl_2 and dried *in vacuo*. X-Ray quality crystals were obtained by redissolving in MeCN and slow evaporation of the solvent. Yield: 0.043 g, 63%. Required for $C_{12}H_{24}I_3O_4S_2Sc$ (721.78): C, 19.95; H, 3.35. Found: C, 19.81; H, 3.17%. ^{1}H NMR (CD_3CN, 293 K): δ 2.75-2.98 (br m, [8H], SC***H***$_2$) 3.56 (br s, [8H], SCH_2C***H***$_2$O), 4.24 (br, [8H], OC***H***$_2$). ^{45}Sc NMR (CD_3CN/MeCN, 298 K): δ 206; (CH_2Cl_2, 295 K): δ 220.

4.4.4 **[ScI_2([15]aneO_3S_2)][I]:** ScI_3 (0.040 g, 9.40 x 10^{-5} mol) was suspended in MeCN (15 mL) and [15]aneO_3S_2 (0.024 g, 9.40 x 10^{-5} mol) added. The ligand dissolved and slowly the MeCN turned pale yellow as the reaction proceeded. Left stirring overnight at room temperature the ScI_3 fully dissolved. The pale yellow solution was exposed to a vacuum until all the volatiles had been removed; the remaining light yellow powder was washed with CH_2Cl_2 and dried *in vacuo*. Yield: 0.040 g, 63%. Required for $C_{10}H_{20}I_3O_3S_2Sc$ (677.75): C, 17.71; H, 2.97. Found: C, 17.61; H, 2.86%. ^{1}H NMR (CD_3CN, 293 K): δ 3.83 (br), 4.38 (br), 4,48 (br), 4.62 (br). ^{45}Sc NMR (CD_3CN/MeCN, 298 K): δ 297.

4.4.5 **$[ScCl_2([18]aneO_4Se_2)][FeCl_4]$:** $ScCl_3(THF)_3$ (0.060 g, 1.63 x 10^{-4} mol) and $FeCl_3$ (0.027 g, 1.63 x 10^{-4} mol) were dissolved together in MeCN (15 mL) and left to stir for 1 h. $[18]aneO_4Se_2$ (0.064 g, 1.63 x 10^{-4} mol) was then added and the yellow solution was allowed to stir overnight at room temperature. The volatiles were removed and the remaining dark ochre solid washed with CH_2Cl_2, filtered and dried *in vacuo*. Yield: 0.070 g, 61%. Required for $C_{12}H_{24}Cl_6FeO_4ScSe_2$ (703.61): C, 20.47; H, 3.44. Found: C, 20.56; H, 3.51%. IR (Nujol, cm^{-1}): 388 ($FeCl_4$), 317 (ScCl). ^1H NMR (CD_3CN, 298K): δ 2.83 (br, [8H], $SeC\boldsymbol{H}_2$), 3.59 (br, [8H], $SeCH_2C\boldsymbol{H}_2O$), 3.75 (br, [8H], $OC\boldsymbol{H}_2$); (230K): δ 2.81 (br, [8H], $SeC\boldsymbol{H}_2$), 3.54 and 3.70 (br m, [16H], $OC\boldsymbol{H}_2$). ^{45}Sc NMR (CD_3CN/MeCN, 298K): δ 205. ^{77}Se NMR (CD_3CN/MeCN, 298K): δ 150; (233K): δ 153.

4.4.6 **$[ScI_2([18]aneO_4Se_2)][I]$:** ScI_3 (0.023 g, 5.40 x 10^{-5} mol) was suspended in MeCN (15 mL) and heated to 83˚C. The mixture was maintained at reflux until a yellow solution remained then allowed to cool and $[18]aneO_4Se_2$ (0.021 g, 5.40 x 10^{-5} mol) added. The reaction was left at room temperature to stir for 45 min, some darkening of the solution was observed. The volatiles were removed *in vacuo* and the oily solid left behind washed with CH_2Cl_2. The ochre solid produced was separated and dried *in vacuo*. Yield 0.026 g, 59%. Required for $C_{12}H_{24}I_3O_4ScSe_2$ (815.76): C, 17.65; H, 2.97. Found: C, 17.54; H, 3.05%. ^1H NMR (CD_3CN, 298 K): δ 2.78-3.16 (br, [8H], $SeC\boldsymbol{H}_2$), 3.64 (s, [8H], $SeCH_2C\boldsymbol{H}_2O$), 4.19-4.38 (br, [8H], $OC\boldsymbol{H}_2$). ^{45}Sc (CD_3CN/MeCN, 295 K): not observed. $^{77}Se\{^1H\}$ NMR (CD_3CN/MeCN, 298 K): not observed.

4.4.7 **$[ScCl_2([18]aneO_4Te_2)][FeCl_4]$:** $[ScCl_3(THF)_3]$ (0.060 g, 1.63 x 10^{-4} mol) and $FeCl_3$ (0.027 g, 1.63 x 10^{-4} mol) were dissolved together in MeCN (15 mL) and left to stir for 1 h. To the yellow solution $[18]aneO_4Te_2$ (0.049 g, 1.63 x 10^{-4} mol) was then added and the solution was allowed to stir overnight at room temperature. The solution darkened to orange. The volatiles were removed and the remaining brown solid washed with CH_2Cl_2, filtered and dried *in vacuo*. Yield: 0.070 g, 53%. Required for $C_{12}H_{24}Cl_6FeO_4ScTe_2$ (801.09): C, 17.98; H, 3.03. Found: C, 17.83; H, 2.91%. IR (Nujol, cm^{-1}): 381 ($FeCl_4$), 336 (ScCl). ^1H NMR (CD_3CN, 295K): δ 3.74 (v.br m, [16H], Te***H***$_2$C***H***$_2$O), 4.19 (v.br, [8H], OC***H***$_2$); (230K): δ 3.72 (v.br m, [16H], Te***H***$_2$C***H***$_2$O), 4.15 (v.br, [8H], OC***H***$_2$)). ^{45}Sc NMR (CD_3CN/MeCN, 238K): (see discussion).

4.4.8 **$[ScCl_2([18]aneO_2S_4)][FeCl_4]$:** $[ScCl_3(THF)_3]$ (0.060 g, 1.63 x 10^{-4} mol) and $FeCl_3$ (0.027 g, 1.63 x 10^{-4} mol) were dissolved together in MeCN (15 mL) and left to stir for 1 h. $[18]aneO_2S_4$ (0.054 g, 1.63 x 10^{-4} mol) was then added along with CH_2Cl_2 (10 mL) to aid in the dissolution of the macrocycle. The yellow suspension was allowed to stir overnight at room temperature. The reaction was filtered and the volatiles removed. Analysis of the minor amount of solid filtered showed minimal difference to the bulk yellow solid obtained from the filtrate. Yield 0.035 g, 33%. Required for $C_{12}H_{24}Cl_6FeO_2S_4Sc$ (641.59): C, 22.44; H, 3.77. Found: C, 22.31; H, 3.82%. IR (Nujol, cm^{-1}): 379 ($FeCl_4$), 328 (ScCl). ^1H NMR (CD_2Cl_2, 293K): δ 2.69 (v.br m, [16H], SC***H***$_2$), 3.55 (br, [8H], OC***H***$_2$); (CD_3CN, 298K): δ 2.74-2.95 (v.br m), 3.75 (br). ^{45}Sc NMR (CD_2Cl_2/CH_2Cl_2, 293K): δ 257.

4.4.9 **[ScI_3([9]aneS_3)]:** ScI_3 (0.019 g, 1.41 x 10^{-4} mol) and [9]aneS_3 (0.060 g, 1.41 x 10^{-4} mol) were heated in acetonitrile at 80˚C for 4 h until a clear yellow solution remained. The volatiles were removed once the reaction had cooled to room temperature. The solid was washed with CH_2Cl_2 isolating a light orange powder. Yield: 0.035 g, 44%. Required for $C_6H_{12}I_3S_3Sc$ (605.68): C, 11.89; H, 2.00. Found: C, 11.73; H, 1.89%. ^{1}H NMR (CD_3CN, 293K): δ 3.09 (s, thiacrown SC***H***$_2$). ^{45}Sc (CD_3CN/MeCN, 295 K): δ 327.

4.4.10 **[$ScCl_3$(MeCN)$_3$]:** [$ScCl_3(THF)_3$] was dissolved in MeCN and allowed to stir at room temperature for an hour. The volatiles were completely removed *in vacuo* and fresh acetonitrile added. The solution was concentrated and left overnight at 5˚C. Small extremely sensitive crystals of the tris acetonitrile product grew. Removal of the volatiles gave a bulk solid which analysed as a mixture of products. ^{45}Sc NMR (CD_3CN/MeCN, 298 K): (see discussion).

4.4.11 **[YCl_2([15]aneO_3S_2)][$FeCl_4$]:** [$YCl_2(THF)_5$][$YCl_4(THF)_2$] (0.107 g, 1.19 x 10^{-4} mol) and $FeCl_3$ (0.039 g, 2.38 x 10^{-4} mol) were dissolved together in MeCN (15 mL) and left to stir for 1 h. [15]aneO_3S_2 (0.060 g, 2.38 x 10^{-4} mol) was then added and the yellow solution was allowed to stir overnight at room temperature. The volatiles were removed and the remaining yellow solid washed with CH_2Cl_2, filtered and dried *in vacuo*. Yield: 0.090 g, 62%. Required for $C_{10}H_{20}Cl_6FeO_3S_2Y$ (609.56): C, 19.69; H, 3.31. Found: C, 20.02; H, 3.67%. IR (Nujol, cm^{-1}): 380 ($FeCl_4$), 262 (YCl). ^{1}H NMR (CD_3CN, 293K): δ 3.20 (v.br, [8H], SC***H***$_2$), 4.17 (v.br, [12H], OC***H***$_2$).

4.4.12 **$[YCl_2([18]aneO_4S_2)][FeCl_4]$:** $[YCl_2(THF)_5][YCl_4(THF)_2]$ (0.060 g, 6.70×10^{-5} mol) and $FeCl_3$ (0.022 g, 1.34×10^{-4} mol) were dissolved together in MeCN (15 mL) and left to stir for 1 h. $[18]aneO_4S_2$ (0.040 g, 1.34×10^{-4} mol) was then added and the yellow solution was allowed to stir overnight at room temperature. The volatiles were removed and the remaining yellow solid washed with CH_2Cl_2, filtered and dried *in vacuo*. X-Ray quality crystals grew by dissolving in MeCN and slow evaporation of the solvent. Yield: 0.034 g, 37%. Required for $C_{12}H_{24}Cl_6FeO_4S_2Y$ (653.58): C, 22.04; H, 3.70. Found: C, 21.87; H, 3.73%. IR (Nujol, cm^{-1}): 375 ($FeCl_4$), 265 (YCl). ^1H NMR (CD_3CN, 293K): δ 2.94 (br, [4H], SCH_2), 3.29 (br, [4H], SCH_2), 4.29 and 4.36 (br m, [16H], OCH_2).

4.5 Structural Data

Compound	$[ScCl_2([18]aneO_4S_2)][FeCl_4]$	$[ScI_2([18]aneO_4S_2)][I]\cdot MeCN$	$[YCl_2([18]aneO_4S_2)][FeCl_4]$
Formula	$C_{12}H_{24}Cl_6FeO_4S_2Sc$	$C_{14}H_{27}I_3NO_4S_2Sc$	$C_{12}H_{24}Cl_6FeO_4S_2Y$
mwt.	609.94	763.15	653.89
crystal system	Orthorhombic	Orthorhombic	Orthorhombic
space group	*Abm*2 (69)	*Pnma* (62)	*Pccn* (56)
a (Å)	16.150(4)	15.2900(10)	23.764(5)
b (Å)	64.370(8)	11.9434(8)	16.180(2)
c (Å)	11.3327(12)	14.4913(8)	12.5376
α (°)	90	90	90
β (°)	90	90	90
γ (°)	90	90	90
U (Å^3)	11781(4)	2646.3(3)	4820.7(14)
Z	20	4	8
μ(Mo Kα) (mm^{-1})	1.777	3.951	3.851
F(000)	6180	1448	2616
total no. reflns	69707	27355	41731
unique reflns	13386	2710	5515
R_{int}	0.0841	0.0610	0.0503
no. of params, restraints	428, 10	144, 8	235, 0
R_1[a] [$I_o > 2\sigma(I_o)$]	0.0963	0.074	0.0301
R_1 (all data)	0.1288	0.100	0.0419
wR_2[a] [$I_o > 2\sigma(I_o)$]	0.2292	0.188	0.0627
wR_2(all data)	0.2517	0.206	0.0664

Compound	$[ScCl_3(MeCN)_3]\cdot MeCN$
Formula	$C_8H_{12}Cl_3N_4Sc$
mwt.	315.53
crystal system	Orthorhombic
space group	*Pbcm* (57)
a (Å)	8.4393(15)
b (Å)	12.293(2)
c (Å)	14.978(3)
α (°)	90
β (°)	90
γ (°)	90
U (Å^3)	1553.8(5)
Z	4
μ(Mo Kα) [mm^{-1}]	0.971
F(000)	640
total no. reflns	11075
unique reflns	1853
R_{int}	0.056
no. of params, restraints	85, 0
R_1[a] [$I_o > 2\sigma(I_o)$]	0.055
R_1 (all data)	0.063
wR_2[a] [$I_o > 2\sigma(I_o)$]	0.121
wR_2(all data)	0.125

[a] $R_1 = \Sigma||F_o| - |F_c||/\Sigma|F_o|$. $wR_2 = [\Sigma w(F_o^2 - F_c^2)^2/\Sigma wF_o^4]^{1/2}$

Common items: temperature = 100K; wavelength (Mo Kα)= 0.71073 Å; θ_{max}= 27.5°

4.6 References

1. B. Cordero, V. Gomez, A. E. Platero-Prats, M. Reves, J. Echeverria, E. Cremades, F. Barragan and S. Alvarez, *Dalton Trans.*, 2008, 2832

2. S. Cotton, in *Comprehensive Coord. Chem. II*, eds. J. A. M. Editors-in-Chief: T. J. Meyer, Pergamon, Oxford, 2003, pp. 93

3. N.G. Connelly, T. Damhus, R.M. Hartshorn and A.T. Hutton, *Nomenclature of Inorganic Chemistry IUPAC*, The Royal Society of Chemistry, King's Lynn, 2005

4. K. J. Fisher, in *Comprehensive Coord. Chem. II*, eds. J. A. M. Editors-in-Chief: T. J. Meyer, Pergamon, Oxford, 2003, pp. 1

5. C. S. Tredget, F. Bonnet, A. R. Cowley and P. Mountford, *Chem. Commun.*, 2005, 3301

6. R. G. Pearson, *C. C. /Eng. Tech. Appl. Sci.*, 1986, 18

7. H. Ma, T. P. Spaniol and J. Okuda, *Angew. Chem. Int. Ed.*, 2006, **45**, 7818

8. C. S. Tredget, E. Clot and P. Mountford, *Organometallics*, 2008, **27**, 3458

9. H. Ma, T. P. Spaniol and J. Okuda, *Dalton Trans.*, 2003, 4770

10. M. Konkol, M. Kondracka, P. Voth, T. P. Spaniol and J. Okuda, *Organometallics*, 2008, **27**, 3774

11. C. Lichtenberg, P. Jochmann, T. P. Spaniol and J. Okuda, *Angew. Chem. Int. Ed.*, 2011, **50**, 5752

12. M. D. Fryzuk, G. Giesbrecht and S. J. Rettig, *Organometallics*, 1996, **15**, 3329

13. S. A. Bartlett, G. Cibin, A. J. Dent, J. Evans, M. J. Hanton, G. Reid, R. P. Tooze and M. Tromp, *Dalton Trans.*, 2013, **42**, 2213

14. M. D. Brown, W. Levason, D. C. Murray, M. C. Popham, G. Reid and M. Webster, *Dalton Trans.*, 2003, 857

15. J. L. Atwood and K. D. Smith, *J. Chem. Soc., Dalton Trans.*, 1974, 921

16. S. Hajela, W. P. Schaefer and J. E. Bercaw, *J. Organomet. Chem.*, 1997, **532**, 45

17. N. J. Hill, W. Levason, M. C. Popham, G. Reid and M. Webster, *Polyhedron*, 2002, **21**, 1579

18. E. Abinet, T. P. Spaniol and J. Okuda, *Chem.-Asian J.*, 2011, **6**, 389

19. H. Ma, T. P. Spaniol and J. Okuda, *Inorg. Chem.*, 2008, **47**, 3328

20. A. Kapelski, J.-C. Buffet, T. P. Spaniol and J. Okuda, *Chem.-Asian J.*, 2012, **7**, 1320

21. W. J. Evans, B. M. Schmiege, S. E. Lorenz, K. A. Miller, T. M. Champagne, J. W. Ziller, A. G. DiPasquale and A. L. Rheingold, *J. Am. Chem. Soc.*, 2008, **130**, 8555

22. Z. Zhang, L. Zhang, Y. Li, L. Hong, Z. Chen and X. Zhou, *Inorg. Chem.*, 2010, **49**, 5715

23. Y. Li, C. Pi, J. Zhang, X. Zhou, Z. Chen and L. Weng, *Organometallics*, 2005, **24**, 1982

24. S. N. Ringelberg, A. Meetsma, B. Hessen and J. H. Teuben, *J. Am. Chem. Soc.*, 1999, **121**, 6082

25. S. Arndt, A. Trifonov, T. P. Spaniol, J. Okuda, M. Kitamura and T. Takahashi, *J. Organomet. Chem.*, 2002, **647**, 158

26. J. M. Bakker, G. B. Deacon, C. M. Forsyth, P. C. Junk and M. Wiecko, *Eur. J. Inorg. Chem.*, 2010, 2813

27. H. Schumann, K. Herrmann, J. Demtschuk and S. H. Mühle, *Z. Anorg. Allg. Chem.*, 1999, **625**, 1107

28. W. M. Haynes, *CRC Handbook of Chemistry and Physics, 94th Edition (CRC Handbook of Chemistry & Physics)*, CRC Press, 2013

29. G. R. Willey, M. T. Lakin, M. Ravindran and N. W. Alcock, *J. Chem. Soc. Chem. Comm.*, 1991, 271

30. G. R. Willey, M. T. Lakin and N. W. Alcock, *J. Chem. Soc. Chem. Comm.*, 1992, 1619

31. K. Kireeva, *Russ. J. Inorg. Chem.*, 1992, **37**, 1822

32. K. Nakamoto, in *Handbook of Vibrational Spectroscopy*, John Wiley & Sons, Ltd, 2006

33. M. Mantina, A. C. Chamberlin, R. Valero, C. J. Cramer and D. G. Truhlar, *J. Phys. Chem. A*, 2009, **113**, 5806

34. C. D. Beard, L. Carr, M. F. Davis, J. Evans, W. Levason, L. D. Norman, G. Reid and M. Webster, *Eur. J. Inorg. Chem.*, 2006, 4399

35. E. G. Hope, T. Kemmitt and W. Levason, *Organometallics*, 1987, **6**, 206

36. E. G. Hope, T. Kemmitt and W. Levason, *Organometallics*, 1988, **7**, 78

37. Igor L. Fedushkin, Alexandra A. Skatova, Valentina A. Chudakova, Georgy K. Fukin, S. Dechert and H. Schumann, *Eur. J. Inorg. Chem.*, 2003, 3336

38. A. J. Blake, A. J. Holder, T. I. Hyde, H. J. Kuppers, M. Schroder, S. Stotzel and K. Wieghardt, *J. Chem. Soc. Chem. Comm.*, 1989, 1600

39. G. R. Willey, P. R. Meehan and M. G. B. Drew, *Polyhedron*, 1996, **15**, 1397

40. G. R. Willey, M. T. Lakin and N. W. Alcock, *J. Chem. Soc. Dalton Trans.*, 1993, 3407

41. M. J. D. Champion, P. Farina, W. Levason and G. Reid, *Dalton Trans.*, 2013, **42**, 13179

5. Mixed Donor Chalcogenoether Macrocyclic Complexes of Lead(II)

5.1 Introduction

Lead has been widely used in many industrial processes; due to this it is heavily distributed [1,2]. Its toxicity has resulted in a significant effort towards lead(II) complexes with aza-, oxa- (crown ether) and thia-macrocycles with the aim to use the macrocyclic ligands in heavy metal sensing and sequestration [1 3 4 5].

Lead is a fairly large metal atom with a covalent radius of 1.46 Å and a Pauling electronegativity of 1.87 [6]. Due to its large radius and modest charge (and hence low charge to radius ratio) lead(II) complexes tend to be heavily dissociated in solution, and it is this property that has led to its persistence in the environment. Lead(II) complexes are extensive and include examples with many neutral and charged donor ligands from Groups 14-17 [3 7 8]. Coordination numbers range from two in diaryllead compounds with bulky substituted aryl groups to seven (in $[(\eta^5\text{-Cp*})Pb(\mu^2\text{-}BF_4)_2Pb(\eta^5\text{-Cp*})]$ (Figure 5.1; the very unusual bridging $[BF_4]^-$ anions are discussed further below) [9], nine in $[Pb(OAc)_2]\cdot 3H_2O$ [10], ten in $[Pb(18\text{-crown-6})(NO_3)_2]$ (Figure 5.2) and eleven in the anionic $[Pb(15\text{-crown-5})(NO_3)_3]^-$ [11]. Unusually for a p-block metal, much of its coordination chemistry surrounds that with oxo-salts such as nitrate, acetate and perchlorate and not the analogous lead(II) halides; lead dihalides are highly insoluble and tend to be intractable in nature [3]. The few halide complexes are $[PbX_2(18\text{-crown-6})]$ (X= Cl, Br, I), which are discrete monomers [12]. The bridged complexes $[Pb_2Br_4(18\text{-crown-6})]$ [13] and $[Pb_2I_3(18\text{-crown-6})_2][SnI_5]$ [14]; in the bromide "$[PbBr_4]^{2-}$" units bridge (μ^2) two $[PbBr(18\text{-crown-6})]^+$ cations, the anions link up to form a linear polymer. The iodide differs in that it is a discrete dimer with two $[PbI(18\text{-crown-6})]$ fragments bridged by a central iodide, $[SnI_5]^-$ provides charge balance. The adduct $[PbI_2(18\text{-crown-6})]\cdot[I_2C{=}CI_2]$ where the lead iodo-ligands also interact with the iodines on tetraiodoethylene, and

the anion/cation pairs [PbI(18-crown-6)][I_3] and [PbCl(18-crown-6)][$SbCl_6$] [15].

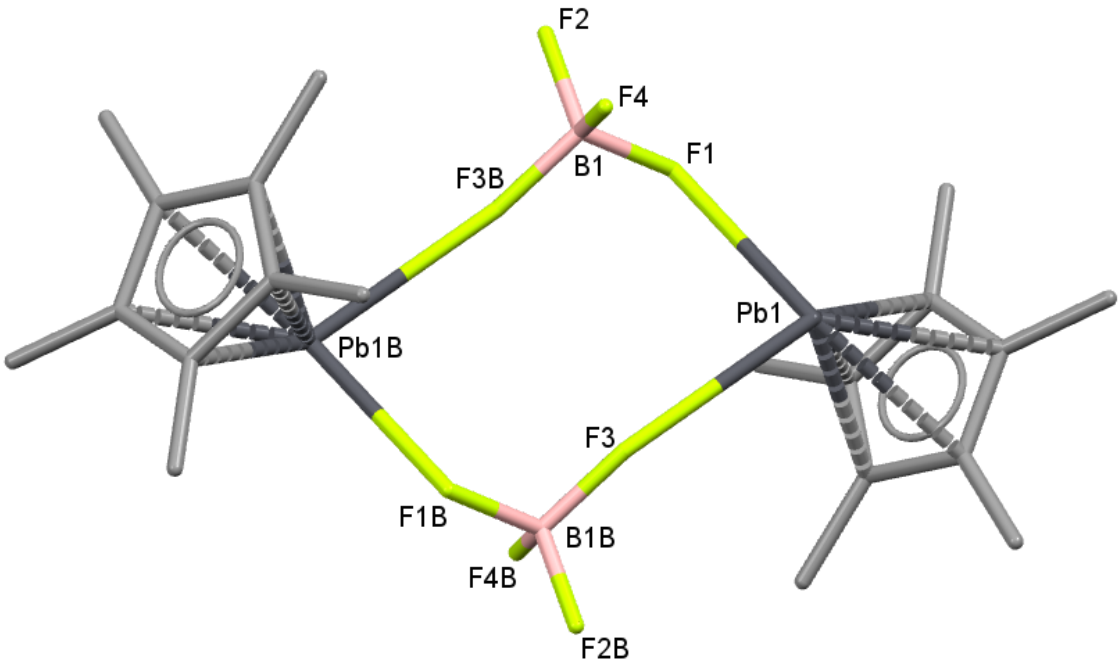

Figure 5.1 Structure of [(η^5-Cp*)Pb(μ^2-BF_4)$_2$Pb(η^5-Cp*)]. H atoms are omitted for clarity.

Typical Pb(II) macrocycle complexes include [Pb(12-crown-4)$_2$(NO_3)][Pb(12-crown-4)(NO_3)$_3$] [11] which has both sandwich and half-sandwich lead-crown adducts, the metal centres are both 10-coordinate. [Pb(dicyclohexane-18-crown-6)($NCS)_2$] [16] has *trans* isothiocyanates and is 8-coordinate, whereas [Pb(18-crown-6)($MeCN)_3$][$SbCl_6$]$_2$ [15] is 9-coordinate, the macrocycle is equatorial to the lead and the three acetonitrile co-ligands occupy a meridian.

Thia-crown complexes also show varied coordination numbers and geometries, for example complexes with the related trithioether macrocycles [9]aneS_3 and [10]aneS_3 differ considerably. [Pb([9]aneS_3)$_2$(ClO_4)$_2$] [17] is an 8-coordinate sandwich complex with two κ^1-coordinated perchlorate groups; [Pb([10]aneS_3)(H_2O)(ClO_4)$_2$] [18] is a half-sandwich complex exhibiting 9-coordinate lead, one perchlorate is monodentate, two other perchlorate groups have contacts within the ΣVdW radii for Pb and O (3.54 Å) and chelate asymmetrically, (the seemingly extra $[ClO_4]^-$ also coordinates to, and provides charge balance for another Pb(II) fragment). The larger thia-macrocycle

[28]aneS$_8$ gives a dinuclear complex with lead(II) perchlorate, [Pb$_2$([28]aneS$_8$)(ClO$_4$)$_4$] [19]. Here the lead centres are 8-coordinate, bidentate (κ^2) and bridging (μ^2) coordination modes are observed for the [ClO$_4$]$^-$ anions.

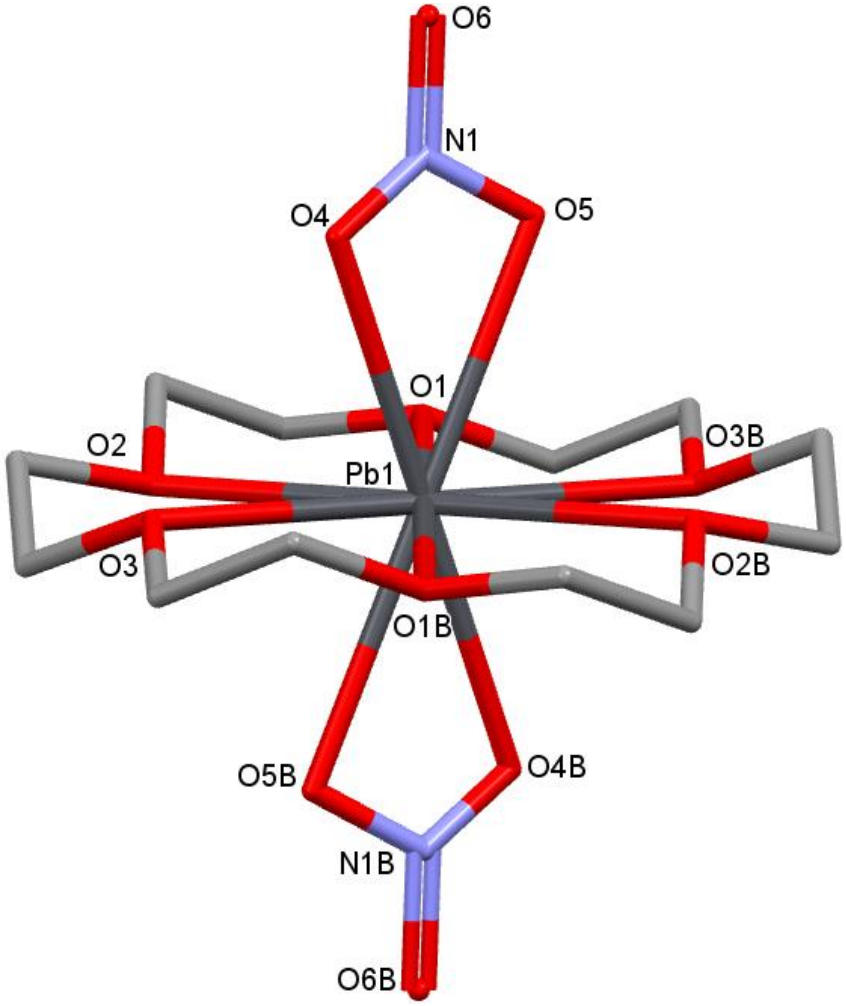

Figure 5.2 Structure of [Pb(18-crown-6)(NO$_3$)$_2$]. H atoms are omitted for clarity [11].

Despite its extensive chemistry the nature of Pb(II) as a Lewis Acid remains debatable, several sources claim it is an exemplar of a soft Lewis Acid, whereas others classify it as borderline Lewis Acid exhibiting both hard and soft characteristics. This study will aim to further resolve this question.

Examples of oxa-thia macrocycles with Pb(II) are rare, and with oxa-selena crowns unknown. The unusual macrocycles mn-15-O$_3$S$_2$ and mn-18-O$_4$S$_2$ coordinate to Pb(ClO$_4$)$_2$ *via* all the macrocycle donors with the perchlorate anions coordinated κ^1 and κ^2 in [Pb(mn-18-O$_4$S$_2$)(ClO$_4$)$_2$]

and monodentate in [Pb(mn-15-O_3S_2)(ClO_4)(H_2O)][ClO_4]·MeCN [20]. In both complexes the O-donors are coordinated preferentially over the sulfur donors. The ligand preorganisation of these maleonitrile containing oxa-thia macrocycles is discussed further in Chapter 7.

The literature examples of complexes with [18]aneO_4S_2 are [Pb([18]aneO_4S_2)(ClO_4)$_2$] (Figure 5.3), [Pb([18]aneO_4S_2)(NO_3)$_2$] (Figure 5.4) [21] and [Pb([18]aneO_4S_2)(NCS)$_2$] (Figure 5.5) [22]. The anions in these complexes are considered moderate to strongly coordinating. Pb(II) salts with weakly or non-coordinating anions such as hexafluorophosphate and tetrafluoroborate will more likely mimic the heavily dissociated nature of Pb(II) in the environment, and hence are useful synthons towards examining their coordination chemistry with the chalcogenoether macrocycles used in this study.

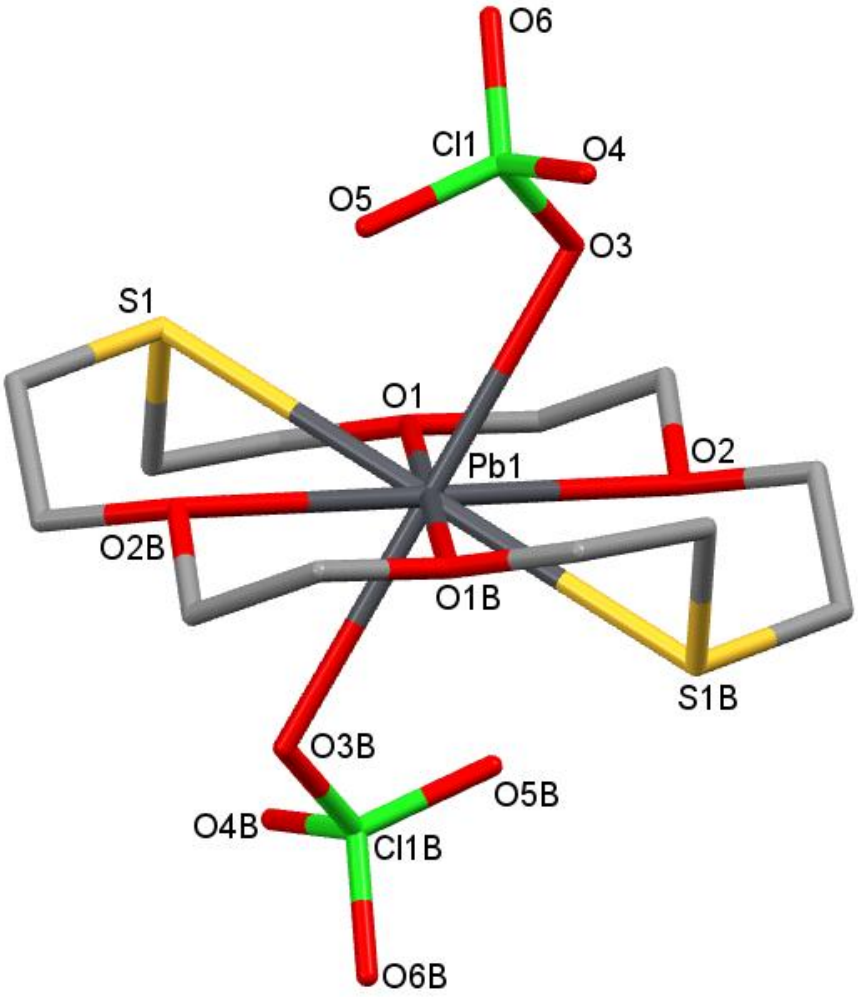

Figure 5.3 Structure of [Pb([18]aneO_4S_2)(ClO_4)$_2$]. H atoms are omitted for clarity [21].

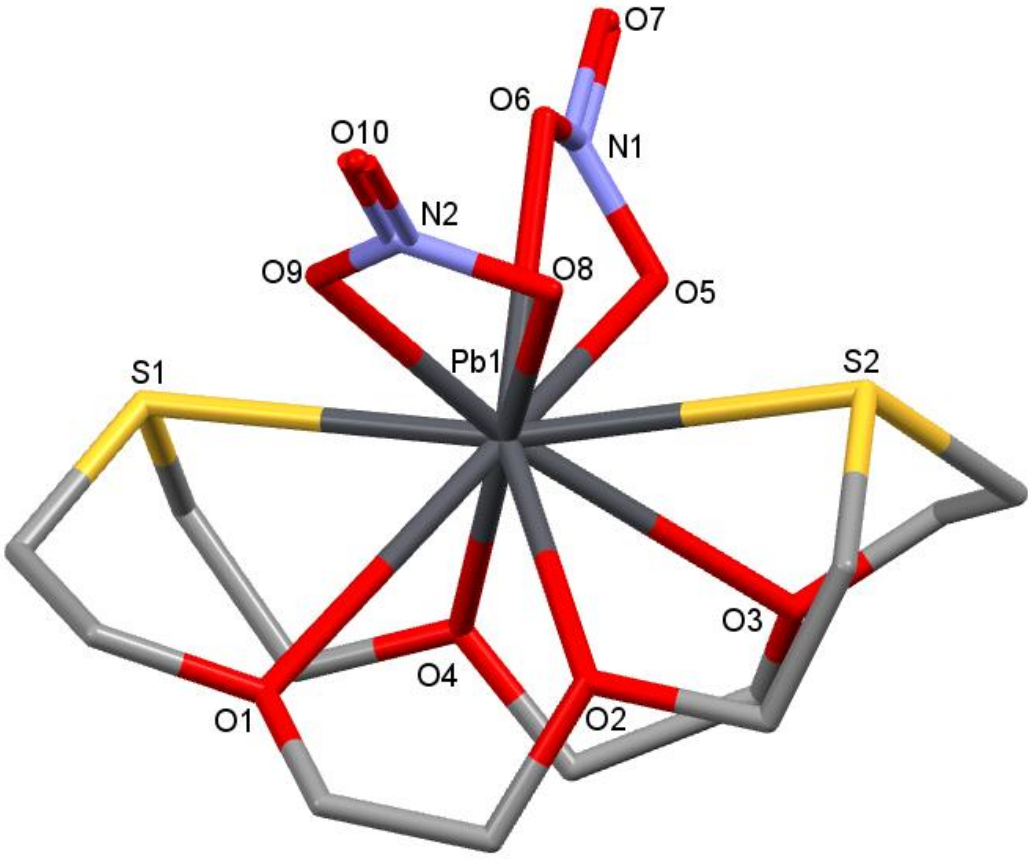

Figure 5.4 Structure of [Pb([18]aneO$_4$S$_2$)(NO$_3$)$_2$]. H atoms are omitted for clarity [21].

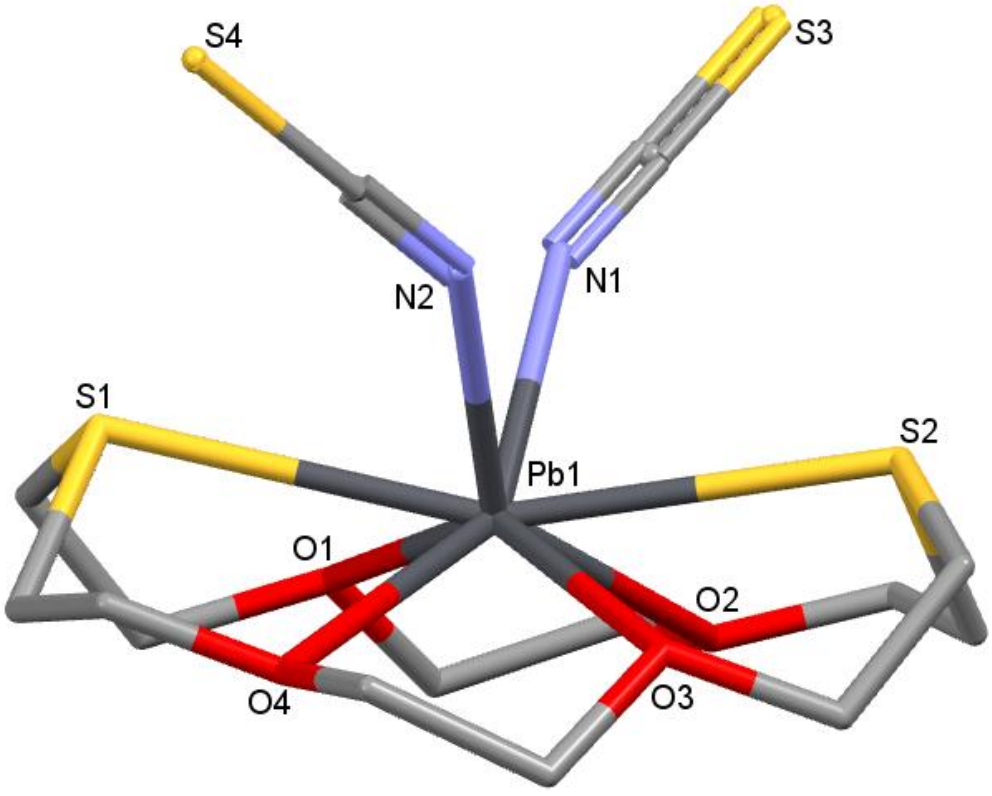

Figure 5.5 Structure of [Pb([18]aneO$_4$S$_2$)(NCS)$_2$]. H atoms are omitted for clarity [22].

5.1.1 Non-/Weakly-Coordinating Fluoroanions

The fluoroanions $[BF_4]^-$ and $[PF_6]^-$ have had a long history in being used to stabilise cationic complexes whilst remaining uncoordinated/weakly coordinated. In recent years, bulkier, more stable and even less coordinating anions have been designed and found widespread use, especially in homogenous catalysis, such as $[B(Ar^F)_4]^-$ (Ar^F= C_6H_3-3,5$(CF_3)_2$ and $[B(C_6F_5)_4]^-$ [23] [24]. Nevertheless the 'simpler' tetrafluoroborate and hexafluorophosphate anions still adequately serve the purpose of a charge stabilising and weakly coordinating anion, especially for metal centres which are not highly electrophilic. For the purpose of this study they also allow for a greater degree of comparison to be made with the coordinating anion Pb(II) complexes prevalent in the literature (perchlorate, nitrate, acetate, isothiocyanate etc.) in that they are more sterically similar (relative to $[B(C_6F_5)_4]^-$ etc.). Comparison with the analogous nitrate or halide complexes, the $[BF_4]^-$ and $[PF_6]^-$ salts will also tend to have better solubility in organic solvents, which overall is more compatible with mixed chalcogenoether macrocycles.

5.2 Results and Discussion

5.2.1 Pb(II) precursors

$Pb(BF_4)_2$ was obtained commercially as a 50 wt. % aqueous solution. The metal salt is indefinitely stable in solution, but will decompose to intractable mixtures of PbF_2 and other products if concentrated. NMR studies (^{19}F Table 5.7 and ^{207}Pb Table 5.1) show just one species present in the commercial solution.

The related hexafluorophosphate salt is also prepared as an aqueous solution by reacting basic lead carbonate, suspended in water and HPF_6. The resulting $Pb(PF_6)_2$ (aq) is unstable and begins to decompose shortly after its formation. The decomposition was followed using NMR spectroscopy and the decomposition products identified using a combination of ^{19}F and ^{31}P NMR and IR spectroscopy. The instability of the $[PF_6]^-$ anion is surprising but its hydrolysis/degradation in the presence of metals such as Ag^+ and other metals has been reported previously [25] [26].

Lead(II) nitrate is also obtained commercially and used as a solid. It is insoluble in acetonitrile.

Table 5.1 ^{207}Pb NMR shifts for relevant Pb(II) salts in D_2O/H_2O

Pb(II) salt	$^{207}Pb_y$ NMR (δ)
$Pb(BF_4)_2$	2903
$Pb(PF_6)_2$	2904
$Pb(NO_3)_2$	2973

[y] ^{207}Pb, 22.1%, *I*= 1/2

Multinuclear NMR studies were undertaken on fresh solutions of the Pb(II) precursors. For the fluoroanion salts the species observed was concluded to be $[Pb(H_2O)_x]^{2+}$, the $[BF_4]^-$ and $[PF_6]^-$ environments in the ^{19}F and ^{31}P NMR are close to free tetrafluoroborate (compared to $[TBA][BF_4]$) and hexafluorophosphate (compared to $[NH_4][PF_6]$). This interpretation is further supported by the conductivity studies performed on the

subsequent complexes (see Table 5.8). The difference in the $Pb(NO_3)_2$ shift can be attributed to the retained coordination of the $[NO_3]^-$ anions in solution; discussed in 5.2.3.1.

5.2.2 Pb(II) complexes with 15-membered macrocycles

Reacting 15-crown-5 in MeCN with $Pb(BF_4)_2$ (aq) gave the sandwich complex $[Pb(15\text{-crown-}5)_2][BF_4]_2$. The same complex was formed regardless of the molar ratios used, either 1:1 or 2:1 ligand to metal stoichiometry.

The ^1H NMR spectrum shows the C***H***$_2$ environment shifted from free ligand (+0.29 ppm). Ill-defined second order patterns are visible even at ambient temperature for the axial and equatorial macrocyclic protons, and on cooling to 228K an AB quartet pattern is revealed as the ligand exchange is slowed. The crowns most likely coordinate in two similar but distinct conformations on the Pb(II) centre.

Crystals of the crown sandwich complex had the constitution $[Pb(15\text{-crown-}5)_2][H_3O][BF_4]_3$, the lead dication (Figure 5.6) is disordered and precludes detailed structural comparisons. Nevertheless it is obvious from the partial structure that the lead(II) centre is 10-coordinate and the three tetrafluoroborate groups remain anionic (a hydroxonium cation is present for charge balance). In the related literature complexes $[Pb(15\text{-crown-}5)_2][Pb(15\text{-crown-}5)(NO_3)_2]_2$, $[Pb(15\text{-crown-}5)_2[SbCl_6]_2$ and $[Pb(15\text{-crown-}5)_2][SbCl_6]_2 \cdot [SbCl_3(15\text{-crown-}5)]$ the cation is likewise disordered [11] [15]. Crystals of $[Sn(15\text{-crown-}5)_2][H_3O][BF_4]_3$ are isostructural with a well-defined cation (see Chapter 6).

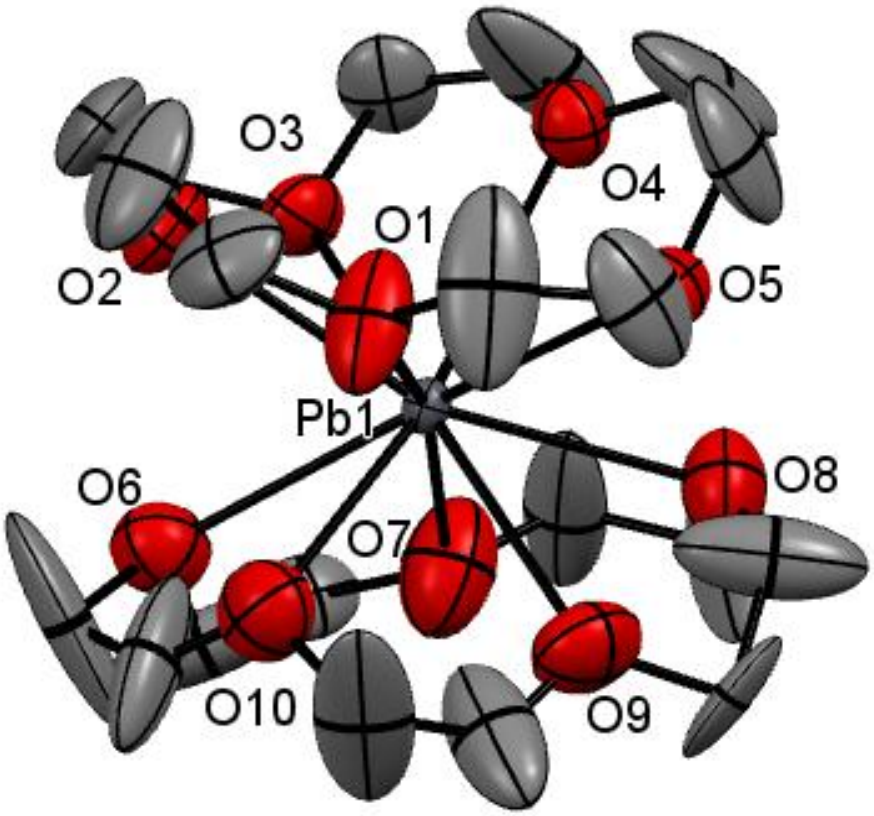

Figure 5.6 Partial Structure of the heavily disordered cation in $[Pb(15\text{-crown-}5)_2][H_3O][BF_4]_3$.

The analogous reaction using the oxa-thia macrocycle $[15]aneO_3S_2$ similarly gave a sandwich complex $[Pb([15]aneO_3S_2)_2][BF_4]_2$ Figure 5.7. In this example the crystals had a well defined cation discrete from the two anionic $[BF_4]^-$. The Pb(II) centre is in a very distorted 10-coordinate environment with all the Pb-donor distances well within the ΣVdW radii. Two of the Pb–O distances (Pb–O3 and Pb–O4) are substantially longer than the rest (2.898(5) and 3.055(5) Å compared to 2.688(5)-2.761(4) Å), a different interpretation thus is the Pb(II) centre has a coordination number of "8+2" with two interactions being weaker, long directional contacts to an 8-coordinate core. Examination of the Pb–S and Pb–O distances show a preference for the S donor, in both coordination interpretations the Pb–S bond length is on average significantly shorter ("10", 0.133 Å shorter or "8+2", 0.052 Å shorter) when comparing the difference in the sum of the covalent radii for O *vs*. S (0.39 Å) [6]. The complex is a rare structural example of an *endocyclic* sandwich complex of $[15]aneO_3S_2$.

The ^{1}H NMR spectrum gives further evidence for the Pb(II) preference for the sulfur in this system. There are four distinct C***H***$_2$ environments all shifted to high frequency from the free ligand, those adjacent to the sulfur donors (SC***H***$_2$ and SC***H***$_2$CH$_2$O) experience a much stronger coordination shift (0.49 and 0.41 ppm) than for those adjacent to the oxygens (~0.2 ppm). The C***H***$_2$ groups adjacent to O also have much broader signals.

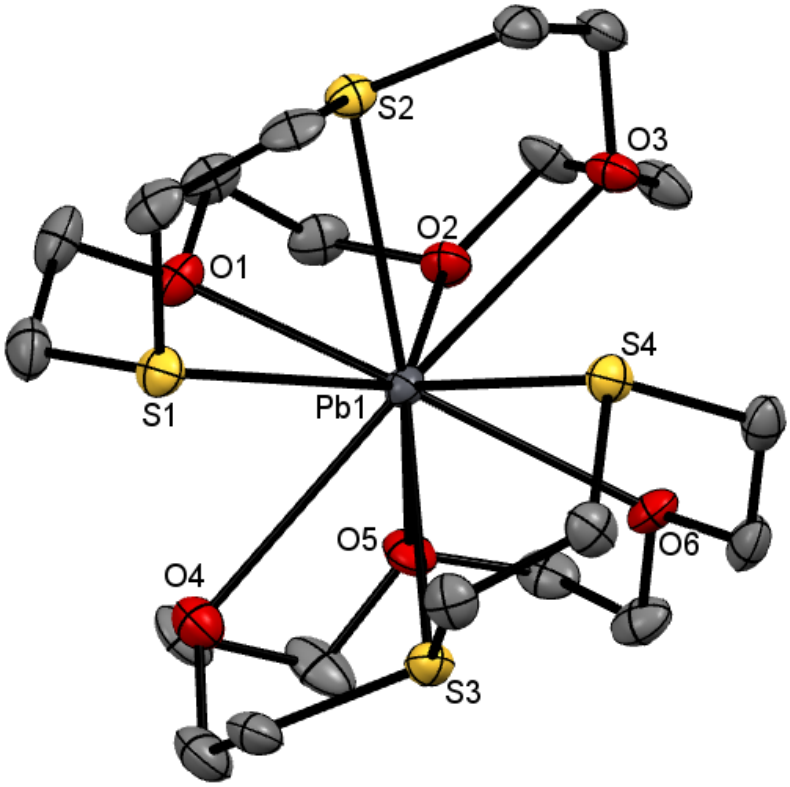

Figure 5.7 Crystal structure of the cation in [Pb([15]aneO$_3$S$_2$)$_2$][BF$_4$]$_2$· *n*CH$_2$Cl$_2$ (*n*= 1.22) showing the atom numbering scheme and the coordination around Pb1. Ellipsoids are drawn at the 50% probability level and H atoms are omitted for clarity.

Table 5.2 Selected bond lengths (Å) and angles (°) for $[Pb([15]aneO_3S_2)_2][BF_4]_2 \cdot n CH_2Cl_2]$ (n= 1.22)

Pb1–S1	3.022(2)	S1–Pb1–S2	66.44(4)
Pb1–S2	3.043(2)	S3–Pb1–S4	65.35(4)
Pb1–S3	3.116(2)	S1–Pb1–O1	68.0(9)
Pb1–S4	3.054(2)	S2–Pb1–O3	60.3(1)
Pb1–O1	2.688(4)	S3–Pb1–O4	58.6(1)
Pb1–O2	2.725(4)	S4–Pb1–O6	67.67(9)
Pb1–O3	2.898(4)	O1–Pb1–O2	63.8(1)
Pb1–O4	3.055(5)	O2–Pb1–O3	59.6(1)
Pb1–O5	2.761(4)	O4–Pb1–O5	57.9(1)
Pb1–O6	2.750(4)	O5–Pb1–O6	63.0(1)

In contrast to the fluoroanion chemistry a few $Pb(NO_3)_2$ complexes were investigated, the nitrate group being much more likely to be coordinated rather than anionic. The complex $[Pb(15\text{-crown-}5)(NO_3)_2]$ was successfully made by addition of the crown to an acetonitrile suspension of lead(II) nitrate. ^{1}H NMR studies show an expected singlet shifted from free crown. The crystal structure (Figure 5.8) is a half-sandwich complex with two *cisoidal* κ^2-nitrate groups, giving 9-coordinate lead. The nitrate groups are coordinated closer to the metal than the crown-O, Pb–O_{crown} 2.691(3)-2.713(3) Å compared to Pb-$O_{nitrate}$ 2.574(4)-2.586(3) Å. The procedures employed in this study only resulted in the neutral complex but previous work has reported a similar reaction of 15-crown-5 and $Pb(NO_3)_2$ in hot MeOH/MeCN solution at a 2:1 molar ratio which gave the salt $[Pb(15\text{-crown-}5)_2][Pb(15\text{-crown-}5)(NO_3)_2]_2$ [11]. Comparison of the Pb(II) anion shows again a half-sandwich arrangement with the crown on one side and the three κ^2-nitrate ligands chelating on the other face of the metal.

Multiple attempts to make the analogous lead(II) nitrate $[15]aneO_3S_2$ complex proved unsuccessful.

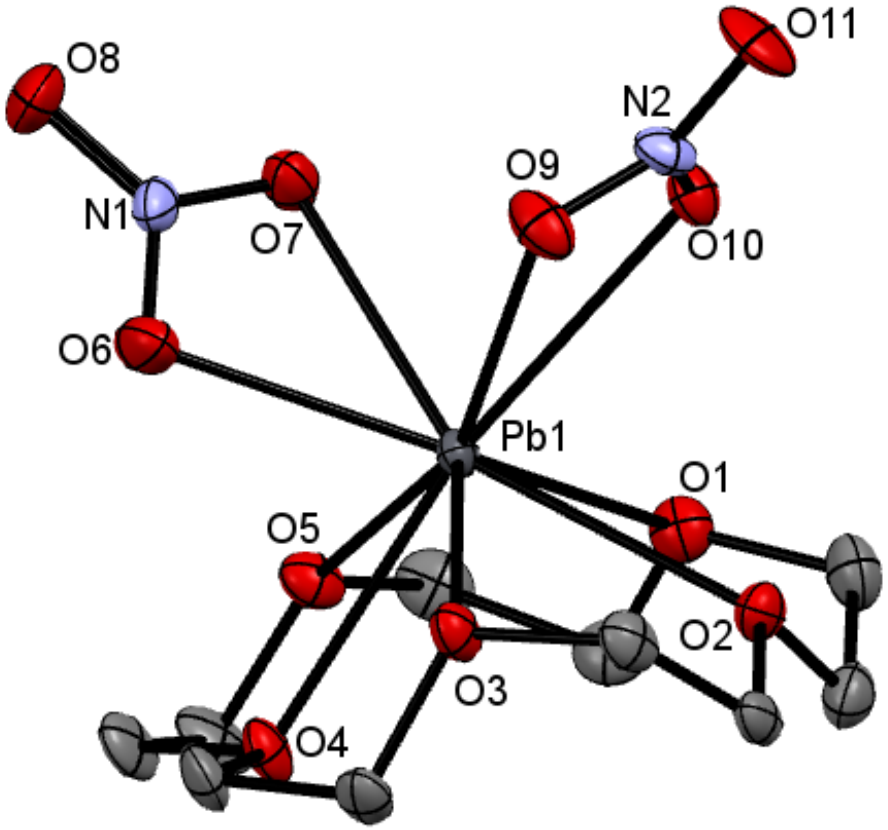

Figure 5.8 Crystal structure of the [Pb(15-crown-5)(NO_3)$_2$] showing the atom numbering scheme. Ellipsoids are drawn at the 50% probability level and H atoms are omitted for clarity.

Table 5.3 Selected bond lengths (Å) and angles (°) for [Pb(15-crown-5)(NO_3)$_2$]

Pb1–O1	2.691(4)	O6–Pb1–O7	49.9(1)
Pb1–O2	2.712(3)	O9–Pb1–O10	48.8(1)
Pb1–O3	2.711(3)	O1–Pb1–O2	64.18(9)
Pb1–O4	2.709(3)	O2–Pb1–O3	62.8(1)
Pb1–O5	2.716(3)	O3–Pb1–O4	61.4(1)
Pb1–O6	2.575(3)	O4–Pb1–O5	61.8(1)
Pb1–O7	2.595(3)	O1–Pb1–O5	63.85(9)
Pb1–O9	2.587(4)		
Pb1–O10	2.680(3)		

5.2.3 $Pb(BF_4)_2$ complexes with 18-membered macrocycles

The Pb(II) cation is too large to fit in the cavity of both 15-membered and 12-membered macrocycle rings and hence give sandwich or half-sandwich complexes. Conversely, with 18-membered macrocycles it fits well within the cavity and a different variety of coordination behaviours are observed for both the macrocycles and the ancillary ligands/anions.

The reaction between $Pb(BF_4)_2$ (aq) and 18-crown-6 gives the unexpected $[BF_4]^-$ bridged dimer $[\{Pb(18\text{-crown-6})(H_2O)(BF_4)\}_2][BF_4]_2$ (Figure 5.9) [9]. Elemental analysis is consistent with the formulation stated and the IR spectrum clearly shows water present and stretches assigned to the tetrafluoroborate anion, although, as with all the related complexes the presence of the macrocycle absorptions makes it necessary to use reference tetrafluoroborate salts for comparison, see 5.2.3.1.

^1H NMR studies show a singlet with very Ill-defined second order effects starting to show and cooling to 228 K failed to resolve any clear pattern, instead a sharpening of the singlet is observed. The chemical shift is to high frequency of the free ligand (+0.39 ppm); also present is a shift at δ 2.15 attributed to the coordinated water.

The crystal structure is only the second known example of a tetrafluoroborate bridged Pb(II) complex, the other being the organolead compound $[(\eta^5\text{-Cp}^*)Pb(\mu^2\text{-}BF_4)_2Pb(\eta^5\text{-Cp}^*)]$ (Figure 5.1). The literature complex has Pb–F distances of 2.831(9) and 2.901(9) Å. In the crown complex they are shorter; Pb1–F3 2.677(5) Å and Pb1–F4a 2.813(4). The ring is slightly buckled and the 9-coordinate lead(II) sits just below the basal plane, an apical water ligand completes the primary coordination sphere and interacts with F atoms *via* two H-bonds to adjacent anionic $[BF_4]^-$ groups. A more detailed discussion of $[BF_4]$ coordination modes is given below (see $[Pb([18]aneO_4Se_2)(BF_4)_2]$).

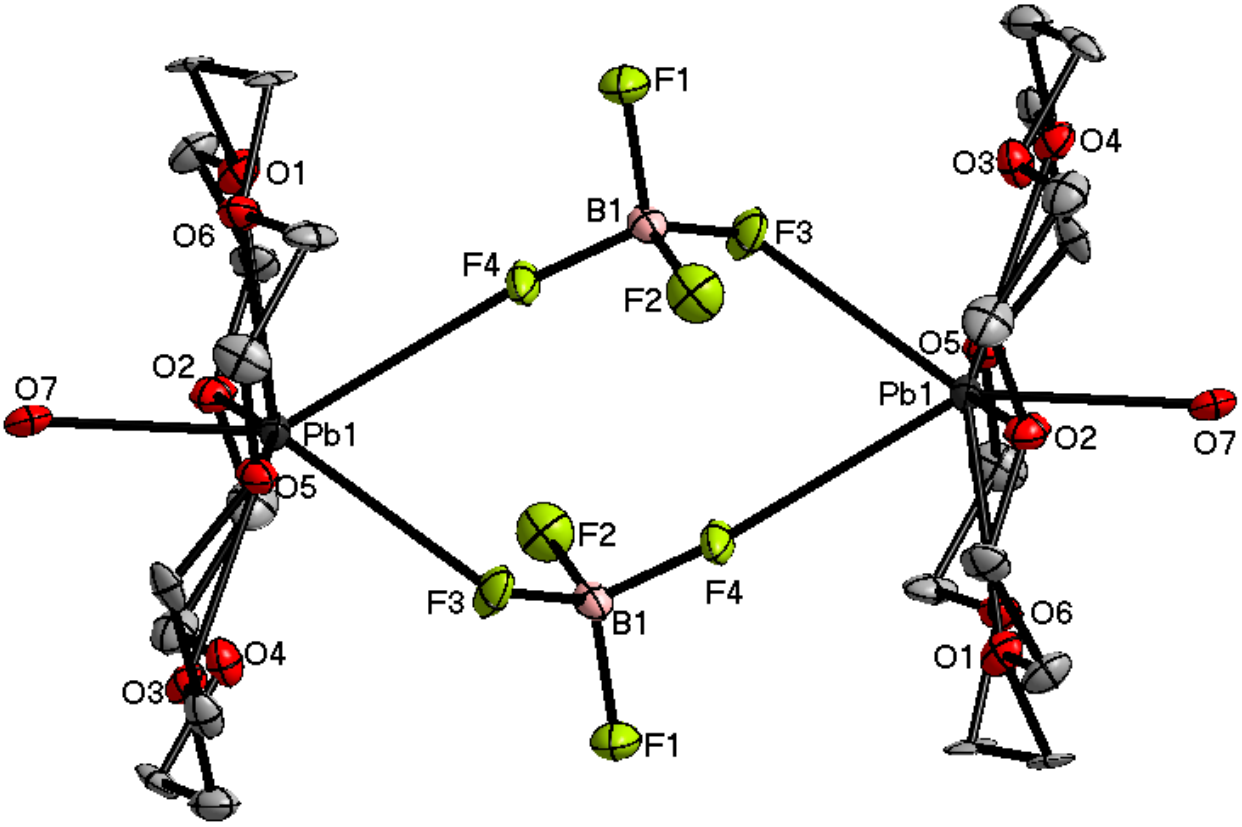

Figure 5.9 Crystal structure of the dimer cation in $[\{Pb(18\text{-crown-6})(H_2O)(BF_4)\}_2][BF_4]_2$ showing the bridging $[BF_4]$ groups. Ellipsoids are drawn at the 50% probability level and H atoms are omitted for clarity. Symmetry operation: a = –x, –y, 2 – z

Table 5.4 Selected bond lengths (Å) and angles (°) for $[\{Pb(18\text{-crown-}6)(H_2O)(BF_4)\}_2][BF_4]_2$

Pb1–F3	2.677(5)	F3–Pb1–F4a	66.3(1)
Pb1–F4	2.812(5)	O1–Pb1–O2	58.9(1)
Pb1–O7	2.405(7)	O2–Pb1–O3	57.7(1)
Pb1–O1	2.745(4)	O3–Pb1–O4	57.8(1)
Pb1–O2	2.803(5)	O5–Pb1–O6	61.1(1)
Pb1–O3	2.895(5)	O5–Pb1–O6	60.8(1)
Pb1–O4	2.733(4)	O1–Pb1–O6	60.1(1)
Pb1–O5	2.710(5)	F1–B1–F2	111.5(7)
Pb1–O6	2.701(5)	F2–B1–F3	109.3(7)
B1–F1	1.40(1)	F3–B1–F4	108.3(7)
B1–F2	1.38(1)	F1–B1–F4	108.4(7)
B1–F3	1.41(1)		
B1–F4	1.411)		

Despite being made the same way, the complex $[Pb([18]aneO_4S_2)(H_2O)_2(BF_4)][BF_4]$ is mononuclear (Figure 5.10). The lead centre sits within the puckered ring cavity and is 10-coordinate, two ligating *cis* water molecules (O5 & 6) sit *trans* to an unusual chelating κ^2-$[BF_4]$ group, the other $[BF_4]^-$ anion remains uncoordinated. Both tetrafluoroborate groups form H-bonds with the coordinated water molecules: O5···F7 2.876(3) Å, O6···F6 2.773(3) Å, O6···F3 2.744(3) Å, forming a network. Analysis of the Pb–donor$_{macrocycle}$ distances again show a preference for the softer donor with the average difference being 0.21 Å which is significantly less than the difference in the covalent radii for S and O (0.39 Å). The spectroscopic data (discussed further below, 5.2.3.1) are in keeping with structure and formulation obtained. The complex was poorly soluble in both $CDCl_3$ and CD_3CN, but weak ^1H NMR spectra were obtained with the expected shifts and there is evidence of water present. The distinct preference for coordination to the sulfur is not retained in

solution with the high frequency shifts being between 0.25-0.3 ppm for all three environments.

Other reported and structurally authenticated Pb(II) [18]aneO$_4$S$_2$ macrocycle complexes include [Pb([18]aneO$_4$S$_2$)(ClO$_4$)$_2$] (Figure 5.3), [Pb([18]aneO$_4$S$_2$)(NO$_3$)$_2$] (Figure 5.4) and [Pb([18]aneO$_4$S$_2$)(NCS)$_2$] (Figure 5.5) [21] [22]. There are large and notable differences between each of the structures.

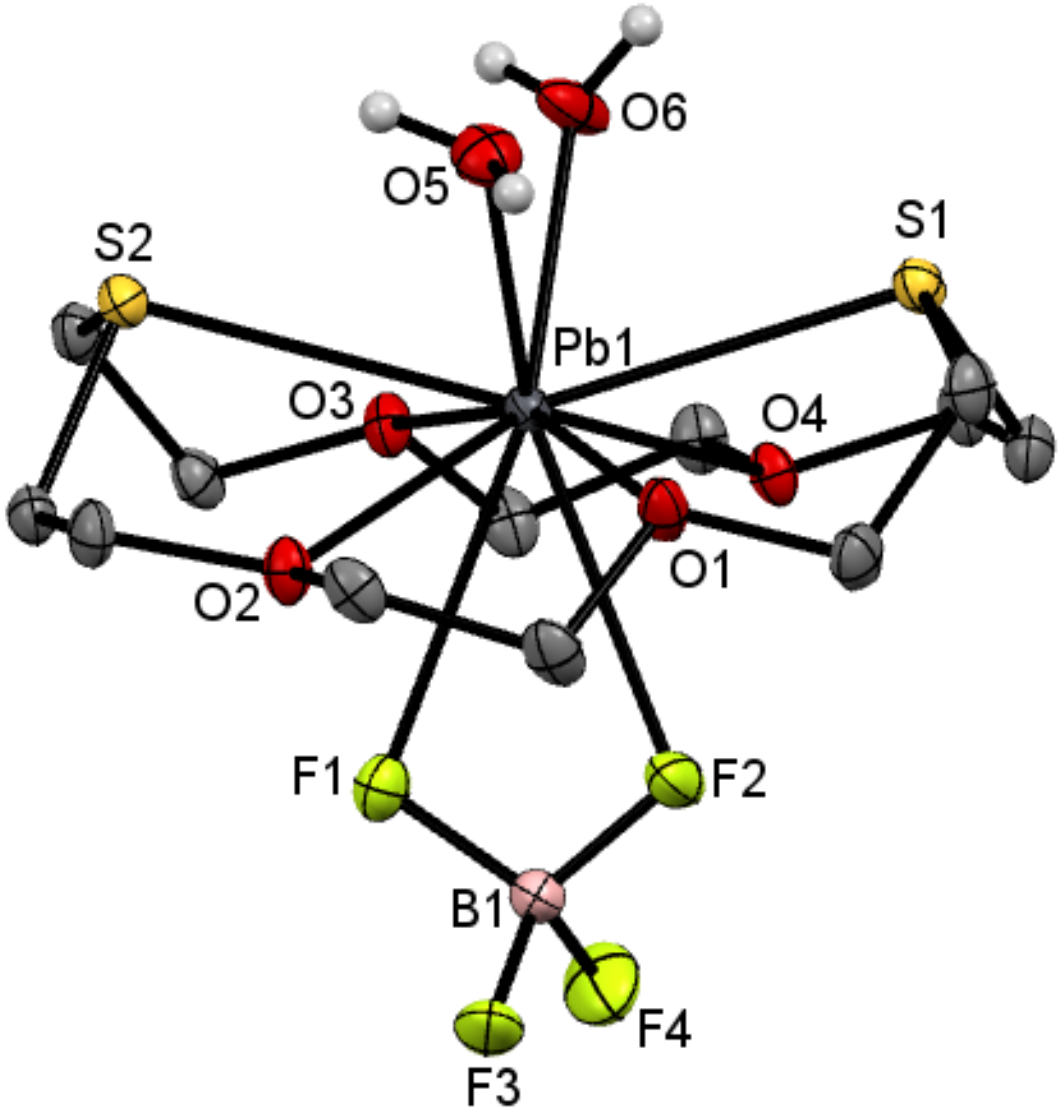

Figure 5.10 Crystal structure of the cation in [Pb([18]aneO$_4$S$_2$)(H$_2$O)$_2$(BF$_4$)][BF$_4$] showing the atom numbering scheme and the coordination around Pb1. Ellipsoids are drawn at the 50% probability level and H atoms bonded to C are omitted for clarity. The uncoordinated [BF$_4$]$^-$ anion is also omitted.

Table 5.5 Selected bond lengths (Å) and angles (°) for $[Pb([18]aneO_4S_2)(H_2O)_2(BF_4)][BF_4]$

Pb1–F1	3.038(2)	O5–Pb1–O6	73.04(7)
Pb1–F2	2.877(2)	S1–Pb1–S2	147.41(2)
Pb1–S1	3.0151(8)	S1–Pb1–O1	64.43(4)
Pb1–S2	3.0191(7)	O1–Pb1–O2	59.03(5)
Pb1–O1	2.888(2)	S2–Pb1–O2	64.90(4)
Pb1–O2	2.842(2)	S2–Pb1–O3	65.07(4)
Pb1–O3	2.726(2)	O3–Pb1–O4	62.68(6)
Pb1–O4	2.731(2)	S1–Pb1–O4	66.64(4)
Pb1–O5	2.559(2)	F1–Pb1–F2	44.93(5)
Pb1–O6	2.471(2)	F1–B1–F2	108.2(2)
B1–F1	1.398(4)	F2–B1–F3	108.5(2)
B1–F2	1.399(4)	F3–B1–F4	110.1(3)
B1–F3	1.404(4)	F1–B1–F4	110.3(2)
B1–F4	1.377(4)		

In the perchlorate analogue there is no significant difference between the Pb-donor$_{macrocycle}$ bond distances. Conversely the isothiocyanate complex, like the tetrafluoroborate analogue in this study, has significantly shorter Pb–S bonds (ave) 0.18 Å longer which is much less than 0.39 Å the difference in covalent radii for O and S [6]. The nitrate structure is disordered (the same problem experienced for $[Pb([18]aneO_4Se_2)(NO_3)_2]$ discussed below) and hence a detailed structural comparison is not possible. Nevertheless it can be seen from the partial structure that the nitrate groups chelate bidentate and are coordinated *cis* to each other with the macrocycle much more encapsulating; in the isothiocyanate and tetrafluoroborate complexes the macrocycle is far more planar being only slightly puckered with the S-donors also *syn* to each other. Contrastingly, in $[Pb([18]aneO_4S_2)(ClO_4)_2]$ the κ^1-perchlorate groups are coordinated *trans*

across the lead to each other, also the macrocycle folds in a more sigmoidal fashion with the S-donors *anti* to one another. The coordination strength of the co-ligands also varies, the Pb–F interactions for $[BF_4]^-$ in $[Pb([18]aneO_4S_2)(H_2O)_2(BF_4)][BF_4]$ are the weakest ligand interaction in the system with the water ligands being the strongest ($Pb–O_{water}$ 2.471(2) and 2.559(2) Å; $Pb–O_{macrocycle}$ 2726(2)-2.888(2) Å). The $[ClO_4]^-$ anions are bound to a similar extent as the macrocyclic donors in $[Pb([18]aneO_4S_2)(ClO_4)_2]$ whereas in $[Pb([18]aneO_4S_2)(NCS)_2]$ the $[NCS]^-$ are bound closer. This follows the predicted ligand behaviours:

$$[BF_4]<[ClO_4]<<H_2O<[NCS]$$

The perchlorate and tetrafluoroborate anions are more weakly coordinating than isothiocyanate or water. A note on the isothiocyanate complex is the Pb(II) coordinates through the harder N-donor over the sulfur donor. The general picture that is beginning to form is that the Pb(II) centre has no clear stereochemical driving force with the primary coordination sphere being dominated by the maximum number of interactions whilst taking into account the inter-ligand repulsions and the steric constraints of the various ligands. In $[Pb([18]aneO_4S_2)(ClO_4)_2]$ and $[Pb([18]aneO_4S_2)(NCS)_2]$ the lead(II) is 8-coordinate, whereas 10-coordinate in the tetrafluoroborate and nitrate analogues.

Table 5.6 Selected bond lengths (Å) and angles (°) for $[Pb([18]aneO_4Se_2)(BF_4)_2]$

Pb1–F1	2.707(5)	F1–Pb1–F4	43.5(1)
Pb1–F4	3.222(5)	Se1–Pb1–Se1a	155.61(2)
Pb1–Se1	3.182(2)	Se1–Pb1–O1	65.4(1)
Pb1–O1	2.717(5)	Se1–Pb1–O2	68.7(1)
Pb1–O2	2.584(5)	O1–Pb1–O2	64.0(1)
B1–F1	1.411(8)	F1–B1–F2	107.6(6)
B1–F2	1.39(1)	F2–B1–F3	111.4(6)
B1–F3	1.371(9)	F3–B1–F4	111.9(6)
B1–F4	1.395(9)	F1–B1–F4	106.6(6)

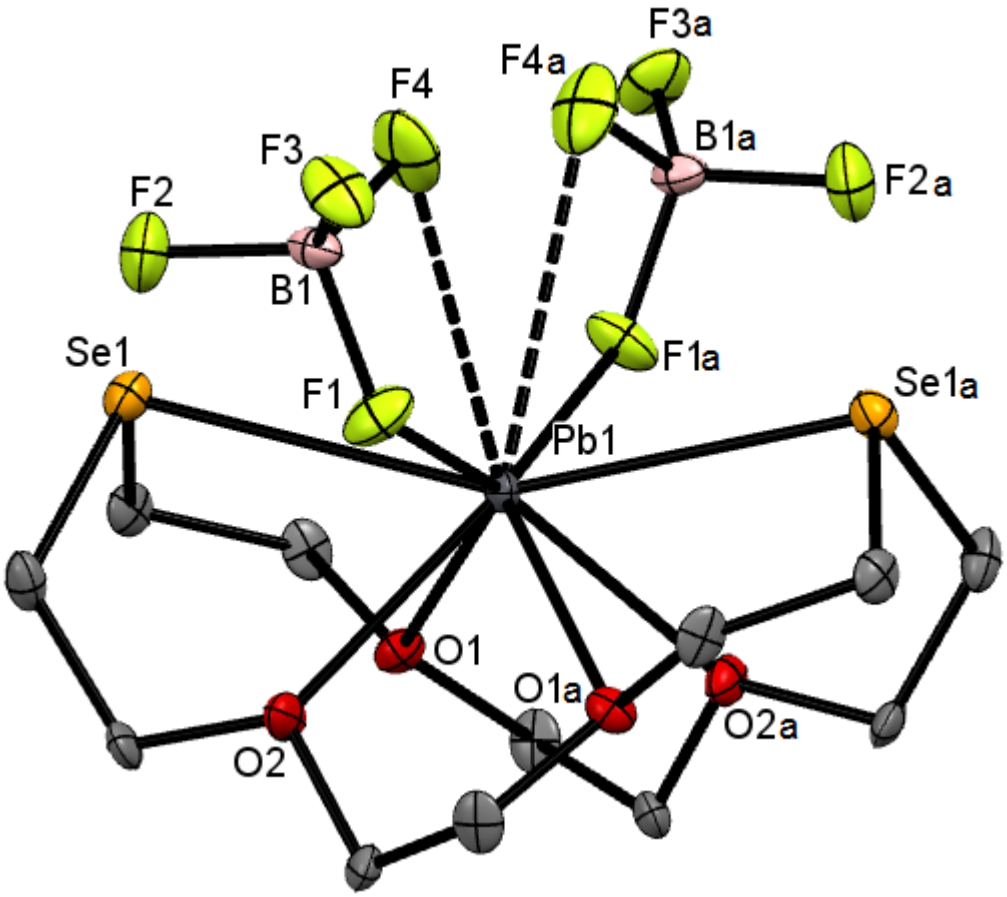

Figure 5.11 Crystal structure of [Pb([18]aneO$_4$Se$_2$)(BF$_4$)$_2$] showing the atom numbering scheme. The cation has two-fold symmetry. Ellipsoids are drawn at the 50% probability level and H atoms have been omitted for clarity. Symmetry operation: a = 1 – x, y, 1/2 – z.

The complex [Pb([18]aneO$_4$Se$_2$)(BF$_4$)$_2$] (Figure 5.11) is different again. The crystal structure does not fully correspond with the spectroscopic data. Both in the IR and ^{1}H NMR spectra there are strong signals attributed to water (see 5.2.3.1), but multiple attempts to grow crystals gave exclusively the neutral complex. Like in [Pb([18]aneO$_4$S$_2$)(NO$_3$)$_2$] (Figure 5.4); the macrocycle has a very folded conformation around the lead(II) centre with the [BF$_4$]$^-$ groups coordinated mutually *cis*. [Pb([18]aneO$_4$Se$_2$)(BF$_4$)$_2$] represents the first structurally authenticated example of any lead species coordinated to an oxa-selena crown. Comparing the Pb-E (E= S, Se) distances in the two mixed chalcogenoether tetrafluoroborate complexes ([Pb([18]aneO$_4$S$_2$)(H$_2$O)$_2$(BF$_4$)][BF$_4$] and [Pb([18]aneO$_4$Se$_2$)(BF$_4$)$_2$]) shows a difference of 0.16 Å which closely corresponds to the difference in the covalent radii between S and Se indicating both donors have a similar affinity for the lead. The Pb–O distances are shorter in the oxa-selena

macrocycle complex than in the oxa-thia complex, comparison with the Pb–Se distances show a mean difference of 0.53 Å, which matches the difference in covalent radii for Se and O (0.54 Å); in this system the lead(II) coordinates equally to both donor types. The most unusual structural feature in this complex is the two Pb–F distances of the chelating $[BF_4]^-$ are highly asymmetric Pb1–F1= 2.707(4), Pb1–F4= 3.223(5) Å, Δ_{Pb-F}= 0.52 Å. This disparity is great enough to consider κ^1-coordination as the coordination mode. A similar situation is apparent in the complex $[Pb([18]aneO_4S_2)(ClO_4)_2]$ (Figure 5.3, mentioned above), both $Pb-O_{perchlorate}$ distances lie well within the ΣVdW radii but as in the tetrafluoroborate example there is a sizeable difference, Δ_{Pb-F}= 0.33 Å. Examination of the non-bonded contacts involving the fluoroborate groups in $[Pb([18]aneO_4Se_2)(BF_4)_2]$ provides a possible explanation; F4···F4a is 2.975(7) Å which is very close to the ΣVdW radius for two fluorines (2 x 1.47 Å) [27], chelating more symmetrically to the lead(II) is hindered by this steric interaction. Interpretation of the coordination number in these systems depends on the perception of what constitutes a coordinate bond, from the point of view of the ΣVdW radii $[Pb([18]aneO_4Se_2)(BF_4)_2]$ is 10-coordinate but if the $[BF_4]$ groups are to be considered monodentate then the coordination number is 8. In the literature the perchlorate groups in $[Pb([18]aneO_4S_2)(ClO_4)_2]$ are reported to be κ^1-coordinated.

A note on the $[BF_4]$ groups in $[\{Pb(18\text{-crown-6})(H_2O)(BF_4)\}_2][BF_4]_2$ (Figure 5.9); although it has been reported as an example of μ^2-coordination by the tetrafluoroborate anion, closer examination of all the Pb···F contacts show an identical situation to $[Pb([18]aneO_4Se_2)(BF_4)_2]$ where the $[BF_4]$ group could also be considered chelating (κ^2) albeit asymmetrically Δ_{Pb-F}= 0.52 Å, (Pb1–F3= 2.677(5), Pb1···F2= 3.201(5) Å). This highlights how difficult it can be to assign asymmetric coordination especially in crowded metal centres. In $[(\eta^5\text{-Cp*})Pb(\mu^2\text{-}BF_4)_2Pb(\eta^5\text{-Cp*})]$ the only $[BF_4]^-$ coordination mode is μ^2.

In all the tetrafluoroborate complexes the effect of the coordination on both the B–F distances and F–B–F angles is small, reflecting the very strong B–F bonding.

5.2.3.1 Spectroscopic studies on $Pb(BF_4)_2$ complexes

Using reference tetrafluoroborate salts such $NaBF_4$ and $[TBA][BF_4]$ (TBA= tetrabutylammonium), the $[BF_4]$ IR stretches can be assigned with reasonable certainty for the macrocycle complexes. The ionic tetrafluoroborate anion absorbs at ~1070 and ~520 cm^{-1}, a broad (often asymmetric) stretching mode and sharp band for the bending mode respectively [28].

Differences from the reference tetrafluoroborate salts are noticeable, furthermore the individual $[BF_4]^-$ absorptions differ from each other from complex to complex. This is all indicative of the different coordination modes for $[BF_4]^-$ observed in the crystal structures for the tetrafluoroborate salts. Unfortunately the broad nature of the bands and presence of other ligand modes preclude detailed analysis of the IR absorptions to the extent where the anion coordination mode is identifiable (from the IR spectra alone). H-bonding to neighbouring groups or site symmetry can cause some ill-defined splitting in the higher frequency band as seen for the 15-membered macrocycle sandwich complexes.

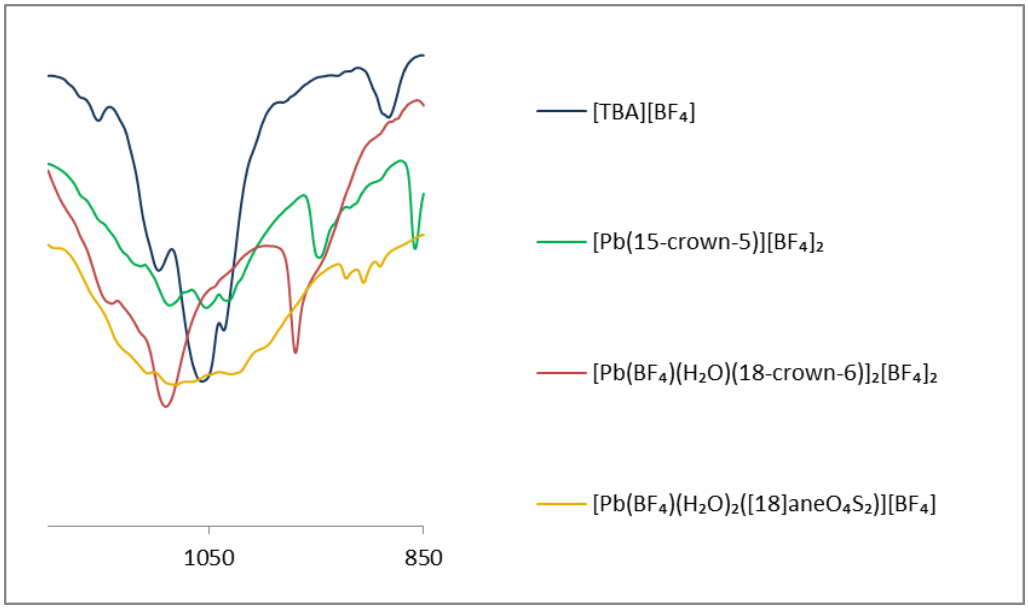

Figure 5.12 IR (Nujol, cm^{-1}) spectra for selected tetrafluoroborate salts showing the stretching region ~1070 cm^{-1}

Attempts to obtain ^{207}Pb and $^{77}Se\{^1H\}$ NMR data on these Pb(II) systems were unsuccessful in that no resonances were observed over the

temperature range 295-220 K even after long accumulations, likely due to the highly labile nature of the species in solution.

From the observed ^{1}H NMR data it seems likely that the Pb-macrocycle interactions are maintained in solution for all the tetrafluoroborate complexes.

The structures and the solid-state data all positively identify unusual coordination of the tetrafluoroborate anion. $^{19}F\{^{1}H\}$ NMR studies differ in that only one $[BF_4]$ environment is seen for all five of the complexes (Table 5.7). Whereas the macrocycles remain coordinated once the complexes are in solution the weakly coordinating tetrafluoroborate anion dissociates. This is further concluded from the results obtained from the conductivity studies performed (Table 5.8).

Table 5.7 $^{19}F\{^{1}H\}$ NMR data for relevant tetrafluoroborate salts

$[BF_4]^-$ salt	$^{19}F\{^{1}H\}$ NMR (δ)
$[TBA][BF_4]$	-151.0[a]
$Pb(BF_4)_2$	-149.8[a], 150.7[d]
$[Pb(15\text{-crown-}5)_2][BF_4]_2$	-152.2[c]
$[Pb([15]aneO_3S_2)_2][BF_4]_2$	-151.3[c]
$[\{Pb(18\text{-crown-}6)(H_2O)(BF_4)\}_2][BF_4]_2$	-150.3[a], -151.8[b]
$[Pb([18]aneO_4S_2)(H_2O)_2(BF_4)][BF_4]$	-148.5[c]
$[Pb([18]aneO_4Se_2)(BF_4)_2]$	-150.5[b]

[a]D_2O, [b]CD_3CN, [c]CD_2Cl_2, [d]CD_3CN/H_2O. The different deuterated solvents reflect the relative solubilities of the products.

In all the $[BF_4]$ complexes, under high resolution, two very closely spaced singlets in an approximate ratio of 1:4 are seen, these are due to the ^{10}B and ^{11}B isotopomers. The $^{1}J_{BF}$ couplings are very small and unresolved [29].

Table 5.8 Conductivity measurements for Pb(II) complexes (10^{-3} mol dm^{-3}, CH_3CN), recorded using a Cambridge conductivity bridge.

Pb(II) complex	Λ_M (ohm^{-1} cm^2 mol^{-1})
$[Pb(15\text{-crown-}5)_2][BF_4]_2$	335
$[Pb([15]aneO_3S_2)_2][BF_4]_2$	350
$[Pb([18]aneO_4S_2)(H_2O)_2(BF_4)][BF_4]$	314
$[Pb(15\text{-crown-}5)(NO_3)_2]$	40
$[Pb(18\text{-crown-}6)(NO_3)_2]$	50

The conductivity measurements Table 5.8 clearly show that solutions of the tetrafluoroborate complexes have high conductivities. When used in conjunction with the evidence from the $^{19}F\{^1H\}$ NMR data, the values can be accounted for by the dissociation of the coordinated $[BF_4]^-$ groups and the sole presence of ionic tetrafluoroborate anions. In contrast, solutions of the nitrate complexes failed to conduct substantially indicating the $[NO_3]^-$ groups remain coordinated in solution. Attempts to collect conductivity data for $[Pb([18]aneO_4Se_2)(NO_3)_2]$ were precluded due to the insoluble nature of the salt.

Despite the $[BF_4]$ anions dissociating in solution, MeCN does not compete as a ligand in the solid state. All the products and their structures in this study are reproducible not only in acetonitrile but also acetone and in some cases dichloromethane; the complexes decomposed in nitromethane.

Even after multiple recrystallisation attempts, analytically pure samples of $[Pb([18]aneO_4Se_2)(BF_4)_2]$ were not obtained. The spectroscopic data showed the expected IR data for $[BF_4]$ and in the ^1H NMR spectrum there are three geometrically distinct C$\boldsymbol{H}_2$ signals substantially shifted from the free ligand (+0.25-0.32 ppm). Both sets of data conclusively showed the presence of water (seemingly coordinated), although the microanalytical data failed to correspond to a sensible hydrate formulation.

Attempts to form Pb(II) oxa-tellura macrocycle complexes failed. Dissolving $Pb(BF_4)_2$ (aq) in an $MeCN/CH_2Cl_2$ solution of $[18]aneO_4Te_2$ (yellow) gave an immediate intense orange solution that deposited a black solid over 12 h. A subsequent preparation isolated an orange oil which produced a black solid on redissolution in CD_3CN (compare $[ScCl_2([18]aneO_4Te_2)][FeCl_4]$, Chapter 4). The ^1H NMR spectrum showed a complex mixture of products, alongside shifts associated with protons on ethers and telluro-ethers (3.4-4.2 ppm) there was an intense and very broad signal at δ 6.78. This is within the range for vinyl protons and indicative of ring opening and breakup of the macrocycle. The C–Te bond is weak and it is conceivable that polarisation by the Pb^{2+} cation initiates a ring-opening mechanism; the black solid produced was assumed to be elemental tellurium.

5.2.4 $Pb(NO_3)_2$ and $Pb(PF_6)_2$ complexes with 18-membered macrocycles

The $[PF_6]^-$ anion is similar to tetrafluoroborate in that they are both considered non-coordinating and relatively stable counterions. The analogous hexafluorophosphate complexes were investigated to see whether the smaller bite angle (if coordinated) would give differing coordination geometries and/or behaviours.

The reaction between 18-crown-6 and $Pb(PF_6)_2$ (aq) in acetonitrile gives the $[PF_6]$ salt, $[Pb(18\text{-crown-6})(H_2O)_2(PF_6)][PF_6]$. Crystals had the constitution $[Pb(18\text{-crown-6})(H_2O)_{1.6}(PF_6)][PF_6] \cdot 0.6H_2O$ (Figure 5.13), the crown is slightly buckled and the 10-coordinate Pb(II) centre sits in the plane of the macrocycle. There are two coordinated waters *trans* to a κ^2-coordinated $[PF_6]^-$ anion, the other $[PF_6]^-$ remains free. The overall structure bears a very close similarity to $[Pb([18]aneO_4S_2)(H_2O)_2(BF_4)][BF_4]$ (Figure 5.10). The two aquo ligands hydrogen bond to another water (O7) and the F4 and F6 atoms from both the hexafluorophosphates; O5···O7= 2.82(3) Å, O6···O7= 2.50(4) Å, O5···F4= 2.60(3) Å, O6···F7= 2.95(1) Å.

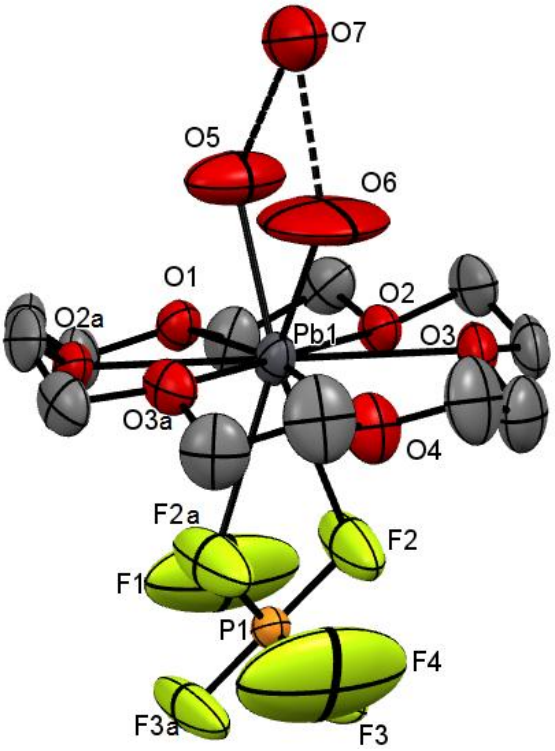

Figure 5.13 Crystal structure of the cation in $[Pb(PF_6)(18\text{-crown-6})(H_2O)_{1.6}][PF_6]\cdot 0.6H_2O$ showing the atom labelling scheme. The P2 centred PF_6 anion is not shown. Ellipsoids are drawn at the 40% probability level and H atoms are omitted for clarity. The molecule drawn has mirror symmetry. Symmetry operation: a = x, 1 – y, z.

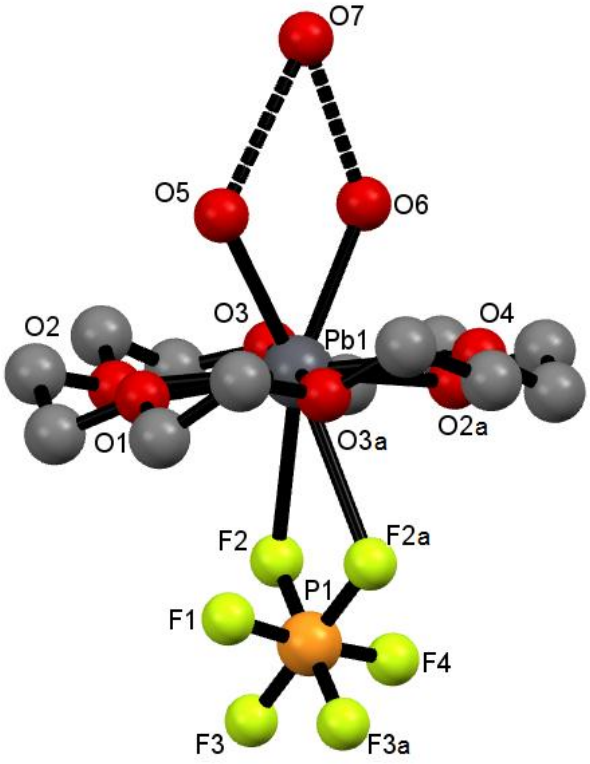

Figure 5.14"Ball and Stick" representation of $[Pb(PF_6)\ (18\text{-crown-6})(H_2O)_{1.6}][PF_6]\cdot 0.6H_2O$

Table 5.9 Selected bond lengths (Å) and angles (°) for $[Pb(PF_6)(18\text{-crown-6})(H_2O)_{1.6}][PF_6]\cdot 0.6H_2O$

Pb1–F2	2.88(1)	F2–Pb1–F2a	43.2(3)
Pb1–O5	2.55(2)	O5–Pb1–O6	57.8(9)
Pb1–O6	2.57(4)	O1–Pb1–O2	60.0(3)
Pb1–O1	2.70(1)	O2–Pb1–O3	60.1(2)
Pb1–O2	2.736(6)	O3–Pb1–O4	61.1(3)
Pb1–O3	2.7318)	F1–P1–F4	175(1)
Pb1–O4	2.73(1)	F2–P1–F3	179.0(6)
P1–F1	1.45(2)	F1–P1–F3	92.5(8)
P1–F2	1.561)	F2–P1–F2a	85.5(6)
P1–F3	1.52(1)	F3–P1–F3a	86.8(6)
P1–F4	1.46(2)	F2–P1–F4	88(1)
O5···O7	2.82(3)		
O6···O7	2.50(4)		

For all the bis-hexafluorophosphate complexes, obtaining analytically pure samples proved to be unachievable. Like the parent Pb(II) salt the complexes were unstable and decomposed rapidly. Although crystals were readily grown and carefully separated from the concentrated reaction mixtures, the products quickly decomposed and analysis of the mother liquors showed considerable amounts of hydrolysis products. Using a combination of $^{19}F\{^1H\}$ and $^{31}P\{^1H\}$ NMR and IR spectroscopy showed the presence of $[PO_3F]^{2-}$, $[PO_2F_2]^-$, F^- and $[PO_4H_{3-n}]^{n-}$ [26].

The above reaction for $[Pb(18\text{-crown-6})(H_2O)_2(PF_6)][PF_6]$ was repeated and *in situ* $^{19}F\{^1H\}$ NMR studies undertaken. During the first hour the sole $[PF_6]^-$ environment began to decrease in intensity and the concentration of $[PO_3F]^{2-}$ (δ -82.8, d) steadily increased. Over time the $[PO_3F]^{2-}$ signal also diminishes and a shift attributable to $[BF_4]^-$ appears. This is evidence for attack on the borosilicate in the glass, other $[PF_6]$ salts

([SnF(18-crown-6-)][PF_6], Sn(PF_6)$_2$ see Chapter 6; and the other complexes) have shown they readily attack the glass (or at least their decomposition products) and analysis of their $^{19}F\{^1H\}$ NMR spectra also show [BF_4]$^-$ and [SiF_5]$^-$/[SiF_6]$^{2-}$ present after sometime.

A different approach towards [Pb(18-crown-6)][PF_6]$_2$ involved making the analogous nitrate and reacting it with an excess of [NH_4][PF_6]. Full metathesis did not occur, instead an interesting mixed anion system, [Pb(18-crown-6)(PF_6)(NO_3)] (Figure 5.15), formed. The spectroscopic data was as expected and X-ray quality crystals were collected.

The lead(II) sits in plane of the ring with the anions coordinated *trans* to each other. The nitrate chelates *via* two oxygens and the [PF_6]$^-$ is tridentate, a rare example of κ^3-coordination. The overall coordination number around the lead is 11. The Pb–F distances are well within the ΣVdW radii (3.49 Å), Pb1–F2= 2.975(9), Pb1–F4= 3.174(8) Å. Interestingly, the P–F bonds that interact with the lead(II) are slightly lengthened compared to the other three non-bonded P–F moieties; P1–F2= 1.605(9), P1–F4= 1.610(7) Å *vs*. P1–F3= 1.564(9), P1–F1= 1.586(9) Å.

Although [Pb(18-crown-6)(PF_6)(NO_3)] itself is stable, this lengthening of the coordinated P–F bonds may provide an insight into why the bis-[PF_6] complexes decompose so rapidly. Coordination to the lead centre weakens the P–F bond and thus undergoes hydrolysis far more readily. Another contributing factor may be the insolubility of lead(II) fluoride which would remove any [F]$^-$ generated from the solution and thereby "push" the equilibrium towards hydrolysis. This is in contrast to the tetrafluoroborate complexes where the [BF_4] group is little perturbed by coordination to the lead(II) and henceforth is far more stable.

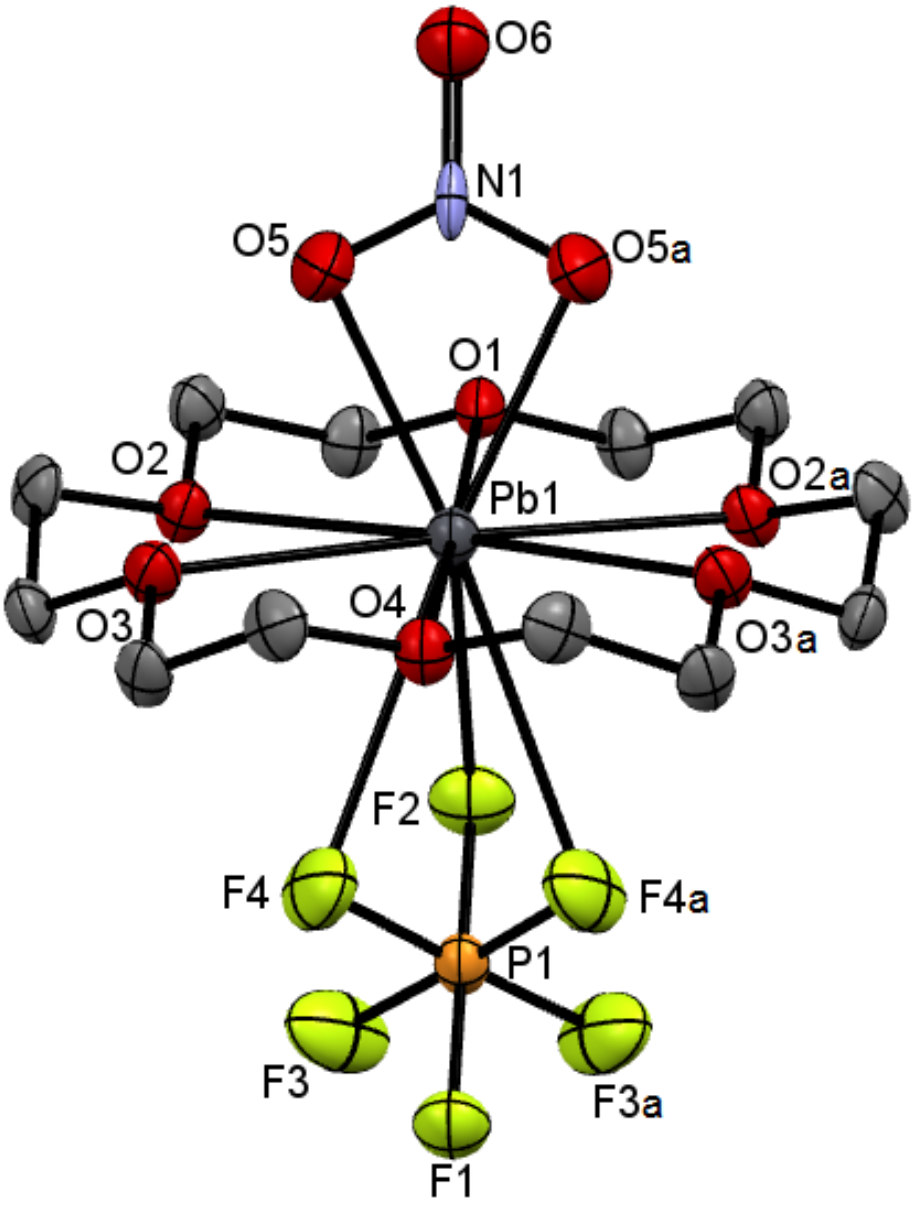

Figure 5.15 Crystal structure of [Pb(18-crown-6)(PF_6)(NO_3)] showing the atom labelling scheme. Ellipsoids are drawn at the 50% probability level and H atoms are omitted for clarity. The molecule has mirror symmetry. Symmetry operation: a = 1 – x, y, z.

Table 5.10 Selected bond lengths (Å) and angles (°) for [Pb(18-crown-6)(PF_6)(NO_3)]

Pb1–F2	2.975(9)	F2–Pb1–F4	42.9(2)
Pb1–F4	3.174(8)	F4–Pb1–F4a	41.1(2)
Pb1–O5	2.526(8)	O5–Pb1–O5a	50.6(2)
Pb1–O1	2.715(9)	O1–Pb1–O2	61.8(2)
Pb1–O2	2.736(5)	O2–Pb1–O3	60.7(2)
Pb1–O3	2.811(7)	O3–Pb1–O4	68.9(2)
Pb1–O4	2.80(1)	F1–P1–F2	179.1(5)
P1–F1	1.59(1)	F3–P1–F4	177.7(5)
P1–F2	1.605(9)	F1–P1–F4	90.3(5)
P1–F3	1.564(9)	F2–P1–F3	90.7(5)
P1–F4	1.610(8)	F2–P1–F4	89.0(5)
		F4–P1–F4a	87.5(4)

Comparison with other Pb(II) 18-crown-6 complexes in the literature show a very similar equatorial arrangement of the crown with the lead in the plane of the ring and the co-ligands arranged mutually *trans*, in the cases where there are three ancillary ligands they occupy a meridian around the lead centre with the crown more buckled/folded away from the two mutually *cis* co-ligands. The complex [PbCl(18-crown-6)][$SbCl_6$] similarly has an octahedral anion providing charge balance. In this example the Pb(II) sits in the plane of the crown with the chloride bound on one side and an open face on the other side to which the [$SbCl_6$]$^-$ anion is directed. However, examination of the Pb$\cdots$$Cl_{Sb}$ show they equal the ΣVdW radii (3.81 Å) which suggests it is simply packing in the crystal structure.

The reaction with the oxa-thia macrocycle [18]aneO_4S_2 failed to give crystals of suitable quality for X-ray diffraction studies but the spectroscopy closely matches that of [Pb(18-crown-6)(H_2O)$_2$(PF_6)][PF_6] indicating a likely constitution of [Pb([18]aneO_4S_2)(H_2O)$_2$(PF_6)][PF_6].

As with the tetrafluoroborate complexes the $[PF_6]^-$ and $[NO_3]^-$ complexes' spectroscopic measurements were referenced to the parent salts ($Pb(NO_3)_2$ and $Pb(PF_6)_2$) and standard salts ($NaPF_6$ and $[NH_4][PF_6]$).

The κ^2-coordinated nitrates (identified crystallographically) have C_{2v} approximate symmetry for which three stretching modes are expected, all of which are IR active. Lanthanide nitrate complexes make good comparisons as they also exhibit high coordination numbers on large metal centres with no strong stereochemical preferences. Typical IR bands for such complexes are in the range ~1470, 1310, 1030 and 820 cm^{-1} (three stretches and one bending mode) [28]. The complexes present herein show these features although the stretch at ~1470 cm^{-1} is obscured. The published IR spectrum of $[Pb([18]aneO_4S_2)(NO_3)_2]$ [21] also shows bands at 1357, 1012 and 801 cm^{-1} consistent with the nitrate coordination present. A closer examination of the coordinate bond lengths show the nitrates in this study bind asymmetrically, but even allowing for lower actually symmetry three stretching modes are still predicted. The frequencies distinguish coordinated from ionic nitrate, but distinguishing κ^1 and κ^2-coordination has been controversial in many systems [28].

Ionic hexafluorophosphate shows stretching and bending modes at ~850 and ~560 cm^{-1} respectively [28]. In the IR spectra only broadened vibrations with no resolved splittings are observed for all of the complexes. Like the $[BF_4]^-$ complexes already described, only one anion environment ($^{19}F\{^1H\}$ and $^{31}P\{^1H\}$ NMR) is seen in solution for $[PF_6]^-$ showing the anion dissociates from the metal centre.

Reactions of both $Pb(NO_3)_2$ and $Pb(PF_6)_2$ (aq) with the oxa-selena crown $[18]aneO_4Se_2$ gave the desired complexes, $[Pb([18]aneO_4Se_2)(NO_3)_2]$ (Figure 5.17) and $[Pb([18]aneO_4Se_2)(PF_6)_2]$ (Figure 5.16). Like the crystals of $[Pb([18]aneO_4Se_2)(BF_4)_2]$ only the neutral anhydrous complexes were isolated. Both products had the expected spectroscopic features.

The crystal structures of all three seleno-ether complexes have a very similar folded conformation of the macrocycle, encapsulating the lead(II) centre. The anions ($[NO_3]^-$, $[BF_4]^-$, $[PF_6]^-$) are mutually coordinated in a *cisoidal* fashion. The major difference between the two fluoroanion structures is where the $[BF_4]^-$ groups are very asymmetrically coordinated

(~κ^1), the $[PF_6]^-$ groups form a symmetrical chelate to the lead centre. This difference can be attributed to the smaller bite angle of the octahedral anion reducing the steric interaction with the other hexafluorophosphate. The P–F bonds that interact with Pb(II) again show a lengthening compared to the non-bonded P–F bonds. The nitrate structure features crystallographic disorder.

The structure of $[Pb([18]aneO_4Se_2)(NO_3)_2]$ was solved in the space group *C*2/*c* and is isomorphous to the tetrafluoroborate analogue. The molecule has two-fold symmetry in which the lead(II) is 10-coordinate with two κ^2-nitrate groups, which are disordered over two sites. Solving the structure in the non-centrosymmetric space group *Cc* removes the disorder in the anions, but the data failed to converge satisfactorily. Similar problems were apparent for $[Pb([18]aneO_4S_2)(NO_3)_2]$, in this case the structure was reported in the space group *Cc* with a large number of restraints. This is a well-known crystallographic problem, and the chemical identity of the complex is not in doubt. Still, in light of the disorder present a detailed comparison of the bond lengths is prevented.

The analogous reaction of $Pb(NO_3)_2$ and $[18]aneO_4Te_2$ only resulted in recovery of the starting oxa-tellura macrocycle.

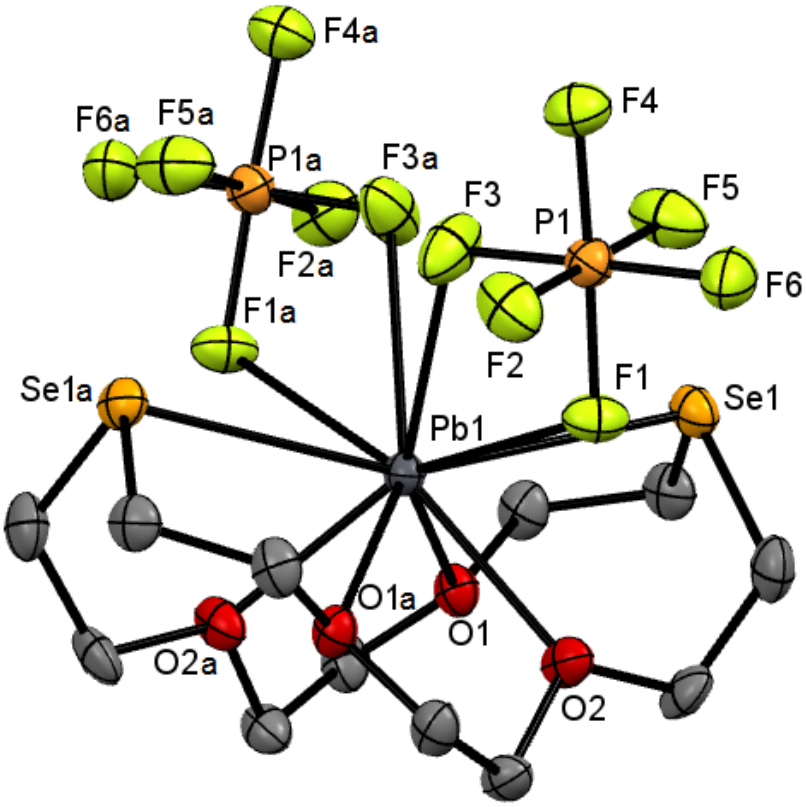

Figure 5.16 Crystal structure of [Pb([18]aneO$_4$Se$_2$)(PF$_6$)$_2$] showing the atom labelling scheme. Ellipsoids are drawn at the 50% probability level and H atoms are omitted for clarity. The molecule has two-fold symmetry. Symmetry operation: a = -x, y, 1/2 - z.

Table 5.11 Selected bond lengths (Å) and angles (°) for [Pb([18]aneO$_4$Se$_2$)(PF$_6$)$_2$]

Pb1-F1	2.921(3)	F1-Pb1-F3	45.2(1)
Pb1-F3	2.907(4)	Se1-Pb1-Se1a	156.01(1)
Pb1-Se1	3.173(1)	Se1-Pb1-O1	65.14(8)
Pb1-O1	2.664(3)	Se1-Pb1-O2	69.60(8)
Pb1-O2	2.5443(4)	O1-Pb1-O2	63.7(1)
P1-F1	1.616(3)	F1-P1-F4	178.1(2)
P1-F2	1.588(3)	F3-P1-F6	178.6(2)
P1-F3	1.610(4)	F1-P1-F3	88.0(2)
P1-F4	1.591(4)	F1-P1-F5	90.4(2)
P1-F5	1.584(4)	F2-P1-F3	90.7(2)
P1-F6	1.592(4)	F4-P1-F6	90.9(2)

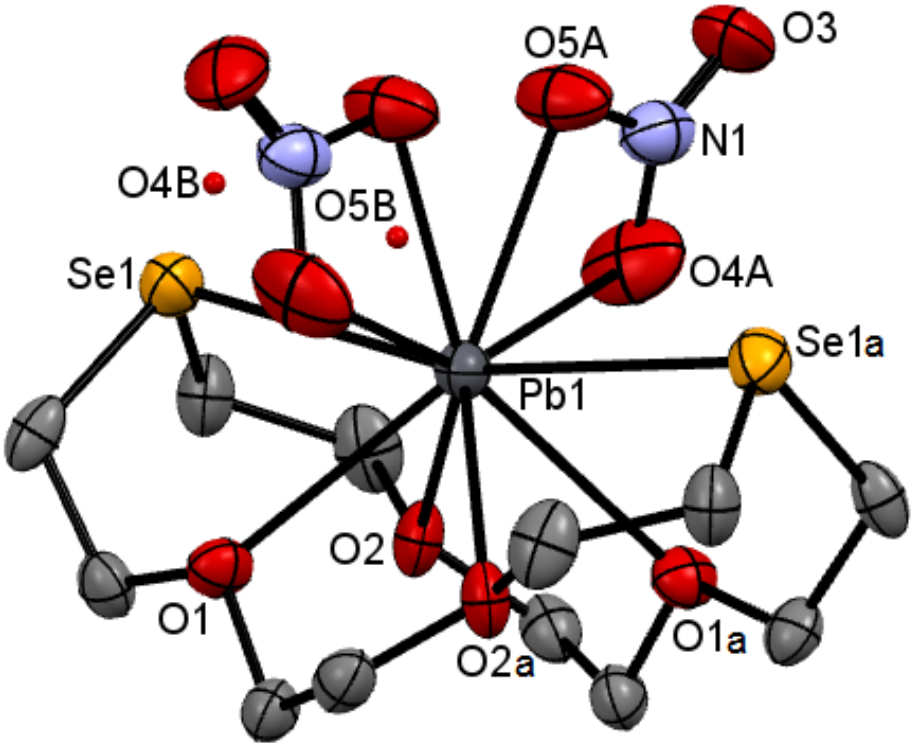

Figure 5.17 Crystal structure of [Pb([18]aneO$_4$Se$_2$)(NO$_3$)$_2$] refined in the space group C2/c showing the atom numbering scheme. The molecule has two-fold symmetry. Ellipsoids are drawn at the 30% probability level and H atoms have been omitted for clarity. The disordered nitrate was modelled as O4A/B and O5A/B. Symmetry operation: i = – x, y, 1/2 – z.

Table 5.12 Selected bond lengths (Å) and angles (°) for [Pb([18]aneO$_4$Se$_2$)(NO$_3$)$_2$]

Pb1–O4A	2.61(2)	O4A–Pb1–O5A	46.2(7)
Pb1–O4B	2.290(3)	O4B–Pb1–O5B	44.1(8)
Pb1–O5A	2.60(2)	Se1–Pb1–Se1a	165.01(4)
Pb1–O5B	2.62(3)	Se1–Pb1–O1	68.0(2)
Pb1–Se1	3.174(2)	Se1–Pb1–O2	62.7(1)
Pb1–O1	2.777(7)	O1–Pb1–O2	60.3(2)
Pb1–O2	2.930(7)		

5.3 Conclusions

The chemistry of Pb(II) tetrafluoroborate and hexafluorophosphate salts has been investigated with mixed chalcogenoether Macrocycles revealing a great variety of unusual and unexpected coordination behaviours for these traditionally non-coordinating anions. Examples of monodentate (κ^1), chelating (κ^2) and only the second structurally authenticated case of bridging (μ^2) $[BF_4]^-$ (in a Pb(II) system), as well as ionic tetrafluoroborate have been observed as part of this study. All three coordination modes are present in complexes with the closely related chalcogenoether macrocycles [18]aneO_4E_2 (E= S, Se (O)). Further inferences of the varying coordination behaviours can be seen in the solid state IR spectra.

The complexes exhibit high coordination numbers (in the range of 8-11), irregular geometries and a large variety in coordinate bond lengths. This breadth of variation alongside the related literature examples shows a large metal centre with no strong stereochemical preferences. Pb(II) accommodates the steric demands of the macrocycles and the different anions/ligands to saturate its primary coordination sphere whilst minimising the inter-ligand repulsions.

With regards to Pb(II) as a Lewis acid (Hard/Soft/Borderline), examination of the Pb-donor bond lengths remains inconclusive. In some examples there is a clear preference for the softer donor (e.g. [Pb([18]aneO_4S_2)$(H_2O)_2$$(BF_4)$][$BF_4$]), in others it is not apparent (e.g. [Pb([18]aneO_4S_2)$(ClO_4)_2$]) and in other cases the harder donor (N over S in NCS) is coordinated (e.g. Pb([18]aneO_4S_2)$(NCS)_2$]). Overall this is further indication of Pb(II) having no clear stereochemical preference, its low charge/radius ratio means it has a relatively weak affinity for the ligands. The potential well about the lead is probably quite shallow and the differing bond length data should not be over interpreted for these systems.

Similar to the tetrafluoroborate complexes, the hexafluorophosphate salts also showed unusual coordination of the $[PF_6]^-$ anion. Examples of bidentate (κ^2) and tridentate (κ^3) coordination were observed. Unexpectedly the $[PF_6]^-$ anion readily hydrolysed in the presence of Pb(II), coordination to the lead centre elongates the P–F bond leaving it susceptible to hydrolysis.

5.4 Experimental

5.4.1 **Aqueous $Pb(PF_6)_2$ solution:** $(PbCO_3)_2 \cdot Pb(OH)_2$ (0.080 g, 1.03 x 10^{-4} mol) was suspended in deionised water (10 mL). HPF_6, as a 65% aqueous solution, was added (0.090 g, 6.19 x 10^{-4} mol), the lead salt began to dissolve and the reaction effervesced. Further $(PbCO_3)_2 \cdot Pb(OH)_2$ was added until none continued to dissolve. The mixture was filtered and concentrated to ~2 mL. If further solid formed the solution was filtered once again. $^{19}F\{^1H\}$ NMR (D_2O/H_2O, 293 K): δ 72.0 (d). $^{31}P\{^1H\}$ NMR (D_2O/H_2O, 293 K): δ -141.4 (sept.). ^{207}Pb NMR (D_2O/H_2O, 293 K): δ 2904.

5.4.2 **$[Pb(15\text{-crown-}5)_2][BF_4]_2$:** $Pb(BF_4)_2$ as a 50% aqueous solution (0.200 g, 5.25 x 10^{-4} mol) was added dropwise to 15-crown-5 (0.231 g, 1.05 x 10^{-3} mol) dissolved in CH_3CN (5 mL). The colourless reaction mixture was left to stir for 24 h, and upon slow evaporation afforded colourless crystals. These were washed with CH_3CN (2 mL) followed by CH_2Cl_2 (2 mL) and dried *in vacuo*. Yield: 0.210 g, 49%. Required for $C_{20}H_{40}B_2F_8O_{10}Pb \cdot CH_2Cl_2$ (906.37): C, 27.80; H, 4.67. Found: C, 28.18, H, 4.51%. IR (Nujol, cm^{-1}): 1087, 1052, 520 (BF_4). ^1H NMR (CD_3CN, 293 K): δ 3.92 (m, [10H], OC***H***$_2$), 3.86 (m, [10H], OC***H***$_2$), 5.30 (s, C***H***$_2Cl_2$); (228 K): 3.89 (d), 3.77 (d); (CD_2Cl_2, 293K): δ 3.86 (m). $^{19}F\{^1H\}$ NMR (CD_3CN, 293 K): δ -152.2. Λ_M (10^{-3} mol dm^{-3}, MeCN) = 335 ohm^{-1} cm^2 mol^{-1}.

5.4.3 **[Pb([15]aneO$_3$S$_2$)$_2$][BF$_4$]$_2$:** Pb(BF$_4$)$_2$ as a 50% aqueous solution (0.150 g, 3.93 x 10^{-4} mol) was added dropwise to [15]aneO$_3$S$_2$ (0.200 g, 7.94 x 10^{-4} mol) dissolved in CH$_3$CN (3 mL). The colourless reaction solution was left to stir for 24 h and upon slow evaporation of the solvent colourless crystals formed, which were washed with CH$_2$Cl$_2$ (2 mL) and dried *in vacuo*. Yield: 0.151 g, 43%. Required for C$_{20}$H$_{40}$B$_2$F$_8$O$_6$PbS$_4$·2CH$_2$Cl$_2$ (1055.20): C, 25.02, H 4.20. Found: C, 24.62; H, 3.75%. IR (Nujol, cm^{-1}): 1051, 1030, 520 (BF$_4$). ^{1}H NMR (CD$_2$Cl$_2$, 293 K): δ 3.13 (t, [4H], SC***H***$_2$CH$_2$O), 3.36 (s, [4H], SC***H***$_2$), 3.86 (br s, [8H], OC***H***$_2$), 3.95 (t, [4H], SCH$_2$C***H***$_2$O), 5.24 (s, C***H***$_2$Cl$_2$). ^{19}F{^{1}H} NMR (CD$_3$CN, 293 K): δ -151.3 (s). Λ_M (10^{-3} mol dm^{-3}, MeCN) = 350 ohm^{-1} cm^2 mol^{-1}.

5.4.4 **[Pb(15-crown-5)(NO$_3$)$_2$]:** 15-crown-5 (0.133 g, 6.03 x 10^{-4} mol) dissolved in a minimum amount of dry CH$_3$CN (5 mL) was slowly added to a suspension of Pb(NO$_3$)$_2$ (0.200 g, 6.03 x 10^{-4} mol) in dry CH$_3$CN (5 mL). The mixture was left to stir for 2 d and the remaining solids were removed by filtration. The filtrate was left to slowly evaporate for 12 h and afforded colourless crystals which were washed with CH$_3$CN (2 mL) and CH$_2$Cl$_2$ (2 mL), then dried *in vacuo*. Yield: 0.080 g, 25%. Required for C$_{10}$H$_{20}$N$_2$O$_{11}$Pb (551.31): C, 21.78; H, 3.66; N 5.08. Found: C, 22.12; H, 3.83; N 5.06%. IR (Nujol, cm^{-1}): 1352, 1025, 805 (NO$_3$). ^{1}H NMR (CDCl$_3$, 293 K): δ 3.70(s, crown C***H***$_2$); (CD$_3$CN): δ 3.79 (s, crown C***H***$_2$). Λ_M (10^{-3} mol dm^{-3}, MeCN) = 40 ohm^{-1} cm^2 mol^{-1}.

5.4.5 **[{Pb(18-crown-6)(H_2O)(BF_4)}$_2$][BF_4]$_2$:** $Pb(BF_4)_2$ as a 50% aqueous solution (0.200 g, 5.25 x 10^{-4} mol) was added dropwise to 18-crown-6 (0.139 g, 5.25 x 10^{-4} mol) dissolved in CH_3CN (5 mL). The resulting colourless mixture was allowed to evaporate at room temperature for 12 h, which afforded colourless crystals that were collected by filtration, washed with CH_3CN (2 mL) and CH_2Cl_2 (2 mL), then dried *in vacuo*. Yield: 0.250 g, 72%. Required for $C_{12}H_{26}B_2F_8O_7Pb$ (663.35): C, 21.73; H, 3.95. Found: C, 21.78; H, 3.38%. IR (Nujol, cm^{-1}): 3470, 1620 (H_2O), 1143, 1090, 969, 517 (BF_4). ^1H NMR (CD_3CN, 293 K): δ 2.35-2.60 (v.br, ***H***$_2$O), 3.81 (m, crown C***H***$_2$). $^{19}F\{^1H\}$ NMR (CD_3CN, 293 K): δ -151.8.

5.4.6 **[Pb([18]aneO$_4$S$_2$)(H_2O)$_2$(BF_4)][BF_4]:** [18]aneO$_4$S$_2$ (0.060 g, 2.03 x 10^{-4} mol) dissolved in CH_3CN (2 mL) and added dropwise to $Pb(BF_4)_2$ in a 50% aqueous solution (0.077 g, 2.03 x 10^{-4} mol). This was stirred at room temperature for 2 h before being concentrated *in vacuo* to colourless oil. CH_2Cl_2 (1 mL) was added which afforded a cloudy white suspension which upon slow evaporation produced colourless crystals. These were washed with CH_3CN (2 mL) followed by CH_2Cl_2 (2 mL) and dried *in vacuo*. Yield: 0.044 g, 20%. Required for $C_{12}H_{28}B_2F_8O_6PbS_2 \cdot CH_2Cl_2$ (798.24): C 19.54, H 3.79. Found: C 19.21, H 3.43%. IR (Nujol, cm^{-1}): 3470, 1612 (H_2O), 1081, 1020, 990, 518 (BF_4). ^1H NMR ($CDCl_3$, 293 K): δ 2.45 (s, ***H***$_2$O), 3.13 (t, [8H], SC***H***$_2$), 3.70 (br s, [8H], OC***H***$_2$), 4.01 (m, [8H], SCH_2C***H***$_2$O), 5.23 (CH_2Cl_2); (CD_3CN): δ 2.45 (br, ***H***$_2$O), 3.06 (t, [8H], SC***H***$_2$), 3.80 (s, [8H], OC***H***$_2$), 3.92 (t, [8H], SCH_2C***H***$_2$O). $^{19}F\{^1H\}$ NMR (CD_3CN, 293 K): δ -148.5 (s). Λ_M (10^{-3} mol dm^{-3}, MeCN) = 314 ohm^{-1} cm^2 mol^{-1}.

5.4.7 **[Pb([18]aneO$_4$Se$_2$)(BF$_4$)$_2$]:** [18]aneO$_4$Se$_2$ (0.084 g, 2.15 x 10^{-4} mol) and 50% aqueous Pb(BF$_4$)$_2$ (0.082 g, 2.15 x 10^{-4} mol) were dissolved in MeCN (20 mL) and allowed to stir overnight. A small amount of very fine white powder precipitated. The solution was filtered and the filtrate was slowly allowed to evaporate, giving colourless crystals identified crystallographically as [Pb([18]aneO$_4$Se$_2$)(BF$_4$)$_2$], but analytically pure samples were not obtained even after recrystallization from MeCN. Yield: 0.050 g, 30%. IR (Nujol, cm^{-1}): 3600, 1630 (H$_2$O), 1068, 1051, 1038, 519 (BF$_4$). ^{1}H NMR (CD$_3$CN, 298 K): δ 2.40 (br, ***H***$_2$O), 3.10 (v.br t, [8H], SeC***H***$_2$), 3.84 (br s, [8H], OC***H***$_2$), 4.02 (br t, [8H], SeCH$_2$C***H***$_2$O). ^{19}F{^{1}H} NMR (CD$_3$CN, 293 K): δ -150.5.

5.4.8 **[Pb(18-crown-6)(H$_2$O)$_2$(PF$_6$)]PF$_6$:** An aqueous solution of Pb(PF$_6$)$_2$ (0.070 g, 1.41 x 10^{-4} mol) was added to MeCN (10 mL) resulting in an immediate white solid forming. To the stirring mixture was added 18-crown-6 (0.037 g, 1.41 x 10^{-4} mol) and the solution began to clear and was left to react overnight. A small amount of fine white solid remained which was removed by filtration, and the filtrate concentrated *in vacuo*. X-ray quality crystals grew upon concentration. These were removed. The solid was recrystallised from MeCN and washed with CH$_2$Cl$_2$. Yield: 0.045 g, 40%. IR (Nujol, cm^{-1}): 3500, 1680 (H$_2$O), 837, 558 (PF$_6$). ^{1}H NMR (CD$_3$CN, 293 K): δ 3.80 (s, crown C***H***$_2$). ^{19}F{^{1}H} NMR (CD$_3$CN, 295 K): δ -72.1 (d). ^{31}P{^{1}H} NMR (CD$_3$CN, 295 K): δ -143.3 (sept.).

5.4.9 **[Pb(18-crown-6)(NO_3)(PF_6)]:** $Pb(NO_3)_2$ (0.100 g, 3.01 x 10^{-4} mol) and 18-crown-6 (0.080 g, 3.01 x 10^{-4} mol) were left to stir in deionised water (40 mL) for 30 mins. To the resulting clear solution $[NH_4][PF_6]$ (0.245 g, 1.51 x 10^{-3} mol) was added and left to stir for 12 h. A small amount of fine white solid formed was filtered off, and the remaining clear solution concentrated *in vacuo*. Large colourless crystals formed which were washed with ethanol and dried *in vacuo*. Yield: 0.115 g, 56%. IR (Nujol, cm^{-1}): 1356, 1025, 813 (NO_3), 836, 560 (PF_6). ^1H NMR ($CDCl_3$, 293 K): δ 3.77 (s, crown C***H***$_2$). $^{31}P\{^1H\}$ NMR ($CDCl_3$, 295 K): δ -143.3 (sept.).

5.4.10 **[Pb(18-crown-6)(NO_3)$_2$]:** 18-crown-6 (0.239 g, 9.06 x 10^{-4} mol) was dissolved in deionised water (3 mL) was added dropwise to a saturated aqueous solution (5 mL) of $Pb(NO_3)_2$ (0.301 g, 9.06 x 10^{-4} mol). A white microcrystalline solid precipitated from the reaction mixture after ~1 h stirring at room temperature. The precipitate was collected by vacuum filtration and washed with 5 mL of deionised water and then dried *in vacuo*. Yield: 0.190 g, 72%. Required for $C_{12}H_{24}N_2O_{12}Pb$ (595.33): C, 24.20; H, 4.06; N, 4.70. Found: C, 24.20; H, 3.96; N, 4.67%. IR (Nujol, cm^{-1}): 1350, 1030, 823 (NO_3). ^1H NMR ($CDCl_3$, 293 K): δ 3.79 (s, crown CH_2). Λ_M (10^{-3} mol dm^{-3}, MeCN) = 50 ohm^{-1} cm^2 mol^{-1}.

5.4.11 **[Pb([18]aneO$_4$S$_2$)(H$_2$O)$_2$(PF$_6$)]PF$_6$:** An aqueous solution of Pb(PF$_6$)$_2$ (0.070 g, 1.41 x 10^{-4} mol) was added to MeCN (10 mL) resulting in an immediate white solid forming. To the stirring mixture was added [18]aneO$_4$S$_2$ (0.042 g, 1.41 x 10^{-4} mol) and the solution began to clear and was left to react overnight. A small amount of fine white solid remained which was removed by filtration, and the filtrate concentrated *in vacuo*. X-ray quality crystals grew upon concentration. These were removed. The solid was recrystallised from MeCN and washed with CH_2Cl_2. Yield: 0.047 g, 39%. IR (Nujol, cm^{-1}): 3500, 1680 (H$_2$O), 840, 558 (PF$_6$). ^{1}H NMR (CD$_3$CN, 293 K): δ 3.03 (t, [8H], SC***H***$_2$), 3.78 (s, [8H], OC***H***$_2$), 3.89 (t, [8H], SCH$_2$C***H***$_2$O). ^{19}F{^{1}H} NMR (CD$_3$CN, 293 K): δ -72.2 (d). ^{31}P{^{1}H} NMR (CD$_3$CN, 293 K): δ -143.3 (sept.).

5.4.12 **[Pb([18]aneO$_4$Se$_2$)(NO$_3$)$_2$]:** [18]aneO$_4$Se$_2$ (0.070 g, 1.79 x 10^{-4} mol) was dissolved in MeCN (20 mL) after which 50% aqueous Pb(NO$_3$)$_2$ (0.059 g, 1.79 x 10^{-4} mol) was added and the granular suspension allowed to stir overnight. Slowly a fine white powder began to form. The solid was filtered off and crystals were grown from the filtrate. Yield: 0.100 g, 77%. Required for $C_{12}H_{24}N_2O_{10}PbSe_2$ (721.26): C, 19.98; H, 3.35; N, 3.88. Found: C, 19.92; H, 3.23; N, 4.06. IR (Nujol, cm^{-1}): 1348, 1027, 816 (NO$_3$). ^{1}H NMR (CD$_3$CN, 298 K): δ 3.01 (t, [8H], SeC***H***$_2$), 3.74 (s, [8H], OC***H***$_2$), 3.91 (t, [8H], SeCH$_2$C***H***$_2$O).

5.4.13 [Pb([18]aneO$_4$Se$_2$)(PF$_6$)$_2$]: An aqueous solution of Pb(PF$_6$)$_2$ (0.070 g, 1.41 x 10^{-4} mol) was added to MeCN (10 mL) resulting in an immediate white solid forming. To the stirring mixture was added [18]aneO$_4$Se$_2$ (0.055 g, 1.41 x 10^{-4} mol) and the solution began to clear and was left to react overnight. A small amount of fine white solid remained which was removed by filtration, and the filtrate concentrated *in vacuo.* X-ray quality crystals grew upon concentration. These were removed. The solid was recrystallised from MeCN and washed with CH_2Cl_2. Yield: 0.047 g, 38%. IR (Nujol, cm^{-1}): 844, 560 (PF$_6$). ^{1}H NMR (CD_3CN, 293 K): δ 3.05 (t, [8H], SeC***H***$_2$), 3.79 (s, [8H], OC***H***$_2$), 3.96 (t, [8H], SeCH$_2$C***H***$_2$O). ^{19}F{^{1}H} NMR (CD_3CN, 293 K): δ -72.2 (d). ^{31}P{^{1}H} NMR (CD_3CN, 293 K): δ -143.3 (sept.).

5.5 Structural Data

Compound	[Pb([15]aneO$_3$S$_2$)$_2$][BF$_4$]$_2$ · nCH$_2$Cl$_2$ (n= 1.22)	[Pb(15-crown-5)(NO$_3$)$_2$]	[{Pb(18-crown-6)-(H$_2$O)(BF$_4$)}$_2$][BF$_4$]$_2$
Formula	$C_{22.22}H_{42.44}B_2Cl_{2.44}F_8O_6PbS_4$	$C_{10}H_{20}N_2O_{11}Pb$	$C_{24}H_{52}B_4F_{16}O_{14}Pb_2$
mwt.	989.18	551.47	1326.28
crystal system	Orthorhombic	Monoclinic	Monoclinic
space group	*Pccn* (56)	$P2_1/c$ (14)	$P2_1/c$ (14)
a (Å)	18.747(3)	15.307(4)	12.818(4)
b (Å)	28.254(10)	8.303(2)	10.661(3)
c (Å)	13.263(2)	13.152(4)	15.298(5)
α (°)	90	90	90
β (°)	90	92.815(4)	94.66(2)
γ (°)	90	90	90
U (Å^3)	7025(3)	1669.5(8)	2083.6(10)
Z	8	4	2
μ(Mo Kα) (mm^{-1})	5.304	10.165	8.199
F(000)	3898	1056	1272
total no. reflns	17991	9241	11962
unique reflns	7968	3811	4753
R_{int}	0.040	0.076	0.083
no. of params, restraints	394, 16	217, 0	277, 11
R_1[a] [$I_o > 2\sigma(I_o)$]	0.046	0.031	0.049
R_1 (all data)	0.071	0.034	0.082
wR_2[a] [$I_o > 2\sigma(I_o)$]	0.096	0.071	0.077
wR_2(all data)	0.107	0.073	0.085

Compound	[Pb([18]aneO$_4$S$_2$)-(H$_2$O)$_2$(BF$_4$)][BF$_4$]	[Pb([18]aneO$_4$Se$_2$)(BF$_4$)$_2$]	[Pb([18-crown-6)(PF$_6$)-(H$_2$O)$_{1.6}$][PF$_6$] · nH$_2$O (n= 0.6)
Formula	$C_{12}H_{28}B_2F_8O_6PbS_2$	$C_{12}H_{24}B_2F_8O_4PbSe_2$	$C_{12}H_{28.4}F_{12}O_{8.2}P_2Pb$
mwt.	713.27	771.04	801.8
crystal system	Orthorhombic	Monoclinic	Monoclinic
space group	*Pbca* (61)	*C*2/*c* (15)	*P*2$_1$/*m* (11)
a (Å)	16.5374(15)	10.953(5)	8.754(3)
b (Å)	15.5893(15)	12.060(5)	15.230(4)
c (Å)	17.703(6)	15.530(7)	9.254(3)
α (°)	90	90	90
β (°)	90	90.693(6)	91.453(6)
γ (°)	90	90	90
U (Å^3)	4564.1(17)	2051.2(14)	1233.4(7)
Z	8	4	2
μ(Mo Kα) (mm^{-1})	7.667	11.862	7.096
F(000)	2752	1440	772
total no. reflns	11444	6169	5846
unique reflns	5184	2340	2908
R_{int}	0.020	0.057	0.030
no. of params, restraints	293, 4	132, 7	178, 2
R_1[a] [$I_o > 2\sigma(I_o)$]	0.021	0.039	0.063
R_1 (all data)	0.030	0.056	0.076
wR_2[a] [$I_o > 2\sigma(I_o)$]	0.047	0.070	0.141
wR_2(all data)	0.050	0.075	0.150

Compound	[Pb(18-crown-6)(NO_3)-(PF_6)]	[Pb([18]aneO$_4$Se$_2$)(NO_3)$_2$]	[Pb([18]aneO$_4$Se$_2$)(PF_6)$_2$]
Formula	$C_{12}H_{24}F_6NO_9PPb$	$C_{12}H_{24}N_2O_{10}PbSe_2$	$C_{12}H_{24}F_{12}O_4P_2PbSe_2$
mwt.	678.48	721.44	887.36
crystal system	Orthorhombic	Monoclinic	Monoclinic
space group	*Pmn*2$_1$ (31)	*C*2/*c* (15)	*C*2/*c* (15)
a (Å)	12.958(5)	10.969(4)	11.012(4)
b (Å)	8.475(3)	11.735(5)	12.949(5)
c (Å)	9.296(3)	15.385(6)	16.105(6)
α (°)	90	90	90
β (°)	90	90.382(6)	95.402(7)
γ (°)	90	90	90
U (Å^3)	1020.8(5)	1980.4(14)	2286.3(14)
Z	2	4	4
μ(Mo Kα) (mm^{-1})	8.441	12.248	10.819
F(000)	652	1360	1664
total no. reflns	6653	9116	9667
unique reflns	2334	2271	2599
R_{int}	0.079	0.109	0.054
no. of params, restraints	148, 1	141, 4	150, 0
R_1[a] [$I_o > 2\sigma(I_o)$]	0.049	0.060	0.031
R_1 (all data)	0.058	0.085	0.033
wR_2[a] [$I_o > 2\sigma(I_o)$]	0.097	0.119	0.076
wR_2(all data)	0.097	0.134	0.077

[a] $R_1 = \Sigma||F_o| - |F_c||/\Sigma|F_o|$. $wR_2 = [\Sigma w(F_o^2 - F_c^2)^2/\Sigma wF_o^4]^{1/2}$

Common items: temperature = 100K; wavelength (Mo Kα)= 0.71073 Å; θ_{max}= 7.5°

5.6 References

1. A. M. Groth, L. F. Lindoy, G. V. Meehan, G. F. Swiegers and S. B. Wild, in *Transition Metal Sulfur Chemistry*, American Chemical Society, 1996, vol. 653, ch. 18, pp. 297

2. M. Wolff and C. Feldmann, *Z. Anorg. Allg. Chem.*, 2010, **636**, 1787

3. E. S. Claudio, H. A. Godwin and J. S. Magyar, in *Prog. Inorg. Chem.*, John Wiley & Sons, Inc., 2003, pp. 1

4. W. Levason, G. Reid and W. Zhang, *Dalton Trans.*, 2011, **40**, 8491

5. W. Levason and G. Reid, *J. Chem. Soc., Dalton Trans.*, 2001, 2953

6. B. Cordero, V. Gomez, A. E. Platero-Prats, M. Reves, J. Echeverria, E. Cremades, F. Barragan and S. Alvarez, *Dalton Trans.*, 2008, 2832

7. J. Parr, in *Comprehensive Coord. Chem. II*, eds. J. A. M. Editors-in-Chief: T. J. Meyer, Pergamon, Oxford, 2003, pp. 545

8. F. A. Cotton, C. Wilikinson, C. A. Murillo and M. Bochmann, *Advanced Inorganic Chemistry, 6th Edition*, Wiley-Interscience, 1999

9. F. X. Kohl, R. Dickbreder, P. Jutzi, G. Müller and B. Huber, *Chem. Ber.*, 1989, **122**, 871

10. R. G. Bryant, V. P. Chacko and M. C. Etter, *Inorg. Chem.*, 1984, **23**, 3580

11. R. D. Rogers and A. H. Bond, *Inorg. Chim. Acta*, 1992, **192**, 163

12. F. Rieger and A.-V. Mudring, *Z. Anorg. Allg. Chem.*, 2008, **634**, 2989

13. A. N. Chekhlov, *Russ. J. Coord. Chem.*, 2008, **34**, 344

14. A. Y. Nazarenko, O. I. Kronikovski, M. S. Fonari, V. C. Kravtsov, Y. A. Simonov and T. J. Malinovski, *Supramol. Chem.*, 1995, **4**, 259

15. H. Von Arnim, K. Dehnicke, K. Maczek and D. Fenske, *Z. Anorg. Allg. Chem.*, 1993, **619**, 1704

16. A. Y. Nazarenko and E. B. Rusanov, *Polyhedron*, 1994, **13**, 2549

17. H. J. Küppers, K. Wieghardt, B. Nuber and J. Weiss, *Z. Anorg. Allg. Chem.*, 1989, **577**, 155

18. M. Helm, K. Loveday, C. Combs, E. Bentzen, D. VanDerveer, R. Rogers and G. Grant, *J. Chem. Crystallogr.*, 2003, **33**, 447

19. A. J. Blake, D. Fenske, W.-S. Li, V. Lippolis and M. Schroder, *J. Chem. Soc. Dalton Trans.*, 1998, 3961

20. H. J. Drexler, Thesis Structure (F.Allen, Acta Crystallographica Section B, 2002, 58, 380-388), 1997

21. I.H. Park, K.M. Park and S. S. Lee, *Dalton Trans.*, 2010, **39**, 9696

22. A. Y. Nazarenko and E. B. Rusanov, *J. Coord. Chem.*, 1995, **34**, 265

23. S. H. Strauss, *Chem. Rev.*, 1993, **93**, 927

24. I. Krossing and I. Raabe, *Angew. Chem. Int. Ed.*, 2004, **43**, 2066

25. R. Fernandez-Galan, B. R. Manzano, A. Otero, M. Lanfranchi and M. A. Pellinghelli, *Inorg. Chem.*, 1994, **33**, 2309

26. A. V. Plakhotnyk, L. Ernst and R. Schmutzler, *J. Fluorine Chem.*, 2005, **126**, 27

27. M. Mantina, A. C. Chamberlin, R. Valero, C. J. Cramer and D. G. Truhlar, *J. Phys. Chem. A*, 2009, **113**, 5806

28. K. Nakamoto, in *Handbook of Vibrational Spectroscopy*, John Wiley & Sons, Ltd, 2006

29. J. Kennedy, in *Multinuclear NMR*, ed. J. Mason, Springer US, 1987, ch. 8, pp. 221

6. Mixed Chalcogenoether Donor Macrocyclic Complexes of Tin(II)

6.1 Introduction

The unusual results from the fluoroanion ($[BF_4]^-$ and $[PF_6]^-$) chemistry with Pb(II) (Chapter 5) provided an alternative to the oxo-salt dominated Group 14 coordination chemistry while also by-passing the possible solubility issues intrinsic to the respective halides in this area of the Periodic Table.

Germanium, tin and lead are the three largest elements that reside in Group 14 with an established coordination chemistry [1]. Tin represents an intermediate between the heavier Pb and lighter Ge, with a covalent radius of 1.39 Å and a Pauling electronegativity of 1.96 [2]. All three elements have two accessible oxidation states, (II) and (IV), and as the metal becomes heavier the emphasis moves to the 2+ oxidation state. Tin being the intermediate element can easily access both Sn(II) and Sn(IV), and has an established coordination chemistry for both oxidation states.

Recent work within Group 14 has reported *endocyclic* germanium(II) crown and oxa-thia crown complexes [3 4 5 6]. With thia- and selena-crown adducts the Ge(II) is coordinated *exocyclic* and the complexes have polymeric structures [5 6 7]. Macrocyclic lead(II) complexes are well-known and a more thorough report can be found in Chapter 5. With regards to Sn(II), crown ether complexes of the type, $[Sn(15\text{-crown-}5)_2][SnCl_3]_2$ and [SnCl(18-crown-6)][X] (X= $SnCl_3^-$ or ClO_4) have been reported with $SnCl_2$ [8 9 10 11]. Similar to the chlorostannate(II) structures are the analogous tin(II) triflate complexes, $[Sn(15\text{-crown-}5)_2][O_3SCF_3]_2$ and $[SnO_3SCF_3(18\text{-crown-}6)][O_3SCF_3]$ [12 13].

The only structurally authenticated example of neutral S-donor coordination to Sn(II) is $[Sn\{PCH(SiMe_3)_2[C_6H_4(SCH_3)]\}_2]$ (Figure 6.1) [14]; attempts to react $SnCl_2$ with thioethers have been reported to be

unsuccessful [15]. This area of chemistry is underdeveloped and the closest other structurally verified examples of neutral soft chalcogenoether (S, Se, Te) coordination to tin are various Sn(IV) complexes [6] [16] .

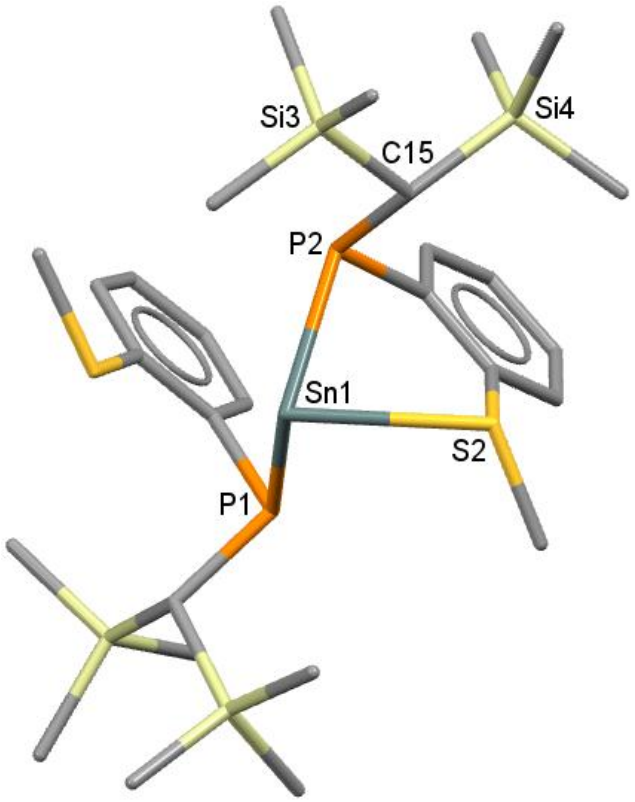

Figure 6.1 Structure of [Sn{PCH(SiMe$_3$)$_2$[C$_6$H$_4$(SCH$_3$)]}$_2$]. H atoms omitted for clarity. [14]

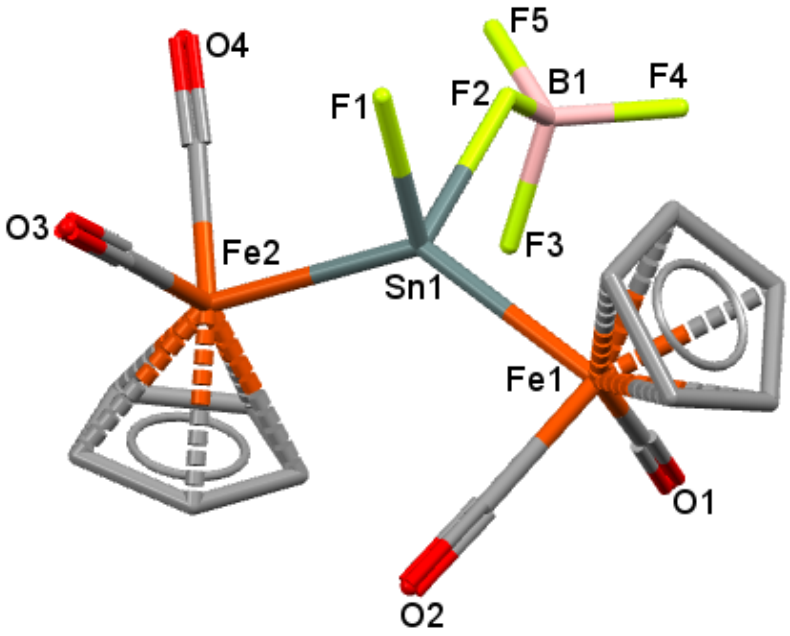

Figure 6.2 Structure of [SnF(BF$_4$){FeCp(CO)$_2$}$_2$]. H atoms omitted for clarity. [17]

As part of the study with Pb(II) fluoroanion chemistry (Chapter 5) , unusual coordination of the fluoroanions (BF_4^- and PF_6^-) was observed. Examples of tin tetrafluoroborate complexes already exist. The majority are with tin(IV) and exhibit no interaction with the fluoroanion, but a series of related cyclopentadienyl organotin(II) derivatives have Sn···FBF contacts ≥2.9 Å [18] [19]. An interesting complex is the heterometallic Sn(II)-centred $[SnF(BF_4)\{FeCp(CO)_2\}_2]$ (Figure 6.2) which has a much shorter Sn···FBF_3 bond distance of 2.149(7) Å [17]. A few tin(IV) complexes have also shown coordination of the tetrafluoroborate anion, with the Sn···FBF_3 distances being 2.387(2) and 2.782(4) Å in $[Sn(CH_3)_3(BF_4)\{C_6H_4(OCH_3)(CH(O))\}]$ (Figure 6.3) and $[SnF(^tBu)_2(CH_2P(Ph)_3)(BF_4)]$ respectively [20] [21]. Of the tin hexafluorophosphate complexes, none exhibit any interaction with the fluoroanion [22] [23] [24] [25].

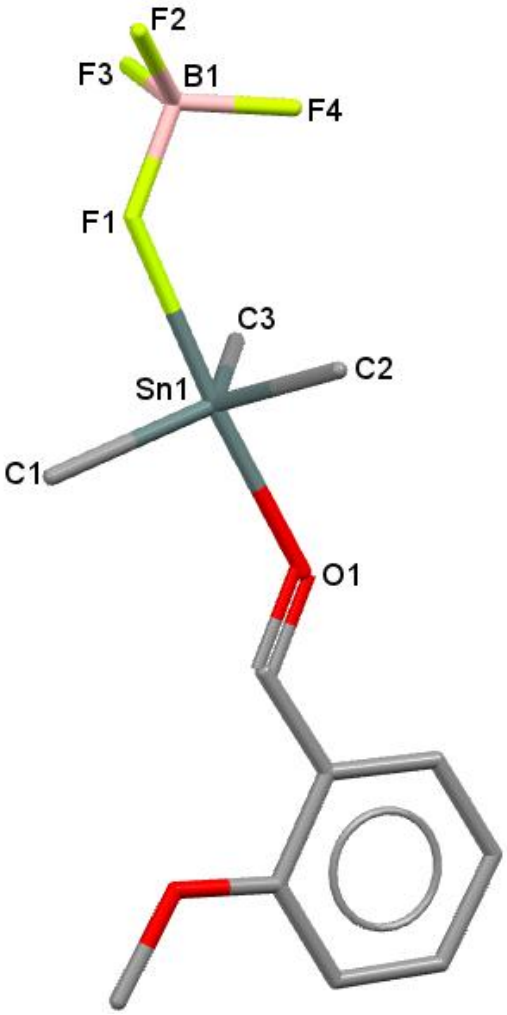

Figure 6.3 Structure of [$Sn(CH_3)_3(BF_4)\{C_6H_4(OCH_3)(CH(O))\}$]. H atoms omitted for clarity. [20]

6.2 Results and Discussion

6.2.1 $Sn(BF_4)_2$ and $Sn(PF_6)_2$ crown ether complexes

Sn(II) fluoroanion salts ($[BF_4]^-$ and $[PF_6]^-$), much like the analogous Pb(II) chemistry (see Chapter 5), readily form crown ether adducts, but due to the ease with which Sn(II) can oxidise to Sn(IV), a more cautious approach using anaerobic handling techniques was employed. Thus, no evidence for any Sn(IV) formation was observed in the present study.

Aqueous solutions of the Sn(II) fluoroanions are not commercially available and have to be synthesised; (6.4 Experimental).

The freshly prepared $Sn(BF_4)_2$ and $Sn(PF_6)_2$ aquaeous solutions showed only single environments for $[BF_4]^-$ and $[PF_6]^-$ ($^{19}F\{^1H\}$ NMR spectra) respectively, and ^{119}Sn NMR spectroscopy showed only single resonances (δ= -901 (BF_4); -866 (PF_6)). Like aqueous $Pb(PF_6)_2$, $Sn(PF_6)_2$ (aq) undergoes relatively rapid hydrolysis, depositing a white precipitate and generating $[F]^-$, $[PO_2F_2]^-$ and $[PO_3F]^{2-}$ [26]; after 5 h most of these species disappear and are replaced by $[BF_4]^-$ and $[SiF_6]^{2-}$ ($^{19}F\{^1H\}$ NMR (D_2O, 298K) δ= -150.6 and -130.2 respectively) which come from fluorination of the borosilicate glass. The $Sn(BF_4)_2$ (aq) was more stable in that it lasts for some days if protected from air; eventually a brown/black precipitate deposited, most likely tin oxide.

The reaction between 18-crown-6 and $Sn(BF_4)_2$ (aq) in acetonitrile gives $[Sn(18\text{-crown-6})(H_2O)][BF_4]_2 \cdot 2H_2O$. All of the spectroscopic data fit with the stated constitution. There is a substantial shift from the free ligand in the ^1H NMR spectrum for the crown protons (+0.35 ppm), typical for analogous *endodentate* crown complexes.

The crystal structure (Figure 6.4) shows the Sn(II) centre sitting asymmetrically within the macrocycle cavity, ($Sn\text{–}O3_{crown}$ 2.984(9) Å, $Sn\text{–}O(other)_{crown}$ 2.537(8)-2.777(8) Å). An apical water molecule completes the primary coordination sphere ($Sn\text{–}O7_{water}$ 2.150(7) Å) giving a 7-coordinate tin centre. Examination of the other contacts within the ΣVdW radii [27] also shows two long contacts to the “open” face of the tin

(Sn···O_{water} 3.304(9), 3.396(8) Å), giving an overall coordination number of "7+2". Analysis of the packing in the structure of [Sn(18-crown-6)(H_2O)][BF_4]$_2$·2H_2O (Figure 6.5) shows that H-bonding plays an important part in the organisation of the crystal, the apical water (O7) forms hydrogen bonds to the two lattice waters (O8 & O9) as does the weakest bound crown oxygen (O3) which forms a H-bond to O9. The [BF_4]$^-$ anions remain uncoordinated and exist within the voids in the lattice.

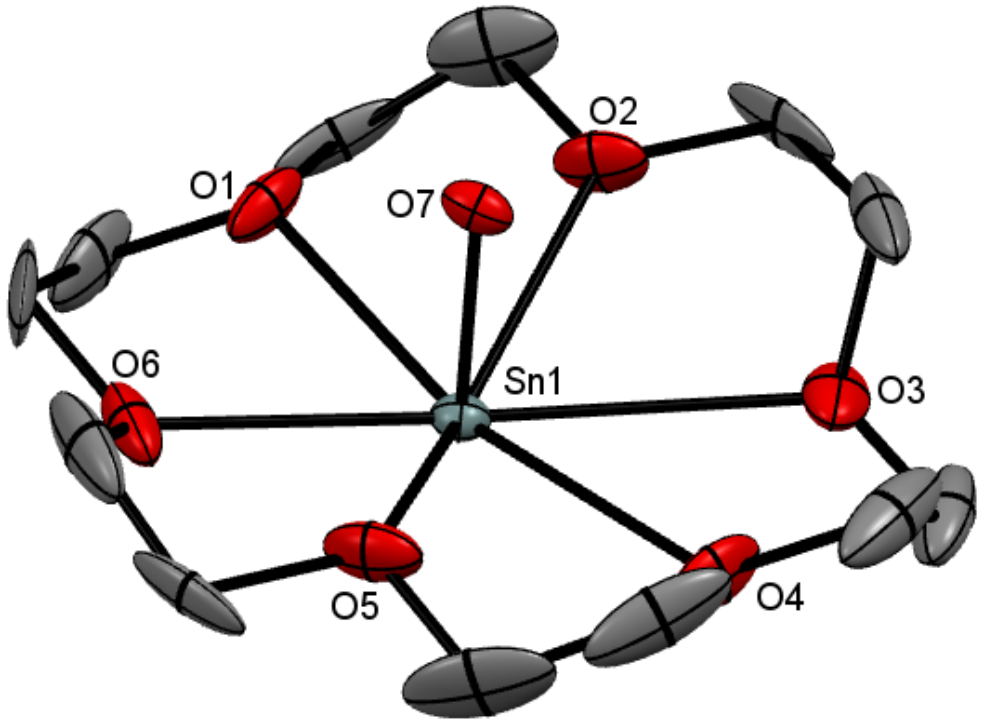

Figure 6.4 Crystal structure of the cation in [Sn(18-crown-6)(H_2O)][BF_4]$_2$·2H_2O showing the atom labelling scheme. The displacement ellipsoids are drawn at the 30% probability level and H atoms are omitted for clarity. Symmetry operation: a = 1/2 + x, 1/2 – y, 1 – z.

Table 6.1 Selected bond lengths (Å) and angles (°) for $[Sn(18\text{-crown-6})(H_2O)][BF_4]_2 \cdot 2H_2O$

Sn1–O1	2.537(9)	O1–Sn1–O2	60.8(3)
Sn1–O2	2.640(9)	O2–Sn1–O3	55.9(3)
Sn1–O3	2.98(1)	O3–Sn1–O4	57.8(3)
Sn1–O4	2.778(9)	O4–Sn1–O5	61.3(3)
Sn1–O5	2.608(9)	O5–Sn1–O6	62.7(3)
Sn1–O6	2.60(1)	O6–Sn1–O1	62.7(3)
Sn1–O7	2.151(7)	O3–Sn1–O9	54.8(2)
Sn1–O8	3.304(9)	O8–Sn1–O9	68.0(2)
Sn1–O9	3.396(8)		
O3···O9	2.91(1)		
O7···O8	2.62(1)		
O7···O9	2.57(1)		

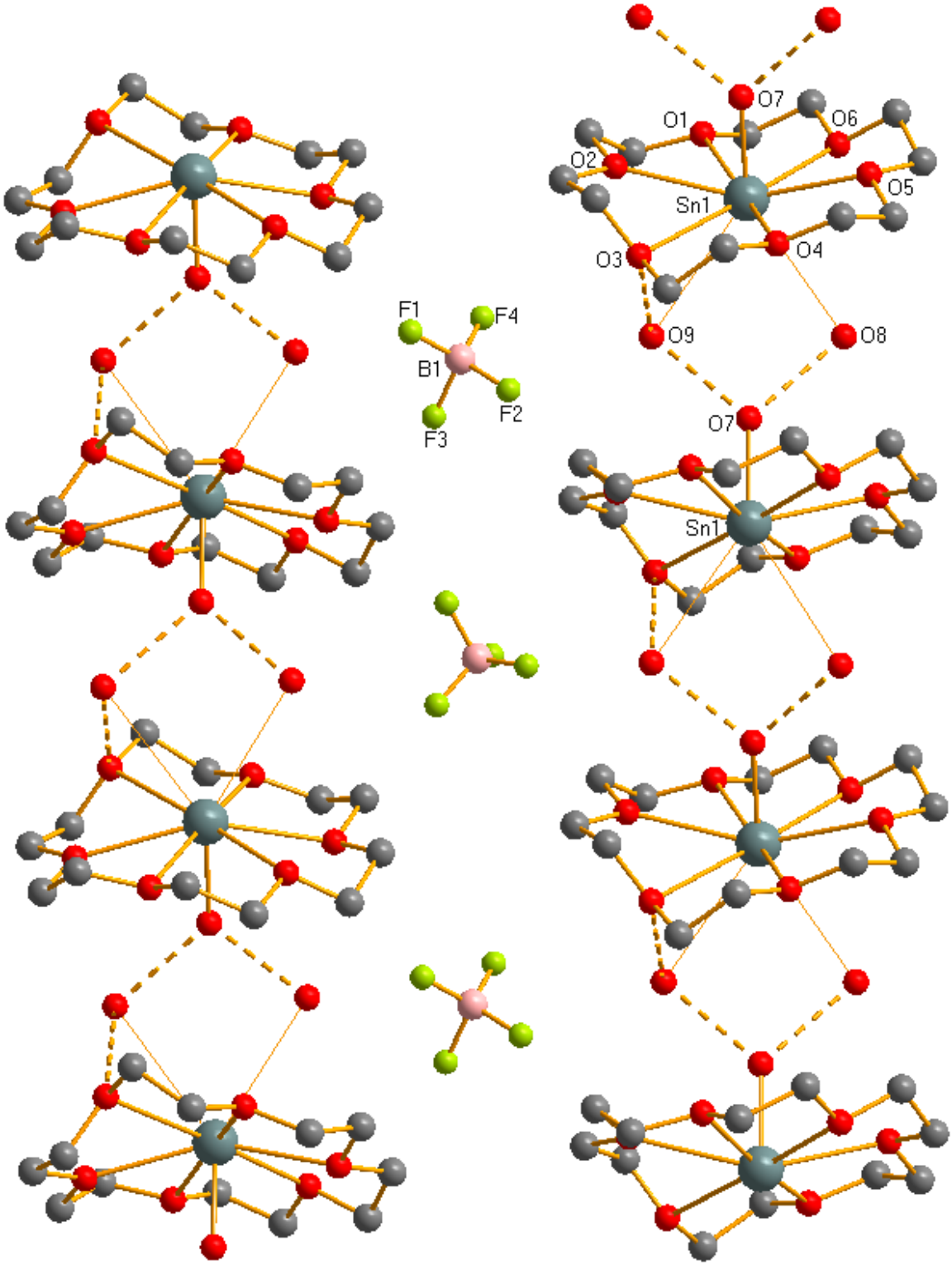

Figure 6.5 View of the packing in the structure of $[Sn(18\text{-crown-6})(H_2O)][BF_4]_2 \cdot 2H_2O$

The analogous reaction using $Sn(PF_6)_2$ (aq) gave a white powder with the composition $[Sn(18\text{-crown-6})][PF_6]_2$. Both the IR spectrum and the microanalysis confirm it is anhydrous, and the ^1H NMR shows the expected high frequency shift in the C***H***$_2$ groups compared to the 'free' ligand. A few crystals grew which had the constitution $[SnF(18\text{-crown-6})][PF_6]$ (Figure 6.6). Decomposition of the $[PF_6]^-$ anion liberates $[F]^-$ which, in contrast to the Pb(II) systems, replaces the hexafluorophosphate and becomes incorporated into the primary coordination sphere of tin(II).

Due to the similar X-ray scattering between F and O, the nature of the apical ligand could not be assigned with certainty from the X-ray data alone, (see also $[ScCl_2([18]aneO_4S_2)][FeCl_4]$, Chapter 4; $[SbI_2([18]aneO_4S_2)]_2[Sb_{2.5}I_{9.5}]$, Chapter 7). Water was dismissed due to the charge balance requirements of the Sn(II) cation leaving either OH^- or F^- as the likeliest ligands. From the other spectroscopic data (discussed below) the final constitution was concluded to be the fluoride.

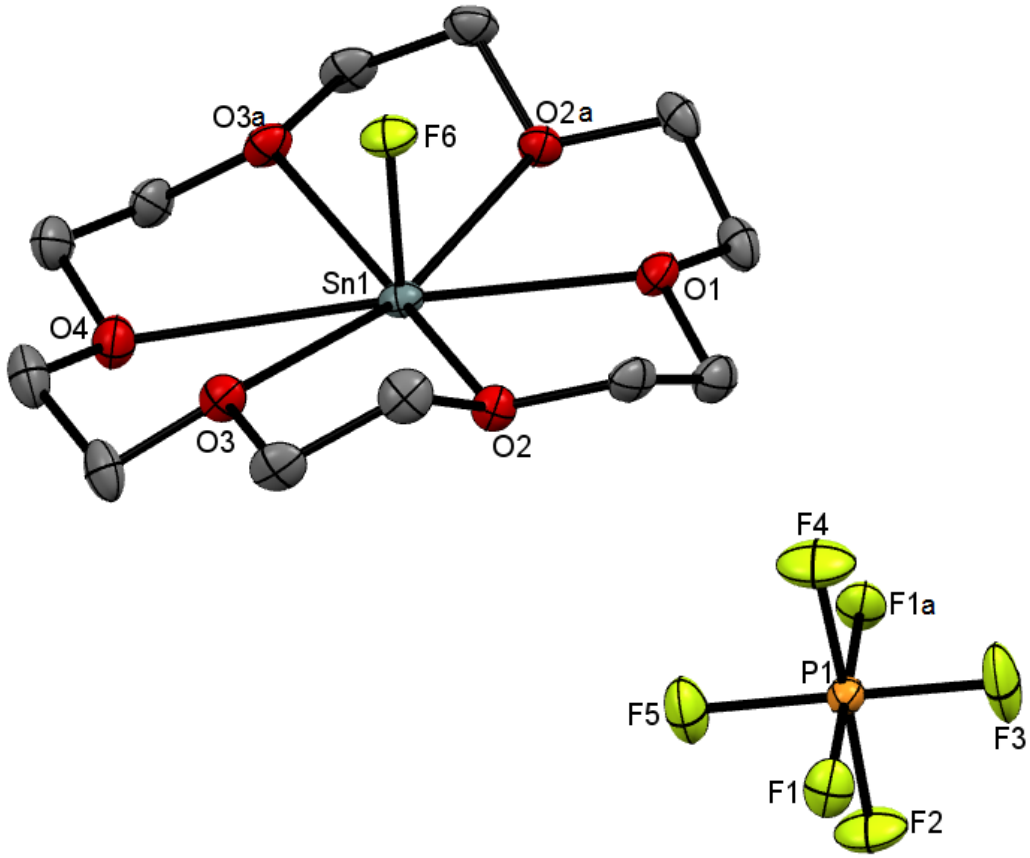

Figure 6.6 Crystal structure of [SnF(18-crown-6)][PF_6] showing the atom labelling scheme. The displacement ellipsoids are drawn at the 50% probability level and H atoms are omitted for clarity. Symmetry operation: a = -x, y, z.

Table 6.2 Selected bond lengths (Å) and angles (°) for [SnF(18-crown-6)][PF_6]

Sn1-O1	2.597(4)	O1-Sn1-O2	62.7(1)
Sn1-O2	2.606(3)	O2-Sn1-O3	61.0(1)
Sn1-O3	2.731(2)	O3-Sn1-O4	57.8(1)
Sn1-O4	2.953(5)	Sn1-O1-Sn1a	132.2(1)
Sn1-F6	1.947(4)		
Sn1-O1a	3.618(4)		

[SnF(18-crown-6)][PF_6] was synthesised directly by reacting [Sn(18-crown-6)][PF_6]$_2$ with KF in acetonitrile, the white solid isolated had the stated composition confirmed by elemental analysis. Comparison of the IR spectra between the two complexes [SnF(18-crown-6)][PF_6] and

[Sn(18-crown-6)][PF_6]$_2$ show clear differences in their [PF_6]$^-$ regions. In the mixed anion system there are two sharp well defined bands at 836 and 555 cm^{-1} (stretch and bend respectively; close to the expected values for ionic [PF_6]$^-$ [28]). For [Sn(18-crown-6)][PF_6]$_2$, instead there was a much more broadened stretching region and two bands in the bending region, this is consistent with some coordination present and hence the more likely constitution is [Sn(18-crown-6)(PF_6)][PF_6].

Comparison of the ^{1}H NMR spectra shows that the resonances are shifted to high frequency from 'free' ligand *viz* coordinating to the tin(II) has a deshielding effect on the C***H***$_2$ crown groups. The two singlets differ by 0.18 ppm, a greater shift being experienced by the crown protons in [Sn(18-crown-6)(PF_6)][PF_6] than in [SnF(18-crown-6)][PF_6]. This is as expected; Sn(II) is less electron rich than [SnF]$^+$ and hence exerts a greater deshielding effect on the crown protons. In [Sn(18-crown-6)(PF_6)][PF_6] the bound [PF_6]$^-$ group dissociates when in solution, whereas in [SnF(18-crown-6)][PF_6] the fluoride remains coordinated; the ^{19}F{^{1}H} and ^{31}P{^{1}H} NMR spectra for both hexafluorophosphate tin(II) crown complexes confirm there being only one [PF_6]$^-$ environment present.

The ^{19}F{^{1}H} NMR spectrum obtained from the crystals of [SnF(18-crown-6)][PF_6] shows a resonance at δ= -96.5 which corresponds to SnF, in keeping with the ^{19}F NMR resonances for other SnF_2 adducts with oxygen donor ligands; SnF_2 in d_4-methanol δ= -98.4 [15]. Analysis of the structure (Figure 6.6) shows a very similar hexagonal pyramidal conformation to that seen in the 7-coordinate [Sn(18-crown-6)(H_2O)]$^{2+}$ cation (Figure 6.4). Again the tin(II) centre is bound asymmetrically by the six crown donor atoms.

Very few examples of SnF_2 adducts with neutral donor ligands are known and the Sn–F distance of 1.947(4) Å in the present crown complex is slightly shorter than those in [Sn(L)F]$^+$ (L= phen, bipy) or [SnF_2(dmso)], which are ~2.02-2.03 Å [15]. Further examination of the structure in [SnF(18-crown-6)][PF_6] again shows packing interactions (Figure 6.7). In this system the "open" face of the tin(II) interacts with one O-donor atom (O1) of the adjacent [SnF(18-crown-6)]$^+$ cation giving an overall coordination number of "7+1", the distance is quite long, but just within ΣVdW radii

(Sn1···O1a 3.618(4) Å; Sn+O= 3.69 Å) [27]. The remaining $[PF_6]^-$ does not interact.

Examples of SnF_2 coordination complexes are few and little studied. The direct synthesis of [SnF(18-crown-6)][PF_6] and the recently synthesised complexes $[SnF(bipy)]_2[SnF_6]$, $[SnF(phen)]_2[SnF_4]$ and $[SnF_2(dmso)]$ suggested that tin(II) fluoride complexes with crown ethers may also be obtainable.

SnF_2 has moderate solubility in MeOH and fully dissolves in the presence of 18-crown-6. Despite this, isolation of a pure material proved difficult. The spectroscopy on the isolated solids showed a mixture of products, including unreacted starting material.

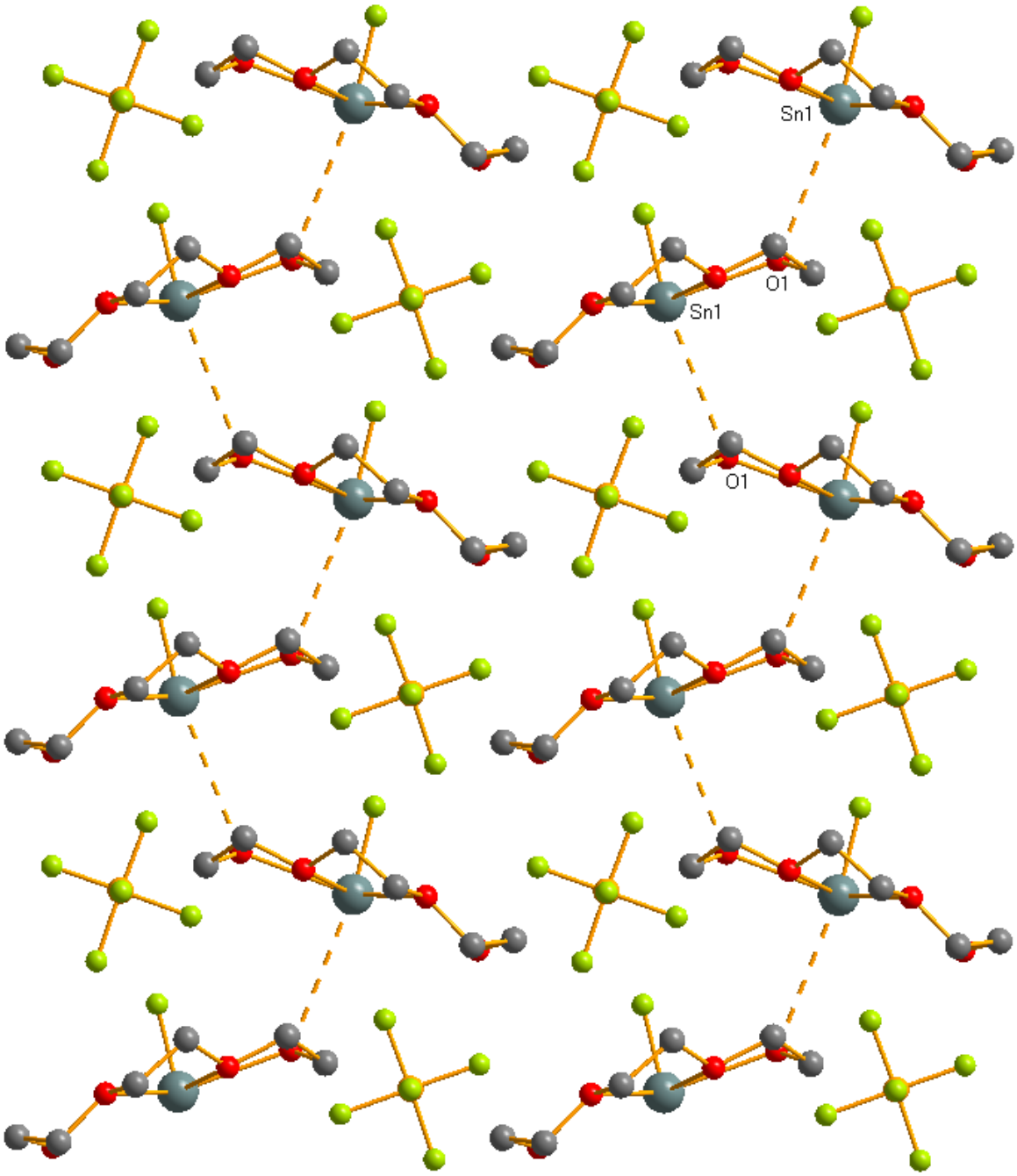

Figure 6.7 View of the packing in the structure of [SnF(18-crown-6)][PF_6]

$Sn(BF_4)_2$ (aq) forms a sandwich complex with 15-crown-5. The same cation, $[Sn(15\text{-crown-}5)_2]^{2+}$ (Figure 6.8), is found in other complexes such as $[Sn(15\text{-crown-}5)_2][X]_2$ (X= $SnCl_3^-$, $CF_3SO_3^-$), the effect of the counter anion is minimal and the $Sn-O_{crown}$ distances differ very little between the complexes [11] [12]. The crystals obtained from the present reaction had the constitution $[Sn(15\text{-crown-}5)_2][H_3O][BF_4]_3$ and were isostructural with its lead counterpart ($[Pb(15\text{-crown-}5)_2][H_3O][BF_4]_3$, Chapter 5). In the lead system the cation was heavily disordered; the tin complex instead had better defined ligands and allowed for a detailed comparison of the bond lengths. The Sn(II) centre coordinates to all the O-donor atoms in a discrete 10-coordinate environment, the Sn–O distances range between 2.588(6)-2.856(6) Å; less variation than in the 18-crown-6 systems, indicating the intermediate crown is a better size match for Sn(II). Only one structurally authenticated 12-crown-4 complex is known with Sn(II), $[Sn(12\text{-crown-}4)_2][CF_3SO_3]_2$ [12]. In this example the Sn–O distances lie over a comparatively larger range (2.474(6)-2.813(4) Å), the tin(II) cation in this case being too large to adequately accommodate the two smaller rings.

For all the tin(II) systems reported to date, assessing the influence of the tin-based lone pair has been difficult in light of the irregular coordination geometries and the range of Sn–O distances present. Computational studies have suggested that the lone pair is predominantly in the 5s orbital and therefore not responsible for the irregular stereochemistry observed. The potential wells about the tin are probably quite shallow (similarly to Pb(II)), and the detailed geometries observed are subtly affected by the electronic and steric interactions of the ligands in the primary coordination sphere, but also the intermolecular interactions, such as hydrogen-bonding and packing forces.

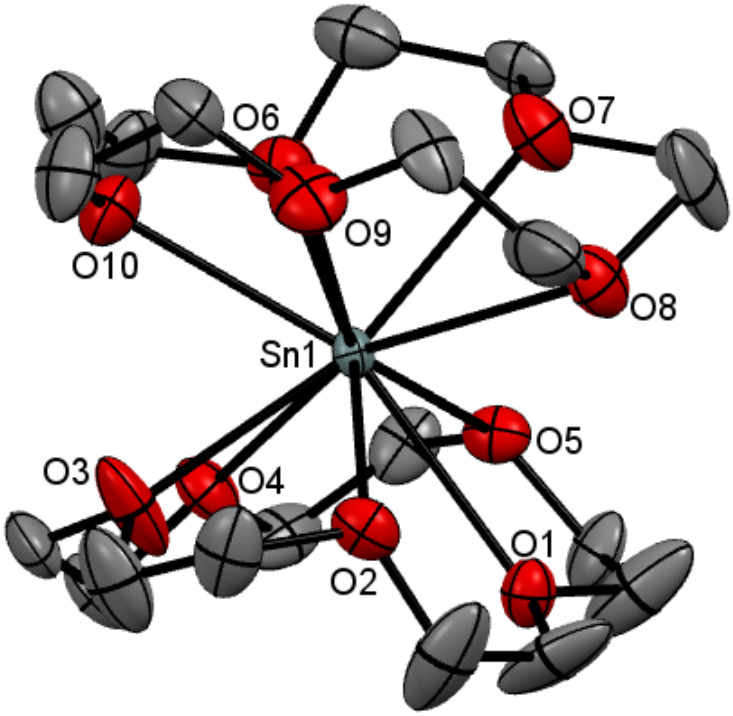

Figure 6.8 Crystal structure of $[Sn(15\text{-crown-}5)_2][BF_4]_3[H_3O]\cdot H_2O$ showing the Sn(II) containing cation. The atom labelling scheme is shown and the displacement ellipsoids are drawn at the 40% probability level with H atoms omitted for clarity.

Table 6.3 Selected bond lengths (Å) and angles (°) for $[Sn(15\text{-crown-}5)_2][BF_4]_3[H_3O]\cdot H_2O$

Sn1–O1	2.752(5)	O1–Sn1–O2	59.7(1)
Sn1–O2	2.771(5)	O2–Sn1–O3	59.6(2)
Sn1–O3	2.588(6)	O3–Sn1–O4	62.2(2)
Sn1–O4	2.678(5)	O4–Sn1–O5	61.0(2)
Sn1–O5	2.741(5)	O5–Sn1–O1	59.8(1)
Sn1–O6	2.725(6)	O6–Sn1–O7	60.5(2)
Sn1–O7	2.747(6)	O7–Sn1–O8	57.8(2)
Sn1–O8	2.856(6)	O8–Sn1–O9	62.0(2)
Sn1–O9	2.676(5)	O9–Sn1–O10	62.5(2)
Sn1–O10	2.620(6)	O10–Sn1–O6	61.5(2)

6.2.2 Oxa-thia and oxa-selena crown complexes with $Sn(BF_4)_2$ and $Sn(PF_6)_2$

Reacting tin(II) fluoroanions with the mixed chalcogenoether donor macrocycles resulted in a more unexpected outcome than the analogous Pb(II) chemistry and the Sn(II) crown chemistry.

Multiple attempts to form $[Sn([15]aneO_3S_2)_2][BF_4]_2$ from $Sn(BF_4)_2$ (aq) and $[15]aneO_3S_2$ in methanol or acetonitrile, were unsuccessful and resulted in oily solids which proved difficult to characterise. This contrasts with the relatively easy and straightforward synthesis of $[Pb([15]aneO_3S_2)_2][BF_4]_2$ under similar conditions.

The analogous reaction with the larger oxa-thia macrocycle, $[18]aneO_4S_2$, also resulted in an intractable oily product. The ^1H NMR spectrum was very complicated and showed a number of different species present. From each attempt at the synthesis a few crystals were isolated. Good quality crystals were obtained from solutions in acetonitrile (as opposed to CH_2Cl_2); they had the constitution $[Sn([18]aneO_4S_2)(HO(CH_2)_2OH)][BF_4]_2$ (Figure 6.9). The structure represents the first neutral oxa-thia donor complex with tin(II), the tin centre coordinates to all six donor atoms from one macrocyclic ring and a chelating ethylene glycol ligand, giving a core coordination number of 8. The presence of ethylene glycol can only be from C–O bond cleavage of the oxa-thia macrocycle, and this, in part, accounts for the complexity of the solution spectroscopic data. The degradation of the saturated oxa-thia macrocycle in the presence of Sn(II) appears to be the first time this type of ring-opening has been observed for any metal. Ring-opening of thia-crowns by Re(II) and Tc(II) has been previously reported and explored, and it has been shown that the $[Rh([9]aneS_3)]^{3+}$ trication can be deprotonated at the α-carbon initiating cleavage of the C–S bonds in one of the macrocyclic rings, resulting in vinyl thioether formation (see also Chapter 4) [29] [30] [31].

The macrocycle adopts a more planar puckered conformation in $[Sn([18]aneO_4S_2)(HO(CH_2)_2OH)][BF_4]_2$ (Figure 6.9) akin to that seen in $[Pb([18]aneO_4S_2)(H_2O)_2(BF_4)][BF_4]$ (Figure 5.10, Chapter 5), and examination of the bond lengths suggests a stronger preference for the S-donor atoms (Sn–S 2.907(1), 2.966(1) Å) over the O-donor atoms ($Sn–O_{macrocycle}$ 2.727(2)-2.892(2) Å) within the macrocycle, the strongest interaction is with the chelating oxygens present in the ethylene glycol (Sn–O 2.340(3), 2.346(3) Å). The O–H protons of the ethylene glycol were easily identified in the electron difference map and are H-bonded to the two charge balancing $[BF_4]^-$ groups. This interaction probably helps stabilise the formation of the complex. Further examination of the long contacts show a weak interaction ($\sim\kappa^2$) between Sn(II) and two of the fluorine atoms on a B2 centred $[BF_4]^-$ anion (Figure 6.10). This gives a total coordination number of "8+2".

The corresponding reaction with $Sn(PF_6)_2$ (aq) resulted in a white solid identified both spectroscopically and *via* elemental analysis as $[Sn([18]aneO_4S_2)(H_2O)_2(PF_6)][(PF_6)]$. Like its lead(II) counterparts the solids eventually degraded and the $[PF_6]^-$ anion underwent hydrolysis to $[F]^-$, $[PO_2F_2]^-$ and $[PO_3F]^{2-}$, based on the evidence from ^{19}F NMR spectroscopy. The ^1H NMR spectrum showed three C$\boldsymbol{H}_2$ environments as expected, all equally shifted to high frequency from the 'free' ligand.

Crystals grew on standing from the mother liquor, which had the composition $[Sn([18]aneO_4S_2)(H_2O)_2]_2[PF_6]_3[F]$ (Figure 6.11). Again, the decomposition of a $[PF_6]^-$ anion has resulted in the incorporation of a fluoride group, in the present case it is in the secondary coordination sphere H-bonded by four coordinated water molecules between two facing $[Sn([18]aneO_4S_2)(H_2O)_2]^{2+}$ cations. The Sn(II) centre has a primary coordination sphere of 8 and two long contacts to a $\sim\kappa^2$ $[PF_6]^-$ group, giving an overall coordination number of "8+2", very similar to $[Sn([18]aneO_4S_2)(HO(CH_2)_2OH)][BF_4]_2$ (Figure 6.10).

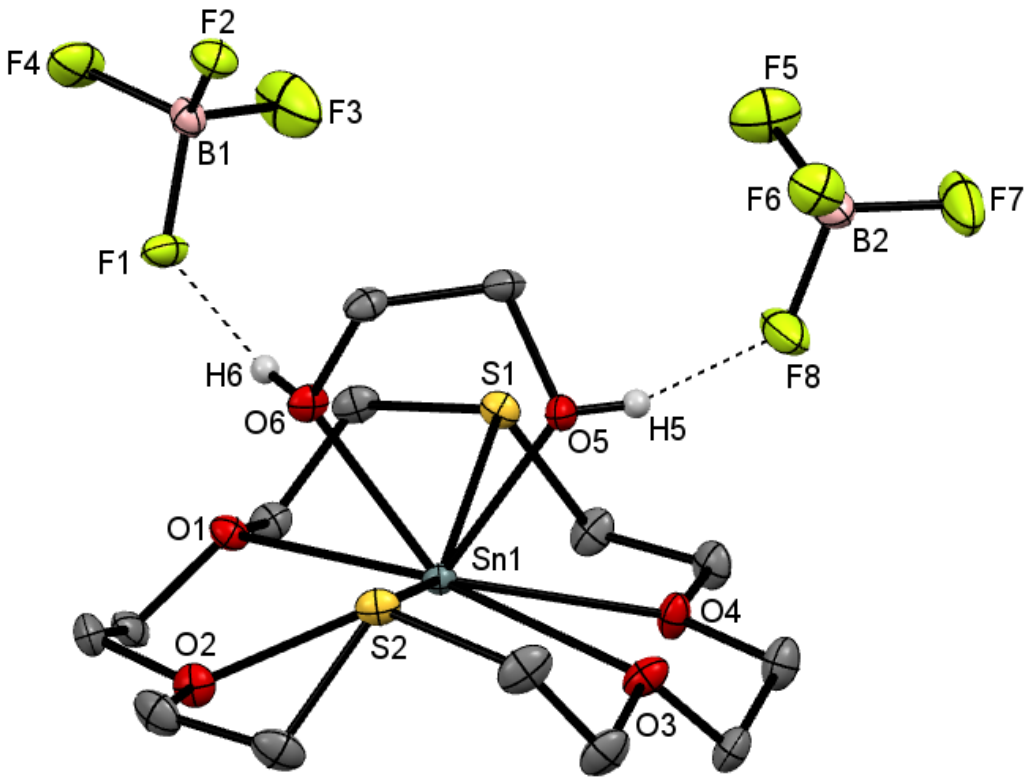

Figure 6.9 Crystal structure of [Sn([18]aneO$_4$S$_2$)(HO(CH$_2$)$_2$OH)][BF$_4$]$_2$ showing the atom labelling scheme. The displacement ellipsoids are drawn at the 50% probability level and non-interacting H atoms are omitted for clarity. The H-bonds to the [BF$_4$] anions are shown as dotted lines.

Table 6.4 Selected bond lengths (Å) and angles (°) for $[Sn([18]aneO_4S_2)(HO(CH_2)_2OH)][BF_4]_2$

Sn1–S1	2.966(1)	O5–Sn1–O6	69.19(8)
Sn1–S2	2.907(1)	S1–Sn1–S2	149.38(2)
Sn1–O1	2.892(2)	S1–Sn1–O1	64.48(4)
Sn1–O2	2.820(2)	O1–Sn1–O2	60.15(6)
Sn1–O3	2.812(2)	S2–Sn1–O2	65.29(5)
Sn1–O4	2.727(2)	S2–Sn1–O3	66.98(5)
Sn1–O5	2.340(3)	O3–Sn1–O4	59.95(7)
Sn1–O6	2.346(3)	S1–Sn1–O4	63.87(5)
Sn1–F5	3.589(3)	F5–Sn1–F6	37.83(5)
Sn1–F7	3.338(2)	F1–B1–F2	108.1(3)
O5···F1	2.696(3)	F1–B1–F3	109.5(3)
O6···F8	2.669(3)	F1–B1–F4	107.7(3)
B1–F1	1.420(4)	F2–B1–F3	110.9(3)
B1–F2	1.389(4)	F2–B1–F4	109.3(3)
B1–F3	1.364(4)	F3–B1–F4	111.3(3)
B1–F4	1.391(4)	F5–B2–F6	109.3(3)
B2–F5	1.385(5)	F5–B2–F7	110.3(3)
B2–F6	1.384(5)	F5–B2–F8	108.7(3)
B2–F7	1.374(4)	F6–B2–F7	111.3(3)
B2–F8	1.416(4)	F6–B2–F8	108.8(3)
		F7–B2–F8	108.4(3)

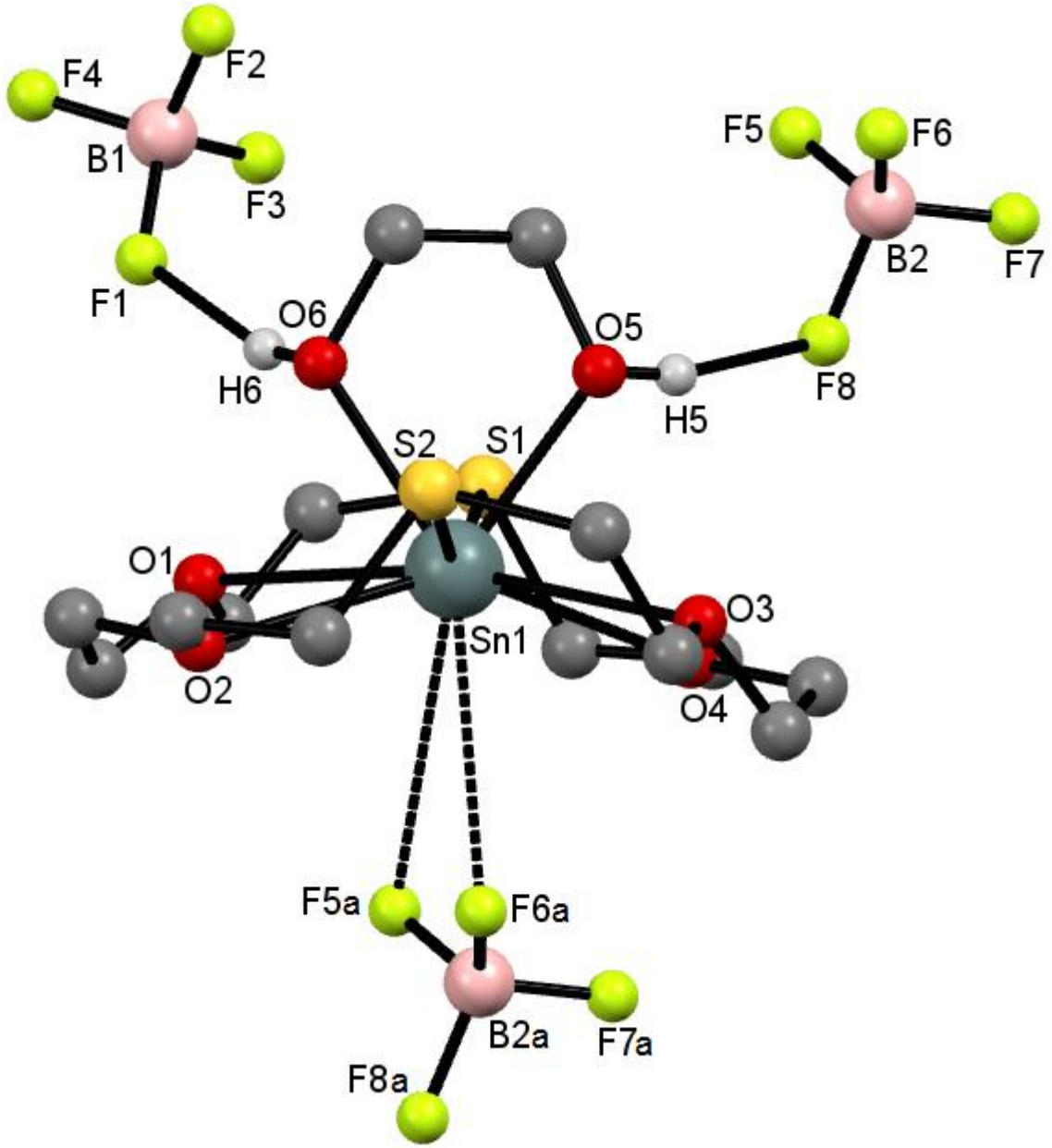

Figure 6.10 "Ball and Stick" structure diagram showing all the Sn(II) contacts in $[Sn([18]aneO_4S_2)(HO(CH_2)_2OH)][BF_4]_2$

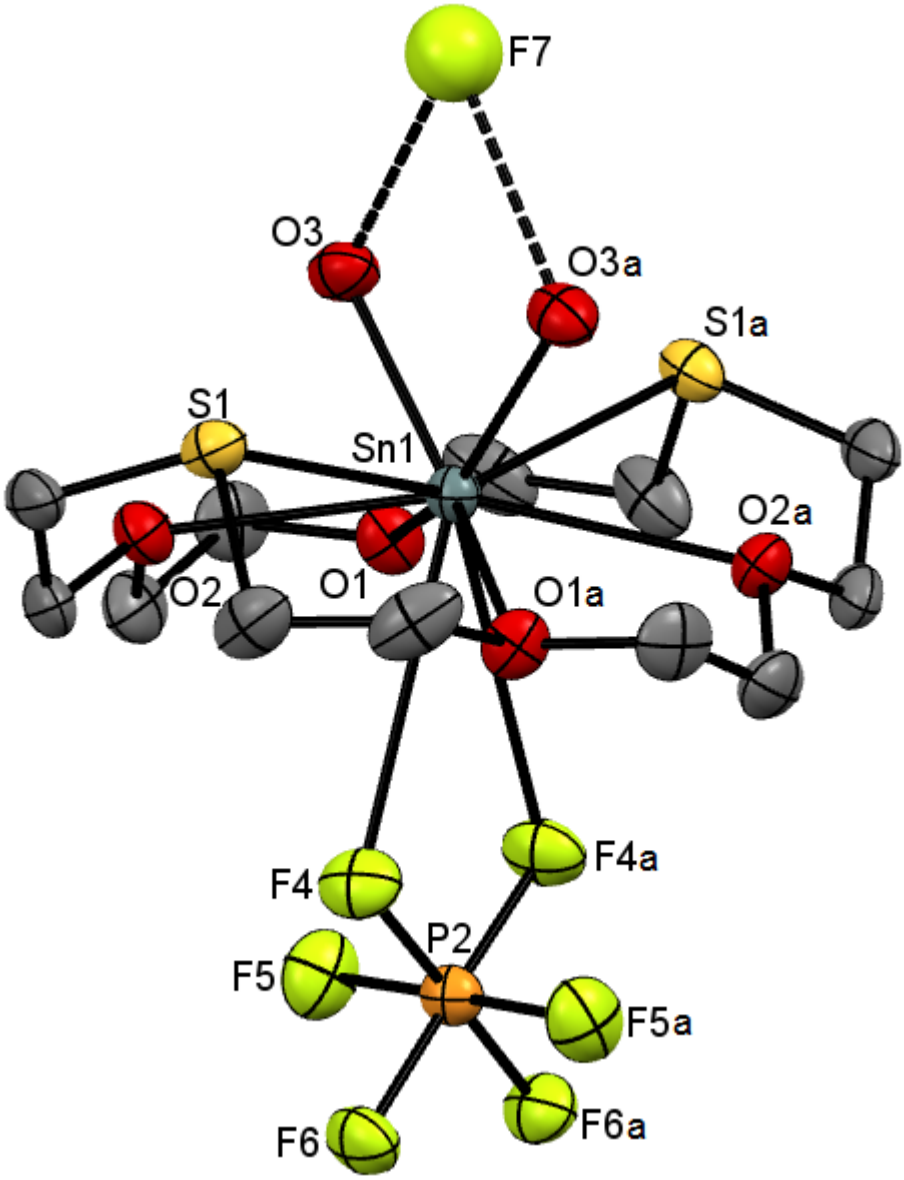

Figure 6.11 Crystal structure of the Sn1 centred molecule in $[Sn(H_2O)_2([18]aneO_4S_2)]_2[PF_6]_3[F]$ showing the atom labelling scheme. The displacement ellipsoids are drawn at the 50% probability level and H atoms are omitted for clarity. The H-bonds to F7 are shown as dotted lines. The molecule has 2-fold symmetry. Symmetry operation: a = y + 1/2, x – 1/2, y, 3/2 – z.

Table 6.5 Selected bond lengths (Å) and angles (°) for $[Sn([18]aneO_4S_2)(H_2O)_2]_2[PF_6]_3[F]$

Sn1–O3	2.282(3)	O3–Sn1–O3a	78.3(1)
Sn1–S1	2.979(1)	S1–Sn1–S1a	151.08(3)
Sn1–O1	2.833(3)	S1–Sn1–O1	65.32(6)
Sn1–O2	2.840(3)	O1–Sn1–O2	60.46(9)
Sn1–F4	3.485(3)	S1–Sn1–O2	64.59(7)
O3···F7	2.561(3)	F4–Sn1–F4a	37.85(7)
P2–F4	1.593(3)	F4–P2–F4a	90.4(2)
P2–F5	1.602(3)	F4–P2–F5	90.8(2)
P2–F6	1.599(3)	F4–P2–F5a	89.9(2)
		F4–P2–F6	90.2(2)
		F4–P2–F6a	178.7(2)
		F5–P2–F6	89.0(2)
		F5–P2–F4a	89.9(2)
		F5–P2–F5a	178.9(2)
		F5–P2–F6a	90.3(2)
		F6–P2–F4a	178.7(2)
		F6–P2–F5a	90.3(2)
		F6–P2–F6a	89.2(2)

The structures of $[Sn([18]aneO_4S_2)(H_2O)_2]_2[PF_6]_3[F]$ (Figure 6.11), $[Sn([18]aneO_4S_2)(HO(CH_2)_2OH)][BF_4]_2$ (Figure 6.9) and $[Pb([18]aneO_4S_2)(H_2O)_2(BF_4)][BF_4]$ (Figure 5.10, Chapter 5) are comparable. In all three complexes the metal centre has contacts with 10 donor atoms, and all three complexes have the same donor set ($S_2O_6F_2$) in a similar arrangement, M(II) (M= Pb, Sn) is bound in the plane of the macrocycle with the S-donors puckered *syn*, two O-donors (water or ethylene glycol)

mutually *cis* opposite to a κ^2-fluoroanion (BF_4^- or PF_6^-). The two tin complexes are very similar and exhibit small differences in the bond lengths, especially for the macrocycle where the Sn(II) favours the S-donor over the $O_{macrocycle}$-donor. The two non-macrocyclic Sn–O interactions represent the strongest coordination bonds in these systems. The same is true for the lead complex.

Comparing the two Group 14 systems, taking into account the metals' respective covalent radii Pb= 1.46 and Sn= 1.39 Å, the average $M–E_{macrocycle}$ distances are little different, with those in the lead complex being slightly shorter reflecting the folding constraints of the macrocycle. The non-macrocyclic O-donor ligands are relatively more strongly bound by the tin(II) centre (Sn–O_{water} 2.282(3), Sn–$O_{ethylene\ glycol}$ 2.340(3), 2.346(3), Pb–O_{water} 2.471(2) Å). The chelating fluoroanions feature the opposite trend, being very weakly bound to tin(II), whereas in the lead(II) system the $[BF_4]^-$ group is comparatively more strongly bound (ave. Sn–F 3.471, ave. Pb–F 2.958 Å), although it is still the weakest metal-ligand interaction in the complex.

An explanation for this is the relative Lewis acidities of the metal cations, Pb^{2+} is softer than Sn(II) and can therefore better accommodate the more diffuse negative charge surrounding the tetrafluoroborate anion, the harder lone pair on water is going to be favoured by the harder tin dication. Another view would be that the tin(II) centre being smaller cannot coordinate as much steric bulk in its primary coordination sphere in comparison to the lead. The likely answer is that both the electronic and steric effects interplay to give the most energetically favourable coordination for the specific system. In all three complexes there are also intermolecular interactions that also influence the observed coordination geometries.

Complexes with the oxa-selena crown [18]aneO_4Se_2 proved challenging. As already seen with the surprising cleavage of the oxa-thia macrocycles the Sn(II) cation is reactive enough to ring open these saturated mixed donor macrocycles, and [18]aneO_4Se_2 contains weaker C–Se bonds. Attempts with $Sn(BF_4)_2$ (aq) and [18]aneO_4Se_2 in acetonitrile resulted in

rapid elimination of elemental selenium (instantly recognisable due to its red colouration).

The analogous reaction with $Sn(PF_6)_2$ (aq) also resulted in the breaking up of the macrocycle and elimination of red selenium. However an analytically pure white solid was able to be isolated by only allowing the reaction to proceed for 4 h and subsequent cooling to 5˚C. The solid proved to be the sought complex, $[Sn([18]aneO_4Se_2)][PF_6]_2$. Expeditious analysis of the solid showed all the expected spectroscopic features. As with all the fluoroanion complexes in this study the solution data only showed one hexafluorophosphate environment. The IR spectrum showed only a single PF_6^- coordination environment, and the ^1H NMR spectrum was typical of coordinated oxa-selena-crown. Prolonged standing of freshly made solutions of $[Sn([18]aneO_4Se_2)][PF_6]_2$ resulted in darkening of these solutions and deposition of red selenium, due to this instability, crystals were unable to be grown and a ^{77}Se NMR spectrum was not obtained. That being said, all the Lewis acid complexes with $[18]aneO_4Se_2$ in this study have a very folded boat-like conformation of the macrocycle with the co-ligands mutually *cis*; the analogous Pb(II) complex $[Pb([18]aneO_4Se_2)(PF_6)_2]$ (Figure 5.15, Chapter 5) has two κ^2–PF_6^- giving 10-coordinate lead, and it is highly likely a similar structure is present in the tin complex.

6.3 Conclusions

Following on from the conclusions in Chapter 5, Sn(II) fluoroanion chemistry is not unlike that of its heavier analogue Pb(II). Nevertheless there are noticeable differences which characterise tin(II) as an intermediate Group 14 metal. Like the lead(II) chemistry, tin(II) readily forms complexes with crowns and mixed donor chalcogenoether macrocycles. Hydrolysis of the [PF_6^-] anion was also observed and in some cases the generated [F^-] was incorporated into the coordination sphere of the tin(II).

One of these mixed fluoride/hexafluorophosphate complexes, [SnF(18-crown-6)][PF_6], was made directly, allowing direct spectroscopic measurements to be made. Despite this, SnF_2 crown ether chemistry proved to be inaccessible under the various conditions employed.

For all the reported complexes the tin(II) centre coordinates to all the donor atoms in the macrocycle as well as other oxo-donor ligands such as water, and in the mixed donor macrocycle complexes the metal forms weak interactions with the fluoroanions. It differs from the analogous lead complexes in that that the fluoroanions tend to have stronger interactions with the lead(II) for all chalcogenoether 18-membered macrocycle complexes. The coordination for tin(II) within the 18-membered crowns is asymmetric, whereas the lead sits well within the cavity. The differences described are due to the smaller and harder nature of Sn(II) relative to Pb(II), decreasing its preference for softer ligands and the amount of steric bulk it can accommodate. Typical coordination numbers are in the range of 7-10 with the higher coordination numbers (9 and 10) a consequence of including weaker longer range contacts as part of the coordination sphere. Both metals form sandwich complexes with 15-crown-5, whereas Ge(II) forms discrete 1:1 adducts.

In addition to encouraging the hydrolysis of hexafluorophosphate, Sn(II) is reactive enough to cleave and ring-open oxa-thia and oxa-selena crowns. Pb(II) only ring-opened the oxa-tellura-crown and afforded stable complexes with the other two mixed donor macrocycles. The ring-opening of saturated oxa-thia crowns was unexpected and the complex

$[Sn([18]aneO_4S_2)(HO(CH_2)_2OH)][BF_4]_2$ represents the first evidence for such a reaction by any metal.

6.4 Experimental

6.4.1 **Aqueous $Sn(BF_4)_2$ solution:** $Cu(BF_4)_2 \cdot 6(H_2O)$ (2.324 g, 6.73 mol) was dried *in vacuo* at 40°C for 2 h. Degassed water (60 mL) was added and an excess of Sn powder (0.821 g, 6.92 mol) was stirred in. The blue solution went colourless overnight and a black precipitate deposited. The solution was filtered and used within a few days. $^{19}F\{^1H\}$ NMR (CD_3CN, 293 K): δ -150.6. ^{119}Sn NMR (D_2O/H_2O, 293 K): δ -901. The solution begins to deposit a black precipitate (possibly SnO) after around 7 d and decomposition of the $[BF_4]$ group can be observed *via* $^{19}F\{^1H\}$ NMR spectroscopy. It must be kept under N_2 at all times.

6.4.2 **Aqueous $Sn(PF_6)_2$ solution:** SnO (0.097 g, 7.20×10^{-4} mol) was suspended in degassed H_2O (4 mL), and HPF_6, as a 65% aqueous solution, (0.210 g, 1.44×10^{-3} mol) was slowly added. Further SnO was added until no more dissolved. The solution was filtered and used immediately. $^{19}F\{^1H\}$ NMR (D_2O, 293 K): δ -72.0 (d). $^{31}P\{^1H\}$ NMR (D_2O, 293 K): δ -144.4 (sept.). ^{119}Sn NMR (D_2O, 293 K): δ -866. The solution fully decomposes within 5 h depositing a lot of white precipitate, both the $^{19}F\{^1H\}$ NMR and $^{31}P\{^1H\}$ NMR showing the relatively rapid hydrolysis of the $[PF_6]^-$ group upon standing.

6.4.3 **[Sn(18-crown-6)(H_2O)][BF_4]$_2$·2H_2O:** Aqueous Sn(BF_4)$_2$ (0.082 g, 2.78 x 10^{-4} mol) was added dropwise to 18-crown-6 (0.072 g, 2.78 x 10^{-4} mol) in MeCN (20 mL) upon which a fine white solid precipitated out. The reaction mixture was left to stir at room temperature for 12 h. The suspension was concentrated, allowed to stand and then filtered. The white solid was then washed with CH_2Cl_2 and dried *in vacuo*. A few X-Ray quality crystals were obtained by slow evaporation from the washings. Yield: 0.019 g, 12%. Required for $C_{12}H_{30}B_2F_8O_9Sn$ (610.89): C, 23.57; H, 4.97. Found: C, 23.39; H, 4.27%. IR (Nujol, cm^{-1}): 3528, 1640 (H_2O), 1095, 1029, 916, 519 (BF_4). ^{1}H NMR (CD_2Cl_2, 298 K): δ 3.84 (s, crown C***H***$_2$; (CD_3CN, 298 K): δ 2.19 (br, ***H***$_2$O), 3.78 (s, crown C***H***$_2$). ^{19}F{^{1}H} NMR (CD_2Cl_2, 298 K): δ -151.4.

6.4.4 **[Sn(18-crown-6)(PF_6)][PF_6]:** Aqueous Sn(PF_6)$_2$ (0.159 g, 3.90 x 10^{-4} mol) was added dropwise to 18-crown-6 (0.103 g, 3.90 x 10^{-4} mol) dissolved in MeOH (15 mL), and left to stir at room temperature for 24 h. The resulting slightly turbid solution was filtered and the filtrate concentrated *in vacuo*. On standing a small amount of white solid began to form, the mother liquor was left at 5°C for 2 d. A large quantity of white solid was filtered and isolated. X-Ray quality crystals grew from the final solution. Yield: 0.100 g, 38%. Required for $C_{12}H_{24}F_{12}O_6P_2Sn$ (672.79): C, 21.40; H, 3.60. Found: C, 21.46; H, 3.45%. IR (Nujol, cm^{-1}): 841, 559 (PF_6). ^{1}H NMR (CD_3CN, 298 K): δ 3.77 (s, crown C***H***$_2$). ^{19}F{^{1}H} NMR (CD_3CN, 298 K): δ −73.2 (d). ^{31}P{^{1}H} NMR (CD_3CN, 298 K): δ −144.1 (sept.).

The crystals grown had the formulation [SnF(18-crown-6)][PF_6], crude ^{19}F{^{1}H} NMR (CD_3CN, 298 K): δ −73.2 (d, PF_6), -98.8 (s, SnF).

6.4.5 **[SnF(18-crown-6)][PF_6]:** [Sn(18-crown-6)][PF_6]$_2$ (0.037 g, 5.50 x 10^{-4} mol) and KF (0.003 g, 5.50 x 10^{-4} mol) were dissolved in MeCN (5 mL) and allowed to stir over 3 d. The reaction began to opalesce, the mother liquor was filtered and the volatiles allowed to evaporate. The crude white solid was taken up in MeCN, refiltered and a pure white solid was obtained on removal of the volatiles. Yield: 0.012 g, 39%. Required for $C_{12}H_{24}F_7O_6PSn$ (546.83): C, 26.33; H, 4.42. Found: C, 26.27; H, 4.56%. IR (Nujol, cm^{-1}): 835, 555 (PF_6). ^{1}H NMR (CD_3CN, 298 K): δ 3.59 (s, crown C***H***$_2$). ^{19}F{^{1}H} NMR (CD_3CN, 298 K): δ -96.5. ^{31}P{^{1}H} NMR (CD_3CN, 298 K): δ −145.7 (sept.).

6.4.6 **[Sn(15-crown-5)$_2$][BF_4]$_2$:** Aqueous Sn(BF_4)$_2$ (0.097 mg, 3.33 x 10^{-4} mol) was added dropwise to 15-crown-5 (0.146 g, 6.63 x 10^{-4} mol) in MeCN (15 mL), upon which a fine white solid precipitated out. The reaction mixture was left to stir at room temperature for 2 h. The suspension was concentrated, allowed to stand and then filtered. The white solid was then washed with CH_2Cl_2 and dried *in vacuo*. Repeated syntheses of this complex gave poor isolated yields which are probably due to the difficulty of isolation of the solid complex rather than to other species present. Yield: 0.018 g, 6%. Required for $C_{20}H_{40}B_2F_8O_{10}Sn$ (732.96): C, 32.74; H, 5.50. Found: C, 32.57; H, 5.36%. IR (Nujol, cm^{-1}): 3401, 1635 (H_2O), 1084, 948 (BF_4). ^{1}H NMR (CD_3CN, 298 K): δ 3.83 (s, crown C***H***$_2$). ^{19}F{^{1}H} NMR (CD_3CN, 298 K): -151.2.

X-Ray quality crystals were grown by redissolving the solid in MeCN and slow evaporation in air and proved to be [Sn(15-crown-5)$_2$][BF_4]$_3$[H_3O]·H_2O.

6.4.7 **Ring-Opening of [18]aneO_4S_2:** Aqueous Sn(BF_4)$_2$ was added dropwise to [18]aneO_4S_2 in MeOH. This mixture was allowed to evaporate slowly in air leaving behind an oily solid and some crystals. Crystals of varying quality were collected from either the residues or CH_2Cl_2 washings. The crystals all had the constitution [Sn([18]aneO_4S_2)(HO(CH_2)$_2$OH)][BF_4]$_2$.

6.4.8 **$[Sn(H_2O)_2([18]aneO_4S_2)][PF_6]_2$:** Aqueous $Sn(PF_6)_2$ (0.158 g, 3.38 x 10^{-4} mol) was added dropwise to [18]aneS_2O_4 (0.100 g, 3.38 x 10^{-4} mol) dissolved in MeOH (15 mL). The reaction was left to stir at room temperature for 12 h, during which a minor amount of fine solid formed. The solution was filtered, concentrated to ~3 mL and cooled for 7 d at 5˚C. Large colourless crystals grew, they were filtered out and dried *in vacuo*. Yield: 0.056 g, 22%. Required for $C_{12}H_{28}F_{12}O_6P_2S_2Sn$ (740.77): C, 19.44; H, 3.81. Found: C, 19.57; H, 3.68%. IR (Nujol, cm^{-1}): 3397, 1635 (H_2O), 837, 557 (PF_6). ^1H NMR (CD_3CN, 298 K): δ 2.88 (br, ***H***$_2O$), 3.02 (t, [8H], SC***H***$_2$), 3.74 (s, [8H], OC***H***$_2$), 3.83 (t, [8H], SCH_2C***H***$_2O$). $^{19}F\{^1H\}$ NMR (CD_3CN, 298 K): δ -72.3 (d). $^{31}P\{^1H\}$ NMR (CD_3CN, 298 K): δ -143.3 (sept.).

The crystals grown had the formulation $[Sn(H_2O)_2([18]aneS_2O_4)]_2[PF_6]_3[F]$.

6.4.9 **$[Sn([18]aneO_4Se_2)][PF_6]_2$:** Aqueous $Sn(PF_6)_2$ (0.102 g, 2.17 x 10^{-4} mol) was added dropwise to [18]aneSe_2O_4 (0.085 g, 2.17 x 10^{-4} mol) dissolved in dry MeOH (15 mL), and left to stir at room temperature for 4 h. The solution was filtered and concentrated to ~5 mL. The filtrate was cooled for 5 d at 5˚C. A substantial quantity of amorphous white solid formed, this was isolated and dried *in vacuo*. Yield: 0.066 g, 35%. Required for $C_{12}H_{24}F_{12}O_4P_2Se_2Sn$ (798.73): C, 18.03; H, 3.03. Found: C, 18.15; H, 3.14%. IR (Nujol, cm^{-1}): 840, 558 (PF_6). ^1H NMR (CD_3CN, 298 K): δ 2.99 (t, [8H], SeC***H***$_2$), 3.72 (s, [8H], OC***H***$_2$), 3.84 (t, [8H], $SeCH_2C$***H***$_2O$). $^{19}F\{^1H\}$ NMR (CD_3CN, 298 K): -72.3 (d). $^{31}P\{^1H\}$ NMR (CD_3CN, 298 K): -143.3 (sept.).

6.5 Structural Data

Compound	[Sn(18-crown-6)(H_2O)]-[BF_4]$_2$·2H_2O	[SnF(18-crown-6)][PF_6]	[Sn(15-crown-5)$_2$]-[BF_4]$_3$[H_3O]·H_2O
Formula	$C_{12}H_{30}B_2F_8O_9Sn$	$C_{12}H_{24}F_7O_6PSn$	$C_{20}H_{45}B_3F_{12}O_{12}Sn$
mwt.	610.67	546.97	856.68
crystal system	Orthorhombic	Orthorhombic	Monoclinic
space group	*Pbca* (61)	*Pmc*2$_1$ (26)	*P*2$_1$/*n* (14)
a (Å)	21.368(6)	10.676(4)	14.116(2)
b (Å)	17.042(4)	10.498(4)	15.118(2)
c (Å)	12.503(2)	8.533(3)	16.137(6)
α (°)	90	90	90
β (°)	90	90	90.793(6)
γ (°)	90	90	90
U (Å^3)	4553.3(19)	956.4(6)	3443.6(14)
Z	8	2	4
μ(Mo Kα) (mm^{-1})	1.227	1,512	0.859
F(000)	2448	544	1736
total no. reflns	18854	544	16402
unique reflns	4461	2302	7805
R_{int}	0.1119	0.0460	0.0295
no. of params, restraints	289, 4	137, 1	432, 2
R_1[a] [$I_o > 2\sigma(I_o)$]	0.0828	0.0381	0.0730
R_1 (all data)	0.1916	0.0870	0.1894
wR_2[a] [$I_o > 2\sigma(I_o)$]	0.1527	0.0432	0.0913
wR_2(all data)	0.1916	0.0895	0.2061

Compound	[Sn([18]aneO$_4$S$_2$)-(HO(CH$_2$)$_2$OH)][BF$_4$]$_2$	[Sn([18]aneO$_4$S$_2$)(H$_2$O)$_2$]$_2$-[PF$_6$]$_3$[F]
Formula	$C_{14}H_{30}B_2F_8O_6S_2Sn$	$C_{24}H_{56}F_{19}O_{12}P_3S_4Sn_2$
mwt.	650.81	1356.22
crystal system	Monoclinic	Tetragonal
space group	*P*2$_1$/*c* (14)	*P*4/*ncc* (130)
a (Å)	8.4182(15)	17.656(3)
b (Å)	15.129(4)	17.656(3)
c (Å)	19.264(7)	15.5791(10)
α (˚)	90	90
β (˚)	100.326(7)	90
γ (˚)	90	90
U (Å^3)	2413.7(11)	4856.5(12)
Z	4	4
μ(Mo Kα) (mm^{-1})	1.321	1.421
F(000)	1304	2704
total no. reflns	27195	54421
unique reflns	5512	2785
R_{int}	0.0590	0.0551
no. of params, restraints	305, 2	148, 0
R_1[a] [$I_o > 2\sigma(I_o)$]	0.0346	0.0470
R_1 (all data)	0.0682	0.1283
wR_2[a] [$I_o > 2\sigma(I_o)$]	0.0551	0.0593
wR_2(all data)	0.0735	0.1350

[a] $R_1 = \Sigma||F_o| - |F_c||/\Sigma|F_o|$. $wR_2 = [\Sigma w(F_o^2 - F_c^2)^2/\Sigma wF_o^4]^{1/2}$

Common items: temperature = 100K; wavelength (Mo Kα)= 0.71073 Å; θ_{max}= 27.5˚

6.6 References

1. J. Parr, in *Comprehensive Coord. Chem. II*, eds. J. A. M. Editors-in-Chief: T. J. Meyer, Pergamon, Oxford, 2003, pp. 545

2. B. Cordero, V. Gomez, A. E. Platero-Prats, M. Reves, J. Echeverria, E. Cremades, F. Barragan and S. Alvarez, *Dalton Trans.*, 2008, 2832

3. F. Cheng, A. L. Hector, W. Levason, G. Reid, M. Webster and W. Zhang, *Angew. Chem. Int. Ed.*, 2009, **48**, 5152

4. P. A. Rupar, R. Bandyopadhyay, B. F. T. Cooper, M. R. Stinchcombe, P. J. Ragogna, C. L. B. Macdonald and K. M. Baines, *Angew. Chem. Int. Ed.*, 2009, **48**, 5155

5. A. L. Hector, W. Levason, G. Reid, M. Webster and W. Zhang, *Dalton Trans.*, 2011, **40**, 694

6. W. Levason and G. Reid, in *Supramol. Chem.*, John Wiley & Sons, Ltd, 2012

7. F. Cheng, A. L. Hector, W. Levason, G. Reid, M. Webster and W. Zhang, *Chem. Commun.*, 2008, 5508

8. R. H. Herber and A. E. Smelkinson, *Inorg. Chem.*, 1978, **17**, 1023

9. R. H. Herber and G. Carrasquillo, *Inorg. Chem.*, 1981, **20**, 3693

10. M. G. B. Drew and D. G. Nicholson, *J. Chem. Soc., Dalton Trans.*, 1986, 1543

11. E. Hough, D. G. Nicholson and A. K. Vasudevan, *J. Chem. Soc., Dalton Trans.*, 1989, 2155

12. R. Bandyopadhyay, B. F. T. Cooper, A. J. Rossini, R. W. Schurko and C. L. B. Macdonald, *J. Organomet. Chem.*, 2010, **695**, 1012

13. C. L. B. Macdonald, R. Bandyopadhyay, B. F. T. Cooper, W. W. Friedl, A. J. Rossini, R. W. Schurko, S. H. Eichhorn and R. H. Herber, *J. Am. Chem. Soc.*, 2012, **134**, 4332

14. K. Izod, E. R. Clark, W. Clegg and R. W. Harrington, *Organometallics*, 2011, **31**, 246

15. C. Gurnani, A. L. Hector, E. Jager, W. Levason, D. Pugh and G. Reid, *Dalton Trans.*, 2013, **42**, 8364

16. J. A. Cabeza, J. M. Fernández-Colinas, P. García-Álvarez and D. Polo, *Inorg. Chem.*, 2012, **51**, 3896

17. K. Merzweiler, L. Weisse and H. Kraus, *Z. Naturforsch. B: Chem. Sci.*, 1994, **49**, 425

18. T. S. Dory, J. J. Zuckerman and C. L. Barnes, *J. Organomet. Chem.*, 1985, **281**, 1

19. P. Jutzi, F. Kohl, P. Hofmann, C. Kruger and Y. H. Tsay, *Chem. Ber. Recl.*, 1980, **113**, 757

20. J. M. Blackwell, W. E. Piers and R. McDonald, *J. Am. Chem. Soc.*, 2002, **124**, 1295

21. H. Gruetzmacher and H. Pritzkow, *Organometallics*, 1991, **10**, 938

22. S. W. Audi Fong, W. Teck Yap, J. J. Vittal, T. S. A. Hor, W. Henderson, A. G. Oliver and C. E. F. Rickard, *J. Chem. Soc., Dalton Trans.*, 2001, 1986

23. R. Y. C. Shin, J. J. Vittal, Z. Y. Zhou, L. L. Koh and L. Y. Goh, *Inorg. Chim. Acta*, 2003, **352**, 220

24. E. C. Constable, F. K. Khan, J. Lewis, M. C. Liptrot and P. R. Raithby, *J. Chem. Soc., Dalton Trans.*, 1985, 333

25. J. Fischer, M. Schürmann, M. Mehring, U. Zachwieja and K. Jurkschat, *Organometallics*, 2006, **25**, 2886

26. A. V. Plakhotnyk, L. Ernst and R. Schmutzler, *J. Fluorine Chem.*, 2005, **126**, 27

27. M. Mantina, A. C. Chamberlin, R. Valero, C. J. Cramer and D. G. Truhlar, *J. Phys. Chem. A*, 2009, **113**, 5806

28. K. Nakamoto, in *Handbook of Vibrational Spectroscopy*, John Wiley & Sons, Ltd, 2006

29. G. E. D. Mullen, P. J. Blower, D. J. Price, A. K. Powell, M. J. Howard and M. J. Went, *Inorg. Chem.*, 2000, **39**, 4093

30. P. Maurer, A. Magistrato and U. Rothlisberger, *J. Phys. Chem. A*, 2004, **108**, 11494

31. A. J. Blake, A. J. Holder, T. I. Hyde, H. J. Kuppers, M. Schroder, S. Stotzel and K. Wieghardt, *J. Chem. Soc. Chem. Comm.*, 1989, 1600

7. Mixed Donor Chalcogenoether Macrocyclic Coordination Complexes of Antimony(III) Halides

7.1 Introduction

Antimony(III) is considered a borderline/soft Lewis acid with a Pauling electronegativity of 2.05 and a covalent radius of 1.39 Å [1].

There are only three structurally authenticated examples of antimony(III) halides with oxa-thia macrocycles known in the literature, all of which show preferential coordination to the hard O donors and in one example no S-donor interaction. This contrasts the expected coordination behaviour for a soft Lewis acid. They are $[SbCl_3(mn\text{-}15\text{-}O_3S_2)]$, $[SbCl_3(mn\text{-}18\text{-}O_4S_2)]$ and $[SbF_3([1.5]\text{-dibenzothia-18-crown-6})]$ (Figure 7.1-7.4) [2 3 4].

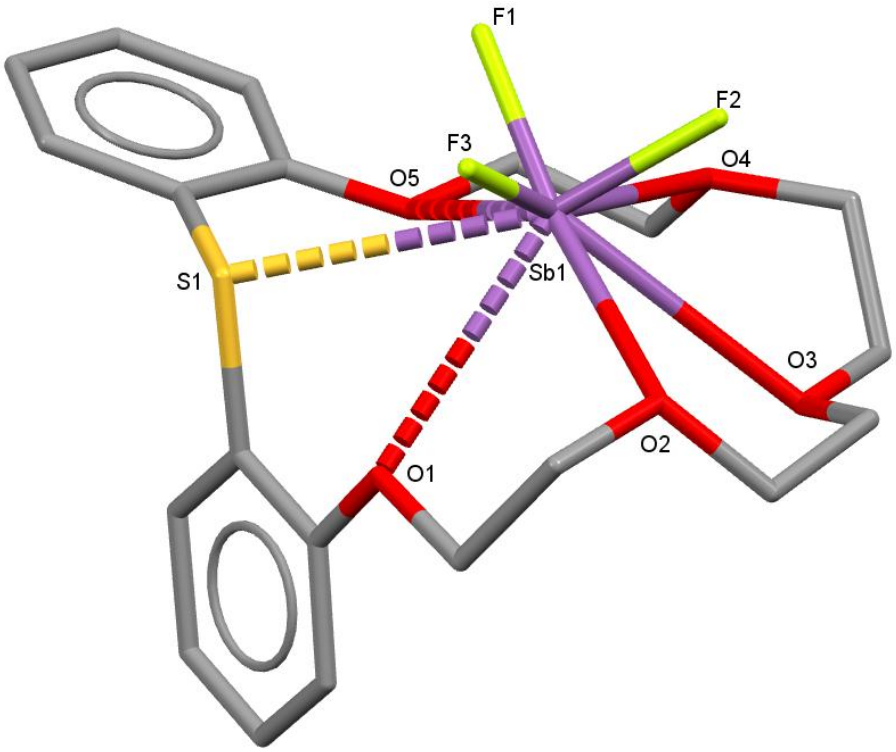

Figure 7.1 Structure of $[SbF_3([1.5]\text{-dibenzothia-18-crown-6})]$. H atoms are omitted for clarity [4].

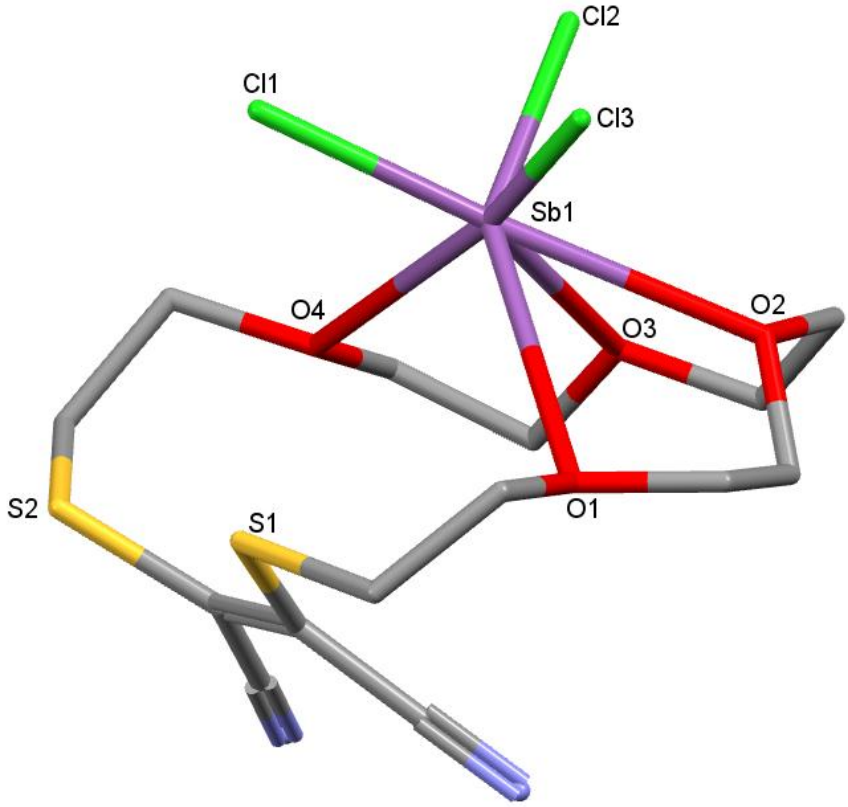

Figure 7.2 Structure of [$SbCl_3$(mn-18-O_4S_2)]. H atoms are omitted for clarity [2] [3].

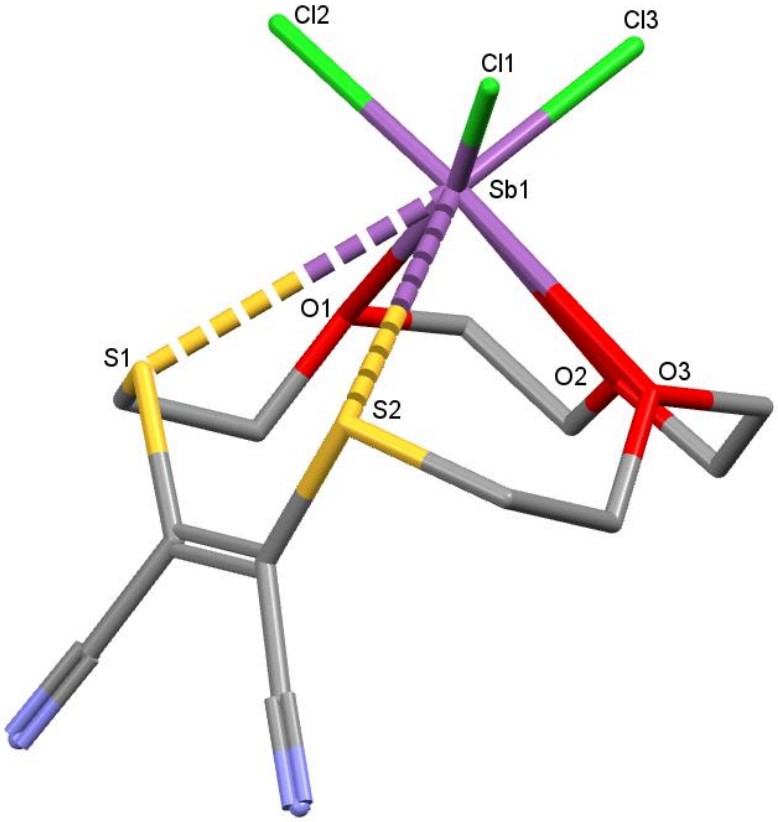

Figure 7.3 Structure of [$SbCl_3$(mn-15-O_3S_2)]. H atoms are omitted for clarity [2] [3].

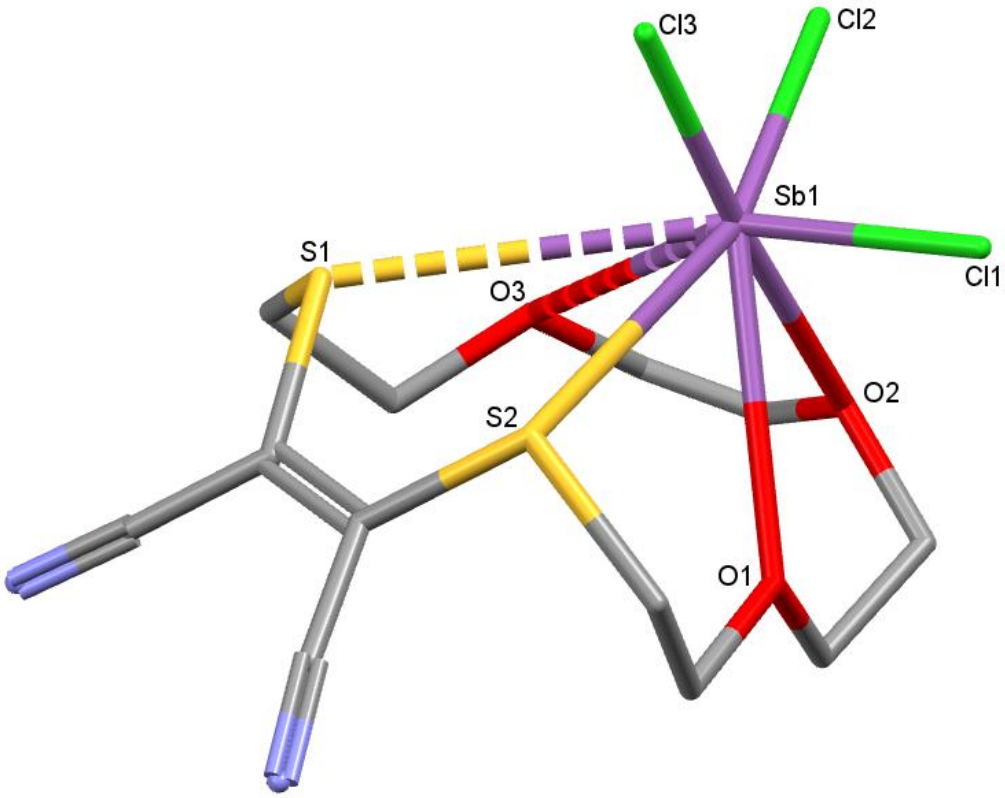

Figure 7.4 Structure of [$SbCl_3$(mn-15-O_3S_2)]. H atoms are omitted for clarity [5].

Structurally the complex [$SbCl_3$(mn-15-O_3S_2)] has two very closely related isomeric forms, in Figure 7.3 the pyramidal $SbCl_3$ unit is centred more symmetrically within the macrocyclic cavity whereas in Figure 7.4 it favours one side and is skewed [5]. A point of comparison is that the valence isoelectronic Lewis acid Pb(II) (see Chapter 5) coordinates to all the donors in both mn-15-O_3S_2 and mn-18-O_4S_2, The covalent radius of Pb(II) is only 0.07 Å larger than Sb(III)[1], although lead(II) still coordinates preferably to the O-donors [3].

Examples of SbX_3 complexes with crowns and thia-crowns are more plentiful. In general, the crown ether complexes are 1:1 half-sandwich adducts (crown= 12-crown-4, 15-crown-5, 18-crown-6, benzo- or dicyclohexyl-18-crown-6) [6 7 8 9 10 11 12 13 14]. [$(SbF_3)_2$(12-crown-4)] is slightly different in that it is polymeric with the second SbF_3 interacting with the coordinated SbF_3 [7]. In all the complexes the Sb(III) ion coordinates to all the O donor atoms. A comparison of [SbX_3(15-crown-5)] (X= F, Cl, Br) complexes shows minimal differences, in all three the pyramidal SbX_3 unit

sits above the basal plane of the macrocycle and remains little perturbed by the influence of the crown, indicating the predominant bonding is to the halide [15] [16] [17]. Minor differences between the complexes reflect the steric constraints and electronic influences put on the Sb(III) centre by the differing halides.

In the presence of halide abstractors, namely $SbCl_5$, cationic species can be formed [18] [19] [20]. The removal of one, two or even all three halides from the metal cation allow for a greater amount of encapsulation by the macrocycle. In $[SbCl_2([18\text{-crown-6})][SbCl_6]$ the macrocycle begins to adopt a more folded conformation akin to that seen for $[18]aneO_4S_2$ complexes discussed as part of this work (see Chapters 3 and 4) [18]. In contrast, for $[SbCl(15\text{-crown-5})][SbCl_6]_2 \cdot MeCN$ the $[SbCl]^{2+}$ unit sits within the macrocyclic cavity and is coordinated in the plane of the macrocycle [19]. Different again is the complex $[Sb(12\text{-crown-4})_2(MeCN)][SbCl_6]_3$ which is a discrete sandwich complex [20].

The thia-crowns adopt more varied geometries compared to the neutral crown complexes. The nine-membered thia-macrocycle $[9]aneS_3$ forms complexes with $SbCl_3$ and SbI_3, in the former it is a chain polymer, whereas the latter is a discrete monomeric complex [21] [22]. The selena-macrocycle $[16]aneSe_4$ and thia-macrocycle $[14]aneS_4$ form *exocyclic* polymeric complexes with $SbBr_3$ [23] [24]. The reaction between $SbCl_3$ and $[18]aneS_6$ forms the discrete dimer $[(SbCl_3)_2([18]aneS_6)]$, where each Sb(III) is coordinated *anti* by a S_3Cl_3 donor set [21].

The work in this chapter discusses the preparation of antimony(III) complexes with mixed donor chalcogenoether macrocycles.

7.2 Results and Discussion

7.2.1 Reactions with $SbCl_3$

Direct reaction of [18]aneO_4S_2 and $SbCl_3$ in acetonitrile with one equivalent of the halide abstractor $SbCl_5$ gives the previously mentioned (See Chapters 3 and 4) yellow complex $[SbCl_2([18]aneO_4S_2)][SbCl_6]$.

The IR spectrum of the isolated solid shows the expected band at 340 cm^{-1} for the v_3 of $[SbCl_6]^-$, and a sharp band at 301 cm^{-1} assigned to the $SbCl_2$ v_{asym} from the cation. This closely matches the corresponding band in $[SbCl_2$(18-crown-6][$SbCl_6$] at 300 cm^{-1} [18]. Other bands attributed to the macrocycle are also present.

The crystal structure $[SbCl_2([18]aneO_4S_2)][SbCl_6]$ is isomorphous with that of the 18-crown-6 analogue in the literature. The discrete octahedral anion $[SbCl_6]^-$ is present, and provides charge balance for the cation in Figure 7.5, $[SbCl_2([18]aneO_4S_2)]^+$. The Sb–Cl distances in the two cations are identical, and in $[SbCl_2$(18-crown-6)]$^+$ there are two short Sb–O distances (2.467(1), 2.485(1) Å) arranged mutually *trans* (O–Sb–O = 170.6°) and four longer Sb–O bonds (2.68(1)–2.76(1) Å). In $[SbCl_2([18]aneO_4S_2)]^+$ the two sulfur atoms (Sb–S= 2.768(2), 2.793(2) Å) have replaced the shorter Sb–O with the S–Sb–S angle more acute (154.07(6)°); the other Sb–O distances are slightly longer (2.779(7)−2.855(7) Å). This suggests a higher affinity of Sb(III) for sulfur over oxygen. Other similar cationic/neutral fragments $[M(cis\text{-}X_2)([18]aneO_4S_2)]^{(n+)}$ (M= Ca, Sr, Sc, Y; X= Cl, I, $[CF_3SO_3]^-$, H_2O; n= 0,1,2) have varyingly shorter $M–O_{macrocycle}$ to M–S distances confirming the macrocycle ([18]aneO_4S_2) is flexible enough to accommodate a variety of conformations; taking into account the difference in covalent radii [1]; and hence the significant differences between the M–E (E= S(Se), O) interactions can be attributed to the different Lewis acid affinities of the metal in these systems.

In CD_3CN solutions at ambient temperature the ^1H NMR spectra show the C***H***$_2$ group resonances shifted to high frequency from those in the parent ligand by 0.2-0.44 ppm. The largest shift being experienced by the C***H***$_2$ groups closest to the sulfur, further confirming the greater affinity of

Sb(III) for the softer donor. Second order multiplets for the SC***H***$_2$ and the SCH$_2$C***H***$_2$O protons were observed indicating slow exchange/dissociation of the macrocycle.

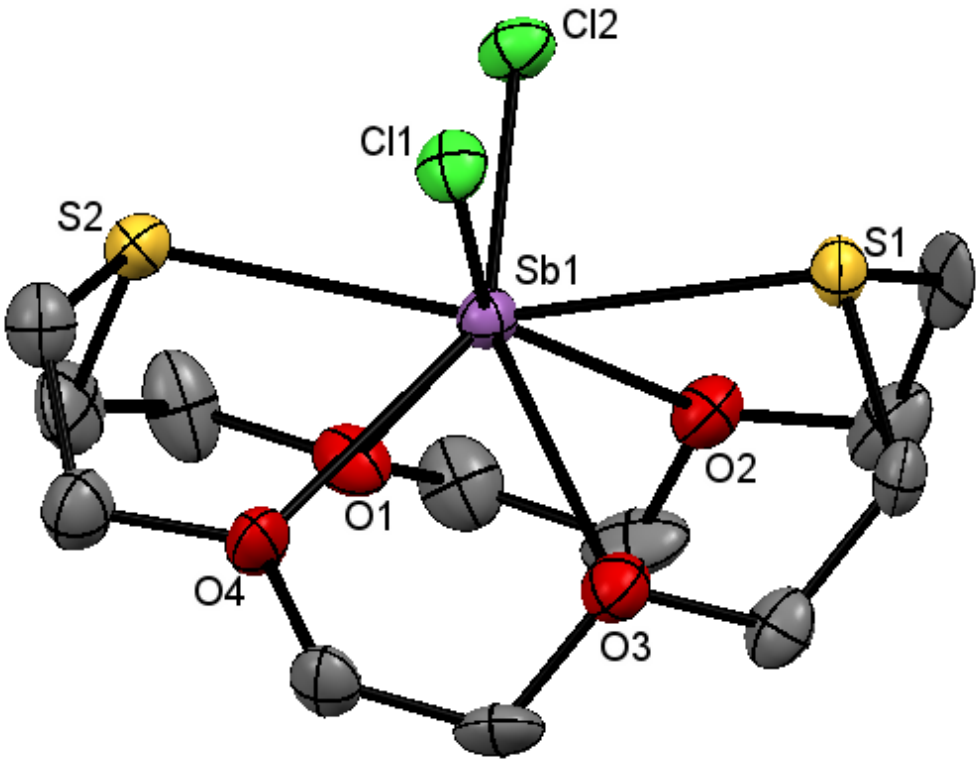

Figure 7.5 Crystal Structure of the cation in [SbCl$_2$([18]aneO$_4$S$_2$)][SbCl$_6$] showing the atom labelling scheme. The displacement ellipsoids are drawn at the 50% probability level and H atoms are omitted for clarity.

Table 7.1 Selected bond lengths (Å) and angles (°) for [SbCl$_2$([18]aneO$_4$S$_2$)][SbCl$_6$]

Sb1–Cl1	2.400(2)	Cl1–Sb1–Cl2	90.68(8)
Sb1–Cl2	2.385(2)	S1–Sb1–S2	154.07(6)
Sb1–S1	2.793(2)	S2–Sb1–O1	67.71(15)
Sb1–S2	2.768(2)	S1–Sb1–O2	67.17(15)
Sb1–O1	2.779(7)	S1–Sb1–O3	68.50(14)
Sb1–O2	2.828(7)	S2–Sb1–O4	64.02(14)
Sb1–O3	2.855(7)	O1–Sb1–O2	59.11(19)
Sb1–O4	2.810(7)	O3–Sb1–O4	59.33(18)

Similar reactions with [18]aneO_2S_4 and [15]aneO_3S_2 proved unsuccessful giving only oils that were difficult to analyse in the former, and a viscous yellow oil plus vivid green crystals in the latter. The ^{1}H NMR spectrum was very difficult to interpret and showed a mixture of unidentified species. The crystals had the structure [MCl([15]aneO_3S_2)][$SbCl_6$] where M was unidentified requiring an oxidation state (2+) and hence ruling out Sb(III), EDX on the crystals also failed to identify a suitable metal cation. Due to the recurring difficulties in these systems the reactions were abandoned. As with previous experiences, the reagent $SbCl_5$ has proven to be unpredictable and very reactive and could be the cause for the difficulties.

Subsequent reactions involved direct reaction of $SbCl_3$ and the macrocycle in MeCN, excluding the use of a halide abstractor. $SbCl_3$ and [9]aneOS_2 react together to form colourless crystals of [$SbCl_3$([9]aneOS_2)] and is the first example of a nine membered oxa-thia macrocycle coordinated to an element outside of the d-block Figure 7.6. The IR spectrum shows the expected bands for the macrocycle present and stretches attributable to SbCl (328, 307, 289 cm^{-1}). The ^{1}H NMR data shows modest high frequency shifts for all the C***H***$_2$ groups compared to the free ligand.

The structure has a pyramidal $SbCl_3$ unit little different from the parent halide, coordinated (*exocyclic*) to one S atom from two different macrocycles Sb1–S1 3.0007(9), Sb1–S2 3.2112(10) Å, and there are two very long (*endocyclic*) contacts to a third macrocycle (3.720 and 3.387 Å), the longest of which is nearing the ΣVdW radii (Sb+S= 3.86 Å) [15 25]. The overall polymeric structure is a double chain shown in Figure 7.7, in which the antimony is in a much distorted seven-coordinate environment. The structure may be compared with [$SbCl_3$([9]aneS_3)] (also seven-coordinate) which has *endo*-coordinated thiacrown (Sb–S= 3.156(3)–3.409(3) Å) and the Sb–S link to the neighbouring thia-crown is 3.171(3) Å [21]. In both cases the "*exo*" interactions are the stronger of the Sb–S bonds. The two chain structures are in contrast to the related discrete monomer [SbI_3([9]aneS_3)], where the antimony is six-coordinate but also bound *endocyclic* with markedly shorter Sb–S bonds (2.840– 2.895 Å) [22]. In the present molecule there is no interaction with the ether oxygens, which

point away from the chains continuing to show the preference $SbCl_3$ has for the S-donor over O.

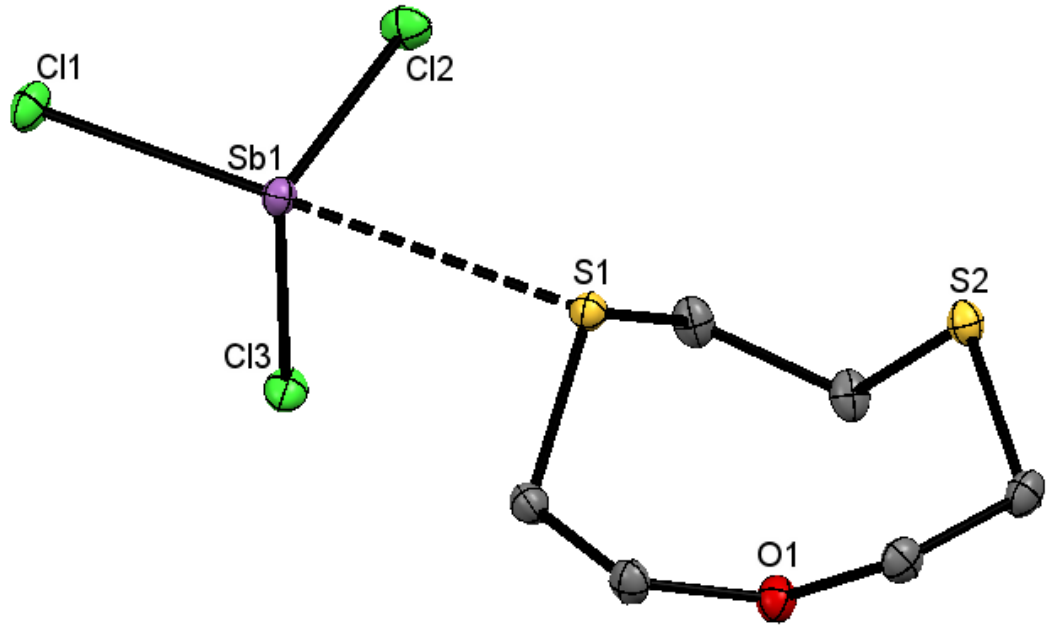

Figure 7.6 Crystal structure of $[SbCl_3([9]aneOS_2)]$ showing the atom labelling scheme. The displacement ellipsoids are drawn at the 50% probability level and H atoms are omitted for clarity. One Sb···S *exocyclic* interaction is shown. Symmetry operation: a = x – 1, y, z.

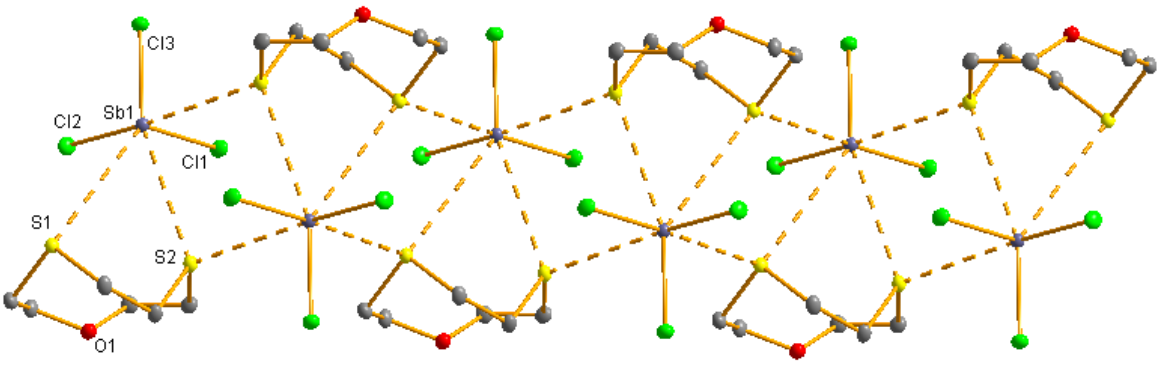

Figure 7.7 View of the double chain network in the crystal structure of $[SbCl_3([9]aneOS_2)]$

Table 7.2 Selected bond lengths (Å) and angles (°) for $[SbCl_3([9]aneOS_2)]$

Sb1–Cl1	2.4428(8)	Cl1–Sb1–Cl2	92.47(2)
Sb1–Cl2	2.3895(8)	Cl2–Sb1–Cl3	90.56(2)
Sb1–Cl3	2.3828(9)	Cl1–Sb1–Cl3	93.59(2)
Sb1–S1(*exo*)	3.0008(9)	S1–Sb1–S2(*endo*)	55.85(1)
Sb1–S2(*exo*)	3.211(1)		
Sb1–S1(*endo*)	3.720(1)		
Sb1–S2(*endo*)	3.387(6)		

The complex $[SbCl_3([15]aneO_3S_2)]$ is a discrete monomer with all the macrocyclic donor atoms coordinated, giving eight-coordinate antimony Figure 7.8. At the time it was a relatively rare example of *endo*-coordination by this ligand, although there are now more examples, the majority of which have emerged from the work in this thesis.

The IR spectrum shows the expected bands for the complex. The ^1H NMR data (in CD_3CN at ambient temperature) show the four different C***H***$_2$ environments close to free ligand. On cooling the solution to 233K, the triplet and singlet associated with the C***H***$_2$ groups adjacent to the O merge into a multiplet ~3.71 ppm, the other signals remain little affected.

The structure has very long Sb–O and Sb–S bonds (>3 Å). Again the pyramidal $SbCl_3$ unit remains relatively unchanged showing the predominant bonding is Sb–Cl [15]. The $SbCl_3$ sits above the basal plane of the macrocycle, with the coordination to the macrocycle favouring the sulfur donor atoms. This can be seen by comparing the Sb–E (E= O, S) bond lengths, Sb–O: 3.12 Å (ave), Sb–S: 3.14 Å (ave), $\Delta_{Sb\text{-}O/Sb\text{-}S}$= 0.02 Å which is significantly smaller than the difference in covalent radii between S and O Δ_{radii}= 0.39 Å, ultimately suggesting that $SbCl_3$ has a softer Lewis acidic character [1].

Comparisons with the structures in the literature include the complex $[SbCl_3$(15-crown-5)] where the Sb–O distances are shorter 2.787(5)-

2.997(3) Å but still significantly longer than the Sb–S interaction in $[SbCl_3([15]aneO_3S_2)]$ [8 10]. An interesting case is in the structure of $[SbCl_3(mn\text{-}15\text{-}O_3S_2)]$ where the Sb–S interaction (3.495(2), 3.460(2) Å) is much longer compared to that seen for Sb–O (2.898(5)-3.009(5) Å), this apparent reversal in coordination behaviour can be explained when looking at the ligand structure Figure 7.3, between the two sulfur atoms is a rigid maleonitrile link rather than the more flexible dimethylene linker present in $[15]aneO_3S_2$ and this would seem to pre-organise the ligand to coordinate the $SbCl_3$ in a manner that favours the O-donor atoms. A more extreme example of this is in the related complex $[SbCl_3(mn\text{-}18\text{-}O_4S_2)]$ (Figure 7.2) where there is no S-coordination evident [2 3].

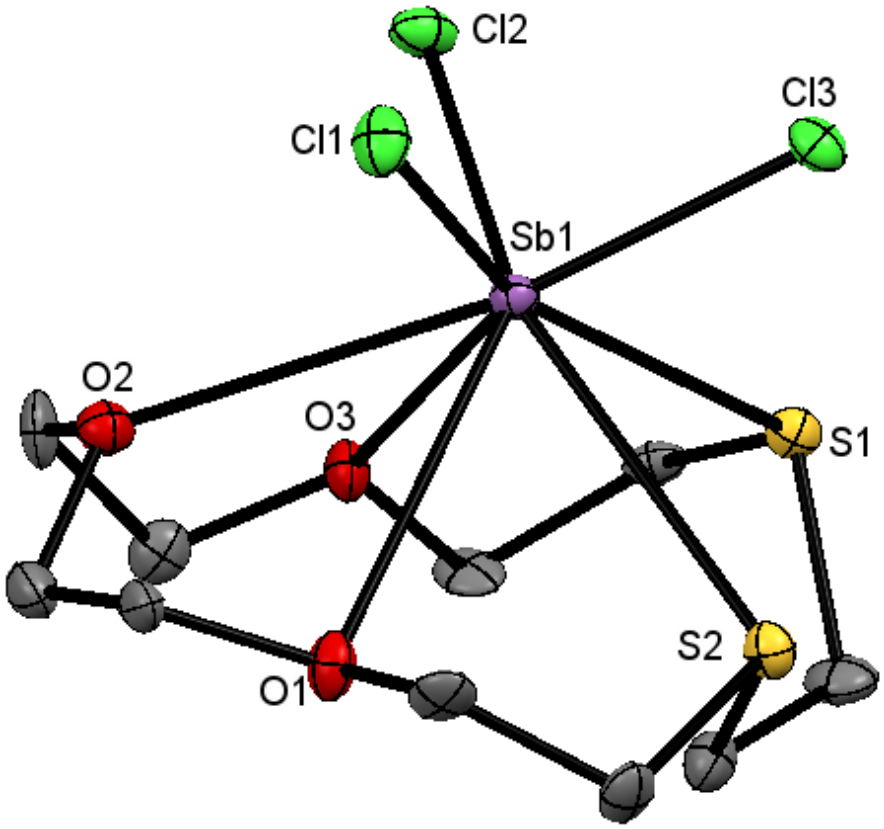

Figure 7.8 Crystal structure of $[SbCl_3([15]aneO_3S_2)]$ showing the atom labelling scheme. The displacement ellipsoids are drawn at the 50% probability level and H atoms are omitted for clarity.

Table 7.3 Selected bond lengths (Å) and angles (°) for $[SbCl_3([15]aneO_3S_2)]$

Sb1–Cl1	2.453(2)	Cl1–Sb1–Cl2	92.58(7)
Sb1–Cl2	2.408(2)	Cl2–Sb1–Cl3	91.63(7)
Sb1–Cl3	2.432(2)	Cl1–Sb1–Cl3	87.33(6)
Sb1–S1	3.061(2)	S1–Sb1–S2	68.05(5)
Sb1–S2	3.205(2)	S1–Sb1–O3	61.6(1)
Sb1–O1	3.205(5)	S2–Sb1–O1	57.64(9)
Sb1–O2	3.011(5)	O1–Sb1–O2	54.9(1)
Sb1–O3	3.117(5)	O2–Sb1–O3	56.1(1)

The reaction of $SbCl_3$ with $[18]aneO_4S_2$ in acetonitrile gives predominantly a white solid $[SbCl_3([18]aneO_4S_2)]$. The neutral formulation was favoured over $[SbCl_2([18]aneO_4S_2)][Cl]$ from the evidence in the far IR spectrum which shows ν(SbCl) as a broad feature at 292 cm^{-1} with ill-defined shoulders to both high and low frequency, this differs from the sharp stretch at 301 cm^{-1} found for $[SbCl_2([18]aneO_4S_2)]^+$ (*vide supra*). The stretches are similar to those obtained in other neutral $[SbCl_3(crown)]$ complexes, which indicates that the pyramidal $SbCl_3$ unit has been influenced little by the different macrocycles coordinated [9, 11, 15, 21].

In solution (CD_3CN, 295 K) the ^1H NMR spectrum is more complicated than expected, with two sets of three C***H***$_2$ resonances observed. The first closely resembles the chemical shifts expected for $[SbCl_2([18]aneO_4S_2)]^+$ and the other shows a small shift to high frequency from the parent ligand, assigned to the neutral complex. All the signals are broadened and the couplings are not clear, suggesting an equilibrium:

$$[SbCl_3([18]aneO_4S_2)] \rightleftharpoons [SbCl_2([18]aneO_4S_2)]^+Cl^-$$

Cooling the solutions to 233 K gives rise to complex second-order patterns, consistent with two species present in unequal amounts.

Conductivity studies give further credence to this interpretation; the MeCN solution has a modest molar conductivity (Λ_M = 26 ohms^{-1} mol^{-1} cm^2) although much less than expected for a 1:1 electrolyte (~120-160 ohms^{-1} mol^{-1} cm^2) [26]. The ^{1}H NMR spectrum in the non-coordinating solvent $CDCl_3$ showed only one set of resonances close to free ligand, suggesting that formation of the cationic species is promoted by polar solvents such as MeCN.

The bulk material analyses close to the above formula but a few crystals were isolated with the constitution $[SbCl_2([18]aneO_4S_2)]_2[Sb_3Cl_{11}]$. The presence of excess Lewis Acid $SbCl_3$ promotes formation of the $[SbCl_2([18]aneO_4S_2)]^+$ cation Figure 7.9. The structure itself does not differ much from the cation in $[SbCl_2([18]aneO_4S_2)][SbCl_6]$ (above). But the dianion $[Sb_3Cl_{11}]^{2-}$ has not been previously reported Figure 7.10. Haloantimonates(III) show an extensive variety in the literature in both stoichiometries and structures, the present example contains a central square pyramidal $SbCl_5$ unit linked *via* single long Cl (*cis*) bridges to $SbCl_4$ groups which are *pseudo* trigonal bipyramidal [27].

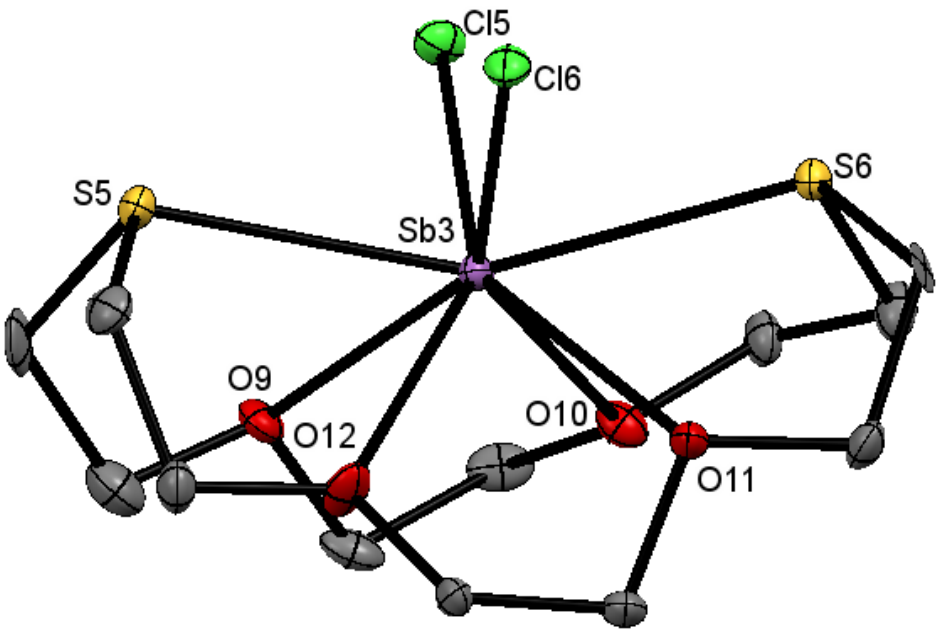

Figure 7.9 Crystal structure of the Sb3 centred cation in $[SbCl_2([18]aneO_4S_2)]_2[Sb_3Cl_{11}]\cdot CH_2Cl_2$ showing the atom labelling scheme. Ellipsoids are drawn at the 50% probability level and H atoms have been omitted for clarity. The other crystallographically independent cation adopts a very similar structure.

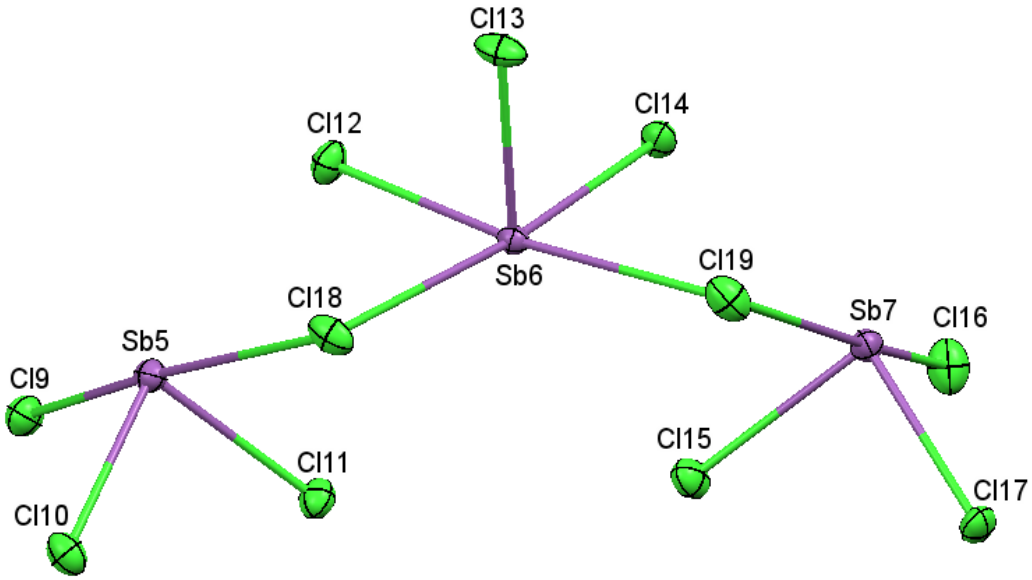

Figure 7.10 Crystal structure of the Sb6 centred dianion in $[SbCl_2([18]aneO_4S_2)]_2[Sb_3Cl_{11}]\cdot CH_2Cl_2$ showing the atom labelling scheme. Ellipsoids are drawn at the 50% probability level and H atoms have been omitted for clarity. The other crystallographically independent anion adopts a very similar geometry.

Table 7.4 Selected bond lengths (Å) and angles (°) for $[SbCl_2([18]aneO_4S_2)][Sb_3Cl_{11}]$

Sb3–Cl5	2.420(2)	Cl5–Sb3–Cl6	89.42(6)
Sb3–Cl6	2.435(2)	S5–Sb3–S6	153.94(6)
Sb3–S5	2.795(2)	S5–Sb3–O9	67.4(1)
Sb3–S6	2.787(2)	S5–Sb3–O12	67.2(1)
Sb3–O9	2.745(5)	S6–Sb3–O10	63.0(2)
Sb3–O10	2.782(6)	S6–Sb3–O11	68.3(1)
Sb3–O11	2.785(5)	O9–Sb3–O10	63.0(2)
Sb3–O12	2.721(5)	O11–Sb3–O12	59.7(2)
Sb5–Cl9	2.451(2)	Cl9–Sb5–Cl18	171.20(7)
Sb5–Cl10	2.393(2)	Sb5–Cl18–Sb6	92.94(6)
Sb5–Cl11	2.382(2)	Cl18–Sb6–Cl19	98.22(6)
Sb5–Cl18	2.864(2)	Sb6–Cl19–Sb7	89.54(6)
Sb6–Cl12	2.543(2)	Cl16–Sb7–Cl19	169.65(7)
Sb6–Cl13	2.342(2)	Cl10–Sb5–Cl1	92.28(7)
Sb6–Cl14	2.521(2)	Cl15–Sb7–Cl17	89.69(7)
Sb6–Cl18	2.810(2)		
Sb6–Cl19	2.789(2)		
Sb7–Cl15	2.396(2)		
Sb7–Cl16	2.418(2)		
Sb7–Cl17	2.383(2)		
Sb7–Cl19	2.941(2)		

Reaction of $SbCl_3$ and the oxa-selena crown [18]aneO_4Se_2 gives only one product, $[SbCl_2([18]aneO_4Se_2)]_2[Sb_3Cl_{11}]$ (the first oxa-selena macrocycle complex of antimony). The IR spectrum shows a sharper Sb–Cl stretch at 301 cm^{-1} in contrast to the [18]aneO_4S_2 complex and only one species in the ^1H NMR. Cooling to 233 K only sharpened the signals present, a further indication for there being only one species. All the C***H***$_2$ signals experienced a shift to high frequency, by 0.22-0.44 ppm from the parent ligand, with the largest shifts being experienced by those adjacent to Se. This is analogous to $[SbCl_2([18]aneO_4S_2)]^+$, but, as well as observing the signal splitting in the SeC***H***$_2$ environment, the four CH_2 groups corresponding to $SeCH_2C\boldsymbol{H}_2O$ also show a well-defined splitting.

The structure is isomorphous with $[SbCl_2([18]aneO_4S_2)]_2[Sb_3Cl_{11}]$ and shows a very similar folded conformation as in the previous $[SbCl_2(macrocycle)]^+$ cationic complexes, the anion is also identical. The Sb–Se distances (2.867(1), 2.884(1) Å) are only on average 0.09 Å longer than the Sb–S distances in former $[SbCl_2([18]aneO_4S_2)]^+$ complexes. When compared to the difference in covalent radii between S and Se of 0.15 Å, the interaction for the selenoether is significantly stronger [1]. This is further evidence for the softness of the Lewis acid $SbCl_3$, SeR_2 being a softer Lewis Base than SR_2. The other Sb-donor (Cl and O) lengths are similar to the sulfur analogues.

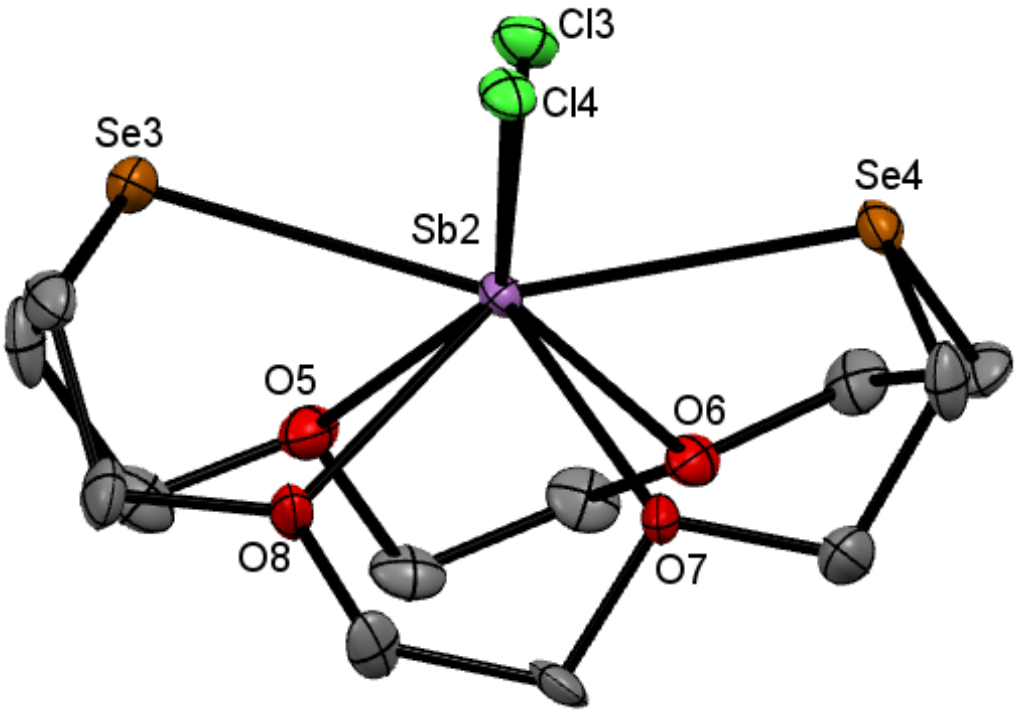

Figure 7.11 Crystal structure of the Sb2 centred cation in $[SbCl_2(C_{12}H_{24}O_4Se_2)]_2[Sb_3Cl_{11}]\cdot MeCN$ showing the atom labelling scheme. Ellipsoids are drawn at the 50% probability level and H atoms have been omitted for clarity. The other crystallographically independent cation adopts a similar structure.

Table 7.5 Selected bond lengths (Å) and angles (°) for $[SbCl_2([18]aneO_4Se_2)][Sb_3Cl_{11}]$

Sb2–Cl3	2.414(3)	Cl3–Sb2–Cl4	90.53(9)
Sb2–Cl4	2.431(2)	Se3–Sb2–Se4	152.87(4)
Sb2–Se3	2.875(1)	Se3–Sb2–O5	68.4(2)
Sb2–Se4	2.870(1)	Se3–Sb2–O8	67.4(1)
Sb2–O5	2.798(7)	Se4–Sb2–O6	68.2(2)
Sb2–O6	2.819(7)	Se4–Sb2–O7	69.4(1)
Sb2–O7	2.866(6)	O5–Sb2–O6	61.5(2)
Sb1–O8	2.789(6)	O7–Sb2–O8	58.8(2)

Similar attempts with the tellurium containing macrocycles, [18]aneO_4Te_2 and [9]aneO_2Te, give orange solutions that rapidly deposit black Te. Most likely the Sb(III) centre polarises the weak Te–C bond and promotes its cleavage in a similar fashion proposed for the analogous reaction with $Pb(BF_4)_2$ (See Chapter 5).

Attempts to increase the ratio of sulfur content in the $SbCl_3$ systems were unsuccessful. The attempted reaction between antimony(III) chloride and the tetrathia-dioxa macrocycle, [18]aneO_2S_4, only results in the recovery of the starting materials. It is unlikely that a low affinity of $SbCl_3$ for the four sulfur donors is the causal factor, since all the evidence so far points to the Lewis acid in fact having an increased preference for soft ligands. Also the existence of [CaI_2([18]aneO_2S_4)] (Chapter 3) is contrary to this, demonstrating the S_4-ligand can coordinate a much harder "incompatible" Lewis acid. It has been seen already that the preorganisation of the ligand can play a big influence on the coordination behaviour of these Lewis acids, the cavity size in [18]aneO_2S_4 may be mismatched for $SbCl_3$. This is also unlikely as the related antimony(III) iodide does successfully form a complex, [SbI_2([18]aneO_2S_4)]$_2$[Sb_4I_{14}] (discussed below), and $SbCl_3$ has shown that it will ionise and form [$SbCl_2$(macrocycle)]$_n$[Sb_xCl_y] salts. A better explanation may be the relative solubilities of the reagents; [18]aneO_2S_4 is not soluble in MeCN, unlike the other oxa-thia macrocycles used, requiring the use of halocarbon solvents (CH_2Cl_2), which in turn $SbCl_3$ is insoluble in. The reaction medium used was MeCN/CH_2Cl_2 which may have hindered the successful isolation of a complex.

7.2.2 Reactions with SbI_3

Investigations into whether SbI_3 would give different complex coordination geometries gave two novel complexes $[SbI_2([18]aneO_4S_2)][Sb_2I_7]$ and $[SbI_2([18]aneO_2S_4)]_2[Sb_4I_{14}]$.

Stirring SbI_3 and $[18]aneO_4S_2$ in MeCN turns the solution yellow, quickly depositing an insoluble bright orange solid. The solid has a constitution close to $[SbI_2([18]aneO_4S_2)][Sb_2I_7]$ and is insoluble in CD_3CN, it has a very limited solubility in CD_2Cl_2 but enough to acquire a weak ^1H NMR spectrum. All the C***H***$_2$ environments are moderately shifted to low frequency by 0.13 ppm. This shift is in contrast to those seen in the chloride systems which all experience shifts to high frequency, here instead there seems to be a shielding effect by the antimony(III) iodide system.

Orange crystals were obtained from the filtrate of the preparation. They contained $[SbI_2([18]aneO_4S_2)]^+$ cations Figure 7.12 and a disordered iodoantimonate anion Figure 7.13 with the constitution $[Sb_{2.5}I_{9.5}]$. The Sb–I bonds are elongated slightly compared to those found in the parent SbI_3, ~0.09 Å. It would appear where the $SbCl_3$ system remains little perturbed by coordination of the macrocycle, the SbI_3 system is more susceptible reflecting the weaker Sb–I bond. But it also has to be considered that the Sb(III) centre is more electron rich when the halide is iodide, suggesting SbI_3 is softer than $SbCl_3$ as a Lewis acid. That said the differences between macrocycle coordination bonds in the chloro and iodo cations with $[18]aneO_4S_2$ are small and irregular.

As mentioned above, the known complex $[SbI_3([9]aneS_3)]$ has shorter Sb–S bonds and coordinates to fewer donors than in the chloride systems. The literature also describes an elongation of the Sb-I bonds in the pyramidal SbI_3 from the parent precursor, a more pronounced lengthening (~0.18 Å) than that observed in the $[SbI_2([18]aneO_4S_2)][Sb_{2.5}I_{9.5}]$ [22]. The stronger Sb–S bonds are also in keeping with, and further evidence that SbI_3 is a softer Lewis Acid.

Discussion of the anion in $[SbI_2([18]aneO_4S_2)]_2[Sb_{2.5}I_{9.5}]$: due to the similar scattering of Sb and I the X-ray experiment has difficulty distinguishing between the two elements (the same issue between O and F in Chapter 6;

Sc and Fe in Chapter 4). The proposed model has Sb3 treated as a disordered mixture of Sb3 and an I atom (I8) giving the required dinegative charge:

$[Sb_nI_m]$ $n + m = 12$ (from the structure solution)

$3n - m = -2$ (the required charge)

giving $n = 2.5$ and $m = 9.5$

Providing the two half atoms occupy the same site, the model fits the experimental result and the bond lengths are plausible. The anion approximates a face-sharing bioctahedral $[Sb_2I_9]$ with an additional I/Sb atom. The anions link to form a chain in the *b* direction Figure 7.14.

Crystals with the constitution $[SbI_2([18]aneO_2S_4)]_2[Sb_4I_{14}]$ were grown from the reaction of SbI_3 and $[18]aneO_2S_4$. A similar, mainly insoluble orange powder formed from the reaction medium $MeCN/CH_2Cl_2$.

Crystals of sufficient quality for X-ray crystallographic studies proved difficult to acquire, the data collected have a reasonable R_{int} of ~3%, but the cation is heavily disordered and proved problematic to model. The cation shown in Figure 7.15 represents only a partial structure solution and hence a comparison of the bond lengths cannot be made.

A common challenge in these macrocyclic systems, (as mentioned in previous chapters), is they regularly exhibit a degree of disorder derived from their flexibility to adopt multiple and closely related conformations even in the solid state. Therefore even when R_{int} is seemingly good, crystallographically a suitable final fit may not be found. In the majority of the cases chemically the compounds are not in doubt.

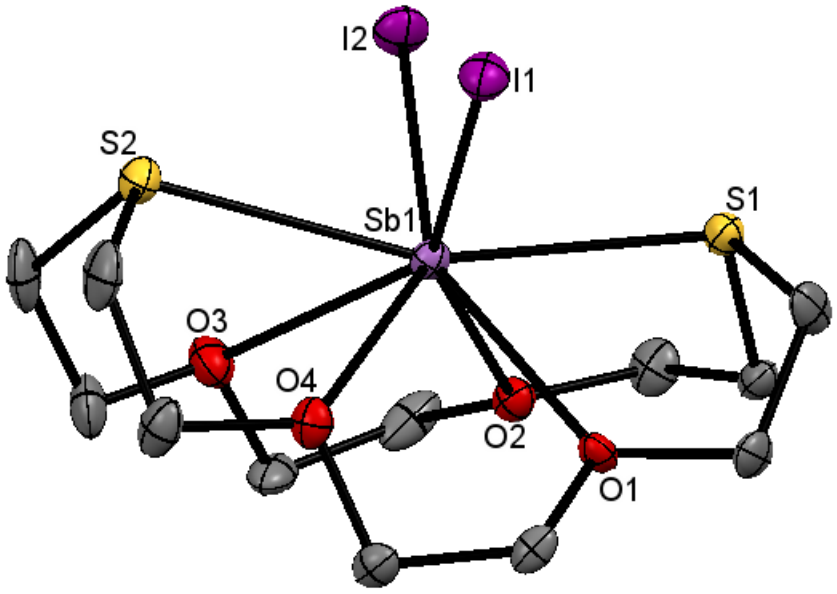

Figure 7.12 Crystal structure of the cation in $[SbI_2([18]aneO_4S_2)]_2[Sb_{2.5}Cl_{9.5}]$ showing the atom labelling scheme. Ellipsoids are drawn at the 50% probability level and H atoms are omitted for clarity

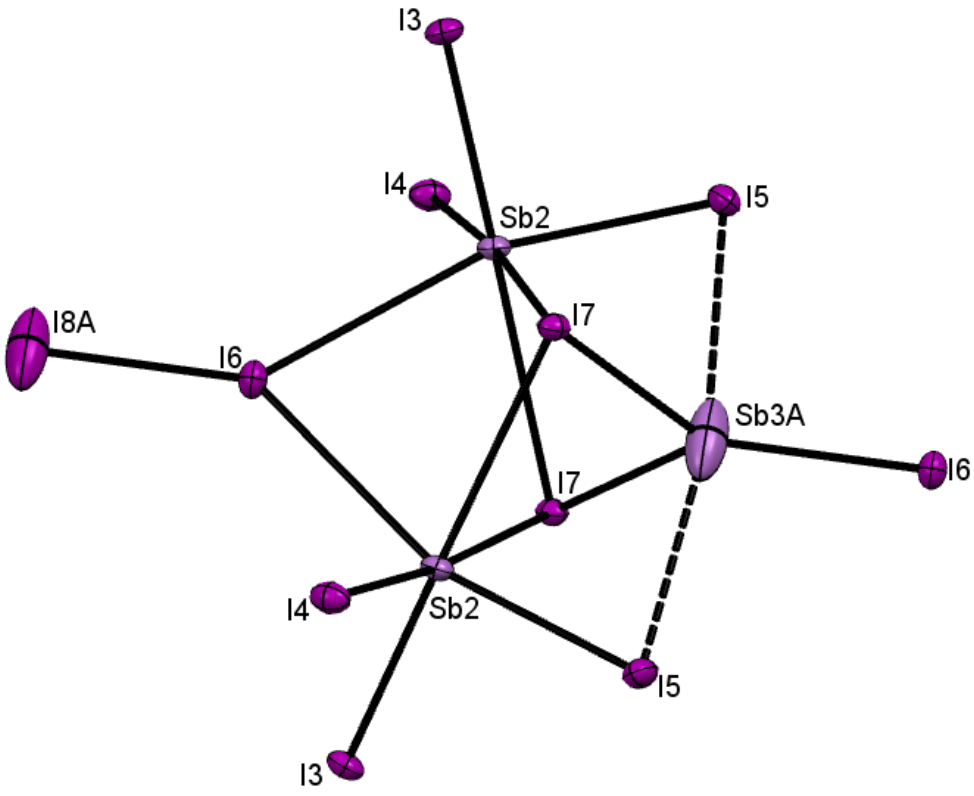

Figure 7.13 Crystal Structure of the anion in $[SbI_2([18]aneO_4S_2)]_2[Sb_{2.5}I_{9.5}]$ showing the atom labelling scheme. Ellipsoids are drawn at the 50% probability level. Atoms labelled Sb3A and I8A are on a disordered atom site and have both been given the same coordinates and atomic displacement parameters. The anions link up to form a chain in the *b* direction. Symmetry operations: a = – x, y, 5/2 – z; b = x, y –

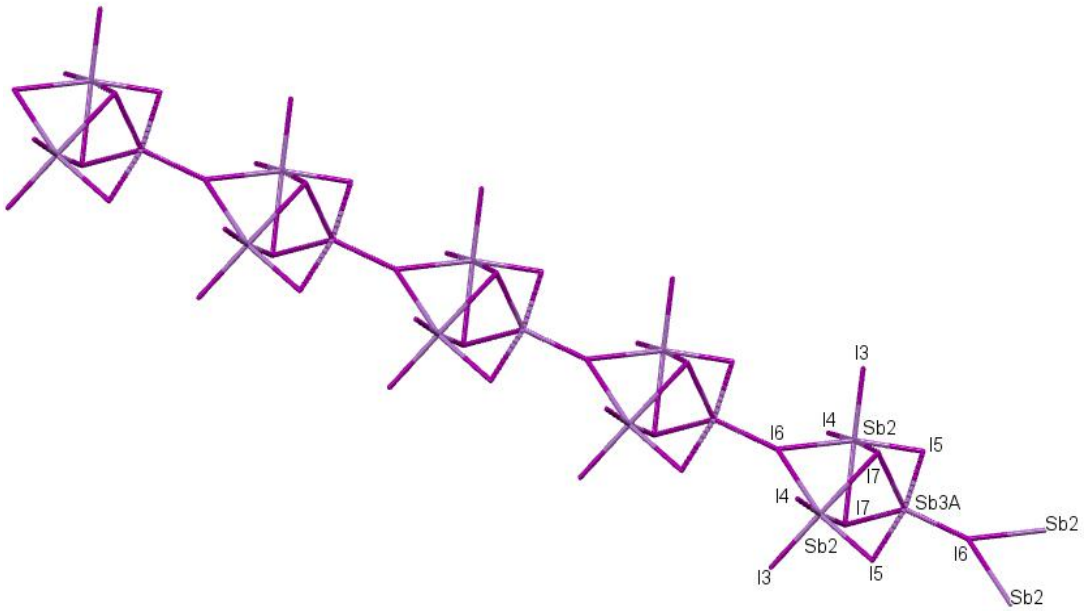

Figure 7.14 View of the anions in $[SbI_2([18]aneO_4S_2)]_2[Sb_{2.5}I_{9.5}]$ linking up and forming a 1D polymeric chain in the *b* direction.

Table 7.6 Selected bond lengths (Å) and angles (°) for $[SbI_2([18]aneO_4S_2)]_2[Sb_{2.5}Cl_{9.5}]$

Sb1–I1	2.766(1)	I1–Sb1–I2	93.18(3)
Sb1–I2	2.786(1)	S1–Sb1–S2	160.05(8)
Sb1–S1	2.766(3)	S1–Sb1–O1	65.9(1)
Sb1–S2	2.853(3)	S1–Sb1–O2	67.7(1)
Sb1–O1	2.744(6)	S2–Sb1–O3	65.7(1)
Sb1–O2	2.794(8)	S2–Sb1–O4	66.7(1)
Sb1–O3	2.968(7)	O1–Sb1–O4	59.3(2)
Sb1–O4	2.801(8)	O2–Sb1–O3	59.0(2)

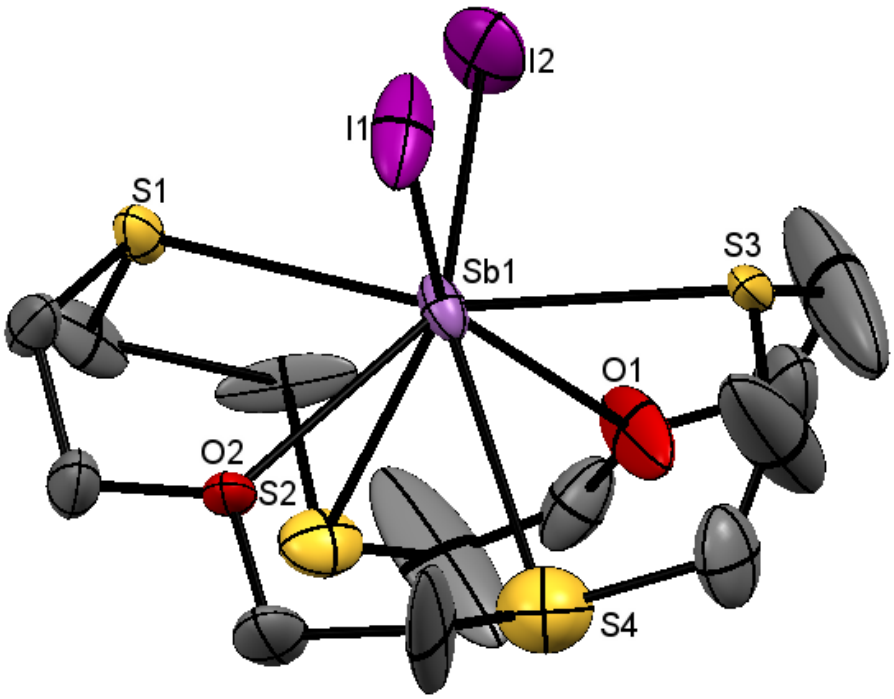

Figure 7.15 Partial Structure of the heavily disordered cation in $[SbI_2([18]aneO_2S_4)]_2[Sb_4Cl_{14}]$.

7.2.3 Reactions with SbF_3

The complexes $[SbF_3([15]aneO_3S_2)]$, $[SbF_3([18]aneO_4S_2)]$ and $[SbF_3([18]aneO_4Se_2)]$ represent the first examples of neutral heavier chalcogen ligand coordination to antimony(III) fluoride. SbF_3 has failed to form complexes with thioethers [28] such as SMe_2 or $MeS(CH_2)_2SMe$, and the related oxa-thia macrocyclic complex $[SbF_3([1.5]$-dibenzothia-18-crown-6)] (Figure 7.1) [4] is mainly coordinated *via* three O donors, the other SO_2 donor set is within the ΣVdW radii but the interactions are substantially longer [25].

Antimony(III) fluoride was dissolved in MeOH and the macrocycles added, (MeOH/MeCN for $[18]aneO_4Se_2$). The white solids that were produced dissolved in CH_2Cl_2 in which SbF_3 is insoluble and all showed broadened resonances compared to the free ligand in their ^1H NMR spectra. The 18-membered macrocycle complexes analysed as the desired 1:1 complexes but failed to form crystals for X-ray analysis.

Crystals of [SbF_3([15]aneO_3S_2)] were successfully grown Figure 7.16. The structure is similar to the chloride (Figure 7.8) in that the SbF_3 sits high above the basal plane of the macrocycle, is 8-coordinate and has fairly long Sb–E bonds (E= S, O). The Sb–F bonds are little affected by coordination of the crown as expected, reflecting the strength of the Sb–F bond. Interestingly the Sb–S bonds in the fluoride are markedly longer than in [$SbCl_3$([15]aneO_3S_2)] (3.31 (ave) *vs*. 3.14 (ave) Å), with the Sb–O bonds showing the opposite trend (2.97 (ave) *vs*. 3.12 (ave) Å) this shows that SbF_3 is the harder Lewis acid.

The known complex [SbF_3(18-crown-6)] was re-prepared for direct spectroscopic comparison with the new antimony(III) fluoride complexes [7]. Free SbF_3 is insoluble in chlorocarbons and has a $^{19}F\{^1H\}$ NMR chemical shift of -83.9 ppm (CD_3CN, 295 K). CD_2Cl_2 solutions of the crown and oxa-thia crown complexes show $^{19}F\{^1H\}$ NMR shifts in a similar environment, Table 7.7.

Table 7.7 Table showing $^{19}F\{^1H\}$ NMR shifts (ppm) for [SbF_3(macrocycle)] complexes.

[SbF_3(macrocycle)]	$^{19}F\{^1H\}$ NMR (δ) (CD_2Cl_2, 295K)	$^{19}F\{^1H\}$ NMR (δ) (CD_2Cl_2, 180K)
[SbF_3(18-crown-6)]*	-83.7	-84.6
[SbF_3([15]aneO_3S_2)]	-81.0	-84.0
[SbF_3([18]aneO_4S_2)]	-84.0	-87.0
[SbF_3([18]aneO_4Se_2)]	-76.2	-76.4

*[SbF_3(18-crown-6)] $^{19}F\{^1H\}$ NMR (CD_3CN, 295 K): -80.9 ppm

The shifts are all attributed to SbF_3.

Structural comparison of the SbX_3-crown (X= Cl, F; crown= 15-crown-5, 18-crown-6) complexes in the literature suggests the binding preference is for the smaller 15-membered macrocycles, although the binding is still weak [6]. The solution data above would also suggest a stronger interaction

for [SbF_3([15]aneO_3S_2)] over both the other 18-membered ring macrocyclic complexes.

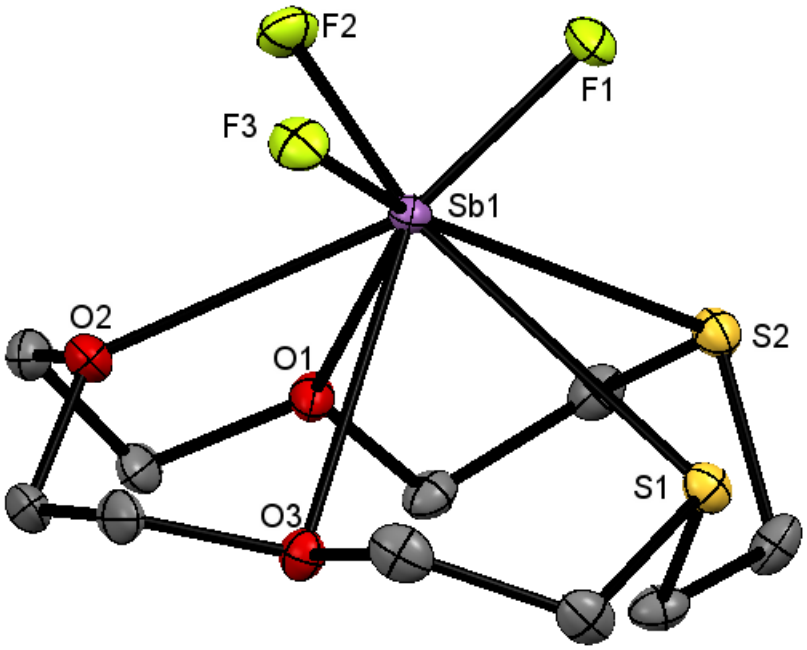

Figure 7.16 Crystal structure of [SbF_3([15]aneO_3S_2)] showing the atom labelling scheme. The displacement ellipsoids are drawn at the 50% probability level and H atoms are omitted for clarity.

Table 7.8 Selected bond lengths (Å) and angles (°) for [SbF_3([15]aneO_3S_2)]

Sb1–F1	1.950(2)	F1–Sb1–F2	86.92(6)
Sb1–F2	1.933(1)	F2–Sb1–F3	90.31(6)
Sb1–F3	1.933(1)	F1–Sb1–F3	87.29(6)
Sb1–S1	3.2998(9)	S1–Sb1–S2	64.76(2)
Sb1–S2	3.3204(8)	S1–Sb1–O3	58.85(3)
Sb1–O1	3.098(2)	S2–Sb1–O1	58.93(3)
Sb1–O2	2.722(2)	O1–Sb1–O2	58.68(5)
Sb1–O3	3.092(2)	O2–Sb1–O3	58.49(5)

7.3 Conclusions

A series of SbX_3 (X= F, Cl, I) adducts with oxa-thia and oxa-selena macrocycles have been prepared and characterised both crystallographically and spectroscopically. The Lewis acidity (Hard to Soft) of Sb(III) has been discussed with the choice of halide proving to be an important factor, not just the metal centre and oxidation state. Analysis of the data revealed a trend SbF_3>$SbCl_3$>SbI_3 where SbF_3 is a borderline Lewis Acid and the chloro and iodo analogues are considerably softer. These findings also fit with the already known SbX_3-macrocycle complexes in the literature.

Interestingly in some cases, attempts to form neutral complexes results in ionisation of antimony(III) chloride/iodide, forming salts of the type $[SbX_2(macrocycle)][Sb_xX_y]$ (X= Cl, I). The 18-membered mixed donor chalcogenoether macrocycles have commonly shown to adopt a very folded conformation beginning to encapsulate the metal centre, this would suggest there is a favourable driving force to coordinate in such a manner. In the antimony(III) halide systems ionisation to $[SbX_2]^+$ allows for a greater amount of encapsulation by the macrocycle and hence a conformational effect by the ligand is seen.

Preorganisation of the macrocyclic ligands has also been shown to affect the binding preference for SbX_3. The more flexible nature of the macrocycles used in this study have shown to allow stronger interaction by Sb(III) with the softer donors (S, Se) over O, more in keeping with the established view that antimony(III) is a soft (borderline) Lewis Acid.

7.4 Experimental

7.4.1 **$[SbCl_2([18]aneO_4S_2)][SbCl_6]$:** $SbCl_3$ (0.080 g, 3.51 x 10^{-4} mol) was dissolved in MeCN (15 mL) and an MeCN solution of $SbCl_5$ (0.66 mL, 0.53 mol dm^{-3}, 3.51 x 10^{-4} mol) added. The solution was stirred for 40 min. before [18]aneO_4S_2 (0.103 g, 3.51 x 10^{-4} mol) was added. An immediate fine yellow precipitate formed leaving behind a pale yellow solution. The mixture was stirred overnight, the yellow solid filtered off and dried *in vacuo*. Yellow needles were deposited from the mother liquor on standing. Yield: 0.170 g, 59%. Required for $C_{12}H_{24}Cl_8O_4S_2Sb_3$ (823.24): C, 17.49; H, 2.94. Found: C, 17.88; H, 2.77%. IR (Nujol, cm^{-1}): 340 ($SbCl_6$), 301 (SbCl). ^{1}H NMR (CD_3CN, 298K): δ 3.09-3.31 (m, [8H], SC***H***$_2$), 3.75 (br s, [8H], OC***H***$_2$), 3.95 (br m, [8H], SCH_2C***H***$_2$O).

7.4.2 **$[SbCl_3([9]aneOS_2)]$:** $SbCl_3$ (0.080 g, 3.51 x 10^{-4} mol) and [9]aneOS_2 (0.058 g, 3.51 x 10^{-4} mol) were dissolved in MeCN (10 mL) and stirred overnight. A white solid formed which was filtered off, washed with a small amount of MeCN and dried *in vacuo*. Large colourless crystals grew on storing the filtrate. Yield: 0.076 g, 55%. Required for $C_6H_{12}Cl_3OS_2Sb$ (392.14): C, 18.36; H, 3.08. Found: C, 17.89; H, 3.01%. IR (Nujol, cm^{-1}): 328, 307, 289 (SbCl).^{1}H NMR (CD_3CN, 298K): δ 2.77 (t, [4H], SC***H***$_2$$CH_2O$), 3.02 (s, [4H], SC***H***$_2$), 3.87 (t, [4H], OC***H***$_2$).

7.4.3 **[$SbCl_3$([15]aneO_3S_2)]:** $SbCl_3$ (0.080 g, 3.51 x 10^{-4} mol) and [15]aneO_3S_2 (0.088 g, 3.51 x 10^{-4} mol) were dissolved in MeCN (10 mL). A white solid precipitated immediately, and the mixture was allowed to stir overnight. The solid was filtered off and dried *in vacuo*. Crystals grew from the filtrate. Yield: 0.106, 63%. Required for $C_{10}H_{20}Cl_3O_3S_2Sb$ (480.19): C, 25.00; H, 4.20. Found: C, 25.10; H, 4.14%. IR (Nujol, cm^{-1}): 316, 292, 277 (SbCl). ^{1}H NMR (CD_3CN, 295K): δ 2.75 (t, [4H], SC***H***$_2$$CH_2O$), 2.89 (s, [4H], SC***H***$_2$), 3.64 (s, [8H], OC*H*$_2$), 3.69 (t, [4H], SCH_2C***H***$_2$O); (233K) 2.83 (t, [4H], SC***H***$_2$$CH_2O$), 2.97 (s, [4H], SC***H***$_2$), 3.67 (t, [4H], OC***H***$_2$), 3.71 (m, [4H], OC***H***$_2$); ($CDCl_3$, 298K): δ 2.81 (t, [4H], SC***H***$_2$$CH_2O$), 2.90 (s, [4H], SC***H***$_2$), 3.72 (s, [8H], OC***H***$_2$), 3.78 (t, [4H], SCH_2C***H***$_2$O).

7.4.4 **[$SbCl_3$([18]aneO_4S_2)]:** $SbCl_3$ (0.050 g, 2.19 x 10^{-4} mol) was dissolved in MeCN (10 mL) and cooled to 0°C. [18]aneO_4S_2 (0.065 g, 2.19 x 10^{-4} mol) was dissolved in MeCN (5 mL), added dropwise, and the solution left to stir at room temperature for 24 h. The solvent was removed *in vacuo* and the remaining residues stirred with CH_2Cl_2 (10 mL). The solid that remained was filtered off and dried. Yield: 0.038 g, 33%. Required for $C_{12}H_{24}Cl_3O_4S_2Sb.CH_2Cl_2$ (609.14): C, 25.61; H, 4.30. Found: C, 25.00; H, 3.35%. IR (Nujol, cm^{-1}): 292 (SbCl).^{1}H NMR (CD_3CN, 295K): δ 3.16 (br m, [4H], SC***H***$_2$), 3.29 (br m, [4H], SC***H***$_2$), 3.76 (br s, [8H], OC***H***$_2$), 3.95 (br m, [8H], SCH_2C***H***$_2$O), 2nd species (see Results and Discussion), 2.80 (br t, [8H], SC***H***$_2$), 3.57 (br s, [8H], OC***H***$_2$), 3.66 (br t, [8H], SCH_2C***H***$_2$O); (233K): 3.12 (m), 3.15 (m), 3.25 (m), 3.28 (m), 3.69-3.77 (m), 3.88-3.96 (m). Λ_M (10^{-3} mol dm^{-3}, MeCN) = 26 ohm^{-1} cm^2 mol^{-1}.

A few crystals grew from the filtrate upon standing, which had the constitution, [$SbCl_2$([18]aneO_4S_2)]$_2$[Sb_3Cl_{11}]·CH_2Cl_2.

7.4.5 **$[SbCl_2([18]aneO_4Se_2)]_2[Sb_3Cl_{11}]$:** $SbCl_3$ (0.040 g, 1.63 x 10^{-4} mol) and $[18]aneO_4Se_2$ (0.070 g, 1.63 x 10^{-4} mol) were dissolved in MeCN (15 mL) and left to stir at room temperature for 24 h. The reaction mixture was concentrated to half volume and left to stand at 5°C. Some of the ligand crystallised and was recovered. The volatiles were removed from the filtrate and the resulting white solid washed with CH_2Cl_2, separated, and dried *in vacuo.* Yield: 0.020 g, 29%. Required for for $C_{24}H_{48}Cl_{15}O_8Se_4Sb_5$ (1920.72): C, 14.99; H, 2.52. Found: C, 15.37; H, 2.57%. IR (Nujol, cm^{-1}): 300 (SbCl). ^1H NMR (CD_3CN, 295K): δ 3.15 (br m [4H], SeC***H***$_2$), 3.33 (br m, [4H], SeC***H***$_2$), 3.78 (br s, [8H], OC***H***$_2$), 3.94 (br m, [4H], $SeCH_2C$***H***$_2O$), 4.03 (br m, [4H], $SeCH_2C$***H***$_2O$); (233K) 3.13 (br m [4H], SeC***H***$_2$), 3.28 (br m, [4H], SeC***H***$_2$), 3.75 (br m, [8H], OC***H***$_2$), 3.90 (br m, [4H], OC***H***$_2$), 4.00 (br m, [4H], OC***H***$_2$).

The solid was recrystallised from MeCN giving crystals of adequate quality for structure characterisation.

7.4.6 **$[SbI_2([18]aneO_4S_2)][Sb_2I_7]$:** SbI_3 (0.100 g, 1.99 x 10^{-4} mol) and $[18]aneO_4S_2$ (0.059 g, 1.99 x 10^{-4} mol) were dissolved in MeCN (10 mL). Within minutes an orange precipitate began to form and the solution turned yellow. The solution was stirred for 5 h, the solid was filtered off and dried. Once formed the bulk orange product is completely insoluble in MeCN and sparingly soluble in CH_2Cl_2. Yield: 0.035 g, 29%. Required for $C_{12}H_{24}I_9O_4S_2Sb_3$ (1803.50): C, 7.98; H, 1.34. Found: C, 7.67; H, 2.02%. ^1H NMR (CD_2Cl_2, 295 K): δ 2.71 (t, [8H], SC***H***$_2$), 3.50 (s, [8H], OC***H***$_2$), 3.59 (t, [8H], SCH_2C***H***$_2O$).

The filtrate formed orange crystals on standing, they had the constitution $[SbI_2([18]aneO_4S_2)]_2[Sb_{2.5}I_{9.5}]$

7.4.7 **$[SbI_2([18]aneO_2S_4)]_2[Sb_4I_{14}]$:** SbI_3 (0.077g, 1.52 x 10^{-4} mol) and an excess of $[18]aneO_2S_4$ (0.100 g, 3.05 x 10^{-4} mol) were dissolved in MeCN (10 mL) and CH_2Cl_2 (10 mL). Within minutes an orange precipitate began to form and the solution turned yellow. The solution was stirred for 4 h, the solid was filtered, washed with CH_2Cl_2 and dried. Once formed the bulk orange product is sparingly soluble. Yield: 0.045 g. ^{1}H NMR (CD_2Cl_2, 298 K): δ 2.67 (t, [8H] SC***H***$_2$$CH_2O$), 2.78 (s, [8H], SC***H***$_2$), 3.59 (t, [8H], OC***H***$_2$); (CD_3CN, 298 K): δ 2.73 (t, [8H] SC***H***$_2$$CH_2O$), 2.83 (s, [8H], SC***H***$_2$), 3.65 (t, [8H], OC***H***$_2$).

Orange crystals were grown by saturating a warm CH_2Cl_2 solution and allowing to cool to room temperature over hours, they had the constitution $[SbI_2([18]aneO_2S_4)]_2[Sb_4I_{14}]$.

7.4.8 **$[SbF_3$(18-crown-6)]:** SbF_3 (0.068 g, 3.78 x 10^{-4} mol) was dissolved in MeOH (20 mL). To the solution, was added solid 18-crown-6 (0.100 g, 3.78 x 10^{-4} mol) which fully dissolved over the course of a few minutes. The clear solution was left to stir for 16 h. The volatiles were removed under reduced pressure and the white powder washed with hexane. The solid was recrystallised from CH_2Cl_2. Yield: 0.108 g, 64%. Required for $C_{12}H_{24}F_3O_6Sb{\cdot}1/2CH_2Cl_2$ (485.37): C, 30.90; H, 5.19. Found: C, 30.56; H, 4.93%. IR (Nujol, cm^{-1}): 593, 544 (SbF). ^{1}H NMR (CD_2Cl_2, 295 K): δ 3.67 (s, crown C***H***$_2$); (180 K): 3.70 (br s, [12H], OC***H***$_2$), 3.50 (br s, [12H], OC***H***$_2$). ^{19}F{^{1}H} NMR (CD_2Cl_2, 295 K): δ -83.7; (180 K): -84.6.

7.4.9 **[SbF_3([18]aneO_4S_2)]:** SbF_3 (0.065 g, 3.64 x 10^{-4} mol) was dissolved in MeOH (20 mL) and [18]aneO_4S_2 (0.108 g, 3.64 x 10^{-4} mol) added, which completely dissolved over the course of minutes. The clear solution was left to stir for 16 h. The volatiles were removed under reduced pressure and the white powder dissolved in CH_2Cl_2; a very small amount of solid with a pink hue did not dissolve (SbF_3) remained. The CH_2Cl_2 extract was evaporated and the white solid produced, rinsed with hexane (5 mL), and dried *in vacuo*. Yield: 0.080 g, 46%. Required for $C_{12}H_{24}F_3O_4S_2Sb$ (474.86): C, 30.32; H, 5.09. Found: C, 31.7; H, 5.2%. IR (Nujol, cm^{-1}): 560, 521 (SbF). ^{1}H NMR (CD_2Cl_2, 295 K): δ 2.81 (s, [8H], SC***H***$_2$), 3.59 (s, [8H], OC***H***$_2$), 3.69 (s, [8H], OC***H***$_2$); (180 K): 2.76 (s, [8H]), 3.56 (s, [8H]), 3.58 (s, [8H]). ^{19}F{^{1}H} NMR (CD_2Cl_2, 295 K): δ -84.0 (s); (180 K): -87.0.

7.4.10 **[SbF_3([15]aneO_3S_2)]:** SbF_3 (0.068 g, 3.78 x 10^{-4} mol) was dissolved in MeOH (20 mL) and [15]aneO_3S_2 (0.096 g, 3.78 x 10^{-4} mol) added, which completely dissolved over the course of minutes. The clear solution was left to stir for 16 h. The volatiles were removed under reduced pressure and the white powder dissolved in CH_2Cl_2; a small amount of solid with a pink hue did not dissolve (SbF_3) remained. The CH_2Cl_2 extract was evaporated and the white solid produced, rinsed with hexane (5 mL), and dried *in vacuo*. Yield: 0.067 g, 39%. IR (Nujol, cm^{-1}): 568, 528 (SbF). ^{1}H NMR (CD_2Cl_2, 295 K): δ 2.73 (s, [4H], SC***H***$_2$), 2.87 (s, [4H], SC***H***$_2$), 3.64 (s, [8H], OC***H***$_2$), 3.70 (s, [4H], OC***H***$_2$); (180 K): 2.68 (s, [4H]), 2.81 (s, [4H]), 3.60 (s, [8H]), 3.61 (s, [4H]); (d_6-acetone, 298K): δ 2.69 (t, [4H], SC***H***$_2$$CH_2O$), 2.84 (s, [4H], SC***H***$_2$), 3.60 (s, [8H], OC***H***$_2$), 3.72 (t, [4H], SCH_2C***H***$_2$O). ^{19}F{^{1}H} NMR (CD_2Cl_2, 295 K): δ -81.0; (180 K): -84.0.

7.4.11 **[SbF_3([18]aneO_4Se_2)]:** SbF_3 (0.060 g, 3.36 x 10^{-4} mol) and [18]aneO_4Se_2 (0.131 g, 3.36 x 10^{-4} mol) were dissolved in a mixture of MeOH (20 mL) and MeCN (5 mL) (to aid solubility). The reactants completely dissolved over the course of minutes and the clear solution was left to stir for 16 h. The volatiles were removed under reduced pressure and the white powder dissolved in CH_2Cl_2; a very small amount of solid with a pink hue did not dissolve (SbF_3) remained. The CH_2Cl_2 extract was evaporated and the white solid produced, rinsed with hexane (5 mL), and dried *in vacuo.* Yield: 0.080 g, 42%. Required for $C_{12}H_{24}F_3O_4SbSe_2$ (568.83): C, 25.32; H, 4.25. Found: C, 24.95; H, 4.16%. IR (Nujol, cm^{-1}): 575, 549 (SbF). ^{1}H NMR (CD_2Cl_2, 295 K): δ 2.83 (s, [8H], SeC**H**$_2$), 3.61 (s, [8H], OC**H**$_2$), 3.76 (s, [8H], OC**H**$_2$); (180 K): 2.77 (br t, [8H]), 3.52 (s, [8H]), 3.69 (br t, [8H]); (CD_3CN, 298K): δ 2.85 (v.br t, [8H], SeC**H**$_2$), 3.59 (br s, [8H], OC**H**$_2$]), 3.75 (br t, [8H], $SeCH_2C$**H**$_2$O). ^{19}F{^{1}H} NMR (CD_2Cl_2, 295 K): δ -76.2; (180 K): -76.4.

7.5 Structural Data

Compound	$[SbCl_2([18]aneO_4S_2)][SbCl_6]$	$[SbCl_3([9]aneOS_2)]$	$[SbCl_3([15]aneO_3S_2)]$
Formula	$C_{12}H_{24}Cl_8O_4S_2Sb_2$	$C_6H_{12}Cl_3OS_2Sb$	$C_{10}H_{20}Cl_3O_3S_2Sb$
mwt.	823.53	392.38	480.48
crystal system	Monoclinic	Monoclinic	Orthorhombic
space group	$P2_1$ (4)	$P2_1/n$ (14)	$P2_12_12_1$ (19)
a (Å)	7.9283(15)	8.238(2)	7.825(2)
b (Å)	12.933(4)	14.896(5)	13.473(4)
c (Å)	12.906(3)	10.186(4)	15.972(6)
α (°)	90	90	90
β (°)	102.322(15)	93.46(4)	90
γ (°)	90	90	90
U (Å^3)	1292.8(5)	1247.7(6)	1683.9(9)
Z	2	4	4
μ(Mo Kα) (mm^{-1})	3.096	3.151	2.362
F(000)	796	760	952
total no. reflns	15409	6606	4683
unique reflns	4899	2836	3575
R_{int}	0.0564	0.0228	0.0343
no. of params, restraints	254, 1	118, 0	173, 0
R_1[a] [$I_o > 2\sigma(I_o)$]	0.0415	0.018	0.045
R_1 (all data)	0.0565	0.021	0.060
wR_2[a] [$I_o > 2\sigma(I_o)$]	0.084	0.038	0.085
wR_2(all data)	0.092	0.039	0.090

Compound	$[SbCl_2([18]aneO_4S_2)]_2[Sb_3Cl_{11}]\cdot CH_2Cl_2$	$[SbCl_2([18]aneO_4Se_2)]_2[Sb_3Cl_{11}]\cdot MeCN$	$[SbI_2([18]aneO_4S_2)]_2[Sb_{2.5}I_{9.5}]$
Formula	$C_{25}H_{50}Cl_{17}O_8S_4Sb_5$	$C_{26}H_{51}Cl_{15}NO_8Sb_5Se_4$	$C_{24}H_{48}I_{13.5}O_8S_4Sb_{4.5}$
mwt.	1818.29	1962.02	2853.89
crystal system	Monoclinic	Monoclinic	Monoclinic
space group	$P2_1/c$ (14)	$P2_1/c$ (14)	$C2/c$ (15)
a (Å)	24.104(3)	24.256(4)	36.076(6)
b (Å)	15.5352(15)	15.466(2)	8.2093(10)
c (Å)	29.615(11)	29.959(7)	23.412(8)
α (°)	90	90	90
β (°)	95.25(4)	95.735(7)	121.70(5)
γ (°)	90	90	90
U (Å^3)	11043(4)	11183(3)	5899(2)
Z	8	8	4
μ(Mo Kα) [mm^{-1}]	3.429	5.746	9.279
F(000)	6976	7392	5060
total no. reflns	50253	64383	16880
unique reflns	24636	25357	6728
R_{int}	0.0361	0.0667	0.058
no. of params, restraints	1058, 10	1050, 0	245, 0
R_1[a] [$I_o > 2\sigma(I_o)$]	0.049	0.064	0.043
R_1 (all data)	0.069	0.117	0.064
wR_2[a] [$I_o > 2\sigma(I_o)$]	0.116	0.152	0.084
wR_2(all data)	0.123	0.152	0.090

Compound	$[SbF_3([15]aneO_3S_2)]$
Formula	$C_{10}H_{20}F_3O_3S_2Sb$
mwt.	431.13
crystal system	Monoclinic
space group	$P2_1/n$ (14)
a (Å)	8.1242(15)
b (Å)	15.210(3)
c (Å)	12.559(4)
α (°)	90
β (°)	100.445(7)
γ (°)	90
U (Å^3)	1526.2(6)
Z	4
μ(Mo Kα) [mm^{-1}]	2.113
F(000)	856
total no. reflns	7280
unique reflns	3466
R_{int}	0.0228
no. of params, restraints	172, 0
R_1[a] [$I_o > 2\sigma(I_o)$]	0.0227
R_1 (all data)	0.0227
wR_2[a] [$I_o > 2\sigma(I_o)$]	0.0484
wR_2(all data)	0.0504

[a] $R_1 = \Sigma||F_o| - |F_c||/\Sigma|F_o|$. $wR_2 = [\Sigma w(F_o^2 - F_c^2)^2/\Sigma wF_o^4]^{1/2}$

Common items: temperature = 100K; wavelength (Mo Kα)= 0.71073 Å; θ_{max}= 27.5°

7.6 References

1. B. Cordero, V. Gomez, A. E. Platero-Prats, M. Reves, J. Echeverria, E. Cremades, F. Barragan and S. Alvarez, *Dalton Trans.*, 2008, 2832

2. H. J. Drexler, I. Starke, M. Grotjahn, H. Reinke, E. Kleinpeter and H. J. Holdt, *Z. Naturforsch. B: Chem. Sci.*, 1999, **54**, 799

3. E. Kleinpeter, M. Grotjhan, K. D. Klika, H. J. Drexler and H. J. Holdt, *J. Chem. Soc. Perkin Trans. 2*, 2001, 988

4. M. S. Fonari, E. V. Ganin, V. O. Gelmboldt, J. Lipkowski, S. A. Kotlyar and G. L. Kamalov, *Acta Crystallogr. Sect. E*, 2006, **62**, 1021

5. H. J. Drexler, Thesis Structure (F.Allen, Acta Crystallographica Section B, 2002, 58, 380-388), 1997

6. J. Lipkowski, M. Fonari, V. Kravtsov, Y. Simonov, E. Ganin and V. Gelmboldt, *J. Chem. Crystallogr.*, 1996, **26**, 823

7. I. Becker, M. Windhaus and R. Mattes, *Z. Naturforsch. B: Chem. Sci.*, 1994, **49**, 870

8. M. Schafer, J. Pebler, B. Borgsen, F. Weller and K. Dehnicke, *Z. Naturforsch. B: Chem. Sci.*, 1990, **45**, 1243

9. N. W. Alcock, M. Ravindran, S. M. Roe and G. R. Willey, *Inorg. Chim. Acta*, 1990, **167**, 115

10. E. Hough, D. G. Nicholson and A. K. Vasudevan, *J. Chem. Soc. Dalton Trans.*, 1987, 427

11. N. W. Alcock, M. Ravindran and G. R. Willey, *Acta Crystallogr. Sect. B*, 1993, **49**, 507

12. M. Schafer, J. Pebler and K. Dehnicke, *Z. Anorg. Allg. Chem.*, 1992, **611**, 149

13. M. Takahashi, T. Kitazawa and M. Takeda, *J. Chem. Soc. Chem. Comm.*, 1993, 1779

14. B. Neumüller and K. Dehnicke, *Z. Anorg. Allg. Chem.*, 2006, **632**, 1681

15. A. Lipka, *Acta Crystallogr. Sect. B: Struct. Sci.*, 1979, **35**, 3020

16. A. J. Edwards, *J. Chem. Soc. A: Inorg. Phys. Theor.*, 1970, 2751

17. D. W. Cushen and R. Hulme, *J. Chem. Soc. Res.*, 1964, 4162

18. A. Neuhaus, G. Frenzen, J. Pebler and K. Dehnicke, *Z. Anorg. Allg. Chem.*, 1992, **618**, 93

19. M. Schäfer, G. Frenzen, B. Neumüller and K. Dehnicke, *Angew. Chem. Int. Ed. Engl.*, 1992, **31**, 334

20. R. Garbe, B. Vollmer, B. Neumüller, J. Pebler and K. Dehnicke, *Z. Anorg. Allg. Chem.*, 1993, **619**, 271

21. G. R. Willey, M. T. Lakin, M. Ravindran and N. W. Alcock, *Journal of the Chemical Society-Chemical Communications*, 1991, 271

22. S. Pohl, D. Haase and M. Peters, *Z. Anorg. Allg. Chem.*, 1993, **619**, 727

23. A. J. Barton, N. J. Hill, W. Levason, B. Patel and G. Reid, *Chem. Commun.*, 2001, 95

24. A. J. Barton, N. J. Hill, W. Levason and G. Reid, *J. Chem. Soc., Dalton Trans.*, 2001, 1621

25. M. Mantina, A. C. Chamberlin, R. Valero, C. J. Cramer and D. G. Truhlar, *J. Phys. Chem. A*, 2009, **113**, 5806

26. W. J. Geary, *Coord. Chem. Rev.*, 1971, **7**, 81

27. G. A. Fisher and N. C. Norman, in *Adv. Inorg. Chem.*, ed. A. G. Sykes, Academic Press, 1994, vol. Volume 41, pp. 233

28. W. Levason, M. E. Light, S. Maheshwari, G. Reid and W. Zhang, *Dalton Trans.*, 2011, **40**, 5291

Appendix 1- General Experimental Techniques

All experiments were performed under a dry N_2 atmosphere using Schlenk line techniques, apart from the $Pb(BF_4)_2$ and $Pb(PF_6)_2$ chemistry which was performed under ambient conditions. Spectroscopic samples were prepared in a glove box purged with dry N_2. Solvents were dried and degassed prior to use. Et_2O and THF were distilled over Na/benzophenone ketyl; hexane was distilled over Na wire; CH_2Cl_2 and MeCN were distilled over CaH; MeOH and EtOH were distilled over Mg/I_2. Reagents were purchased from Sigma-Aldrich. $CaCl_2$, $Ca(CF_3SO_3)_2$ and SbF_3 were dried *in vacuo* with heating over several hours prior to use. $[ScCl_3(THF)_3]$ and $[YCl_2(THF)_5][YCl_4(THF)_2]$ were made according to the literature [1] [2]. $SbCl_3$ was sublimed under reduced pressure and $SbCl_5$ was distilled under reduced pressure. 18-crown-6 was dried for the Group 2 reactions by refluxing in CH_2Cl_2 and $SOCl_2$ for 1 h, the solvent and excess $SOCl_2$ were removed *in vacuo* and the ligand used immediately. All other reagents were used as received.

IR spectra were recorded over the range 4000-200 cm^{-1} using a Perkin Elmer Spectrum 100 spectrometer. Samples were prepared as nujol mulls between CsI plates. NMR spectra were recorded using Bruker AV300 or DPX400 spectrometers. ^{1}H and ^{13}C spectra were referenced to the solvent reference, ^{19}F to external $CFCl_3$, ^{31}P to external aqueous 85% H_3PO_4, ^{45}Sc to external aqueous $[Sc(H_2O)_x]^{3+}$ at pH = 1, ^{77}Se to neat external Me_2Se, ^{125}Te to neat external Me_2Te, ^{119}Sn to external Me_4Sn without proton decoupling and with a 3 s pulse delay, ^{207}Pb to external $PbMe_4$. Microanalyses were undertaken by Medac Ltd. or London Metropolitan. ESI MS was carried out in MeCN solution using a VG Biotech platform. Conductivity measurements were carried using a platinum electrode conductivity cell on a PYE & Co conductance bridge.

Single crystal X-ray data was collected using a Rigaku AFC 12 goniometer equipped with an enhanced sensitivity (HG) Saturn724+ detector mounted at the window of an FR-E+ SuperBright molybdenum rotating anode generator with HF or VHF Varimax optics. Mo-Kα radiation was used (λ= 0.71073 Å). Crystals were held at 120K under a nitrogen gas stream. Solution and refinement of structures was carried out as standard using SHELX [3] [4] [5], with hydrogen atoms added to the model in calculated positions using default C–H distances.

References for Appendix 1

1. L. E. Manzer, *Inorg. Synth.*, 1982, **21**, 135

2. P. Sobota, J. Utko and S. Szafert, *Inorg. Chem.*, 1994, **33**, 5203

3. G. M. Sheldrick, University of Göttingen, Germany, 1997, p. Structure Refinement.

4. G. M. Sheldrick, *Acta Crystallogr.*, *Sect A*, 2008, **A64**, 112

5. H. D. Flack, *Acta Crystallogr., Sect. A (Foundations of Crystallography)*, 1983, **A39**, 876.

Future Aims and Recommendations

The systematic coordination of very soft chalcogenoether Lewis bases to hard Lewis acids has been shown to be attainable and reproducible under the correct conditions. The implications of this present the coordination chemist with a much greater scope for different ligand-metal interactions than previously thought, and inturn the possibility of new compounds with more tailored properties.

With regards to the compounds presented in this thesis, further investigation into the nature of the metal-donor interaction should be pursued. Both DFT calculations and X-ray crytallogaphic charge density mapping could be used to further characterise the electronic character of the coordinate bond. It would be interesting to see if there is a difference in the O–M compared to the E–M (E=S, Se) interactions by ascertaining to what degree these bonds have an ionic or covalent nature. The complexes from this work are unique in that they contain both hard and soft donor types within the same flexible macrocyclic framework all coordinating to one metal centre and are ideal for this further characterisation, thus warranting it.

The strategies employed in synthesising the coordination complexes in this study relied heavily on the macrocyclic effect inherent to the ligands of choice. It would be interesting to see if similar hard/soft metal to ligand interactions can be achieved in the absence of this effect i.e. using polydentate but acyclic ligands. It is unlikely that an analogous saturated -CH_2- backbone will sufficiently preorganise the donors towards coordination to a metal centre or help overcome the inter-donor lone-pair repulsions, therefore the new ligands to be investigated should have a more rigid backbone incorporating aromatic/unsaturated linkers. A possible benefit of these “new” complexes is that the metal centre could be made less crowded liberating new coordination sites so that the coordination chemist can further diversify the coordination environment around the metal centre.

Given that there is a worldwide interest in green chemistry and also the biological importance of both sulfur and calcium. The Group 2 complexes in

this study should provide a basis for the chemistry required to investigate green catalysts and biomimetic systems based on calcium. Many of the structures in this thesis showed mutually *cis* (possible) coordination sites a prerequisite to many organometallic mechanisms that underpin cataysis.

Similar synthetic investigations should be undertaken with the smaller and harder Group 2 cation Mg(II). This work will require overcoming similar challenges encountered with Ca(II), Sc(III) and Sr(II). It will be necessary to move to smaller macrocycle sizes, e.g. 12-,14-, 15- membered rings, to better accommodate the smaller metal ion. Mg(II) is a harder Lewis acid than Ca(II) and thus neutral thioether coordination is likely to be more difficult to achieve. That being said magnesium is equally vital in biological systems especially in photosynthesis and further research into the metal's coordination chemistry could provide new model systems to investigate this biochemistry. This is especially relevant on the back of the success of the calcium chemistry presented in this work.